DIPARTIMENTO SCIENZE DELLA VITA

DOTTORATO DI RICERCA IN SCIENZE DELLA VITA

CICLO XXXV

COORDINATORE Prof. Massimo Valoti

DEVELOPMENT OF NOVEL GPR55 LIGANDS AND GPR55/CB_2R MULTITARGET MODULATORS FOR NEURODEGENERATIVE DISEASES

SETTORE SCIENTIFICO-DISCIPLINARE: CHIM/08

TUTOR: Prof. Marco Macchia **DOTTORANDA: Dott.ssa Costanza Ceni**

A.A. 2022-2023

Contents

1. Introduction

1.1 Endocannabinoid system

Precisely defining the complex endocannabinoid system (ECS) is becoming more and more difficult, considering the high number of potential components which may belong to this system. The ECS was identified in the early 1990, exploring the possible targets of Δ9-tetrahydrocannabinol (THC), the principal psychoactive constituent of *Cannabis Sativa*, whose effects were already well known. The ECS is distributed ubiquitously throughout the mammalian body and, in the last twenty-five years, it has emerged as a fundamental neuromodulatory system, involved in several physiological and pathological processes. [1]

The ECS consists of:

1. Endogenous cannabinoids (endocannabinoids). [1]
2. Enzymes responsible for the synthesis and degradation of endocannabinoids. [1]
3. Cytosolic and membrane transporters. [1]
4. CB_1 and CB_2 cannabinoid receptors. [2]

1.1.1 Endocannabinoids

Endocannabinoids (eCBs) are lipid metabolites which are considered the endogenous ligands of cannabinoid receptors (CBRs). The first discovered and best-characterized endocannabinoids are anandamide (AEA, *figure 1.1*) [3] and 2-arachidonoylglycerol (2-AG, *figure 1.1*) [4]. While 2-AG acts as a full agonist of both CB receptors, with a low preference for CB_1R, [4] AEA is a partial agonist of CB_1R, [3] almost inactive at CB_2R. Moreover, both 2-AG and AEA have been reported to interact also with other targets, including the transient receptor potential cation channel subfamily V member 1 (TRPV1) and GPR55 receptor, although data regarding their pharmacological profiles appear to

be quite controversial. [5] [6] Later, endogenous peptides and other arachidonic acid derivatives were shown to generate endocannabinoid-like effects. [7] Among the ω-6 fatty acid compounds, N-dihomo-γ-linolenoylethanolamine, N-arachidonoyldopamine (NADA, *figure 1.1*), 2-arachidonoylglycerylether (noladin ether, *figure 1.1*) and O-arachidonoylethanolamine (virodhamine, *figure 1.1*) are able to interact with CB receptors (even though with different potency and efficacy). [8] Furthermore, two important ω-3 (n-3) fatty acid ethanolamines, N-eicosapentaenoylethanolamine (EPEA, *figure 1.1*) and N-docosahexaenoylethanolamine (DHEA, *figure 1.1*), have been proposed as CBRs agonists, but their pharmacology and biological relevance remain to be clarified. [9] Recently, allosteric eCBs have been identified, including pregnenolone and lipoxin A4 (*figure 1.1*), which act as a allosteric modulators of CB_1R, with possible therapeutic implications. [10]

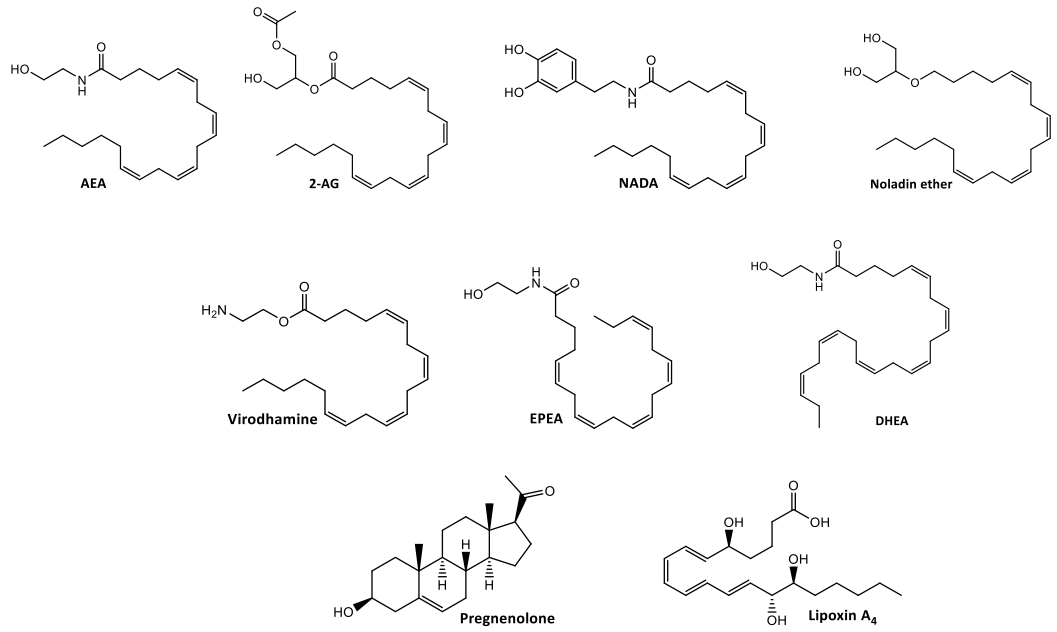

Figure 1.1 *Structures of the most important eCBs.*

1.1.1.1 Synthesis and degradation of eCBs

Endocannabinoids are produced and released in the synaptic space "on demand", following the increase of intracellular Ca^{2+} concentration, and then rapidly deactivated by re-uptake transport or by degrading enzymes, [10] depending on the target tissues.

[11] Biosynthesis and degradation of AEA is reported in *figure 1.2*: the synthesis starts largely from N-arachidonoyl phosphatidyl ethanol (NAPE) and is featured in multiple pathways, depending on the physiological and pathophysiological processes involved, as summarized in *figure 1.2*. Hydrolysis of N-arachidonoyl phosphatidyl ethanol (NAPE) by a phospholipase (NAPE-PLD) result in the one step synthesis of AEA. Otherwise, NAPE can be converted into phospho-AEA by phospholipase C (PLC), which gives AEA through the removal of phosphate group, by a specific phosphatase. The hydrolysis of one of the ester groups by phospholipase A2 (PLA2) or α/β-hydrolase 4 (ABHD4) transforms AEA into 2-lyso-NAPE. A further hydrolysis promoted by ABHD4 produces glycerol-phospho-AEA, which is quickly converted in AEA by glycerophosphodiester phosphodiesterase 1 (GDE-1). Alternatively, 2-lyso-NAPE can also be directly transformed into AEA by lyso-phospholipase *D* (lyso-PLD) enzyme. [1] [12]

In the central nervous system (CNS), AEA is mainly degraded by the enzyme fatty acid amino hydrolase (FAAH), which converts the endocannabinoid in arachidonic acid and ethanolamine, as reported in *figure 1.2*. Other degradation mechanisms involve N-acylethanolamine-hydrolyzing acid amidase (NAAA) and cyclooxygenase-2 (COX-2). Considering this latter enzyme, the structural differences between arachidonic acid and AEA inhibits AEA oxidation, by development of COX-2 inhibitors, without affecting prostaglandin formation. [1]

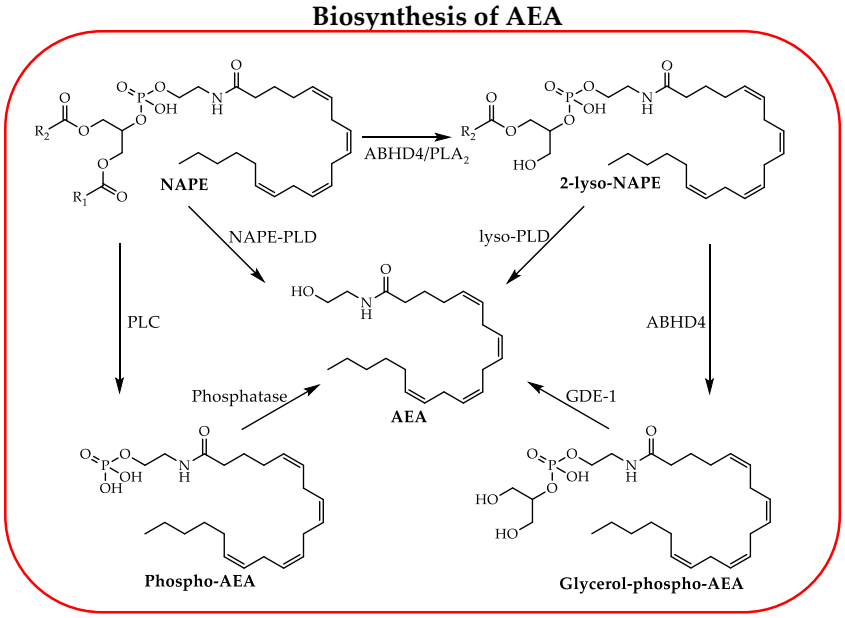

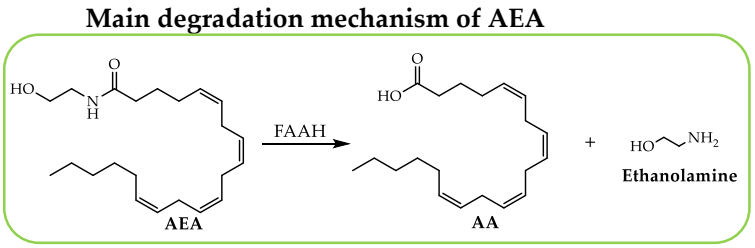

Figure 1.2 *Biosynthesis and main degradation mechanism of AEA.*

2-AG may be produced from several precursors too (*figure 1.3*) [1]: the intermediate 2-arachidonoyl-diacylglycerol, which is transformed in 2-AG through a diacylglycerol lipase (DAGL), is obtained from three different precursors: 2-Arachidonoyl-inositol phospholipids, after hydrolysis through a specific PLC, and 2-arachidonoyl phosphatidic acid or 2-arachidonoyl-phosphocholine; after loss of a phosphate; and a phosphocholine group promoted by specific phosphatase. 2-AG can also be obtained by hydrolysis of 2-arachidonoyl-lysophosphatidic acid or 2-arachidonoyl-lysophosphatidylinositol. This latter intermediate is synthesized from 2-Arachidonoyl-inositol phospholipids, thanks to the phospholipase DDHD1. [13]

Degradation of 2-AG (*figure 1.3*) is primarily due to three hydrolytic enzymes, monoacylglycerol lipase (MAGL) and alpha/beta domain hydrolases 6 and 12 (ABHD6 and 12). In addition, 2-AG can also be oxidized by COX-2 or by P450, phosphorylated by a MAG kinase or hydroxylated by Lipoxigenase (12-LOX). [11]

Biosynthesis 2-AG

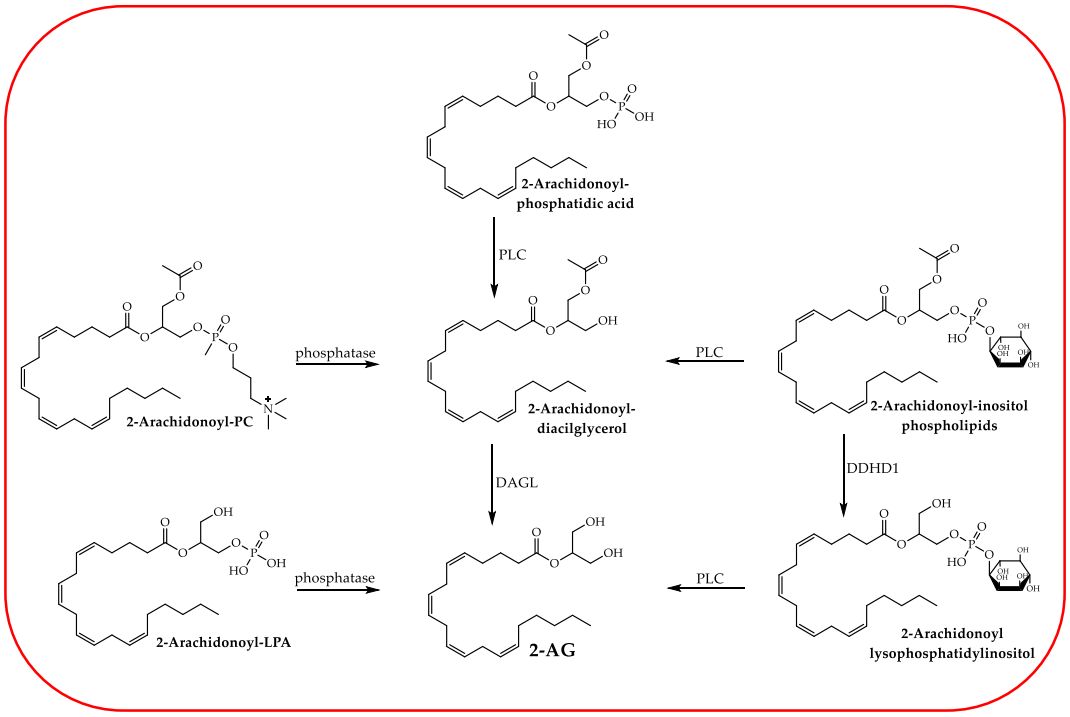

Degradation mechanisms of 2-AG

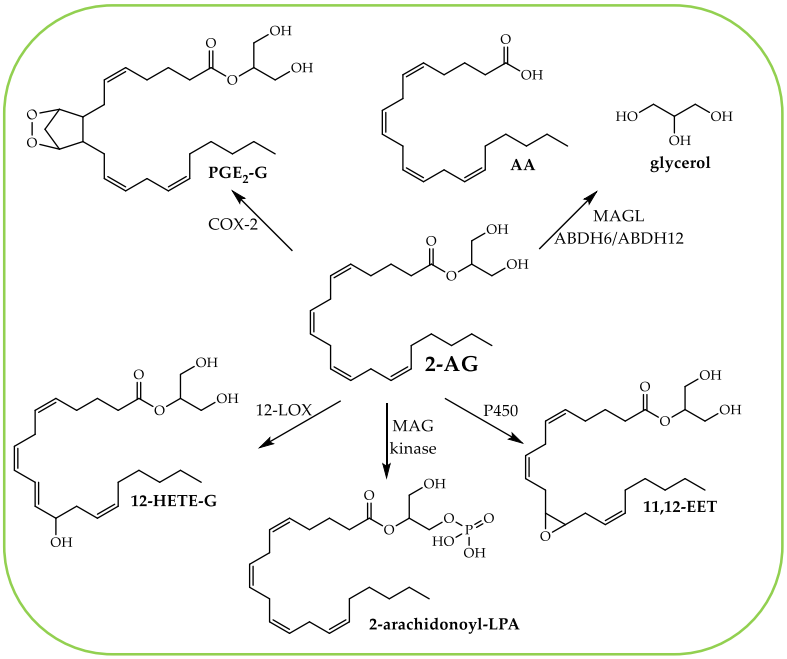

Figure 1.3 *Biosynthesis and degradation mechanisms of 2-AG.*

1.1.2 Endocannabinoid Cytosol and Membrane Transporters

The driving force for the passage of AEA in the intracellular space is the FAAH enzyme, which is localized in the endoplasmic reticulum (ER) and which converts the endocannabinoid in arachidonic acid and ethanolamine, leading to the decrease of extracellular concentration. Thus, FAAH inhibitors disrupt the equilibrium of AEA outside and inside the cells, increasing its extracellular concentration and therefore its binding with cannabinoid receptors. [14] Considering the lipid nature of AEA, after passing through the lipid membrane, it must be delivered through the aqueous cytoplasm to ER. Thus, Fatty acid binding proteins (FABPs) and in particular FABP5 and FABP7, as the main carriers of this endocannabinoid, shuttle AEA through the cytosol up to ER. [15] Albeit to a lesser extent, also albumin, heat shock protein (Hsp70), FAAH-like AEA transporter (FLAT) and steroid carrier protein-2 (SCP-2) act as AEA cytosolic carriers.

Even though no Endocannabinoid Membrane Transporters (EMTs) has been cloned yet, several hypothetical models of AEA uptake have been proposed. Early investigation in 1993 showed a temperature and time-dependent, rapid and saturable uptake process of anandamide, which did not compete with N-acylethanolamines, N-stearoylethanolamine, N-linolenylethanolamine or N-palmitoylethanolamine, highlighting the existence of a membrane carrier-mediated transport. Later, several research groups focused on the mechanism of AEA uptake, showing that this process was not dependent on either ATP or coupled to an ion gradient (Na^+, Cl^-, H^+), suggesting a facilitated or energy-independent membrane transport, similar to those for catecholamines and amino acids. Recently, the discovery of new probes which show potent AEA uptake reduction, without inhibiting FAAH or cytoplasmic-binding proteins corroborated previously hypothesis. [16] Further investigations are required in order to provide new evidences as regards the real existence of EMT. Additionally, it is also necessary to understand if AEA membrane uptake involves proper competition mechanism and if it can be also applied to 2-AG and other eCBs.

1.1.3 Cannabinoid Receptors

Endocannabinoids exert their effect interacting with cannabinoid receptors (CBRs, *figure 1.4*), which include the cannabinoid receptor type-1 (CB_1R) and type-2 (CB_2R), the two main receptors of the ECS identified more than 20 years ago. [17] CBRs are G protein-coupled receptors (GPCRs) and belong to the rhodopsin receptor family, with seven transmembrane helical domains, three extracellular loops and three intracellular loops. Comparing their total protein sequences, CB_2R has about 44% shared identity with CB_1R, but if the focus is the transmembrane region, the protein sequence identity rises to 68% (*figure 1.4*). [18]

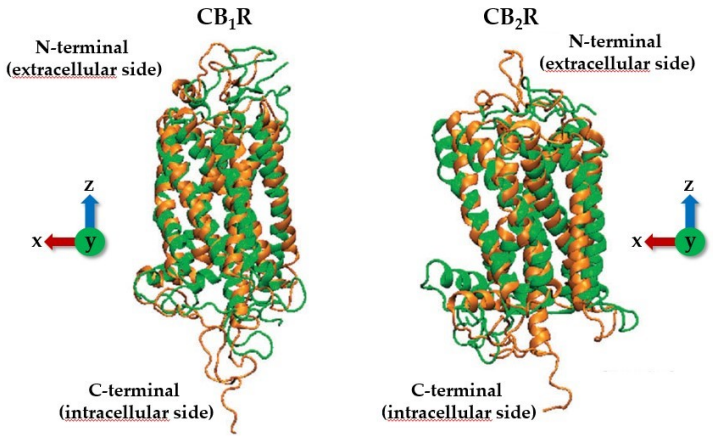

Figure 1.4 *Cannabinoid receptor structures.* [19]

1.1.3.1 CBRs Pathways

The signalling pathways of cannabinoid receptors can be divided into three different waves: the first one which includes both protein G- dependent and independent mechanisms, the second one which results in receptor desensitization, mediated by β-arrestins activation, and the third one which comes from receptor localization in intracellular compartments, such as endosomes and lysosomes (*figure 1.5*). [20]

Both CB_1R and CB_2R belong to the GPCR family and are primarily coupled with the pertussis toxin (PTX)-sensitive $G_{i/o}$ proteins. Their stimulation decreases adenylate cyclase (AC) activity and of intracellular cAMP concentration, with the consequent reduction of Ca^{2+} conductance, as well as the increase in K^+ conductance. Moreover, activation of $G\alpha_{i/o}$ subunits lead to the increase of mitogen-activated protein kinase

(MAPK) signalling pathways, such as extracellular signal-regulated kinase (ERK 1/2), c-Jun N-terminal kinases (JNKs) and p38, while Gβ/γ stimulation activates the phosphoinositide 3-kinase (PI3K). [11] Furthermore, CBRs bind other G-proteins (G_s, $G_{q/11}$, $G_{12/13}$) in a cell type- and ligand- dependent manner. [18] For example, CB_1R increases the release of cAMP through activation of G_s protein, when the dopamine receptor 2 (D_2R) is simultaneously stimulated in cultured striatal neurons and when G_i is blocked by PTX in transfected CHO-K1 cells. Additionally, WIN 55, 212-2 (WIN), a CB_1R agonist, stimulates the increase of intracellular Ca^{2+} due to activation of $G_{q/11}$ protein in transfected HEK-293 cells and in cultured hippocampal neurons with endogenous receptor expression. [11] It has been proposed that CBRs also regulate ion permeability in a G protein-independent manner: in particular, CB_1R stimulation reduces intracellular levels of Ca^{2+}, negatively and directly modulating N-, P-, Q- and R-type voltage gate channels, and increases intracellular concentration of K^+ through activation of G-protein-coupled inwardly rectifying K^+ channels (GIRKs). [11]

The second signalling cascade promoted by CBRs ligands occurs because of receptor phosphorylation, which leads to GPCR internalization. βarrestins play a key role in receptor desensitization, working as a scaffold for the endocytic machinery. This signalling wave starts as a G protein-independent process which result in the activation of MAPKs, including ERK, JNK and Src. [20]

Finally, following the internalization in endo/lysosomes, CBRs phosphorylate ERK 1/2 and promote Ca^{2+} release from intracellular compartments. [20]

Beside the above-reported signalling waves ($G\alpha_{i/o}$ and β-arrestins pathways), it has been shown that MAPK activation can also be promoted by phosphatidylinositol-3-kinase (PI3K) or by transactivation of tyrosine kinase receptors. [21]

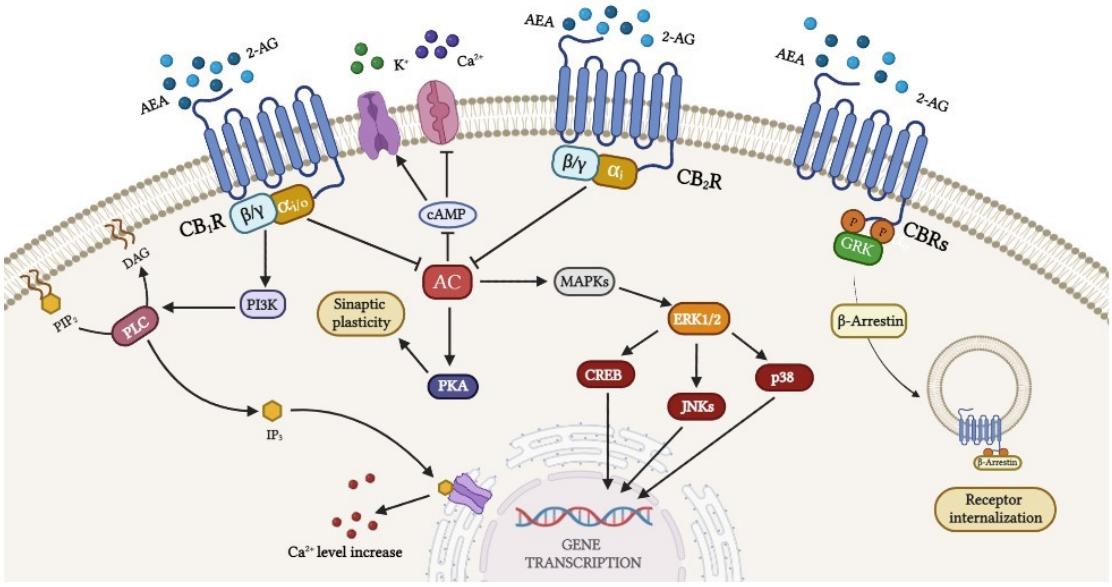

Figure 1.5 *Main CBRs signalling pathways. (figure created by author)*

1.1.3.2 Body distribution of cannabinoid receptors

CBRs differ from each other in terms of tissue distribution. CB_1R was first discovered in the CNS, where it is most abundant, inhibiting the release of several excitatory and inhibitory neurotransmitters. In particular, the human brain regions with highest level of CB_1R include olfactory bulb, hippocampus, basal ganglia, and cerebellum, where it modulates many physiological processes such as memory, cognition, motor coordination and pain. [22] Lower concentrations of CB_1R have been also found in cortex, amygdala, hypothalamus, thalamus and spinal cord. Previous studies suggested a presynaptic localization of CB_1R, mediating retrograde signalling of endocannabinoids, even if its presence in the postsynaptic terminals cannot be excluded. Moreover, functional studies showed a self-inhibition pathway in neocortical neurons, promoted by eCBs. CB_1R is not only distributed in the CNS, it is also expressed at lower levels in astrocytes, oligodendrocytes, microglia, neurons of the Peripheral Nervous System (PNS), gastro-intestinal mucosa including enteroendocrine cells, immune cells, liver, pancreas, cells of the cardiovascular system, adipose tissue, skeletal muscle, and bones. [11]

Initially, CB_2R was identified in macrophages and in the spleen. Further studies revealed its predominant expression in immune cells and lower concentration in other peripheral

tissue, including the cardiovascular system, GI tract, liver, adipose tissue, bone, and reproductive system. [11] At the beginning, reverse transcription quantitative real-time polymerase chain reaction (qRT-qPCR) and *in situ* hybridization (ISH) analysis did not detect CB_2R mRNA in the brain, [23] because of the low concentration of CB_2R mRNA under physiological conditions (about 100-300- fold lower than CB_1R mRNA in the brain). [24] Thus, CB_2R has been considered for a long time a peripheral receptor of the ECS, compared with CB_1R. Recently, more advanced techniques, such as the use of isoform-specific probes in RT-qPCR, RNAscope-ISH, fluorescence-activated cell sorting (FACS) and immunoblot and immunohistochemical (IHC) assays, have detected CB_2R in several areas of CNS including cortex, striatum, amygdala, brainstem, cerebellum, dopamine (DA) neurons of the ventral tegmental area (VTA) and microglial cells. [25] Despite the low expression of CB_2R mRNA in CNS, CB_2R is inducible under pathological conditions like addiction, anxiety, epilepsy, and neuroinflammation (this latter associated with several neurodegenerative diseases). CB_2R expression is upregulated in different brain areas, [26] and in microglia cells, where it play a key neuroprotective role, maintaining neuronal homeostasis and preventing neuroinflammatory disorders.

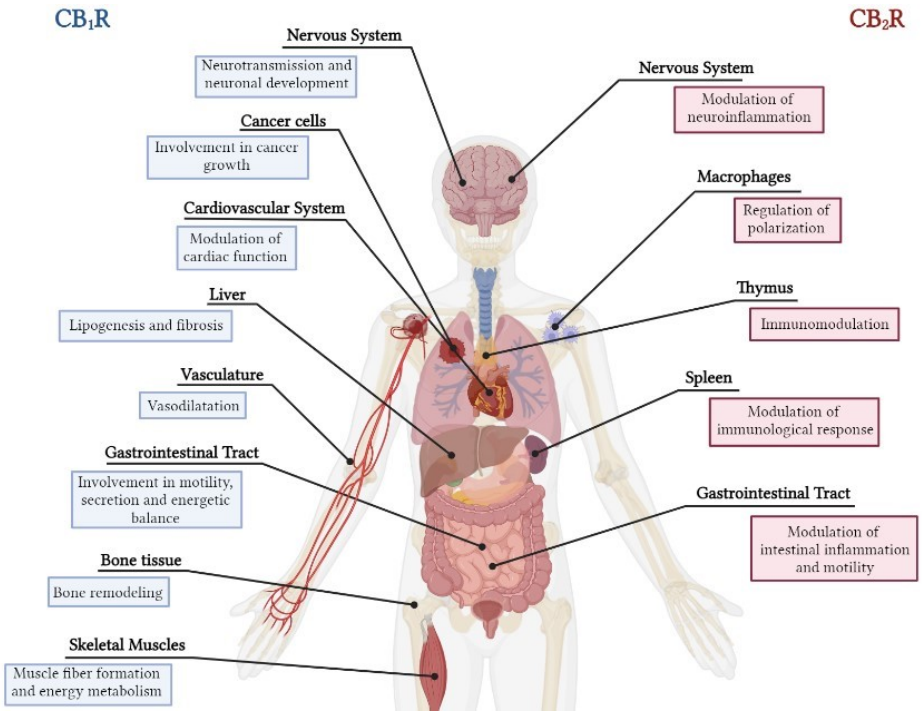

Figure 1.6. *Tissue distribution and involvement of CBRs. (figure created by author)*

1.1.3.3 CB_2 receptor and neurodegenerative diseases [25]

Following the discovery of the CB_2R in several regions of the brain, various studies highlighted its neuroprotective role in CNS due to the modulation of the neuronal excitability and the involvement of glia cells, as reported in *figure 1.7*. [25]

The activation of CB_2R through agonists and the consequent stimulation of $G\alpha_{i/o}$-mediated signalling cascade led to the reduction of neuronal excitability in a cell type-specific manner due to the inhibition of AC, but also modulation of MAP kinase pathway and activation of ERK. In addition, suppression of neuronal activity due to CB_2R stimulation involves other specific signalling mechanisms, including inwardly-rectifying potassium channels (GIRKs) in cortical neurons, [27] M-type K^+ channel (KCNQ7.4) function in VTA DA neurons, [28] Ca^{2+}-dependent chloride channels in pyramidal cells and in prefrontal cortical neurons due to inositol trisphosphate receptor (IP3R) activation and Na^+/ bicarbonate co-transporter in hippocampal CA3/CA2 pyramidal neurons. [29] [30]

Microglia cells play a crucial role in the development of CNS under physiological conditions, providing nutritional and structural support. They also represent the primary defence line of immune system for the brain and spinal cord and can be activated by any type of pathological event or change in brain homeostasis, including brain injury, infections and neurodegenerative disorders, [31] adopting two possible phenotypic variants: M1 and M2. [32] The neurotoxic M1 state (classical activation) is associated with release of several pro-inflammatory factors such as inducible nitric oxide synthase (NOS2)-derived nitric oxide (NO), prostanoids and interleukins (IL-1β, IL-18, and IL-6). On the other hand, the neuroprotective M2 state (alternative activation) is characterized by the release of anti-inflammatory factors, including nerve growth factor (NGF), IL-4 and IL-10. [33] [34] Under physiological conditions, the M1 state is triggered first from the M0 homeostatic state in order to eliminate a pathogen or restrain an injury. However, the shift from the classical to the alternative neuroprotective M2 state allows to damp the pro-inflammatory response, preventing neurotoxicity and chronic neuroinflammation which are strictly involved in the onset of neurodegenerative diseases.

Under pathological conditions, CB_2R expression in microglia cells increases and its activation through CB_2R agonists shift from M1 state to M2 neuroprotective and M0 homeostatic states, allowing the resolution of neuroinflammation. Furthermore, selective stimulation of CB_2R avoids the adverse psychotropic effects related to CB_1R activation. [35] In conclusion, CB_2R seems to be a more promising neuroprotective target than CB_1R, taking into account the lower expression of CB_2R in neurons of healthy brains and its inducibility under pathological conditions. In this context, CB_2R selective agonists could be potentially useful in the prevention and the treatment of neurodegenerative diseases with a neuroinflammatory background, including Parkinson's disease (PD) and Alzheimer's disease (AD). [25]

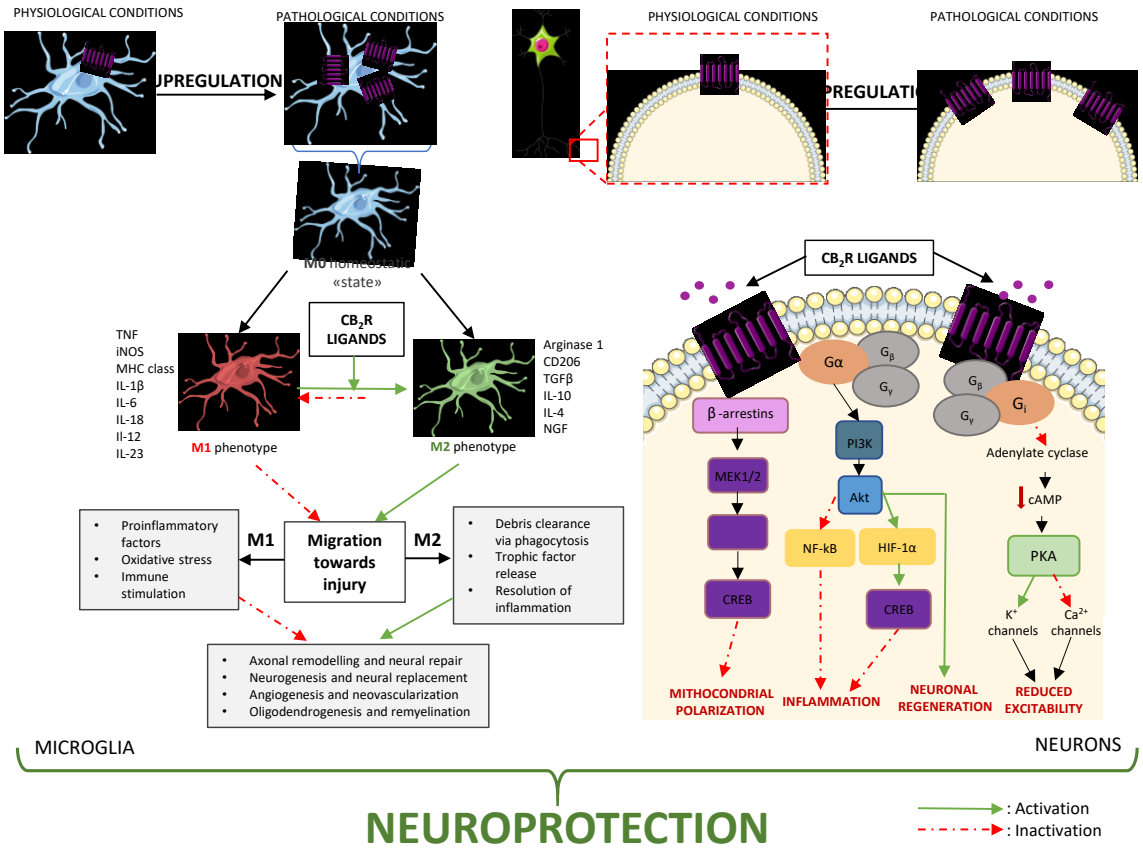

Figure 1.7 *Diagram summarizing brain CB2R involvement in neuroprotection.* [25]

1.1.4 Ligands of CB_2 receptor

Modulation of CB_2R has been correlated with a variety of physio-pathological processes. [36] In particular, regarding its involvement in neuroinflammation and in neurodegenerative diseases, [37] the development of CB_2R ligands has become more and more important in the last few years. In this paragraph the main non-selective and selective CB_2R ligands will be discussed, dividing them according to their chemical structure.

1.1.4.1 Δ^9-tetrahydrocannabinol derivatives

The Δ^9-tetrahydrocannabinol (Δ^9-THC, *figure 1.8*) is the best characterized compound of the classical cannabinoid class and it is considered the main psychoactive component of the *Cannabis Sativa*. This compound has similar affinities for both CBRs, but it behaves ad a partial agonist at CB_1Rs. [38] Structural modifications of its isomer Δ^8-THC (*figure 1.8*), a CB_1R agonist also present in the *Cannabis Sativa*, resulted in the development of synthetic derivatives. Among them, HU-210 (*figure 1.8*) displays higher affinity and potency for CB_1R and CB_2R compared with Δ^9-THC, which seems to be mainly caused by the insertion of the dimethylheptyl side chain. [22] The removal of a phenolic group from HU-210 to obtain JWH-051 (*figure 1.8*) does not significantly influence the affinity for CB_1R, but enhances CB_2R affinity and selectivity. Indeed, JWH-051 has stronger affinity for CB_2R, with a K_i in the low nanomolar range. [39] Further modifications of alkyl chain and the deletion of alcoholic group lead to compound JWH-133 (*figure 1.8*), a potent and selective CB_2R agonist (around 200 folds for CB_2R over CB_1R), with a K_i of 3.4 nM. [38]

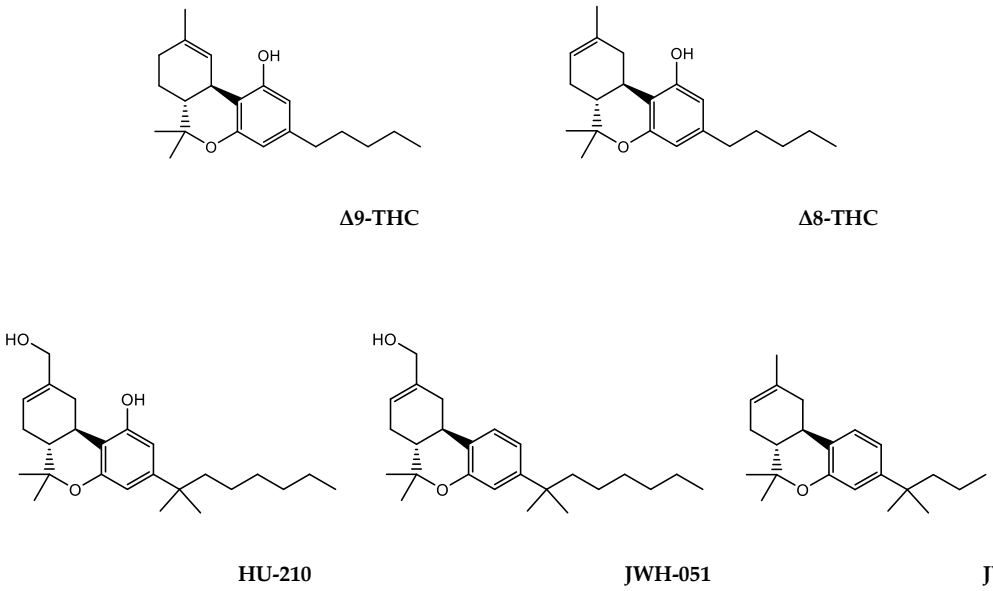

Figure 1.8. *Main Δ⁹-tetrahydrocannabinol derivatives.*

1.1.4.2 Bicyclic derivatives

Bicyclic derivatives differ from classical cannabinoids by the absence of the tetrahydropyran ring. The best known compound of this series is CP 55,940 (*figure 1.9*), a non-selective CBRs full agonist [40] widely used as a reference compound in biological evaluations. [41] In some instances, the removal of the tetrahydropyran ring, together with additional modifications, allowed for improved selectivity towards the CB_2R. In particular, HU-308 (*figure 1.9*) is distinguished by high affinity and selectivity for CB_2R (K_i = 22.7 ± 3.9 nM for CB_2R, K_i = > 10 mM for CB_1R). [42]

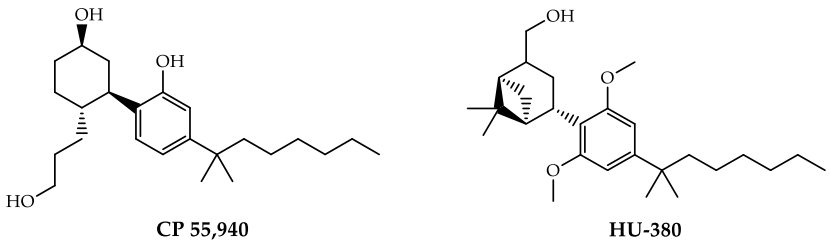

Figure 1.9 *Chemical structures of bicyclic compounds CP 55,940 and HU-380.*

1.1.4.3 Aminoalkylindoles

Derivatives belonging to this class have a distinctly different structure relative to those of the previously seen compounds. WIN 55212-2 (*figure 1.10*) is the best characteristized aminoalkylindole of this class, marked by high affinity for CBRs and a slight CB_2R selectivity. [43] The elimination of the morpholine ring, condensed with the aminoalkylindole scaffold, allowed to achieve compounds with high selectivity towards CB_2R. Among them JWH-015, AM 1241 and GW 405,833 (*figure 1.10*) are noteworthy, [25] turning out to have high affinity for CB_2R and combined low affinity for CB_1R. [44] [45] [46]

This class also includes derivatives with antagonist/inverse agonist activity towards CBRs. One of the most characteristic compound of this series is AM-630 (*figure 1.10*), originally proposed as a selective CB_2R antagonist [47] and later classified as a CB_2R inverse agonist. [48] [49] Additionally, BML-190 (*figure 1.10*), achieved from structural modification of AM-630, was originally described as a CB_2R agonist, [50] with a K_i value included in the nanomolar range and 50-fold selectivity over CB_1R. Later, the research group of *New D.C. et al.* demonstrated its inverse agonist properties. [51]

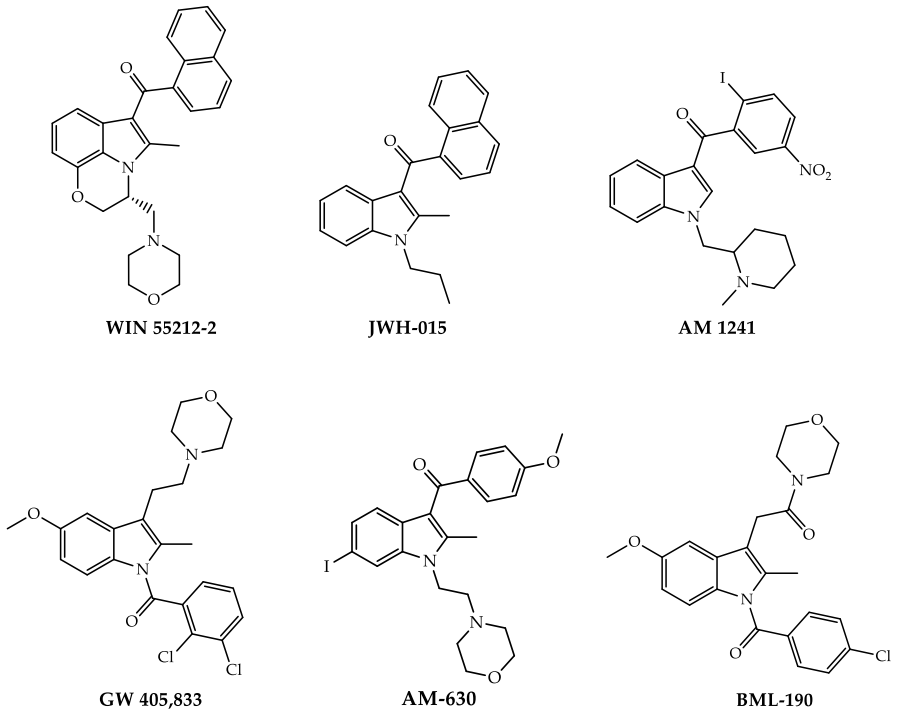

Figure 1.10 *Non selective and selective CB2R aminoalkylindoles.*

1.1.4.4 Diarylpyrazoles

SR144528 (*figure 1.11*) is the first potent, selective and orally active CB_2R antagonist developed, with sub-nanomolar affinity for CB_2R, largely used also in biological assays to reverse the effects of CB_2R agonists. [52] Moreover, it has been showed to display inverse agonist properties in transfected COS cells, stimulating adenylyl cyclase V and inhibiting adenylyl cyclase II in a temperature and dose-dependent manner. [53]

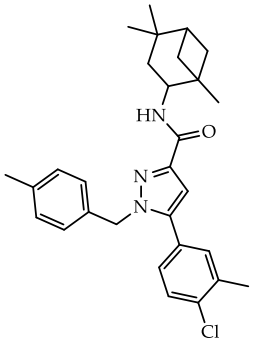

SR144528

Figure 1.11 *Structure of the first selective CB_2R antagonist/inverse agonist SR144528.*

1.1.4.5 Tri-aryl derivatives

The compounds belonging to this series combine aspects of two distinct cannabinoid series, the resorcinol derivatives and bicyclic HU-308 with the aim of achieving new and potent CB_2R ligands. Among them, SMM-189 (*figure 1.12*) is a selective and potent CB_2R inverse agonist [54] marked by high affinity for CB_2R [55] and able to behave also as a non-competitive antagonist at CB_2R against CP 55,940. [55]

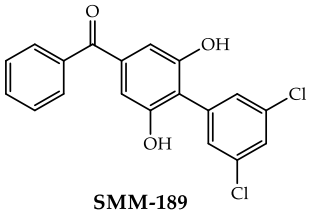

SMM-189

Figure 1.12 *Structure of SMM-189.*

1.1.4.6 Naphthyridin derivatives

In recent years, naphthyridin emerged as a promising and versatile scaffold for the development of novel CB_2R ligands. [56] Thus, various 1,8-naphthyridines resulted as potent and affine CB_2R agonists and showed high selectivity over CB_1R. [57] [58] [59] [60] Concerning the structure-activity relationships (SAR) reported in *figure 1.13*, substitution of the nitrogen in position 1 seems to be extremely important to improve affinity toward CB_2R, especially with bulky alkyl or aryl residues, as well as the insertion of carboxamide in position 3. Substitution of amide group is well tolerated: the 4-methylcyclohexyl represent the best option to improve both affinity and selectivity toward CB_2R and *cis* isomer show in general higher affinity for CB_2R than the *trans* isomer. [57] [60] At position 8 both a nitrogen and a carbon atom are tolerated, as well as the introduction of electron-donating groups, such as methyl and methoxy groups. The insertion of an electron-withdrawing group, including nitro, led instead to a loss of CB_2R selectivity. [61] Surprisingly, substitution of position 6 of the naphthyridine scaffold causes a functionality switch from agonist to antagonists/inverse agonists, [59] while contemporary substitution of positions 6 and 8 is not beneficial. [61]

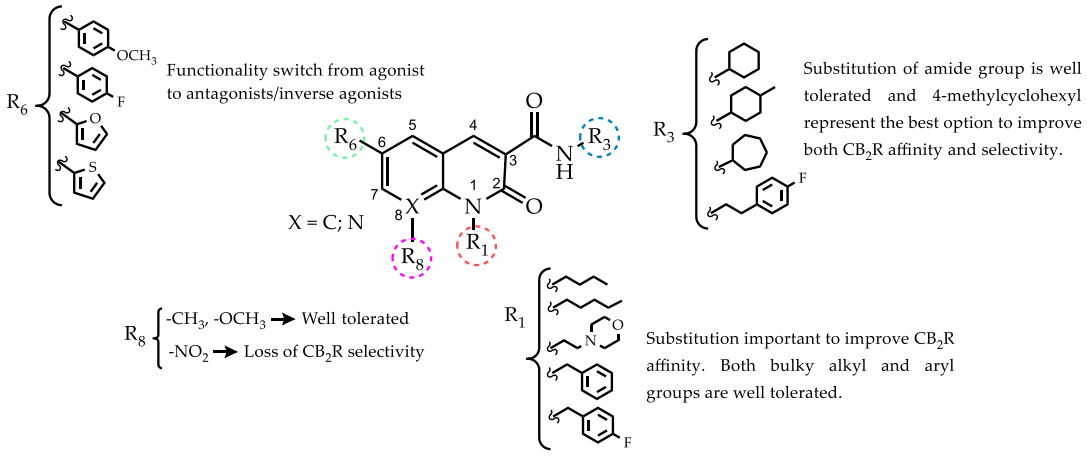

Figure 1.13 *SAR study of 1,8-naphthyridine derivatives.*

Compounds CB74 and CB91 (*figure 1.14*) has been tested in activated lymphocytes isolated from patients with Multiple sclerosis (MS) relative to healthy controls, to evaluate their immune-modulatory effects. All of them down-regulated TNF-α production, NF-κB phosphorylation and Akt and ERK expression, reducing also COX-2

activation. Additionally, they also inhibit some T-cell activation markers, including Cluster of Differentiation 54 (CD54) and CD69. [25]

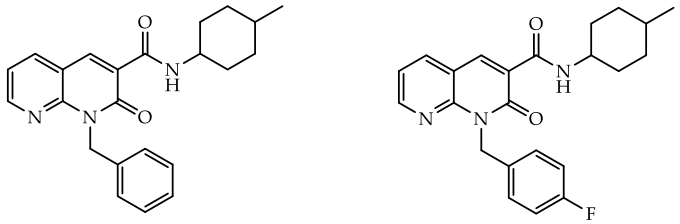

CB74 **CB91**

Figure 1.14 *Chemical structure of CB74 and CB91.*

1.1.4.7 CB_2R allosteric modulation

While an orthosteric ligand is able to interact with the orthosteric binding site of receptor, [62] allosteric modulators (AM) bind to a spatially and topologically distinct site, which is called allosteric site, [63] producing a change in the receptor conformation and therefore transferring this change to the orthosteric site and/or effective site. [62] This results in a modification of orthosteric ligand's binding affinity with a consequent positive or negative effect on cellular responses. [64]

Allosteric modulation could be useful to overcome some drawbacks of orthosteric modulation. First, AMs activate receptor signalling pathways only where the endogenous or orthosteric ligands are present, providing spatial and temporal signalling selectivity, especially in disorders where the endogenous ligand is produced "on demand". Secondly, the saturability of the signal avoids the risk of overdose: indeed, an increasing concentration of AM above the saturation threshold of allosteric binding site does not result in an increase of allosteric effects. [65] Furthermore, the aminoacidic sequences of allosteric sites are usually less conserved than orthosteric sites, offering an higher receptor subtype selectivity. [63] Finally, AMs induce and stabilize specific conformations of the orthosteric site, with the consequent activation or inhibition of different biased signalling by orthosteric ligands which involve certain signalling interactions rather than other. [65]

The presence of an allosteric binding pocket adjacent to the CB_2R orthosteric ligand-binding site was firstly proposed by the research group of *Feng Z. et al.* in 2014, building comparative CB_2R models based on the structural similar GPCRs. [66] Moreover, very recently, *Pandey P.* and co-workers characterized CB_2R allosteric sites using the complex of the CB_2 receptor with bound orthosteric agonist CP55,940, through different computational approaches. [67]

CB_2R allosteric modulators can be classified, according to their mechanisms of action, as positive allosteric modulators (PAMs), negative allosteric modulators (NAMs) or neutral allosteric ligands (NALs). PAM enhances the binding affinity and/or efficacy of orthosteric ligands (*figure 1.15*), whereas NAM decreases them (*figure 1.15*). NAL, instead, binds the allosteric binding site, competing also with PAM and NAM, but without having any effect on binding affinity and/or efficacy of orthosteric ligands (*figure 1.15*). [65] PAMs may also be characterized by intrinsic agonist properties, and in this case they are described as ago-PAMs. Finally, AMs can have a combined PAM-NAM activity, depending on the signalling output evaluated. [65]

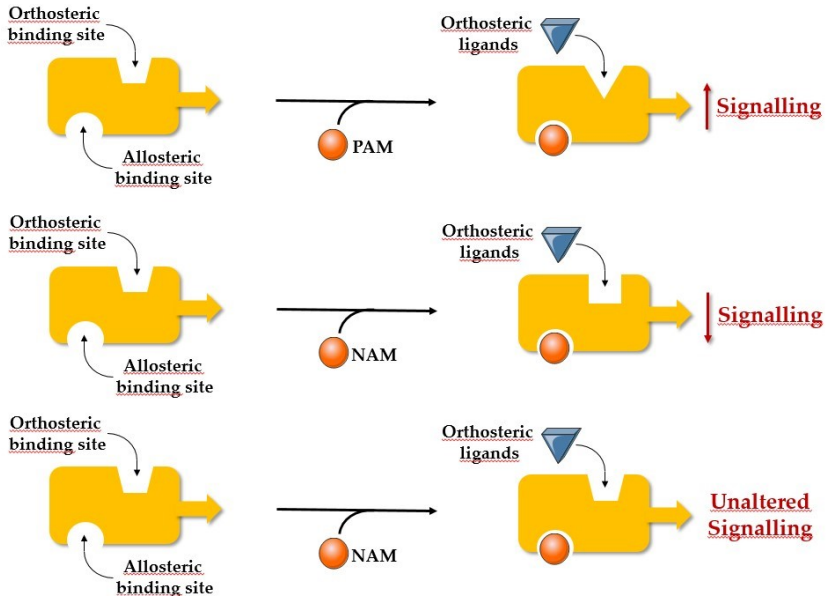

Figure 1.15 *General classification of AMs in PAM, NAM and NAL. (figure created by author)*

Even though several CB_1R AMs are known, to date the number of CB_2R AMs is very limited. Considering the natural compounds, the dodecapeptide Pepcan-12 (*figure 1.16*),

a CB_1R NAM, has recently reported also as a CB_2R PAM, enhancing the potency of CB_2R agonists, including 2-AG. [68]

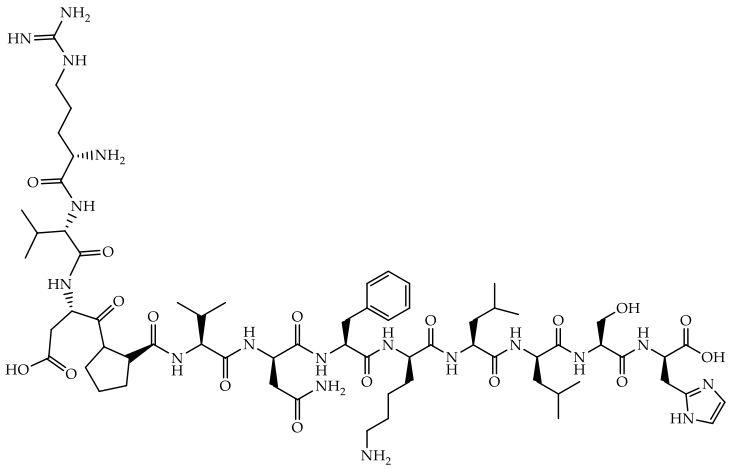

Figure 1.16 *CB_1R NAM and CB_2R PAM.*

However, the first synthetic CB_2R AM, developed by *Gado F. et al.*, is C2 (*figure 1.17*), which acts as CB_2R PAM in favour of CP55940 and 2-AG over AEA, without significantly alter the cellular responses arising from CB_1R orthosteric activation. [69]

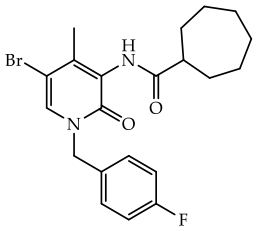

Figure 1.17 *The first CB_2R PAM.*

However, allosteric modulators are reliant upon the presence of the endogenous ligand and this could represent an important limitation for their efficacy, especially in disorders where receptor's inactivation is connected with a reduction of endogenous ligand's production.

1.2 GPR55 Receptor

Identified and cloned in 1999, [70] GPR55 receptor was initially included among the orphan receptors. Later, it was deorphanized and joined to the ECS, being actually proposed as *type-3* cannabinoid receptor (CB_3R), [71] even if its categorization is still being studied. Recent studies highlighted the involvement of GPR55 receptor in the modulation of several physio-pathological processes, [72] currently representing an innovative target in the treatment of various disorders, including neurodegenerative diseases. [73] [74]

1.2.1 Structure and pathways

GPR55 is a membrane-bound receptor which belongs to the rhodopsin-like seven-transmembrane G protein-coupled receptor (GPCR) superfamily. It is composed of 319 amino acids (*figure 1.18*) and exhibits the highest amino acid identity to GPR35 (27%), P2Y (29%), GPR23 (30%), and CXCR4 (26%) receptors. [70]

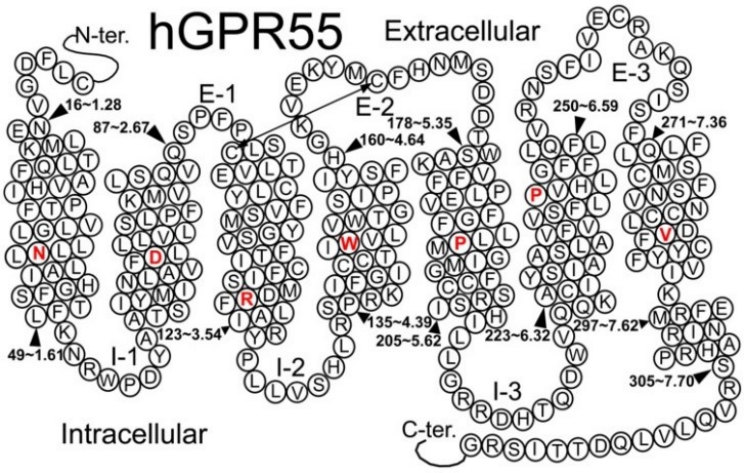

Figure 1.18 *Schematic representation of the GPR55 receptor.* [70]

GPR55 is a peculiar GPCR, since it does not bind classical G proteins, but only G_q and $G_{12,13}$ proteins, [75] [76] leading to the direct or indirect (through RhoA and ROCK pathways) activation of the phospholipase C (PLC) and to the increase of intracellular Ca^{2+}. [75] Moreover, RhoA stimulation causes the phosphorylation of ERK1/2, due to the

activation of Rac and cdc42, [71] which are also involved in the regulation of mitogen-activated protein kinase p38 and the release of the transcription activator factor ATF-2. [77] On the other hand, ERK1/2 cascade can also be activated directly by PLC and by protein-kinase MEK1/2. [78] All these pathways lead to the activation of several transcription factors including CREB, NF-κB and ATF-2, which play an essential role in regulating cellular processes.

Moreover, GPR55 stimulation by agonists causes receptor down-regulation due to the involvement of β-arrestin, [79] promoting its internalization into endosomes. The GPCR-associated sorting protein 1 (GASP-1) seems to be play a crucial role in the degradation of GPR55. Indeed, after forming a complex with GASP-1, GPR55 colocalizes with lysosomal markers LAMP 1/2, targeting the receptor to the degradative pathway. In the absence of GASP-1, it is rapidly recycled and expressed again on the plasmatic membrane. [80]

In addition, β-arrestin seems also to be capable of mediating G protein-independent signalling pathways by activating MAPK. [78]

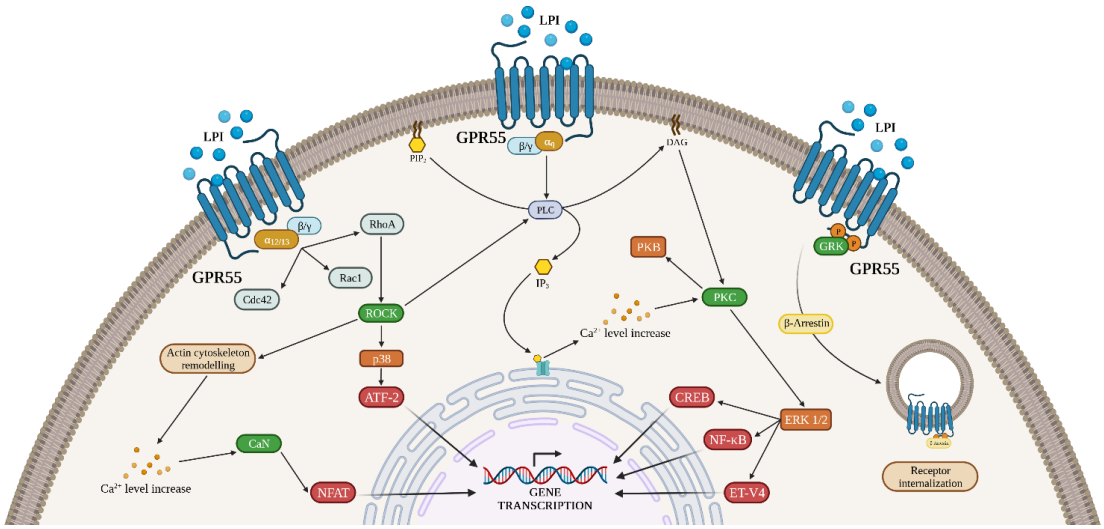

Figure 1.19 *Signalling pathways mediated by GPR55 receptor. (figure created by author)*

1.2.2 GPR55 endogenous ligands

1.2.2.1 LPI

To date, several studies classify the Lysophosphatidylinositol (LPI, *figure 1.20*) as the endogenous ligand of GPR55 receptor, increasing the release of intracellular Ca^{2+}, promoting the phosphorylation of ERK1/2, the activation of p38 mitogen protein kinase and GTPγS binding signals. [81] [82] [83] LPI is a subspecies of lysophospholipid, a glycerophospholipid that contains a glycerol backbone esterified with a single fatty acid and an inositol in its head group. [84] Although bioactive roles of phospholipids were highlighted for the first time more than thirty years ago, the discovery of LPI as endogenous ligand in 2007 was an important step forward in considering LPI not only as component of plasmatic membrane but also as bioactive lysophospholipid mediator. The main synthesis mechanism of LPI involve phospholipase A2 enzyme (PLA2) which hydrolyses the sn-2 ester position of phosphatidylinositol, leading to the production of LPI and arachidonic acid (*figure 1.20*).

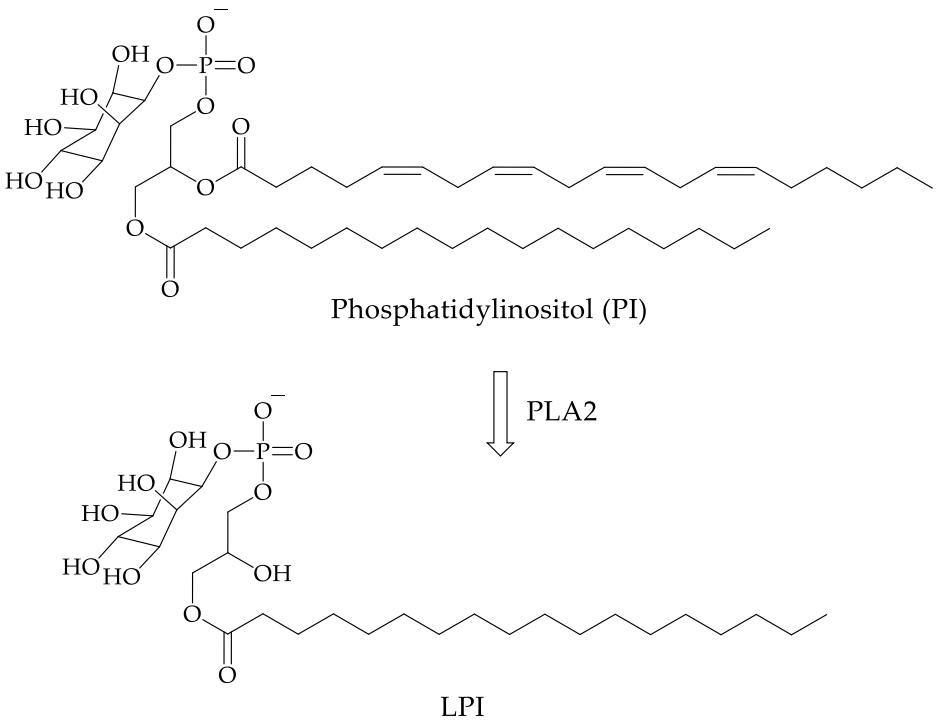

Figure 1.20 *Synthesis of LPI by PLA2.*

1.2.2.2 2-AGPI

To date, LPI is considered the endogenous ligand of GPR55 receptor. However, the complexity of the cellular downstream signalling pathways related to GPR55 activation led to the research of other endogenous ligands able to activate this receptor. 2-arachidonoylglycerolphosphoinositol (2-AGPI, *figure 1.22*) represents one of the most abundant LPI fatty acid species in rat brain and displays the highest potency and efficacy for GPR55 receptor compared with other molecular species identified in rat brain. Indeed, it induces the release of intracellular Ca^{2+} and the phosphorylation of ERK with EC_{50} value of 30 nM. [85] [86] Thus, it has been proposed as GPR55 endogenous ligand too, even if additional studies are required to corroborate this hypothesis.

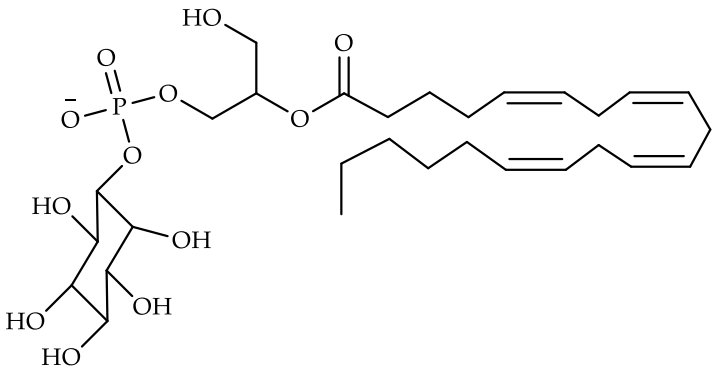

Figure 1.22 *Structure of 2-AGPI.*

1.2.2.3 NAGly

Recently, the N-arachidonoyl glycine (NAGly, *figure 1.23*) has been proposed as GPR55 endogenous agonist, inducing concentration dependent increases in Ca^{2+} mobilization and MAPK activity in triple hemagglutinin-tagged GPR55 stable Chinese Hamster cells (HAGPR55/CHO). These effects were both attenuated by a selective GPR55 antagonist, corroborating receptor mediated signalling. [87]

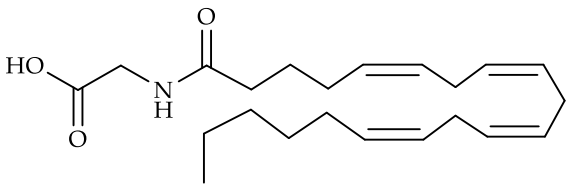

Figure 1.23 *Structure of NAGly.*

1.2.3 GPR55 as a putative CB_3R

As previously reported, classical cannabinoid receptors include CB_1R and CB_2R. However, the complexity of the ECS makes it difficult to define, leading to research of novel receptors, which could belong to this system. Among them, GPR55 is one of the most studied, being actually proposed as a putative CB_3R. [71] Indeed, several cannabinoids were found to interact with GPR55, including the partial CBRs agonist Δ^9-THC and its synthetic derivative HU-210, the nonselective CBRs full agonist CP55,940 and the CB_1R selective antagonist/inverse agonist Rimonabant (figure 2.13). [80] Additionally, GPR55 is also correlated to CBRs from a functional point of view, often regulating the same physio-pathological processes and sometimes forming heterodimers. [88] On the other hand, GPR55 features low ammino acid identity with both CB_1R (13.5 %) and CB_2R (14.4 %) [6] and it is coupled with different G proteins compared with CBR, leading to the activation of different signalling pathways. [88] Thus, to date its categorization is still being studied.

1.2.3.1 Altered signalling in GPR55-CBRs heteromers

As previously mentioned, several findings highlighted the existence of a crosstalk between GPR55 and cannabinoid receptors through heteromerization processes. Like other GPCRs, GPR55 can directly interact with other receptor types by forming a functional complex, which mediates distinct biological responses compared to the single entity. Indeed, heteromers often exhibit variations in the extent of coupling to the G protein, but also its type, leading to signalling alteration. [89]

GPR55 forms heterodimers with both CBRs in various tissue and organs, even if their precise role is not yet completely understood. GPR55 was found to be co-expressed with CB_1R in CNS and with CB_2R in immune tissues and in neoplastic cells. In human embryonic kidney (HEK293) cells which co-express both GPR55 and CB_1R, these two receptors alter each other's signalling properties. CB_1R specifically inhibits the effects mediated by GPR55, like ERK 1/2 phosphorylation and NFAT activation. At the same time, the presence of GPR55 enhances CB_1R signalling pathways, inducing the release of nuclear factor of activated T-cell activation. [90]

GPR55 is also co-expressed with CB_2R on the surface of HEK293 cells. At this level the inhibition of CB_2R through CB_2R antagonists seems to inhibit GPR55 response in presence of LPI or GPR55 agonists according to a cross-antagonism mechanism (*figure 1.24*). [91] Furthermore, another study conducted on the same cell line demonstrated that simultaneous activation of GPR55 and CB_2R inhibited the signalling pathway of the latter, thus indicating the existence of a negative cross-talk phenomenon, as reported in *Figure 2.6*. [92]

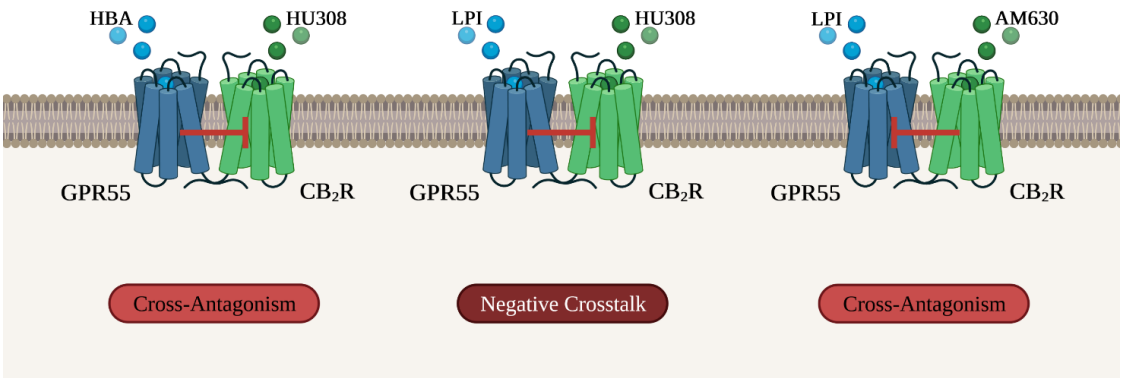

Figure 1.24 *Schematic representation of altered signalling in GPR55-CB_2R heteromers (HU308: CB_2R agonist, HBA: GPR55 antagonist, AM630: CB_2R antagonist). (figure created by author)*

1.2.4 GPR55 localization and therapeutic implications

GPR55 is both a central and a peripheral receptor (*figure 1.25*), taking part in the regulation of several physio-pathological processes.

It is expressed in organs and tissues which are involved in metabolism and in the maintenance of energetic homeostasis, including gastrointestinal tract, liver, adipose tissue, and pancreas; regulating food intake, intestinal motility and insulin release, being actually proposed as innovative target for the treatment of the type-2 diabetes. Indeed, GPR55 stimulation on insulin-secreting βcells leads to the increases of insulin secretion, reducing plasmatic levels of glucose. [78] Moreover, following long-term treatment with GPR55 agonists, glucose tolerance and insulin sensitivity are markedly improved, and total cholesterol and triacylglycerol are decreased. [93]

GPR55 is also expressed in bone tissue and several studies highlighted its involvement in the regulation of bone metabolism. Although its precise role has not been yet completely understood, its activation in osteoclasts appears to result in osteoclastogenesis, cell polarization and bone resorption. Thus, it has been proposed as innovative potential target in the treatment of osteoporosis and in bone loss associated with arthritis. [94]

It has also been found in mesenteric arterial endothelial cells and, to a lesser extent, in the heart. At this level, its activation through LPI induced vasodilation leads to the reduction of blood pressure. In addition, this receptor appears to be involved in the regulation of heart function and in particular the pathogenesis of heart failure. Indeed, GPR55 knock-out mice exhibited systolic dysfunction and ventricular remodelling in comparison with wild-type mice. [78]

Furthermore, this receptor has also been found in many cancer cells from very different origins (brain, breast, pancreas, hematopoietic) and its stimulation is correlated with an increase of the proliferation and migration rate of neoplastic cells, [95] essential for the tumour progression. [96] Additionally, GPR55 is over-expressed in different tumour tissues compared with their healthy counterpart, representing a novel potential biomarker in oncology associated with poor diagnosis. [6]

GPR55 receptor is also expressed in organs and tissue involved in the regulation of immune system response, including spleen, lymphocytes, and macrophages. At this level, its activation through GPR55 agonists seems to increase pro-inflammatory cytokines and cell cytotoxicity in monocytes and NK cells stimulated with LPS. [97] Similar results were obtained in GPR55 knockout mice too, corroborating the involvement of GPR55 receptor in inflammatory processes. [98]

Finally, significant expression of GPR55 was detected in kidney and adrenal glands, bladder, [72] thymus, [77] uterus [72] and placenta, [93] but its role has not been yet understood.

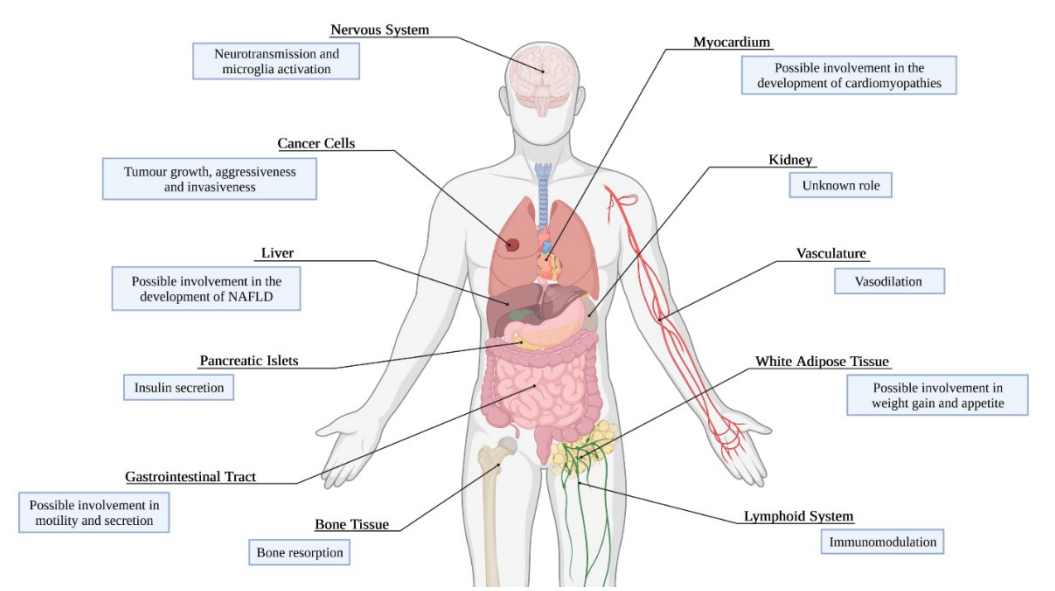

Figure 1.25 *Localization of GPR55 receptor in human body and therapeutic involvement. (figure created by author)*

In the SNC, GPR55 is expressed in several areas, including hippocampus, putamen, bone marrow striatum and thalamic nuclei, [6] but also sub-thalamic nucleus, substantia nigra and cortex, as reported in *figure 1.26*. [99] For this reason, it could be involved in the regulation of several physio-pathological processes, such as food intake, memory, cognitive functions, movements, motor coordination, [88] anxiety modulation and pain. [78] In these areas, GPR55 is less expressed than CB_1R, except for hippocampus, striatum and brain stem, where the distribution of these two receptors is comparable. [6] However, GPR55 is mostly expressed on microglia cells, [99] which play a key role in maintaining neuronal homeostasis and in regulating neuroinflammatory response. [100]

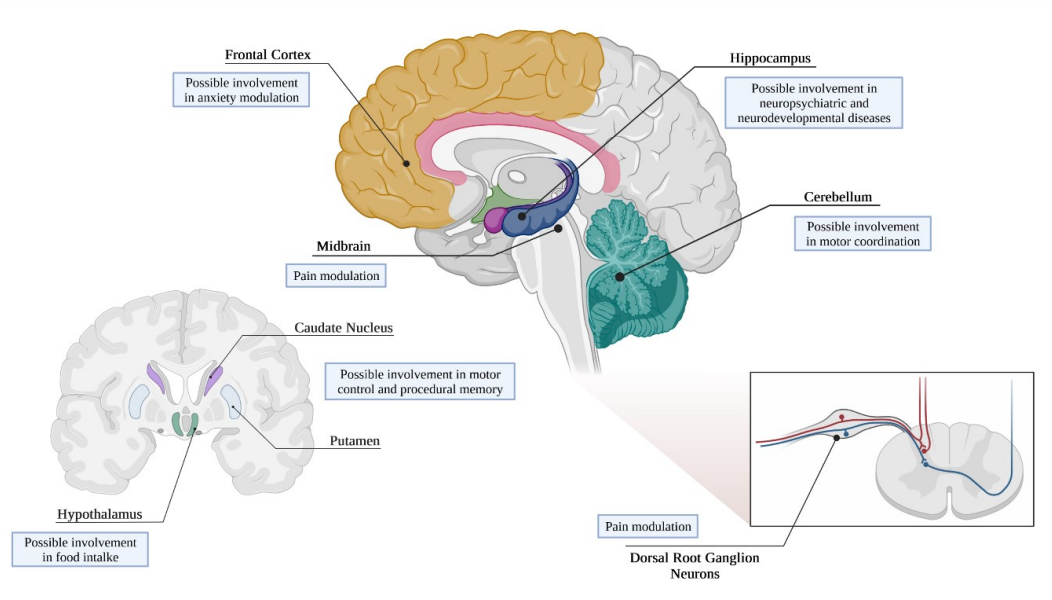

Figure 1.26 *GPR55 localization in CNS. (figure created by author)*

It is not clear if GPR55 is presynaptic and/or postsynaptic receptor in the CNS. In the hippocampus its stimulation seems to be correlated with an increase of glutamate release from intracellular vesicles, suggesting a main presynaptic expression of this receptor. This effect could be also correlated with an increase of intracellular Ca^{2+} release as well as an inhibition of K^{+} flow, due to stimulation through LPI. All these data suggest that GPR55 could exert inhibitory effects on neuronal activity. [88]

1.2.5 GPR55 and neurodegenerative diseases

As previously reported, neurodegenerative disorders, including PD and AD, provide a progressive loss of specific neuron population, leading to the development of several impairments in cognitive function, movement and memory. Despite specific pathological triggers, all these disorders are characterized by common molecular mechanisms, including microglia-mediated neuroinflammation, oxidative stress and mitochondrial dysfunctions. [101] [102]

GPR55 is mainly expressed in CNS, in particular on microglia cells, which plays a key role in maintaining neuronal homeostasis and in regulating neuroinflammatory response. As previously reported, long-term stimulation of microglia cells prevents the

resolution of neuroinflammation, resulting in the development of multiple neurodegenerative pathways. For this reason, targets implicated in the modulation of microglia activation could provide new therapeutic strategies in the treatment of neurodegenerative diseases, such as PD and AD.

Several studies highlighted the involvement of GPR55 in the modulation of microglia-mediated neuroinflammation, even if its precise role has not been yet completely understood. In an *in vitro* model of rat organotypic hippocampal slice cultures (OHSC), LPI exerted neuroprotective effects, reducing the number of activated microglia after NMDA (50 μM) induced lesions. [103] In addition, neural stem cells (NSCs) exposed to IL-1β showed a reduction of neural damage and a downregulation of pro-inflammatory cytokines expression following the treatment with the GPR55 selective agonist O-1602. [74] GPR55 knock-out mice maintained normal synaptic transmission and short-term as well as long-term synaptic plasticity, showing at the same time impaired movement coordination. [104] Moreover, in an *in vivo* mouse model of PD striatal expression of GPR55 receptor was downregulated and the treatment with abn-CBD (GPR55 agonist) prevented MPTPp induced motor impairment by protecting dopaminergic cell bodies. [99]

Furthermore, it has been recently observed that GPR55 antagonists/inverse agonists featuring a coumarin-based scaffold significantly inhibited the release of PGE_2 in primary microglia, which may partially dependent on reduced protein synthesis of mPGES-1 and COX-2. [73]

All these data suggest that the modulation of GPR55 receptor could represent a new and interesting therapeutic strategy for the treatment of neurodegenerative disorders with neuroinflammatory background.

1.2.6 Targeting GPR55 receptor

As previously reported, GPR55 is involved in the regulation of several physiological and pathological processes. In this context, potent and selective GPR55 ligands could represent potential tool compounds to validate this receptor as pharmacological target

and to provide important information about structural requirements for the interaction with GPR55 binding site.

The number of GPR55 ligands is rather limited. Moreover, they are structurally heterogeneous and in general poorly selective, modulating other targets, including CBRs. In addition, their biochemical properties are strictly affected by the functional assay employed, making it difficult to classify them according to their activities. These discrepancies depend on the intrinsic properties of this receptor, including the presence of different receptor active states, heteromerization processes, allosteric phenomena and the agonist functional selectivity, also known as biased agonism, which indicates the ability of a receptor to activate different downstream signalling pathways depending on the binding molecule. [6] [78]

Most of the available data about GPR55 ligands have been obtained through functional assays in transfected cells expressing GPR55, by evaluating the ability of compounds to induce intracellular Ca^{2+} elevation, ERK phosphorylation, β-arrestin recruitment, receptor internalization, activation of the Rho small GTPase proteins (i.e., RhoA, Rac1 and Cdc42), or binding of [^{35}S]GTPγS. [78] [6]

1.2.6.1 LPI and derivatives

As previously reported, LPIs, and particularly 2-AGPI, are nowadays widely recognized as the endogenous ligands for GPR55. Recently, several derivatives of LPI have been synthesized to identify the chemical groups involved in the interaction with the receptor. In particular, lysophosphatidyl-β-D-glucoside (*figure 1.27*) activated sensory neuron axons through GPR55 activation while its galactose analogue (*figure 1.27*) was inactive. Moreover, starting from a glucosylamine as precursor, it was obtained a squaryldiamide (SDA) which was linked to amino glycerol derivatives with the aim of identifying novel LPI derivatives. Among them, *sn-2* arachidonylated and *O*-benzyl-substituted analogues (*figure 1.27*) resulted to be GPR55 agonists. [105]

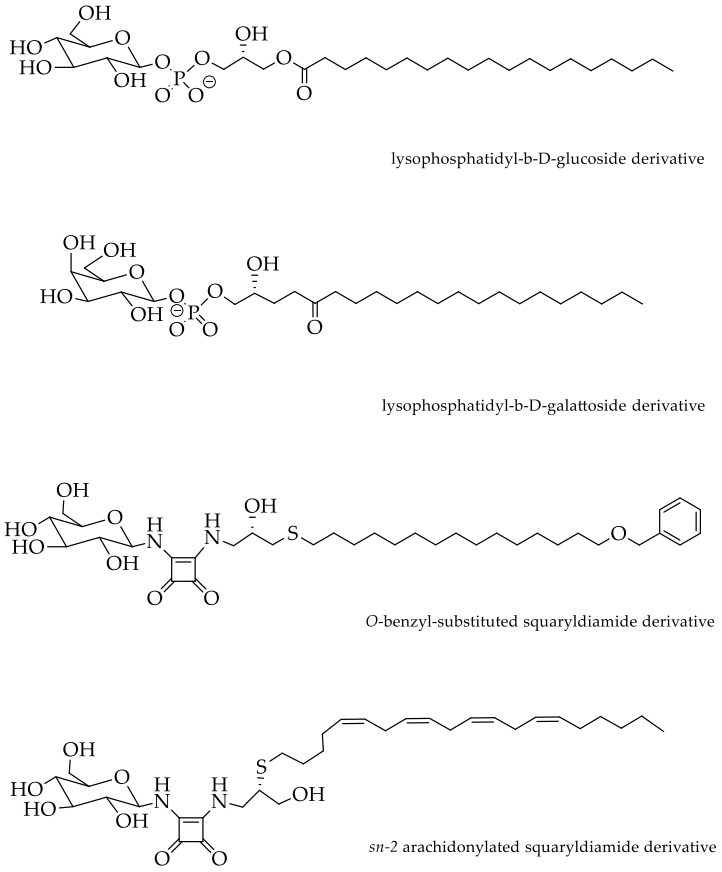

Figure 1.27 *Synthetic derivatives of LPI.*

1.2.6.2 Cannabinoid ligands of GPR55 receptor

In recent years, GPR55 has been related to the ECS, being actually proposed as putative CB_3R. For this reason, the research of potential GPR55 modulators began from cannabinoids. As expected, several cannabinoid ligands were found to be able to bind this receptor, showing sometimes conflicting results. [72]

1.2.6.2.1 Eicosanoid derivatives

Endocannabinoids are deemed for all intents the endogenous ligands of CBRs. However, some of them also modulate GPR55. AEA and 2-AG, the first discovered and best-characterized endogenous ligands of CBRs, seems to act as GPR55 agonists. In particular, AEA stimulated GTPγS binding to GPR55 in HEK-293 transfected cells in the nanomolar range [76] and caused Ca^{2+} mobilization in a micromolar range, [106] [76] even if it did not affect ERK phosphorylation and receptor internalization mediated by β-arrestin. [76]

[82] [107] On the other hand, 2-AG showed agonist properties in the GTPγS binding assay but it seems not to induce the increase of intracellular Ca^{2+}. Additionally, 2-AG did not stimulate ERK phosphorylation and receptor internalization, as well as AEA. [22] This could depend on the different position of LPI and 2-AGP in the in the lipid bilayer, comparing with AEA and 2-AG. Indeed, the lipid derivatives are located higher in the bilayer allowing easier solvation than AEA and 2-AG. [6]

Furthermore, noladin ether, virodhamine, palmitoylethanolamide (PEA, *figure 1.28*) and oleoylethanolamide (OEA, *figure 2.10*) are able to stimulate GTPγS binding, with EC_{50} values of 10, 4, 12 and 440 nM, respectively. [6] In addition, virodhamine is a GPR55 partial agonist in the β-arrestin recruitment assay. [108]

Figure 1.28 *Eicosanoid derivatives which act as GPR55 agonists.*

1.2.6.2.2 Δ⁹-tetrahydrocannabinol and derivatives

Δ⁹-THC, major psychoactive component of the *Cannabis Sativa* and partial agonist of CBRs, is also able to activate GPR55, promoting GTPγS binding with an EC_{50} value of 4 nM, [76] stimulating RhoA protein and increasing Ca^{2+} release. [75] At the same time, it seems not to affect both p-ERK1/2 [81] and β-arrestin activation. [82] Similarly, the potent CB_1/CB_2 receptor agonists HU-210 and CP-55940, synthetic derivatives of Δ⁹-THC, were found to activate GPR55, inducing [^{35}S]GTPγS binding, with EC_{50} values of 26 and 5 nM, respectively. [76] Yet, while no response has been obtained in other assays for the former compound, the latter has been reported to antagonize LPI-mediated effects. [81] [79] [78] Lastly, Tetrahydrocannanivarin (Δ⁹-THCV, *figure 1.29*), a non-psychoactive molecule deriving from THC degradation, did not show any activity towards GPR55, whereas its synthetic analogue JWH-133 turned out to be an inverse agonist by reducing basal phosphorylated ERK levels. [76] [109]

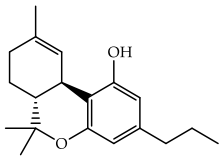

Δ9-THCV

Figure 1.29 *Structure of Δ9-THCV.*

1.2.6.2.3 Cannabidiol and derivatives

Cannabidiol (CBD, *figure 1.30*) is the major non-psychoactive component of *Cannabis Sativa* and it was approved by the Food and Drug Administration (FDA) in 2018 and by the European Medicines Agency (EMA) in 2019 with the trade name of Epidiolex for the treatment of two forms of childhood treatment-resistant epilepsy. [110] [111] Even if its mechanism of action has not been yet completely understood, [6] one of the most likely explanation for its antiepileptic properties seems to involve the antagonism toward GPR55 receptor. [112] Indeed, CBD prevents both GTPγS binding and RhoA stimulation without affecting β-arrestin activation and Ca^{2+} recruitment. [76] [113] Additionally, it proved to be an inhibitor of LPI with a percentage inhibition of 32% (at concentration of 3 μM), as well as the cannabidivarin (CBDV, *figure 1.30*), *n*-propyl analogue of CBD, which showed a percentage inhibition of 56% (at concentration of 1 μM). [109] In contrast to CBD and CBDV, abnormal Cannabidiol (abn-CBD, *figure 1.30*), a positional isomer of CBD, and O-1602 (*figure 1.30*), a synthetic isomer of CBD, are selective GPR55 agonists that induce GPR55-dependent GTPγS activity with EC_{50} values included in the micromolar and nanomolar range, respectively. [76] [114]

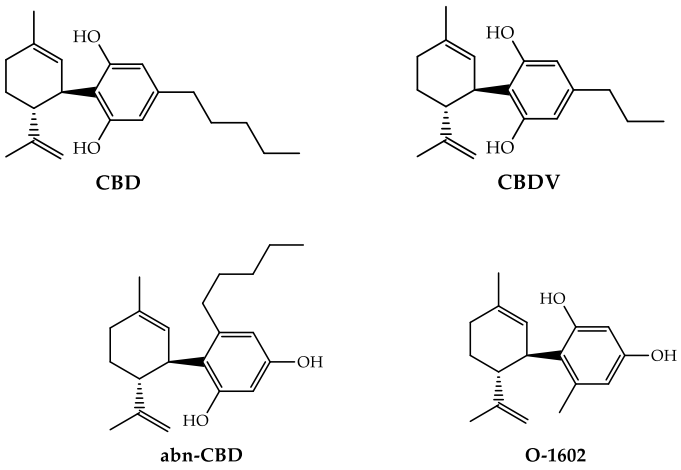

Figure 1.30 *CBD and derivatives.*

1.2.6.2.4 Diarylpyrazoles

Rimonabant (or SR141716A, *figure 1.31*), is the most representative compound of diarylpyrazole class and the first developed CB_1R antagonist. Beside its CB_1R antagonist/inverse agonist properties, it also modulates GPR55, inducing β-arrestin trafficking [82] and internalization, [79] stimulating Ca^{2+} release, activating ERK1/2, MAPK, and CREB transcription factor. [79] [109] Moreover, AM251 and AM281 (*figure 1.31*), CB_1R inverse agonists structurally related to SR141716, behaved as GPR55 agonists in different biochemical experiments, although the latter appeared to possess a negligible activity compared to the other. [79] [82] [109] [107]

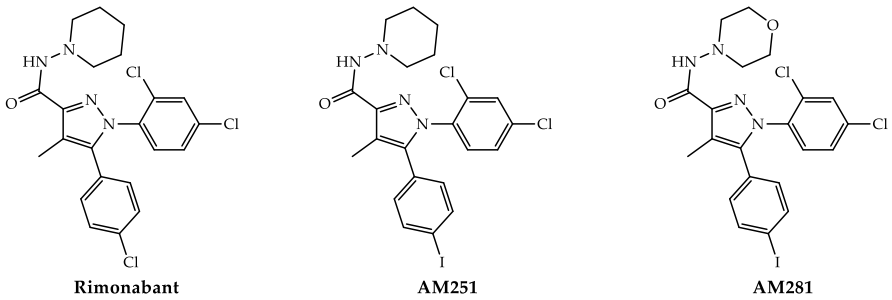

Figure 1.31 *GPR55Rs ligands belonging to arylpyrazole class.*

Remarkably, AM251 and AM-281 were found not only to activate GPR55 by themselves, but also to prevent the LPI-mediated ERK phosphorylation. This result suggests that there might be two topographically distinct binding sites on GPR55, an orthosteric binding site that associates with LPI and an allosteric binding site. In this contest,

arylpyrazoles may represent allosteric inhibitors or even bitopic ligands of GPR55 receptors, interacting with both the orthosteric site (as agonists) and the allosteric site (as negative modulators), as reported in *figure 1.32*. [109]

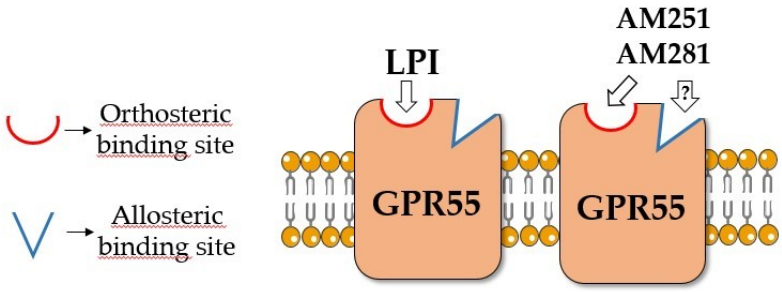

Figure 1.32 *Possible pharmacological mechanism of AM251 and AM281 for the modulation of GPR55 compared with the endogenous ligand LPI. (figure created by author)*

1.2.6.2.5 Aminoalkylindoles

The best characterized compound of this class is WIN 55212-2, a CBRs agonist with a slight selectivity toward CB_2R, as previously reported. [43] Even if it did not display any activity towards GPR55 receptors, [76] [75] its structural analogue JWH-015, a CB_2R selective agonist, shown to act as GPR55 agonist in [^{35}S]GTPγS binding assay as well as in the calcium mobilization assay, with an EC_{50} value in the nanomolar range and in the micromolar range, respectively. [71] Moreover, the partial CB_2R agonist GW-405833 not only showed to be a GPR55 partial agonist on its own in ERK phosphorylation assay, but also a positive allosteric modulator, enhancing LPI-mediated signalling. [109]

1.2.6.2.6 Cumarines

The coumarine scaffold showed high potential and versatility in the development of potent CBRs modulators. In particular, the 7-alkyl-3-benzylcoumarin derivatives showed to be modulators of CB_1R or CB_2R or both receptor subtypes, with high affinity and potency. [115] Since they share some structural features with Δ^9-THCV and CBDV, a possible activity towards GPR55 has been investigated in β-arrestin assay. Remarkably, data showed that these compounds can interact either as an antagonist or inverse agonist, with EC_{50} values in the sub-micromolar range. [116]

The SAR of the benzylcoumarin derivatives are summarized in *Figure 1.33*. The substitution of the 5-position with small groups appears to be essential for GPR55 affinity and activity, and, among various substituents, methoxyl or hydroxyl groups gave the best results in terms of potency. Both small groups and bulkier aliphatic chains are well tolerated at the 7-position. The sidechain length seems also to influence the affinity of these compounds towards cannabinoid receptors. In fact, compounds with either no or small substituents were in fact found to interact almost selectively as GPR55 antagonists, especially when combined with a methyl group at position 8. On the other hand, large and branched aliphatic residues resulted in an increased affinity towards cannabinoid receptors.

As for the 6-position, it can remain unsubstituted, but the insertion of small groups is tolerated when combined with small residue in other positions. Lastly, both *ortho*-methoxy- and *ortho*-hydroxy-substituted benzyl group result to be the best substituent at position 3 of the central scaffold, since they provided a high degree of potency. [116]

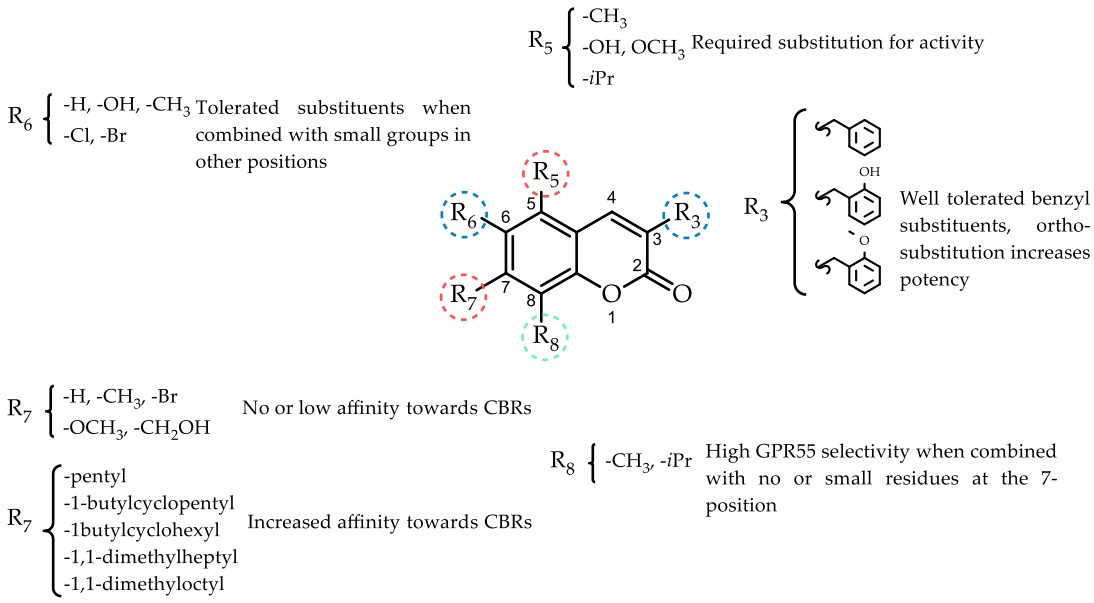

Figure 1.33 *Summary of SAR study related to 7-alkyl-3-benzylcoumarin derivatives.* [116]

Among them, compounds KIT-3, KIT-17 and KIT-21 (*figure 1.34*) were tested in primary rat microglial cells activated by LPS and displayed neuroprotective effects, blocking the inflammatory cascade. [73]

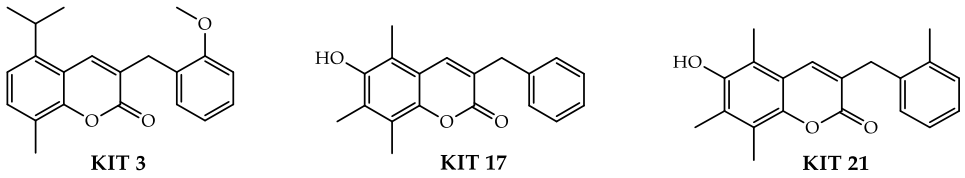

Figure 1.34 *Structures of the above-described benzylcoumarin derivatives.*

1.2.6.2.7 Magnolol derivatives

Magnolol (*figure 1.35*) is the major bioactive compound of *Magnolia Officinalis*, [117] and is a partial agonist of both CB_1R and CB_2R, [118] but no activity is detected towards GPR55. [119] However, its main metabolite tetrahydromagnolol (*figure 1.35*) is a potent peripheral CB_2R agonist, which also displayed weak antagonist properties towards GPR55 receptors in β-arrestin assay with an EC_{50} value included in the low micromolar range, being used as a lead compound for a SAR study. [119] As a result, the methylation of one of the hydroxyl groups led to an increase in the antagonist activity, and particularly, 5'-hexyl-2'-methoxy-5-propyl-[1,1'-biphenyl]-2-ol (*figure 1.35*), resulted as the most potent compound of this series. [120]

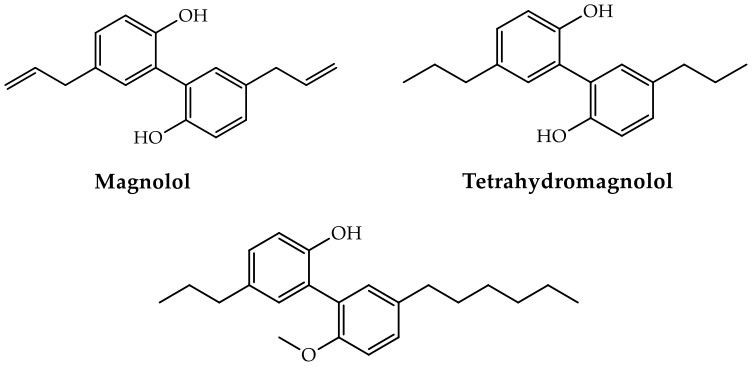

Figure 1.35 *Structure of Magnolol and its analogues.*

1.2.6.3 Non cannabinoid ligands of GPR55 receptor

The need to obtain selective and potent GPR55 ligands led to the investigation of novel molecular scaffolds. A collaborative project between individual laboratories and the Sandford-Burnham screening centre of the Molecular Libraries Probe Production Centre Network (MLPCN), consisting in a high-throughput screening of a library of compounds and consequent SAR studies, allowed the discovery of novel potent and sometimes selective GPR55 modulators. [121] [122] Their activity was assessed via the β-arrestin assay in U2OS cells permanently expressing a hemagglutinin antigen-tagged (HA)-GPR55E and βarr2-green fluorescent protein (GFP). [82] Among them, the phenylpiperazine CID 2440433, the tricyclic triazoloquinoline CID 1374043 and the morpholinosulfonylphenylamide CID 15945391, reported in *figure 1.36*, were identified as agonists with sub-micromolar potencies. [121]

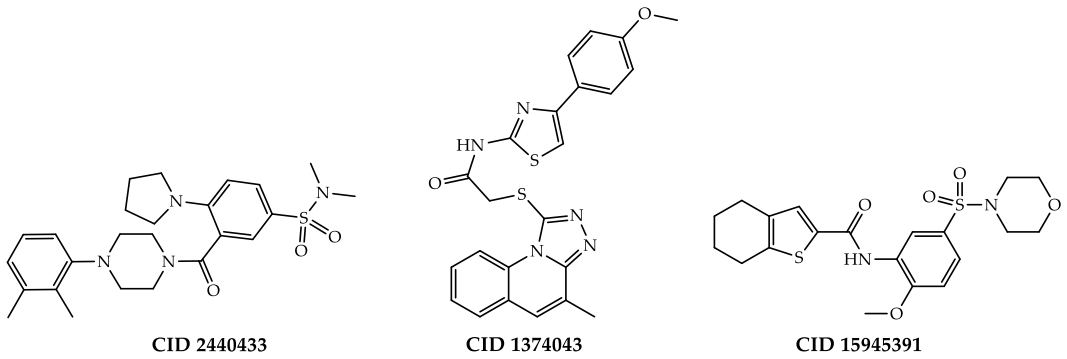

Figure 1.36 *Novel GPR55 agonists.*

Furthermore, the screening of a 5,000 compound set performed at GlaxoSmithKline using yeast *Saccharomyces Cerevisiae* and in HEK293 cells identified 1-benzoyl-4-phenylpiperazine as a novel chemotype for GPR55 agonism, and among these, GSK575594A and GSK494581A (*Figure 1.37*) were the most interesting ones. These benzoylpyperazine were originally identified and patented as inhibitors of the glycine transporter subtype 1 (GlyT1). However, both compounds showed higher affinity for GPR55R, compared with GlyT1. In particular, GSK575594A appeared to be the most selective ligand with approximately 60-fold selectivity for GPR55R over GlyT1, whereas GSK494581A the most potent one (EC_{50} ~ 0.16 μM). [123]

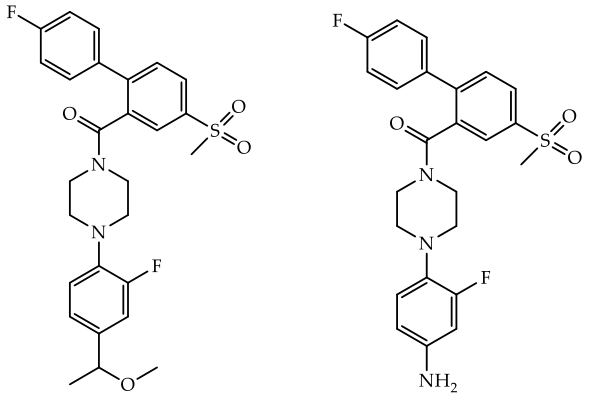

Figure 1.37 *Benzoylpyperazines initially patented as inhibitors of GlyT1.*

As previously reported, the high-throughput screening (HTS) provided novel GPR55 modulators, including three GPR55 selective antagonists, the piperidinyloxadiazolone CID 23612552, the thienopyrimidine CID 1434953 and the quinoline aryl sulfonamide CID 1261822, reported in *figure 1.38*. [122] Even in this case, the activity of these compounds was assessed via β-arrestin assays in recombinant U2OS cells. Moreover, in 2013 the research group of *Kargl J. et al.* identified CID 16020046 (*figure 1.38*) as a GPR55 antagonist too. Indeed, it showed potent and selective antagonist activity, inhibiting LPI-mediated Ca^{2+} release, extracellular signal-regulated kinases activation and GPR55 internalization in HEK293 cells. [124]

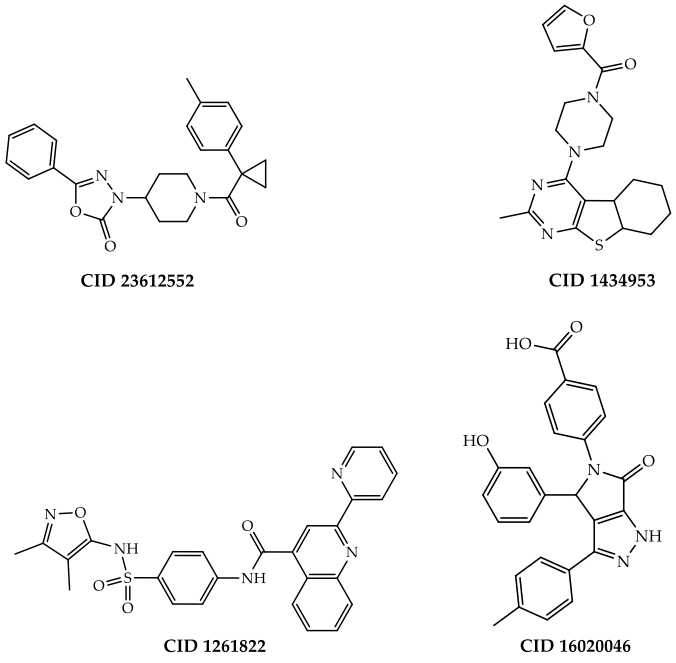

Figure 1.38 *Novel GPR55 antagonists.*

Recently, a derivative of the short-acting β_2-adrenergic fenoterol, (R,R')-4'-Methoxy-1-naphthylfenoterol (MNF, *figure 1.39*), was found to block GPR55 internalization and ERK1/2 phosphorylation promoted by O-1602 and AM251. Furthermore, MNF provides changes in cellular morphology and cell migration induced by GPR55 agonists, highlighting a therapeutic implication of GPR55 receptor in cancer disease. [125]

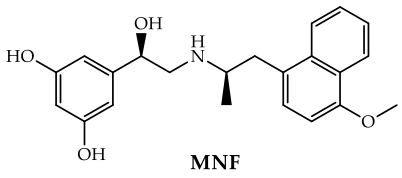

MNF

Figure 1.39 *(R,R')-4'-Methoxy-1-naphthylfenoterol (MNF).*

2. Aim of the thesis

As described above, neurodegenerative diseases cause a progressive loss of specific neuron populations, with the consequent development of several impairments in cognitive functions, movement and memory. In particular, PD lead to the development of motor symptoms, such as tremors, bradykinesia and muscle stiffness, as well as non-motor manifestations, including depression, anxiety, sleep disturbance and dementia, due to slow destruction of dopaminergic neurons in the nigrostriatal pathway. [126] On the other hand, AD provided a progressive cognitive decline and a loss of volume in the cerebral cortex (e.g., hippocampus) and in some subcortical regions, with the consequent development of neurological manifestations (e.g., short-term memory loss, spatial disorientation, language impairment, mood swings, personality changes). [127] Despite the specific pathological triggers, microglia-mediated neuroinflammation has been identified as a common pathological process of neurodegenerative disorders and several lines of evidence highlight the involvement of the cannabinoid receptors in the modulation of neuroinflammatory processes. In particular, CB_2R is mostly expressed in immune cells and tissues but it has also been detected in microglia cells, especially under neuroinflammatory conditions and its activation through CB_2R agonists shifts the microglia from the M1 neurodegenerative state to the M2 neuroprotective state, promoting the resolution of the neuroinflammation. [25] Recently, GPR55 receptor has emerged as an innovative therapeutic target for the treatment of neurodegenerative diseases with a neuroinflammatory background. GPR55 is a GPCR initially included among the orphan receptors and later deorphanized, when LPI was identified as its endogenous ligand. It has also been correlated with the ECS, being proposed as CB_3R, even if its categorization is still being studied. It is located both in the CNS and in the peripheral tissues, taking part in the regulation of various physiological processes. However, its highest expression is in microglia cells and several studies highlighted its involvement in the regulation of microglia-mediated neuroinflammation. Although the molecular mechanism has not been yet completely elucidated, recent data have highlighted a neuroprotective effect following GPR55 activation in neural stem cells [74] and in an *in vitro* model of rat organotypic hippocampal slice cultures. [103] Moreover,

in an *in vivo* mouse model of PD the treatment with abn-CBD (GPR55 agonist) prevented MPTPp induced motor impairment by protecting dopaminergic cell bodies. [99] Another recent study reported an anti-neuroinflammatory effect produced by GPR55 antagonists/inverse agonists [116] in LPS-activated primary microglial cells. [73] To date, there are only a limited number of GPR55 ligands reported in literature and most of them are poorly selective, modulating other targets, including CBRs. In addition, the lack of a crystal structure for GPR55 and the general inconsistency in pharmacological data of the few ligands available have long hampered the research in this field, increasing at the same time the scientific interest.

Thus, in the framework of the development of novel molecules useful in neurodegenerative disorders, my PhD project was focused on two parallel objectives:

1. Design and synthesis of novel GPR55 ligands, which also represents a key step to understand the role of GPR55 in neuroinflammation, as well as providing potential tool compounds to investigate the structural requirements for the interaction with its binding site.
2. Design and synthesis of multi-target compounds featuring two different pharmacophoric portions, able to modulate both GPR55 and CB_2R.

3. Novel ligands of GPR55 receptor

3.1 First series of 3-benzylquinolin-2(1*H*)-ones [128]

3.1.1 Design and Synthesis

Recently, a class of 3-benzylcoumarin derivatives (general structure **A**, *figure 3.1*) has been identified, showing a GPR55 antagonist profile, evaluated through the β-arrestin assay, with IC_{50} values in the low micromolar range. [116] In an effort to identify novel, potent, and selective GPR55 ligands, we designed and synthesized a first series of 3-benzylquinolin-2(1H)-ones **1B** - **4B** (general structure **B**, *figure 3.1*) by changing the stereo-electronic properties of the central coumarin scaffold through the replacement of the lactone group with an amide moiety. Additional modifications concern N-methylation and the insertion of a *n*-butyl group at position 7 as a sidechain of intermediate length with respect to those reported for the coumarin derivatives. Furthermore, we introduced methoxyl or hydroxyl groups in positions 5 and 2', taking into account that the insertion of small polar substituents at the same positions of the 3-benzylcoumarin scaffold led to the best results in terms of activity at GPR55.

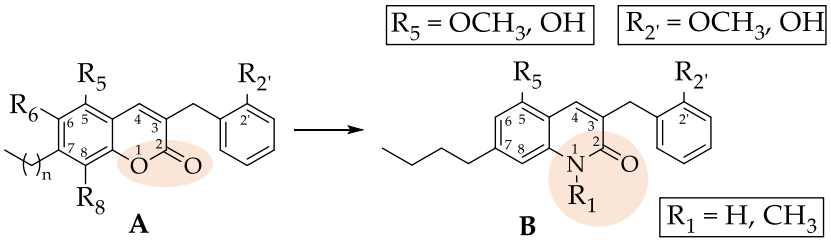

Figure 3.1. *Structural modifications leading to the novel class of 3-benzylquinolin-2(1H)-ones (**B**) from 3-benzylcoumarins (**A**).*

These structural modifications led to the final compounds reported in *figure 3.2*. Specifically, both compounds **1B** and **2B** show methoxyl groups at positions 5 and 2', while N-position is methylated in the latter, but not in the former. The same occurs in

derivatives **3B** and **4B**, however, in this case, hydroxyl groups are attached at positions 5 and 2′.

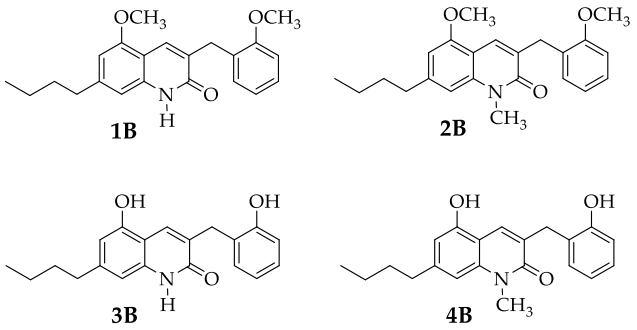

Figure 3.2. *First series of 3-benzylquinolin-2(1H)-ones.*

The synthetic route that lead to the key intermediate **7B** is reported in *Scheme 3.1*. The commercially available 3-bromo-5-nitroanisole **5** firstly underwent a Suzuki-Miyaura cross-coupling reaction with the 1-*n*-butylboronic acid, in the presence of tris(dibenzylideneacetone)dipalladium(0) ($Pd_2(dba)_3$), 2-dicyclohexylphosphino-2′,6′-diisopropoxybiphenyl (RuPhos) and sodium tert-butoxide (NaOtBu). Therefore, the nitro group of the resulting compound **6B** was reduced to give the corresponding aniline derivative **7B** with iron powder and ammonium chloride (NH_4Cl).

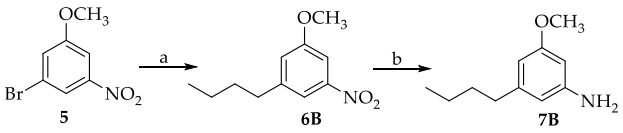

Scheme 3.1: Synthetic Route. ***a)*** *n-Butylboronic acid, $Pd_2(dba)_3$, Ruphos, t-BuONa, toluene/H_2O (10:1), 80 °C, overnight;* ***b)*** *Fe^0, NH_4Cl, EtOH/H_2O (2:1), reflux, 3 h.*

The synthetic route that provided the first series of 3-benzylquinolin-2(1*H*)-ones **1B** - **4B** is illustrated in *Scheme 3.2* reported below. The commercially available 3,4-dihydrocumarine **8** was treated with concentrated sulphuric acid (H_2SO_4) in anhydrous MeOH, providing intermediate **9**, which underwent a methylation reaction in the presence of methyl iodide (CH_3I) and sodium hydride (NaH, 60% dispersion in mineral oil) in DMF, affording compound **10**. After the hydrolysis of the ester group with LiOH, intermediate **11** was treated with thionyl chloride ($SOCl_2$) in toluene, obtaining

compound **12**, which provided the amide derivative **13B** by reaction with compound **7B** in the presence of triethylamine (Et_3N) in DCM. The amide **13B** was converted into the 2-chloroquinoline derivative **14B** through a cyclization with phosphoryl chloride ($POCl_3$) and N,N-dimethylformamide (DMF) as a Vilsmeier-Haack type reaction and separate from the other positional isomer **15B** formed in this reaction by flash chromatography. The intermediate **14B** was then treated with hydrochloric acid (HCl) 6N, to afford compound **1B**, and the subsequent methylation of the nitrogen atom with CH_3I and NaH provided derivative **2B**. Lastly compounds **3B** and **4B** were obtained via O-demethylation reaction in presence of boron tribromide (BBr_3) in DCM.

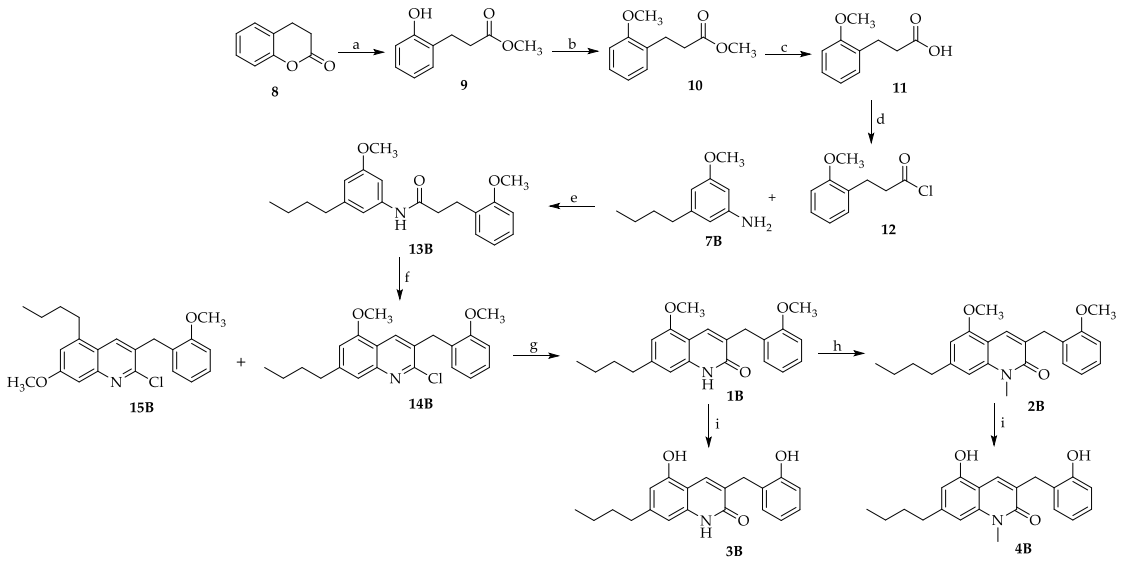

Scheme 3.2: Synthetic Route. ***a)*** *conc. H_2SO_4, dry MeOH, reflux, overnight;* ***b)*** *CH_3I, NaH, DMF, rt, overnight;* ***c)*** *LiOH, EtOH/H_2O (3:1), rt, 3 h;* ***d)*** *$SOCl_2$, toluene, reflux, 3 h;* ***e)*** *Et_3N, CH_2Cl_2, rt, overnight;* ***f)*** *DMF, $POCl_3$, 80 °C, overnight;* ***g)*** *HCl 6 N, reflux, overnight;* ***h)*** *NaH, CH_3I, DMF, rt, overnight;* ***i)*** *BBr_3, DCM, rt, overnight.*

The Vilsmeier-Haack type cyclization reaction represents a critical step in the synthetic route since it leads to a mixture of two regioisomers in equal amounts, compounds **14B** and **15B**, thus dramatically reducing the reaction yield. It is important to point out that the cyclization may occur at both *ortho* positions of the phenyl ring respect to the amide nitrogen atom, as reported in *Figure 3.2*. Thus, besides the desired 2-chloroquinoline derivative **14B**, its regioisomer **15B** was also obtained, where the position of the methoxyl group and the *n*-butyl side chain are swapped.

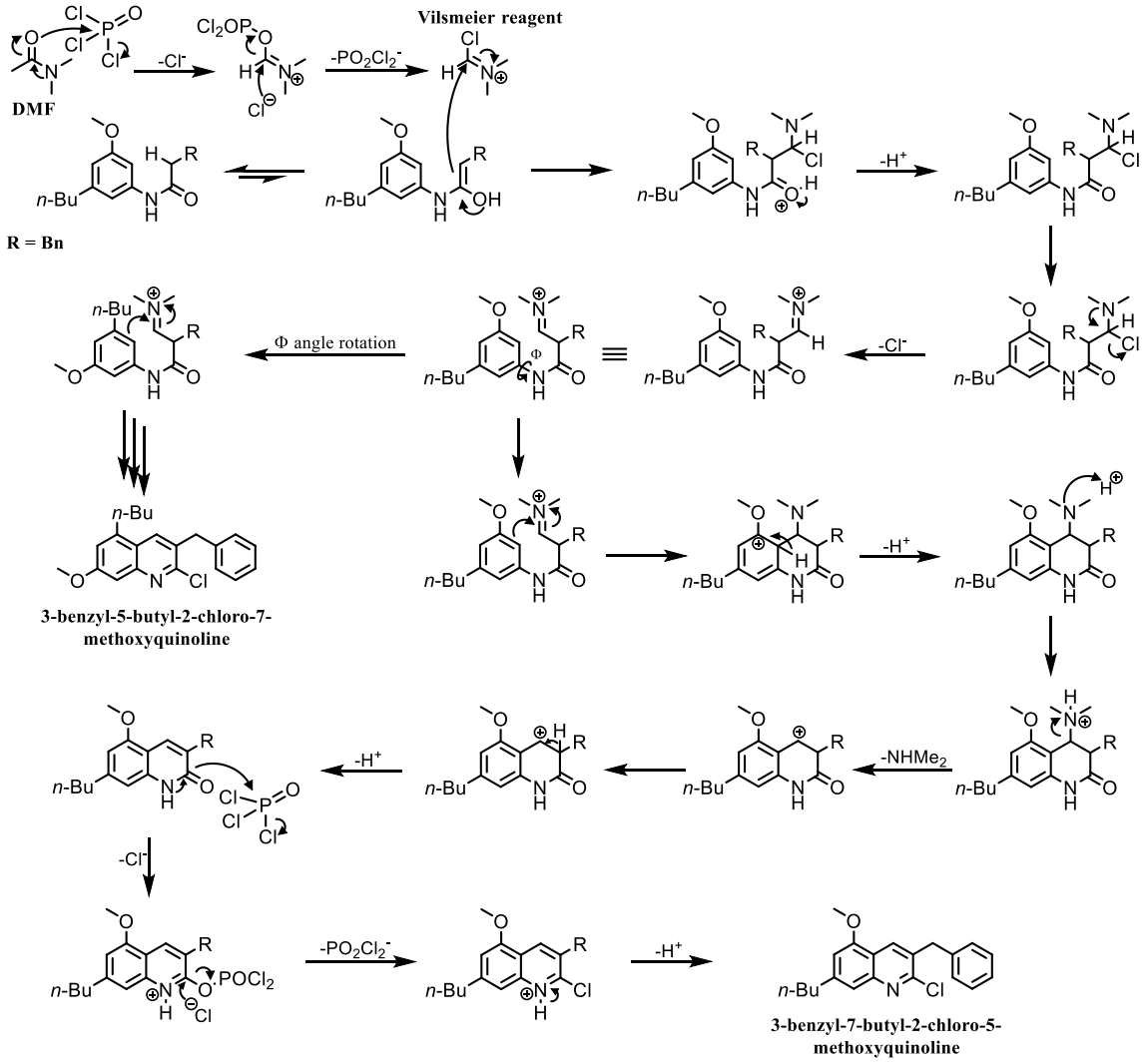

Figure 3.2. *A possible mechanism for the formation of the two regioisomers via Vilsmeier cyclization.*

Once separated by flash column chromatography (see the Experimental Section for further details), the two compounds were characterized via ^{1}H-NMR analysis. In particular, the proton at position 4 (H_4) appears to be more deshielded in derivative **14B** (δH = 8.19 ppm) rather than **15B** (δH = 7.92 ppm), due to the close spatial contact with the electronegative oxygen of the adjacent methoxyl group (*figure 3.3*).

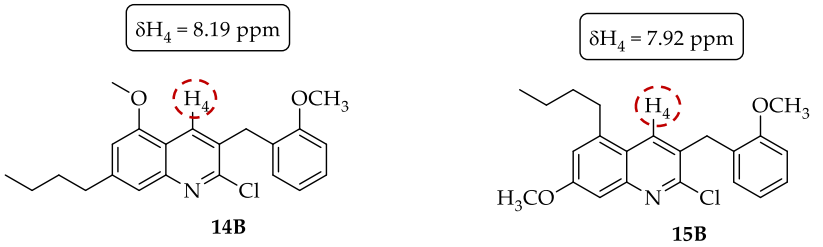

Figure 3.3. *Chemical shift values of the proton at position 4 in the two regioisomers.*

Lastly, two-dimensional experiments were performed to unequivocally identify the structure of the two regioisomers. For this purpose, Nuclear Overhauser Effect Spectroscopy (NOESY) spectra were recorded so as to determine which signals arise from protons that are spatially close to each other. Concerning derivative **14B**, as shown in *figure 3.4*, the proton at position 4 interacts with those of the methylene bridge at position 9 and the methoxyl group at position 5. Moreover, both hydrogen atoms at positions 6 and 8 are affected by the proximity of the *n*-butyl side chain protons.

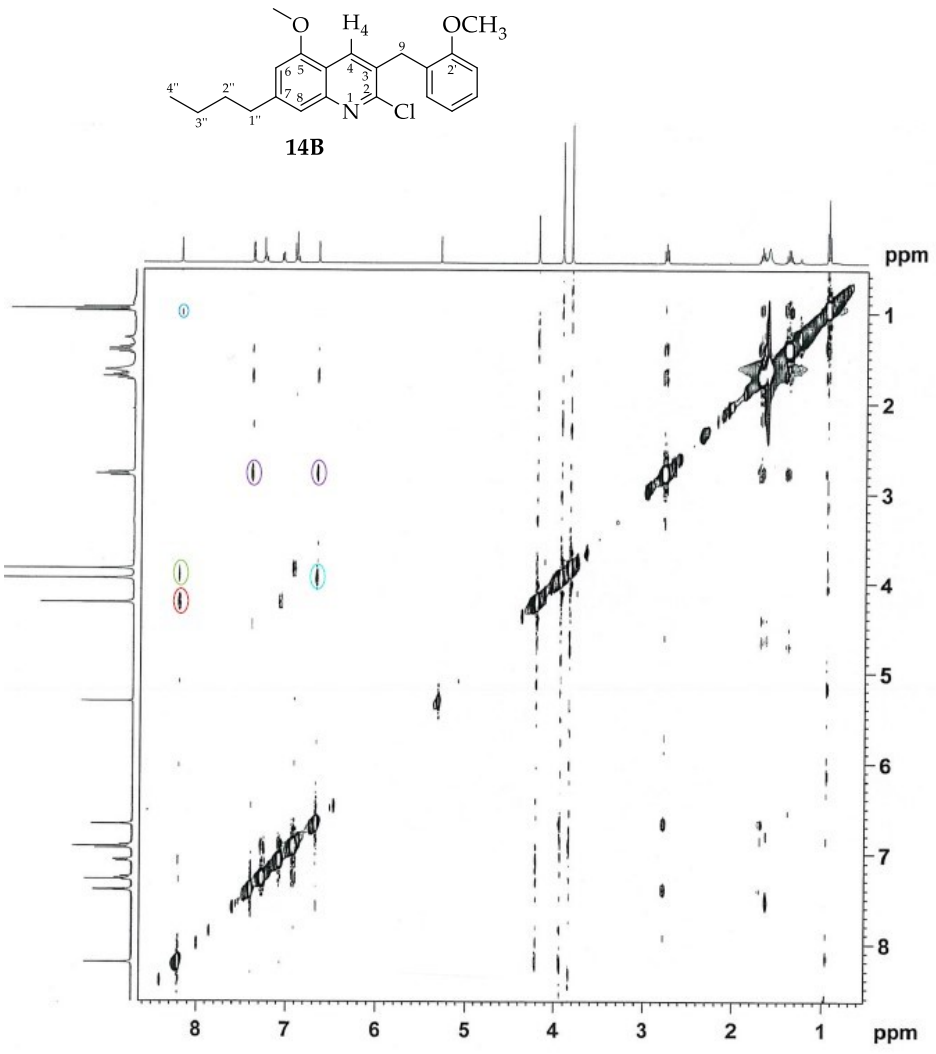

Figure 3.4. *NOESY spectrum of the derivative **14B** in CDCl3 at 400 MHz with a total acquisition time of 12 h.*

In case of isomer **15B**, spatial interactions have been observed between the proton at position 4 and the carbon atom of *n*-butyl chain at position 1'', as well as with the

methylene bridge at position 9. In addition, methoxyl group at position 7 interacts with both hydrogen atoms at positions 6 and 8 (*figure 3.5*).

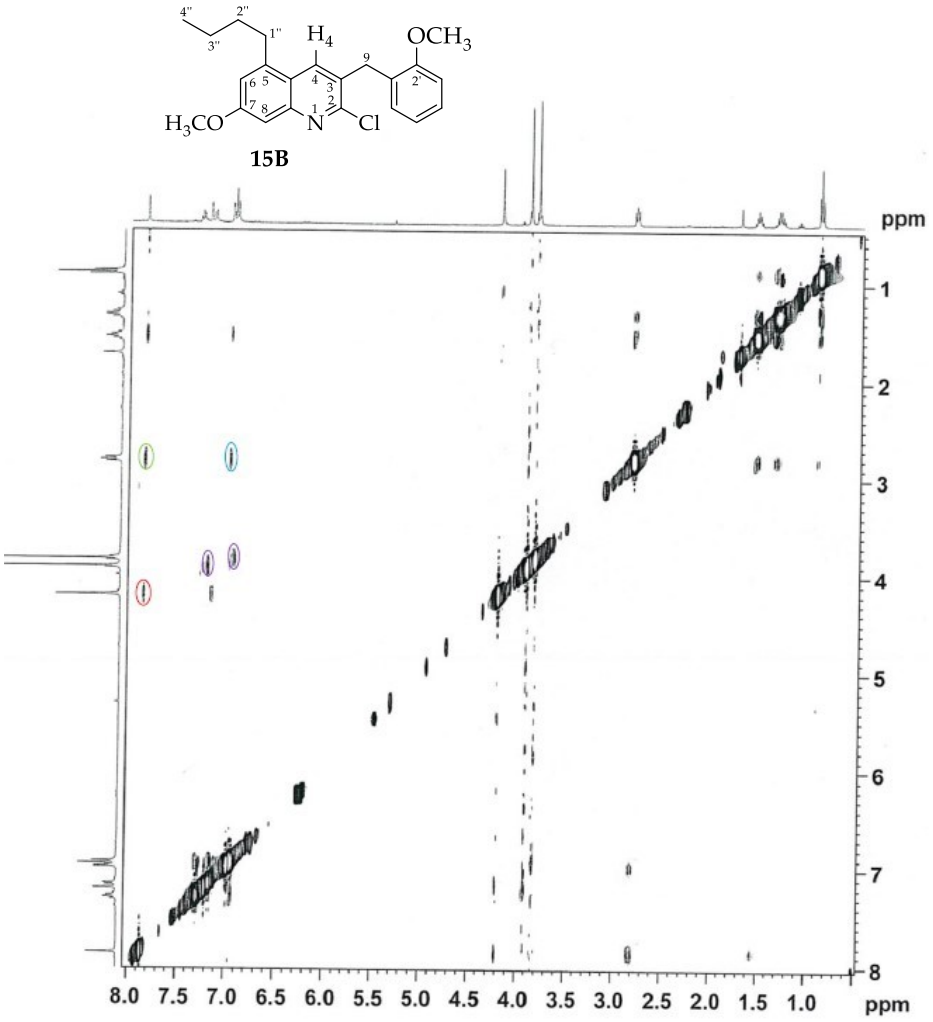

Figure 3.5. *NOESY spectrum of the derivative **15B** in CDCl3 at 400 MHz with a total acquisition time of 12 h.*

3.1.2 Biological evaluation

For this first series of compounds, biological evaluation was conducted at the University of Saskatchewan by Kawthar Mohamed and Michael Benko prior to my arrival at the institution. The affinity of the compounds toward GPR55 has been evaluated via radioligand binding using [^{3}H]CP55,940, which allowed for the estimate of K_i (i.e. affinity) values. Their selectivity over both CB_1R and CB_2R was also evaluated. The estimated experimental data values for the binding experiments are reported in *Table 3.1* and graphs are shown in *Figure 3.6*. Two reference ligands were also tested in this assay:

CP55,940, a full CBR agonist with high affinity toward GPR55 and O-1602, a synthetic compound closely related to abnormal-cannabidiol (abn-CBD) that has been shown to activate the GPR55 receptor.

All the synthesized compounds displayed high affinity toward GPR55, with K_i values included in the low nanomolar range (1.2 nM - 14 nM), and almost complete selectivity over one or both CBRs. Among them, compound **2B**, bearing methoxyl groups at positions 5 and 2′ and a methyl residue on the nitrogen atom at position 1, displayed the greatest affinity towards GPR55 within the series (K_i = 1.2 nM), showing also complete selectivity over CB_1R (K_i > 10,000 nM) and a remarkable affinity for CB_2R (K_i = 6.9 nM). Derivative **1B**, featuring methoxyl groups at positions 5 and 2′, resulted as the most promising of the set, showing not only high affinity toward GPR55 (K_i = 14 nM), but also complete selectivity over both CBRs (K_i > 10,000 nM). [128]

Table 3.1 Radioligand binding assays on *h*GPR55 and *h*CBRs.[a]

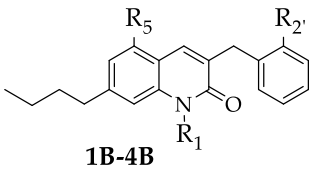

1B-4B

Compound	R_1	R_5	$R_{2'}$	K_i *h*GPR55 (nM)	K_i *h*CB_1R (nM)	K_i *h*CB_2R (nM)
CP55,940				13 (9.4 – 19)	12 (5.8 – 26)	128 (14 – 58)
O-1602				10 (7.6 – 14)		
1B	H	OCH_3	OCH_3	14 (8.1 – 24)	>10000	>10000
2B	CH_3	OCH_3	OCH_3	1.2 (0.58 – 3.3)*	>10000	6.9 (2.4 – 17)
3B	H	OH	OH	6.2 (4.6 – 8.4)*	5.1 (1.0 – 26)	>10000
4B	CH_3	OH	OH	7.1 (6.0 – 8.4)*	29 (14 – 65)	7.9 (4.8 – 13)

[a]*Affinity (K_i) was estimated for each compound using cell membranes (25 μg/sample) derived from CHO cells expressing either human GPR55, CB_1R, or CB_2R. Membranes were incubated with 1 nM [^{3}H]CP55,940 and 0.1 nM – 10 μM of each compound for 2 h and radioactivity was measured as previously described* [129]. *Data were fit to a 3-parameter non-linear regression in GraphPad (v. 9.0). Data are means with 95% confidence interval (CI). n = 3-4 independent experiments. Statistical analyses were by non-overlapping CI. *p < 0.05 relative to GPR55 within compound. Concentration-response curves are shown in Figure 4.6*

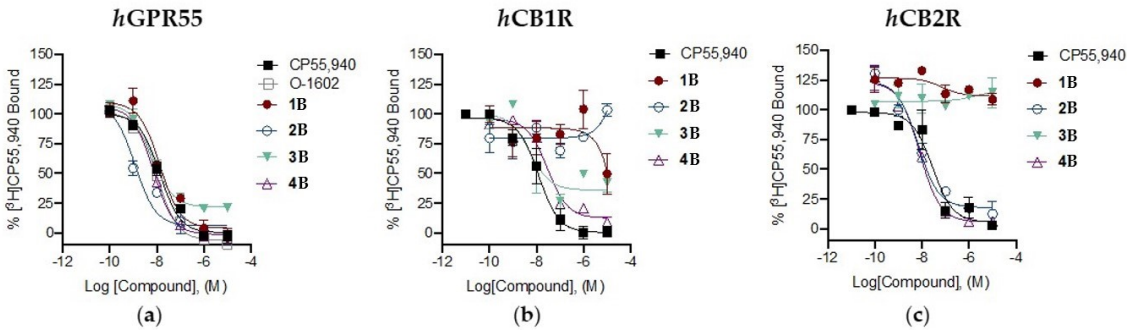

Figure 3.6. *In vitro characterization of [³H]CP55,940 binding in the presence of compounds* ***1B-4B*** *at hGPR55 (**a**), hCB₁R (**b**), or hCB₂R (**c**). Data are expressed as % change from 1 nM [³H]CP55,940 binding and are means ± SEM (n = 3-4). All data were fit to a 3-parameter non-linear regression in GraphPad (v. 9.0). Analyses are presented in Table 4.1.*

Functional activity at *h*GPR55 was investigated in the p-ERK activation assay. Functional data are reported in *Table 3.2* and GPR55 p-ERK activation graphs are shown in *Figure 3.7*.

All compounds displayed a functional activity of full agonists of GPR55 relative to CP55,940 and O-1602, resulting to be among the most potent and selective GPR55 agonists developed to date, with EC_{50} values included in the low nanomolar range (1.1 nM – 6.4 nM). [128]

Table 3.2 p-ERK1/2 activation assay at *h*GPR55.[a]

Compound	**EC_{50} 95% CI (nM)**	**E_{max} (Fold)**
CP55,940	4.2 (1.2 – 12)	1.3 ± 0.06
O-1602	61 (19 – 190)*	1.3 ± 0.03
1B	6.4 (0.38 – 48)	1.5 ± 0.06
2B	1.1 (0.31 – 28)	1.4 ± 0.07
3B	1.4 (0.15 – 22)	1.2 ± 0.04
4B	11 (1.0 – 56)	1.3 ± 0.03

[a] *Potency (EC_{50}) and efficacy (E_{max}) were estimated for each compound in CHO cells expressing human GPR55 and treated with 0.1 nM – 10 μM compounds for 30 min. Data were fit to a 3-parameter non-linear regression in GraphPad (v. 9.0). Data are means with 95% CI (EC_{50}) or means with SEM (E_{max}). n = 6 independent experiments performed in duplicate. Statistical analyses were by non-overlapping CI. *p < 0.05 relative to CP55,940. Concentration-response curves are shown in Figure 4.7.*

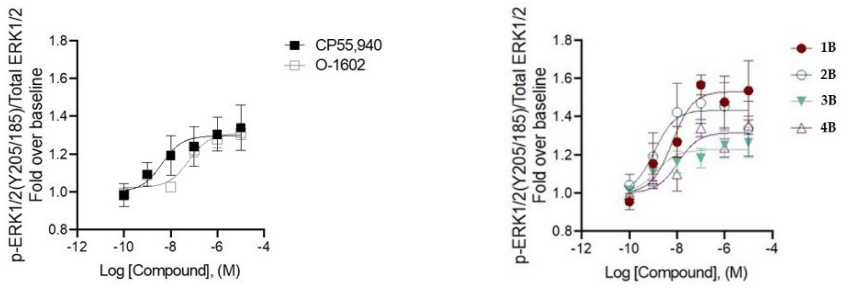

Figure 3.7. *In vitro characterization of p-ERK1/2 in the presence of compounds **1B**-**4B** at hGPR55. CHO cells expressing hGPR55 were treated with 0.1 nM – 10 μM compounds for 30 min. Data are expressed as fold over vehicle and are means ± SEM (n = 6 independent experiments performed in duplicate). All data were fit to a 3 parameter nonlinear regression in GraphPad (v. 9.0). Analyses are presented in Table 4.2.*

3.1.3 Computational studies and pharmacokinetic properties prediction

In addition, a computational study was carried out to predict the key interactions of the ligands with the GPR55 binding site. Since no X-ray structure is available for the receptor, the computational model was obtained through homology modelling techniques by using the X-ray structure of zebrafish lysophosphatidic acid (LPA) receptor LPA6 in complex with LPA as a template. Indeed, it displayed the highest sequence identity (29%) among all proteins with known structural data. [130] In order to identify some structure-based hypotheses for explaining the preliminary SAR data emerging from the biological evaluation results obtained for the series of 3-benzylquinolin-2-(1*H*)-ones, computational studies including homology modeling, molecular dynamics simulations, docking and binding free energy evaluations were employed for identifying the potential binding disposition of these compounds. For this reason, derivative **2B** was used as a reference compound for this analysis, given its highest potency (EC_{50} = 1.1 nM) and affinity for the receptor (K_i = 1.2 nM) among this series of compounds. As reported in *figure 3.8*, the ligand appears to assume an L-shaped conformation inside the GPR55 binding pocket, where the quinolinone scaffold is placed between the TM3 and TM7, forming π-π stacking interactions with Y3.32 and F3.33 as well as Met-aromatic interactions with M3.36 and M7.39. This is noteworthy since such residues constitute the toggle switch, which is involved in the receptor activation. Moreover, the quinolone scaffold is held in place through hydrogen-bond interactions.

The alkyl side chain seems to be accommodated within a hydrophobic pocket at TM5 and the benzyl group is located between Q1.35 and M7.39. Lastly, a H-bond is formed between the carbonyl group and K2.60, while the methoxyl group at position 5 interacts with a serine residue (S7.42). [128]

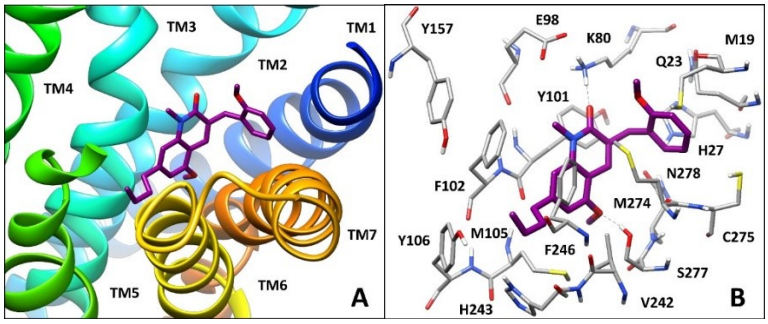

Figure 3.8. *Minimized average structure of compound 2 within the binding site of the hGPR55 model.* ***A)*** *The ligand (purple) and the different transmembrane domains of the receptor are shown;* ***B)*** *the protein residues (grey) surrounding the ligand within the receptor binding site are shown, with ligand-protein H-bonds highlighted with black dashed lines.*

In addition, blood-brain barrier (BBB) permeation and gastrointestinal absorption were calculated with the aim of getting insight the pharmacokinetic profile of final compounds **1B**-**4B**. All four derivatives were predicted as BBB permeable with good confidence and to be well-absorbed by the gastrointestinal tract, [128] thus representing a promising starting point to evaluate their effect in *in-vivo* models of neurodegenerative diseases.

3.2 Second series of 3-benzylquinolin-2(1*H*)-ones

3.2.1 Design and Synthesis

According to the above-mentioned computational study, *n*-butyl side chain is inserted in a hydrophobic pocket, of which the shape and the length have not been yet completely elucidated, and substitution at position 2′ seems not to be essential in the interaction with the binding site of the GPR55 receptor. [128] Based on these results, we expanded the first set of 3-benzyl-7-*n*-butyl-quinolin-2(1*H*)-ones, to deepen the preliminary SAR for this class of molecules and provide further information about the features of the GPR55 binding site. In particular, we change the length (series **C** and **D**, *figure 3.9*) or the isomerism (series **E**, *figure 3.9*) of the side chain at position 7 and we removed the substituent at position 2′ (series **F**, *figure 3.9*).

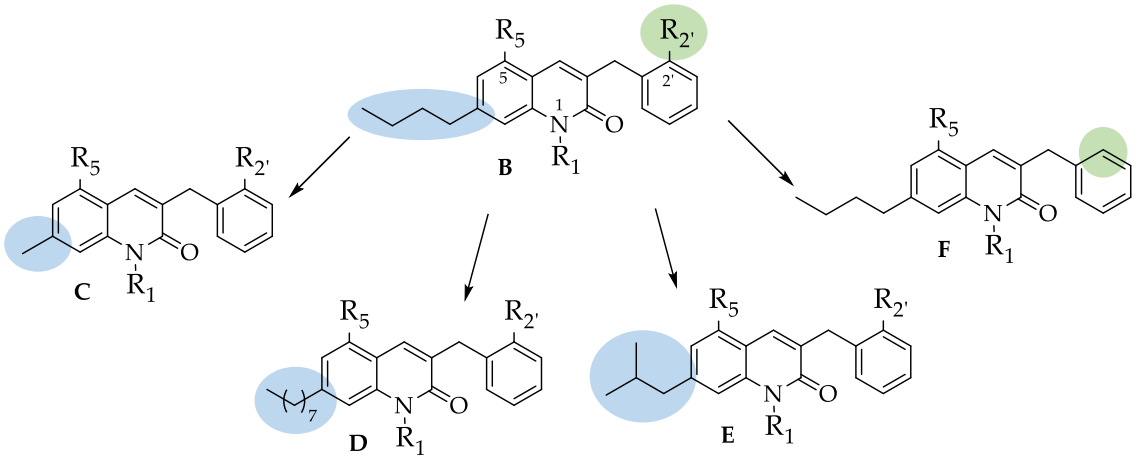

Figure 3.9. *Structural modifications providing the novel series of 3-benzylquinolin-2(1H)-ones (**C**, **D**, **E** and **F**) from series **B**.*

Newly synthesized 3-benzylquinolin-2(1*H*)-ones are reported in *figure 3.10*. In addition to the peripheral structural modifications already discussed for derivatives of the first series, the substitution of the *n*-butyl group at position 7 with a *n*-octyl residue, a methyl group or an *iso*-butyl chain led to the final compounds **1C**-**4C**, **1D**-**4D** and **1E**-**4E**, respectively. On the other hand, the removal of substituent at position 2′ provided derivatives **1F**-**4F**. All compounds were characterized via 1H-NMR and 13C-NMR, but

also via ultra-high performance liquid chromatography combined with high resolution mass spectrometry (HPLC-HRMS), that I performed during my training in Toscana Life Sciences (TLS), Siena (*see experimental section 6.5*).

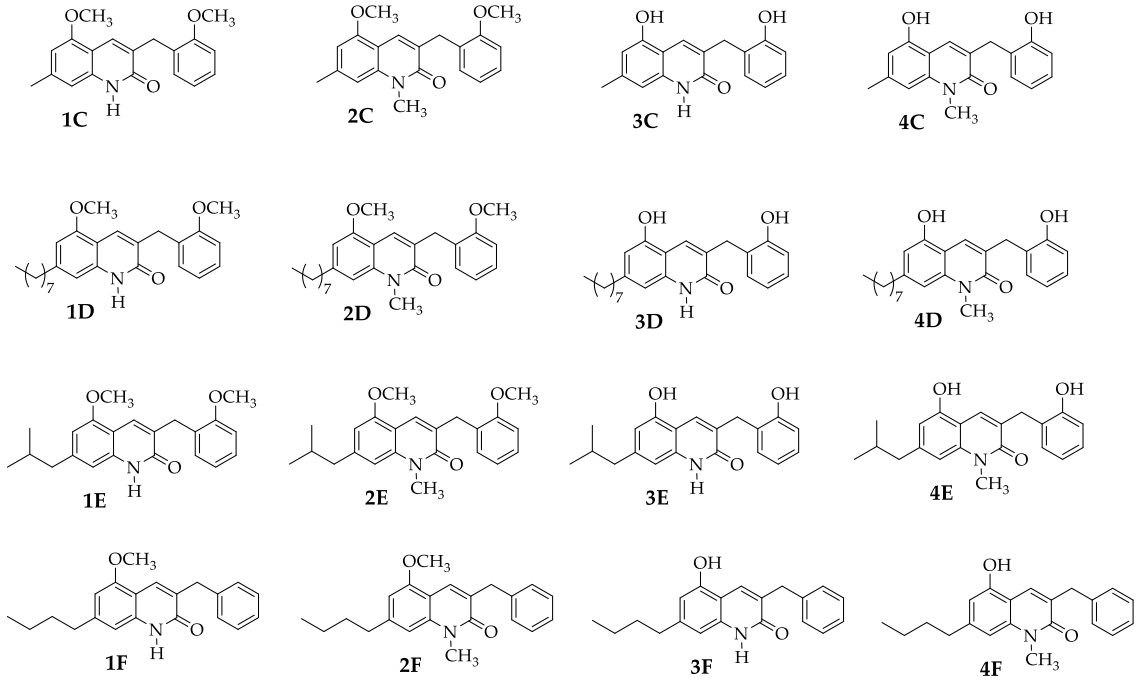

Figure 3.10. *Novel synthesized 3-benzylquinolin-2(1H)-ones belonging to series **C**, **D**, **E** and **F**.*

The synthetic route which led to the aniline derivatives **7C**, **7D** and **7E** is reported in *Scheme 3.3*, following the same reaction conditions formerly applied for the obtaining of intermediate **7B**.

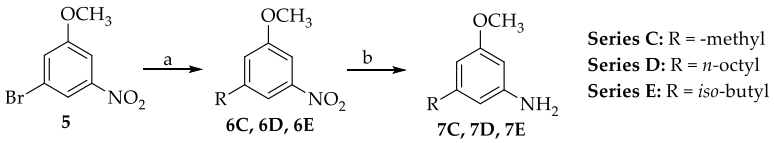

Scheme 3.3: Synthetic Route. ***a)*** *Suitable boronic acid, $Pd_2(dba)_3$, Ruphos, t-BuONa, toluene/H_2O (10:1), 80 °C, overnight;* ***b)*** *Fe^0, NH_4Cl, EtOH/H_2O (2:1), reflux, 3 h.*

The general synthesis of final compounds belonging to series **C**, **D** and **E** is illustrated in *Scheme 3.4* and involved the same synthetic procedure formerly applied to achieve 3-benzyl-7-*n*-butyl-quinolin-2(1*H*)-ones **1B**-**4B**.

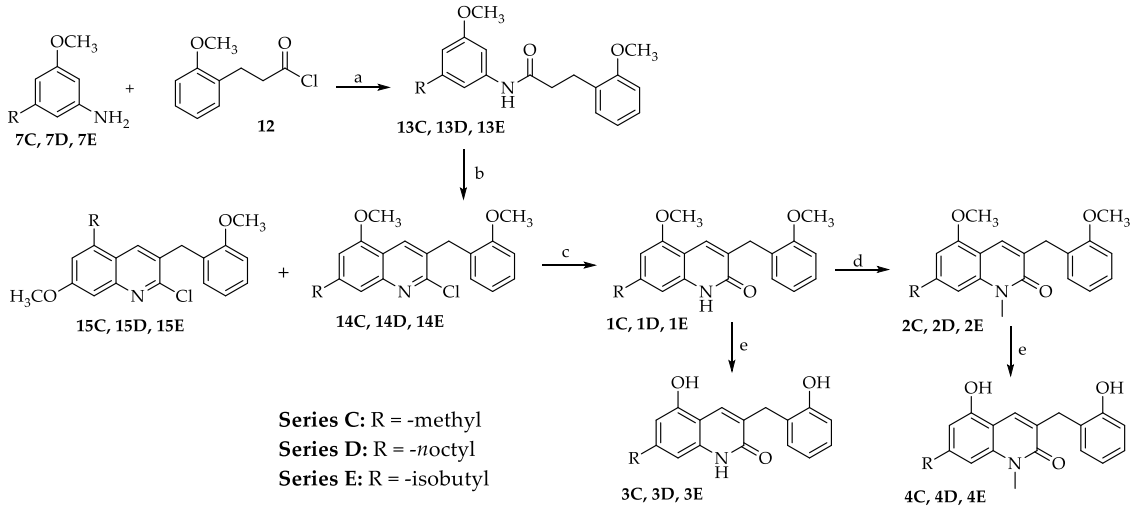

Scheme 3.4: Synthetic Route. ***a)*** *Et_3N, DCM, rt, overnight;* ***b)*** *DMF, $POCl_3$, 80 °C, overnight;* ***c)*** *6N HCl, reflux, overnight;* ***d)*** *NaH, CH_3I, DMF, rt, overnight;* ***e)*** *4 eq BBr_3, DCM, rt, 1h.*

The synthetic procedure to afford final compounds belonging to series **F** is reported in *Scheme 3.5* and followed the same reaction conditions previously described, but starting from the commercially available hydrocinnamic acid **16**.

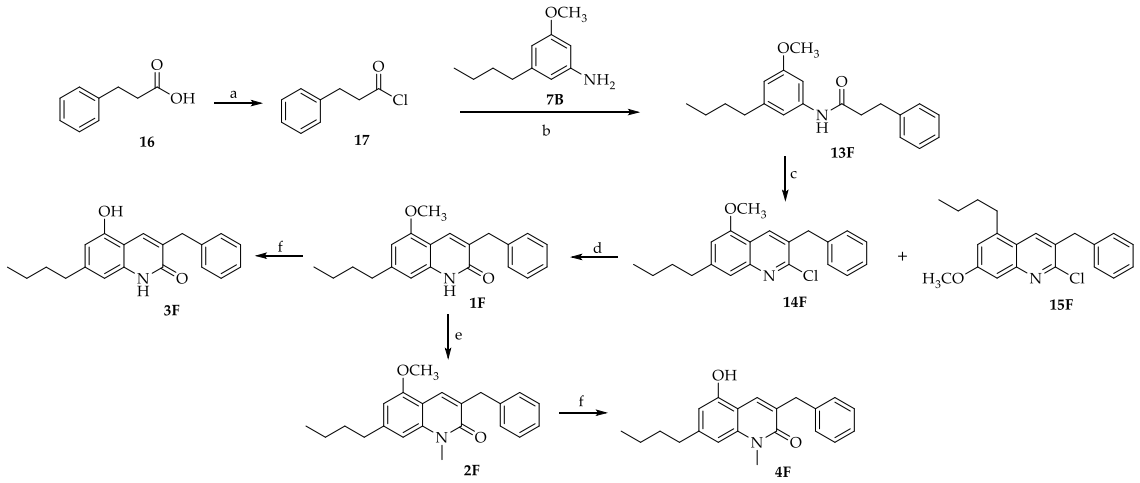

Scheme 3.5: Synthetic Route. ***a)*** *$SOCl_2$, toluene, reflux, 3 h.* ***b)*** *Et_3N, DCM, rt, overnight;* ***c)*** *DMF, $POCl_3$, 80 °C, overnight;* ***d)*** *6N HCl, reflux, overnight;* ***e)*** *NaH, CH_3I, DMF, rt, overnight;* ***f)*** *4 eq BBr_3, DCM, rt, 1h.*

As previously reported, the Vilsmeier-Haack type cyclization reaction is a critical step in the synthetic route and led to a mix of two isomers. For all series, the isomers were separated through flash liquid chromatography and characterized via ^{1}H-NMR and NOESY analysis, showing same interactions previously reported for compounds **14B** and **15B**.

3.2.2 Biological evaluation

During my study abroad experience at University of Saskatchewan, Canada, I worked on the pharmacological evaluation of these synthesized compounds (*see experimental section 6.2*). Affinity toward GPR55 receptor was assessed via radioligand binding using [^{3}H]CP55,940 under the same conditions as the first series. Derivatives which displayed affinity for GPR55 were then tested through p-ERK activation assay in order to evaluate their activity toward GPR55 and their selectivity over CBRs. For these new series only CP55,940 was used as reference compound in these assays.

New compounds belonging to series **C**, featuring a methyl group at position 7 of the quinolone scaffold, generally showed very high affinity toward GPR55 receptor, as illustrated in *Table 3.3*. In particular, derivative **3C**, bearing hydroxyl groups at positions 5 and 2', displayed the greatest affinity towards GPR55 within this set, with K_i value of 0.51 nM. In addition, compound **1C**, characterized by the presence of methoxyl groups at positions 5 and 2', maintained a remarkable affinity for GPR55, showing also complete selectivity over CB_1R (K_i > 10000) and about 7-fold selectivity over CB_2R (K_i = 73 nM). Lastly, concerning derivative **2C**, the combine reduction of *n*-butyl chain and insertion of methoxyl residues at position 5 and 2' lead to a consistent reduction of affinity toward GPR55 (K_i = 250 nM) comparing with the analogue of the first series **2B** (K_i = 1.2 nM).

Table 3.3 Radioligand binding assays on *h*GPR55 and *h*CBRs.[a]

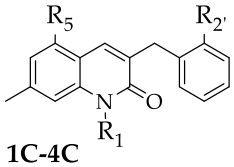

1C-4C

Compound	R_1	R_5	$R_{2'}$	K_i *h*GPR55 (nM)	K_i *h*CB_1R (nM)	K_i *h*CB_2R (nM)
CP55,940				30 (5.6 – 110)	26 (6.5 – 60)	56 (6.1 – 230)
1C	H	OCH_3	OCH_3	11 (1.8 – 130)	>10000	73 (6.8 – 110)
2C	CH_3	OCH_3	OCH_3	250 (1.5 – 560)	n.c.	6.9 (2.4 – 17)
3C	H	OH	OH	0.51 (0.11 – 3.1)	^	^
4C	CH_3	OH	OH	2.2 (0.33 – 19)	1.5 (0.35 – 68)^	230 (25 – 360)

[a]Affinity (K_i) was estimated for each compound using cell membranes (25 μg/sample) derived from CHO cells expressing either human GPR55, CB_1R, or CB_2R. Membranes were incubated with 1 nM [^{3}H]CP55,940 and 0.1 nM – 10 μM of each compound for 2 h and radioactivity was measured as previously described [129]*. Data were fit to a 3-parameter non-linear regression in GraphPad (v. 9.0). Data are means with 95% confidence interval (CI). n = 3-4 independent experiments. Statistical analyses were by non-overlapping CI. *p < 0.05 relative to GPR55 within compound. Concentration-response curves are shown in Figure 4.11. ^Preliminary data.*

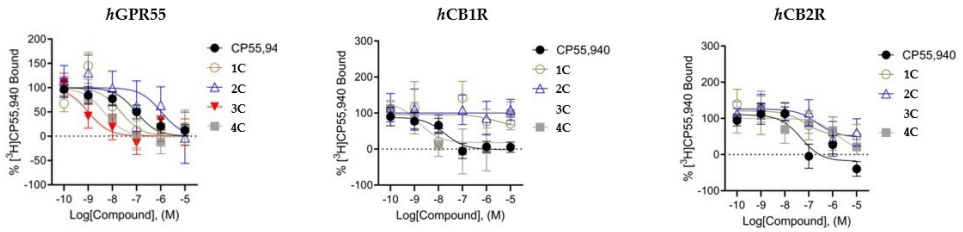

Figure 3.11. *In vitro characterization of [^{3}H]CP55,940 binding in the presence of compounds **1C**-**4C** at hGPR55 (a), hCB_1R (b), or hCB_2R (c). Data are expressed as % change from 1 nM [^{3}H]CP55,940 binding and are means ± SEM (n = 3-4). All data were fit to a 3-parameter non-linear regression in GraphPad (v. 9.0). Analyses are presented in Table 4.3.*

Functional data are reported in *Table 3.4* and GPR55 p-ERK activation graphs are shown in *Figure 3.12*. Only compounds **1C** and **3C** were able to modulate the p-ERK pathway, both showing an inverse agonist profile compared to CP55,940. In particular, derivative **1C**, which differs from the reference compound of the first series **1B** only for the length of the alkyl side chain, displayed the greatest potency towards GPR55 within this new series (EC_{50} = 28 nM).

Table 3.4 p-ERK1/2 activation assay at *h*GPR55.[a]

Compound	EC_{50} 95% CI (nM)	E_{max} (Fold)
CP55,940	0.66 (0.13 – 9.7)	1.24 ± 0.02
1C	28 (9.2 – 81)	0.87 ± 0.03
2C	> 10000	0.91 ± 0.07
3C	300 (36 – 580)	1.1 ± 0.03
4C	> 10000	0.69 ± 0.05

[a]*Potency (EC_{50}) and efficacy (E_{max}) were estimated for each compound in CHO cells expressing human GPR55 and treated with 0.1 nM – 10 μM compounds for 30 min. Data were fit to a 3-parameter non-linear regression in GraphPad (v. 9.0). Data are means with 95% CI (EC_{50}) or means with SEM (E_{max}). n = 6 independent experiments performed in duplicate. Statistical analyses were by non-overlapping CI. *p < 0.05 relative to CP55,940. Concentration-response curves are shown in Figure 4.12.*

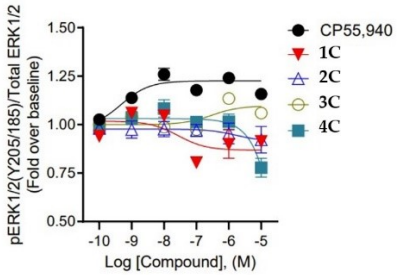

Figure 3.12. *In vitro characterization of p-ERK1/2 in the presence of compounds **1C**-**4C** at hGPR55. CHO cells expressing hGPR55 were treated with 0.1 nM – 10 μM compounds for 30 min. Data are expressed as fold over vehicle and are means ± SEM (n = 6 independent experiments performed in duplicate). All data were fit to a 3 parameter non-linear regression in GraphPad (v. 9.0). Analyses are presented in Table 4.4.*

Concerning 3-benzyl-quinolin-2(1*H*)-ones of series **D**, characterized by a *n*-octyl chain at position 7, methylation of nitrogen atom at position 1 appears to be important to afford compounds with high affinity toward GPR55 receptor, as reported in *Table 3.5*. Among them, derivative **4D**, featuring also hydroxyl groups at positions 5 and 2′, showed a K_i value of 0.29 nM, displaying the highest affinity toward GPR55 within compounds developed to date. Moreover, it also showed complete selectivity over CB_1R (K_i > 10000), as well as derivative **2D**, bearing methoxyl groups at positions 5 and 2′. The extension of alkyl side chain lead in general to an increase of affinity toward CB_2R, except for derivative **3D** (K_i CB_2R > 10000).

Table 3.5 Radioligand binding assays on *h*GPR55 and *h*CBRs.[a]

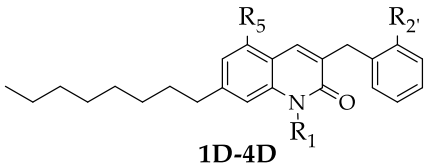

1D-4D

Compound	R_1	R_5	$R_{2'}$	K_i *h*GPR55 (nM)	K_i *h*CB$_1$R (nM)	K_i *h*CB$_2$R (nM)
CP55,940				30 (5.6 – 110)	26 (6.5 – 60)	56 (6.1 – 230)
1D	H	OCH_3	OCH_3	480 (65 – 1000)	13 (4.8 – 79)	5.1 (0.22 – 97)
2D	CH_3	OCH_3	OCH_3	4.6 (0.4 – 180)	> 10000	8.3 (3.4 – 86)^
3D	H	OH	OH	420 (22 – 580)	0.82 (0.16 – 78)	> 10000
4D	CH_3	OH	OH	0.29 (0.02 – 5.1)	> 10000	0.73 (0.12 – 28)

[a]Affinity (K_i) was estimated for each compound using cell membranes (25 μg/sample) derived from CHO cells expressing either human GPR55, CB$_1$R, or CB$_2$R. Membranes were incubated with 1 nM [^{3}H]CP55,940 and 0.1 nM – 10 μM of each compound for 2 h and radioactivity was measured as previously described [129]*. Data were fit to a 3-parameter non-linear regression in GraphPad (v. 9.0). Data are means with 95% confidence interval (CI). n = 3-4 independent experiments. Statistical analyses were by non-overlapping CI. *p < 0.05 relative to GPR55 within compound. Concentration-response curves are shown in Figure 4.13. ^Preliminary data.*

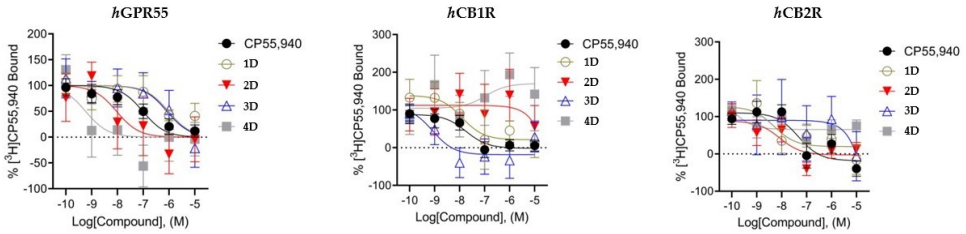

Figure 3.13. *In vitro characterization of [^{3}H]CP55,940 binding in the presence of compounds **1D**-**4D** at hGPR55 (a), hCB$_1$R (b), or hCB$_2$R (c). Data are expressed as % change from 1 nM [^{3}H]CP55,940 binding and are means ± SEM (n = 3-4). All data were fit to a 3-parameter non-linear regression in GraphPad (v. 9.0). Analyses are presented in Table 4.5.*

Functional results are reported in *Table 3.6* and GPR55 p-ERK activation graphs are shown in *Figure 3.14*. All compounds were unable to modulate the p-ERK pathway, except for derivative **1D**, featuring methoxyl groups at positions 5 and 2', which proved to be an inverse agonist compared to CP55,940 with an EC_{50} value of 41 nM. Interestingly, concerning functional data observed for compounds of series **C**, both an increase and a reduction of the *n*-butyl chain shifted functional activity from agonism to antagonism or weak inverse agonism.

Table 3.6 p-ERK1/2 activation assay at *h*GPR55.[a]

Compound	EC_{50} 95% CI (nM)	E_{max} (Fold)
CP55,940	0.66 (0.13 – 9.7)	1.24 ± 0.02
1D	41 (7.8 – 81)	0.88 ± 0.02
2D	n.c.	1.04 ± 0.06
3D	> 10000	0.78 ± 0.09
4D	> 10000	0.78 ± 0.02

[a] *Potency (EC_{50}) and efficacy (E_{max}) were estimated for each compound in CHO cells expressing human GPR55 and treated with 0.1 nM – 10 μM compounds for 30 min. Data were fit to a 3-parameter non-linear regression in GraphPad (v. 9.0). Data are means with 95% CI (EC_{50}) or means with SEM (E_{max}). n = 6 independent experiments performed in duplicate. Statistical analyses were by non-overlapping CI. *p < 0.05 relative to CP55,940. Concentration-response curves are shown in Figure 4.14.*

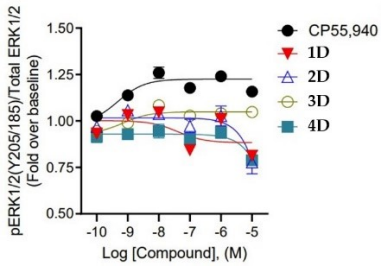

Figure 3.14. *In vitro characterization of p-ERK1/2 in the presence of compounds **1D**-**4D** at hGPR55. CHO cells expressing hGPR55 were treated with 0.1 nM – 10 μM compounds for 30 min. Data are expressed as fold over vehicle and are means ± SEM (n = 6 independent experiments performed in duplicate). All data were fit to a 3 parameter non-linear regression in GraphPad (v. 9.0). Analyses are presented in Table 4.6.*

Spatial variation of alkyl side chain through the substitution of *n*-butyl group with an *iso*-butyl residue led to compounds belonging to series **E**, which showed in general lower affinity for GPR55 receptor and CBRs (*Table 3.7*), comparing with analogues of series **B**. Among them, only derivative **2E**, bearing methoxyl groups at positions 5 and 2′ and a methyl group on the nitrogen atom at position 1, displayed high affinity toward GPR55 receptor (K_i = 5.6 nM), as well as complete selectivity over CB_1R (K_i > 10000) and about 20-fold selectivity over CB_2R (K_i = 110 nM).

Table 3.7 Radioligand binding assays on *h*GPR55 and *h*CBRs.[a]

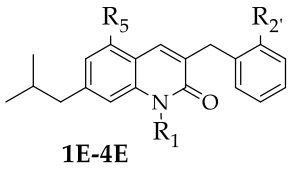

1E-4E

Compound	R_1	R_5	$R_{2'}$	K_i *h*GPR55 (nM)	K_i *h*CB$_1$R (nM)	K_i *h*CB$_2$R (nM)
CP55,940				30 (5.6 – 110)	26 (6.5 – 60)	56 (6.1 – 230)
1E	H	OCH_3	OCH_3	1800 (190 – 3000)	0.14 (0.06 – 12)	> 10000
2E	CH_3	OCH_3	OCH_3	5.6 (0.92 – 44)	> 10000	110 (95 – 390)
3E	H	OH	OH	23 (2.4 – 270)	24 (4.8 – 52)	9.0 (0.67 – 16)
4E	CH_3	OH	OH	870 (93 – 2300)	n.c.	1300 (540 – 7900)

[a]Affinity (K_i) was estimated for each compound using cell membranes (25 μg/sample) derived from CHO cells expressing either human GPR55, CB$_1$R, or CB$_2$R. Membranes were incubated with 1 nM [^{3}H]CP55,940 and 0.1 nM – 10 μM of each compound for 2 h and radioactivity was measured as previously described [129]*. Data were fit to a 3-parameter non-linear regression in GraphPad (v. 9.0). Data are means with 95% confidence interval (CI). n = 3-4 independent experiments. Statistical analyses were by non-overlapping CI. *p < 0.05 relative to GPR55 within compound. Concentration-response curves are shown in Figure 4.15.*

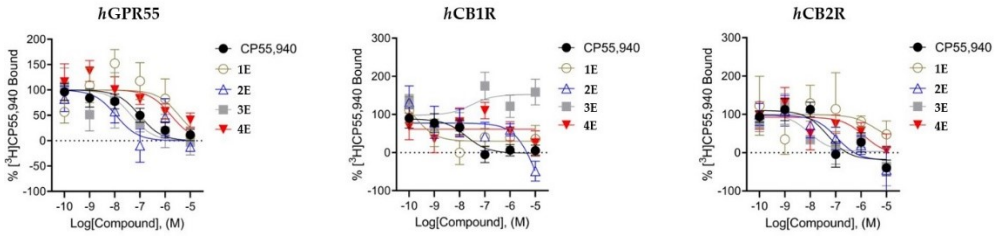

Figure 3.15. *In vitro characterization of [^{3}H]CP55,940 binding in the presence of compounds **1E**-**4E** at hGPR55 (a), hCB$_1$R (b), or hCB$_2$R (c). Data are expressed as % change from 1 nM [^{3}H]CP55,940 binding and are means ± SEM (n = 3-4). All data were fit to a 3-parameter non-linear regression in GraphPad (v. 9.0). Analyses are presented in Table 4.7.*

Functional data are illustrated in *Table 3.8* and GPR55 p-ERK activation graphs are showed in *Figure 3.16*. All compounds belonging to this series proved not to be able to modulate the p-ERK pathway, thus suggesting a possible "linear" shape of the hydrophobic pocket inside the binding site which could explain the reduction of affinity and the loss of activity due to a substitution with a branched-chain.

Table 3.8 p-ERK1/2 activation assay at *h*GPR55.[a]

Compound	EC_{50} 95% CI (nM)	E_{max} (Fold)
CP55,940	0.66 (0.13 – 9.7)	1.24 ± 0.02
1E	> 10000	0.80 ± 0.11
2E	> 10000	0.87 ± 0.10
3E	> 10000	0.73 ± 0.05
4E	> 10000	0.72 ± 0.07

[a] *Potency (EC_{50}) and efficacy (E_{max}) were estimated for each compound in CHO cells expressing human GPR55 and treated with 0.1 nM – 10 μM compounds for 30 min. Data were fit to a 3-parameter non-linear regression in GraphPad (v. 9.0). Data are means with 95% CI (EC_{50}) or means with SEM (E_{max}). n = 6 independent experiments performed in duplicate. Statistical analyses were by non-overlapping CI. *p < 0.05 relative to CP55,940. Concentration-response curves are shown in Figure 4.16.*

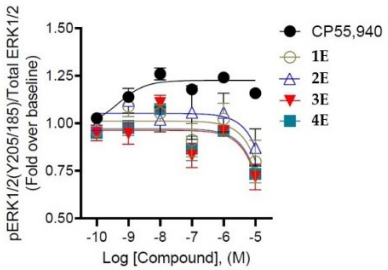

Figure 3.16. *In vitro characterization of p-ERK1/2 in the presence of compounds **1E**-**4E** at hGPR55. CHO cells expressing hGPR55 were treated with 0.1 nM – 10 μM compounds for 30 min. Data are expressed as fold over vehicle and are means ± SEM (n = 6 independent experiments performed in duplicate). All data were fit to a 3 parameter non-linear regression in GraphPad (v. 9.0). Analyses are presented in Table 4.8.*

New compounds belonging to series **F** are illustrated in *Table 3.9*. The introduction of the hydrogen atom at position 2′ resulted in a decrease of affinity toward both GPR55 and CBRs compared with analogues of series **B** featuring methoxyl or hydroxyl groups. These results suggest that substituent at position 2′ is well tolerated and important, even if not essential, for the interaction with GPR55 binding site.

Table 3.9 Radioligand binding assays on *h*GPR55 and *h*CBRs.[a]

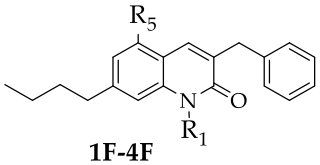

1F-4F

Compound	R_1	R_5	K_i *h*GPR55 (nM)	K_i *h*CB_1R (nM)	K_i *h*CB_2R (nM)
CP55,940			30 (5.6 – 110)	26 (6.5 – 60)	56 (6.1 – 230)
1F	H	OCH_3	n.c.	-	-
2F	CH_3	OCH_3	67 (4.3 – 300)	180 (13 – 480)	> 10000
3F	H	OH	330 (57 – 3200)	> 10000	> 10000^
4F	CH_3	OH	340 (56 – 3400)	> 10000	> 10000

[a]Affinity (K_i) was estimated for each compound using cell membranes (25 μg/sample) derived from CHO cells expressing either human GPR55, CB_1R, or CB_2R. Membranes were incubated with 1 nM [^{3}H]CP55,940 and 0.1 nM – 10 μM of each compound for 2 h and radioactivity was measured as previously described [129]. *Data were fit to a 3-parameter non-linear regression in GraphPad (v. 9.0). Data are means with 95% confidence interval (CI). n = 3-4 independent experiments. Statistical analyses were by non-overlapping CI. *p < 0.05 relative to GPR55 within compound. Concentration-response curves are shown in Figure 4.17. ^Preliminary data.*

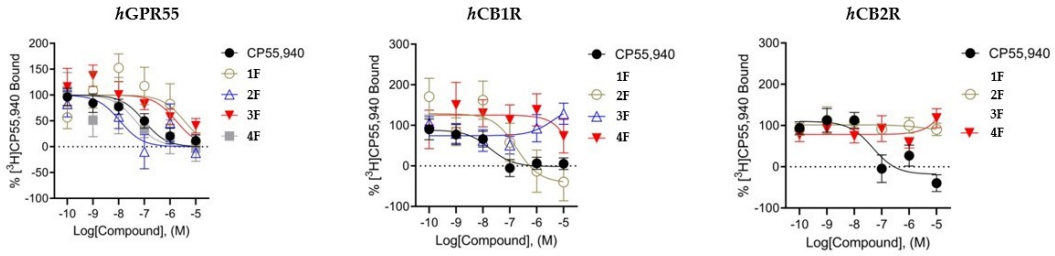

Figure 3.17. *In vitro characterization of [^{3}H]CP55,940 binding in the presence of compounds **1F**-**4F** at hGPR55 (a), hCB_1R (b), or hCB_2R (c). Data are expressed as % change from 1 nM [^{3}H]CP55,940 binding and are means ± SEM (n = 3-4). All data were fit to a 3-parameter non-linear regression in GraphPad (v. 9.0). Analyses are presented in Table 4.9.*

Functional results are reported in *Table 3.10* for 3-benzyl-quinolin-2(1*H*)-ones **2F**-**4F** and GPR55 p-ERK activation graphs are showed in *Figure 3.*18. Only compound **4F**, featuring hydroxyl groups at positions 5 and 2′ and a methyl residue on the nitrogen atom of the quinolin-2(1*H*)-one scaffold, proved to be able to modulate the p-ERK pathway as a weak inverse agonist compared to CP55,940, showing an EC_{50} value of 85 nM.

Table 3.10 p-ERK1/2 activation assay at *h*GPR55.[a]

Compound	EC_{50} 95% CI (nM)	E_{max} (Fold)
CP55,940	0.66 (0.13 – 9.7)	1.24 ± 0.02
1F	-	-
2F	> 10000	0.77 ± 0.05
3F	> 10000	0.77 ± 0.09
4F	85 (24 – 470)	0.82 ± 0.03

[a] *Potency (EC_{50}) and efficacy (E_{max}) were estimated for each compound in CHO cells expressing human GPR55 and treated with 0.1 nM – 10 μM compounds for 30 min. Data were fit to a 3-parameter non-linear regression in GraphPad (v. 9.0). Data are means with 95% CI (EC_{50}) or means with SEM (E_{max}). n = 6 independent experiments performed in duplicate. Statistical analyses were by non-overlapping CI. *p < 0.05 relative to CP55,940. Concentration-response curves are shown in Figure 4.18.*

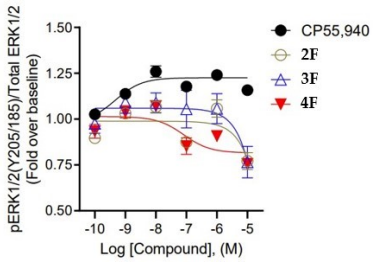

Figure 3.18. *In vitro characterization of p-ERK1/2 in the presence of compounds **1F**-**4F** at hGPR55. CHO cells expressing hGPR55 were treated with 0.1 nM – 10 μM compounds for 30 min. Data are expressed as fold over vehicle and are means ± SEM (n = 6 independent experiments performed in duplicate). All data were fit to a 3 parameter non-linear regression in GraphPad (v. 9.0). Analyses are presented in Table 4.10.*

3.3 Metabolic assays

In order to investigate *in-vitro* cytochrome P450-dependent metabolic behaviour of this class of 3-benzyl-quinolin-2(1*H*)-ones, we selected derivatives **1B** and **1C** as the most promising compounds of the first and the second series, respectively, and I performed metabolic assays during my training in Toscana Life Sciences (*see experimental section 6.4*). Indeed, **1B** was a potent GPR55 agonist with high affinity, showing complete selectivity over both CBRs. On the other hand, **1C** proved to be a potent inverse agonist of GPR55 receptor, displaying complete selectivity over CB_1R and good selectivity over CB_2R. Both compounds demonstrated good metabolite kinetics in human liver (HLM) microsomes, thus giving preliminary prediction of their human *in vivo* behaviour. In addition, the early characterization of the metabolic profile could provide information that might be

useful to guide structural modification, with the aim of achieving derivatives endowed with more favourable metabolic properties.

Each compound was incubated at concentration of 10 μM together with phosphate buffer, human microsomal protein and nicotinamide adenine dinucleotide phosphate (NADPH), following the experimental procedure reported in the Experimental Section.

3.3.1 Metabolic properties of compound 1B

Our study performed on human liver microsomes showed that compound **1B** represents a good substrate for CYP-dependent metabolism, as illustrated in the kinetic curve reported in *figure 3.19*. In particular, **1B** follows a first-order kinetic curve, being probably metabolized only by one specific isoform of CYP450.

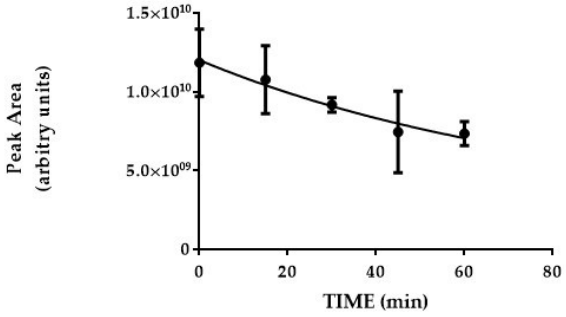

Best-fit values	
Y0	1.201e+010
Plateau	2.423e+009
K	0.01211
Half Life	57.22
Tau	82.55
Span	9.585e+009

Figure 3.19. *Kinetic curve of compound **1B**.*

To predict metabolic transformation of derivative **1B**, an initial computational study was carried out by using MetaSite program, identifying derivatives reported in *figure 3.20* as possible metabolites.

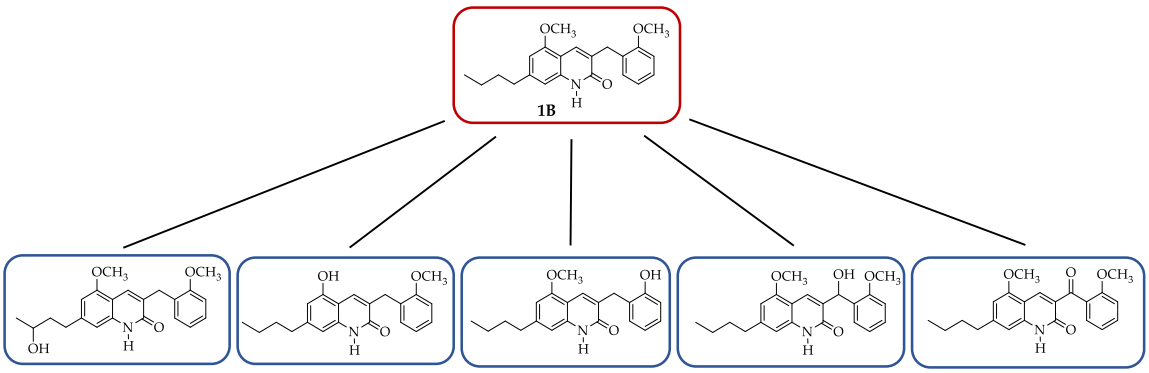

Figure 3.20. *Possible metabolites of compound **1B** predicted by using MetaSite.*

Based on these results, *in vitro* metabolism of **1B** was evaluated in human liver microsomes by using HPLC-HRMS. The structures of the metabolites were characterized by accurate mass, elemental composition and mass fragmentation. Among all the metabolites predicted by MetaSite, we identified derivatives reported in *Figure 3.21*. In particular, **M1** and **M2** underwent the same metabolic reaction which consists in the hydroxylation of the carbon atom of *n*-butyl chain at position 3'' or methylene bridge at position 9, respectively, resulting as the most abundant ones. Compound **M3** features a carboxyl group on the methylene bridge, probably because of an oxidation reaction of compound **M2**.

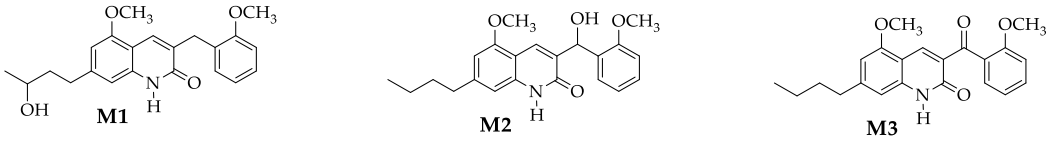

Figure 3.21. *Metabolites of compound **1B** identified by using HPLC-HRMS in human liver microsomes.*

In particular, **M1** represent the most abundant metabolite of derivative **1B**. The kinetic curve reported in *figure 3.22* shows that the amount of the compound increase during the first 45 minutes, being subsequently metabolized in turn.

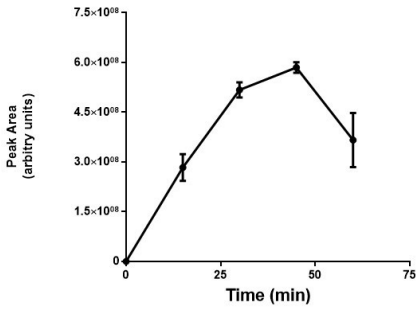

Figure 3.22. *Kinetic curve of main metabolite **M1**.*

3.3.2 Metabolic properties of compound 1C

As reported in *Figure 3.23*, compound **1C** represent a good substrate for CYP-dependent metabolism and it follows a first-order kinetic curve. So, as reported for compound **1B**, probably even derivative **1C** is metabolized only by one specific isoform of CYP450.

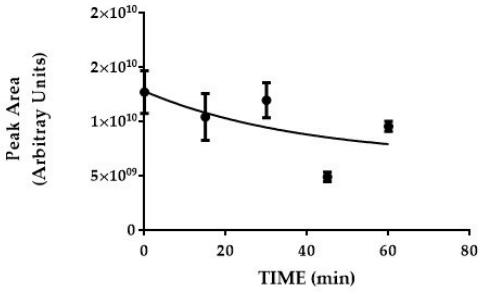

Y0	1.278e+010
Plateau	6.582e+009
K	0.02570
Half Life	26.97
Tau	38.91
Span	6.195e+009

Figure 3.23. *Kinetic curve of compound **1C**.*

As previously discussed, an initial computational study was performed by using MetaSite program, with the aim of predicting the possible metabolites of derivative **1C**, reported in *figure 3.24*.

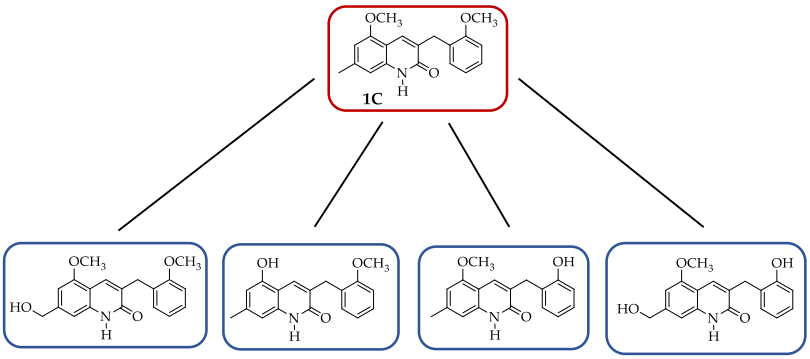

Figure 3.24 *Possible metabolites of compound **1C** predicted by using MetaSite.*

These results were later confirmed by evaluating **1C** *in vitro* metabolism in human liver microsomes via HPLC-HRMS. Derivative **1C** was metabolized mainly through hydroxylation of methyl group at position 7, providing compound **M4** (*figure 3.24*). The subsequent demethylation of methoxyl group at position 2' lead to the second metabolite **M5** (*figure 3.25*).

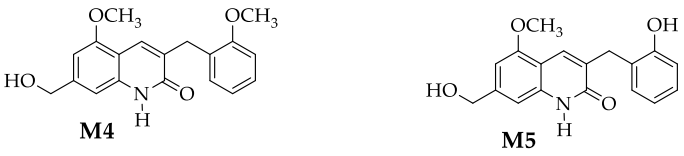

Figure 3.25 *Metabolites of compound **1C** identified by using HPLC-HRMS in human liver microsomes.*

In particular, **M4** is the major metabolite of compound **1C**. The kinetic curve reported in *figure 3.26* highlights that the amount of the compound increase during the first 30 minutes. Subsequently, it starts decreasing, being converted into the metabolite M5, until reaching the plateau after 45 minutes.

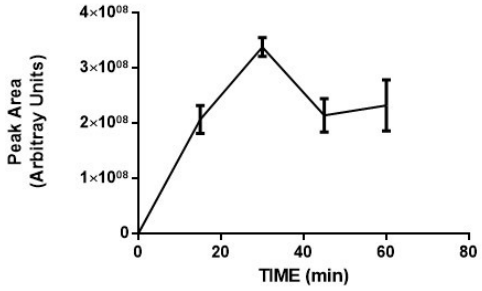

Figure 3.26 *Kinetic curve of main metabolite **M4**.*

4. Novel multitarget compounds

4.1 Design and Synthesis

Traditional pharmacological approaches rely on the design and synthesis of drugs, as selective as possible for the target of interest, with the aim of reducing the collateral effects caused by interaction with other biological structures. However, it is well known that neurodegenerative disorders involve complex pathways, linked to the dysfunction of several biological targets. Traditional therapies have highlighted the boundaries of the one-drug-one-target approach. Thus, in the last few years, the multitarget approach has gained more and more relevance in the treatment of neurodegenerative disorders. The multitarget approach can be pursued by two different strategies: cocktail of monofunctional drugs (combination therapy), active on different targets and administrated in association (drug-combination) or in the same formulation (fixed-dose combination), or treatment with a single multifunctional compound able to selectively act on multiple biological targets (multi-targets-directed ligand, MTDL). [131] [132] This latter strategy overcomes some drawbacks of the combination therapy, such as the different bioavailability of compounds and possible drug-drug interactions, as well as improving the compliance of patients. [133]

As previously reported, GPR55 and CB_2R represent innovative therapeutic targets for the treatment of neurodegenerative diseases due to their involvement in the modulation of neuroinflammatory processes. Moreover, in HEK293 cells these receptors seem to exist also as heterodimers (see section 1.2.3.1). [91] [92] To achieve molecules with enhanced neuroprotective effects, I designed and synthetized multi-target compounds by connecting two pharmacophoric portions able to modulate both receptors through alkyl-triazole linkers of different length, obtaining compounds with general structure **H** (*figure 4.1*). To modulate GPR55 we chose a 3-benzylcoumarine derivative (**KIT17**, *figure 4.1*), which proved to be a GPR55 antagonist in the β-arrestin assay [116] and showed neuroprotective properties in LPS-activated primary microglia cells. [73] Concerning CB_2R, we selected naphthyridine-2-ones (general structures **G**, *figure 4.1*), which resulted as potent and selective CB_2R agonists. [134]

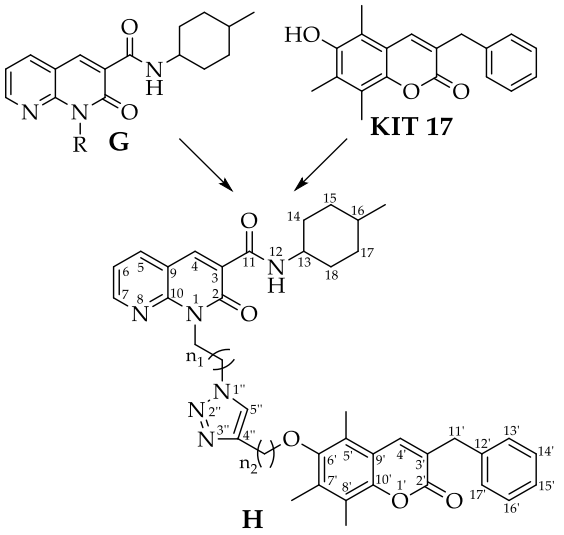

Figure 4.1. *Design of multitarget compounds by connecting naphthyridine-2-one derivatives* ***G*** *and* ***KIT17*** *through triazole linkers of different length.*

Final compounds are reported in *figure 4.2*. Three alkyl chains of different lengths were chosen to connect the naphthyridine-3-carboxamide scaffold **G** to the triazole group, while the 3-benzylcoumarine **KIT17** was linked through a methylene bridge or a *n*-propyl group, achieving derivatives **18**-**20** and **21**-**23**, respectively. All compounds below were characterized via ^{1}H-NMR and ^{13}C-NMR, but also via ultra-high performance liquid chromatography combined with high resolution mass spectrometry (HPLC-HRMS), that I performed during my training in Toscana Life Sciences (*see experimental section 6.5*).

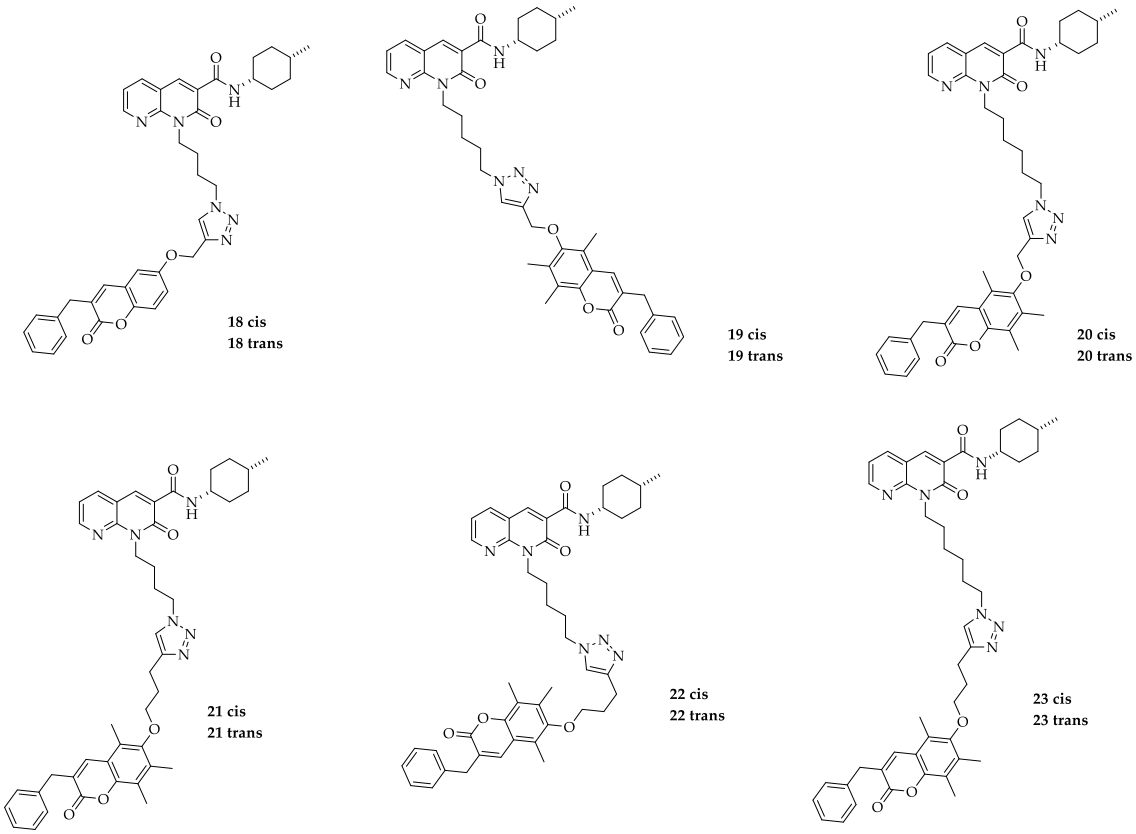

Figure 4.2 *Structures of newly synthesized multitarget compounds.*

The synthetic route that led to the key intermediates **29** and **30** is illustrated in *Scheme 4.1*. The commercially available trimethylhydroquinone **23** underwent a methylation reaction in presence of CH_3I and NaH (60% dispersion in mineral oil) in DMF, affording compound **25**, which was subsequently formylated with hexamethylenetetramine and trifluoroacetic acid, providing derivative **26**. After the demethylation of methoxyl groups with BBr_3, intermediate **27** was treated with cinnamaldehyde, 1,3-dimethylimidazolium dimethylphosphate and K_2CO_3, achieving compound **28**, which underwent a demethylation reaction with BBr_3, to afford compound **KIT17**. Lastly, the alkylation of hydroxyl group of **KIT17** with the suitable bromoalkyne in presence of K_2CO_3 provided intermediates **29** and **30**.

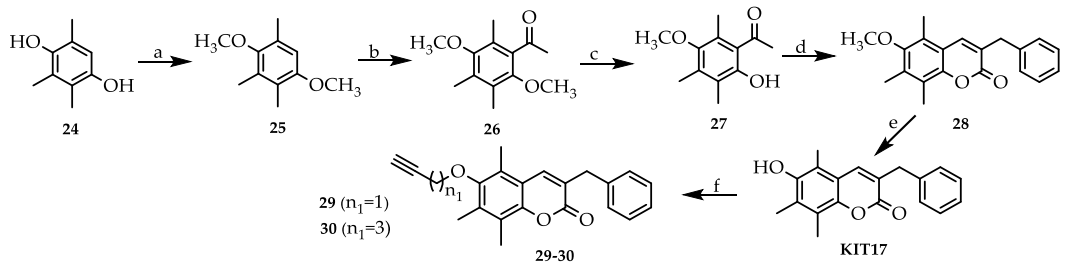

Scheme 4.1: Synthetic Route. ***a)*** *CH_3I, NaH, DMF, rt, 2h;* ***b)*** *hexamethylenetetramine, trifluoroacetic acid, reflux, 20 h;* ***c)*** *0.8 eq BBr_3, DCM, rt, overnight;* ***d)*** *cinnamaldehyde, 1,3-dimethylimidazolium dimethylphosphate, K_2CO_3, toluene, 100 °C, 24 h;* ***e)*** *2 eq BBr_3, DCM, rt, overnight;* ***f)*** *suitable bromoalkyne, K_2CO_3, DMF, 60 °C, 5 h.*

The synthetic procedure to afford intermediates **37-39** is reported in *Scheme 4.2*. The commercially available 2-amino-3-pyridinecarboxaldehyde **31** underwent a cyclization reaction in presence of diethyl malonate and piperidine to achieve compound **32**, which was then treated with a mixture of cis/4-methylcyclohexan-1-amine, providing derivative **33**. After the alkylation of the nitrogen atom with the suitable alkyldibromide, to afford compounds **34**-**36**, cis and trans isomers were separated through flash liquid chromatography. Finally, the treatment with sodium azide (NaN_3) provided the other key intermediates **37**-**39**.

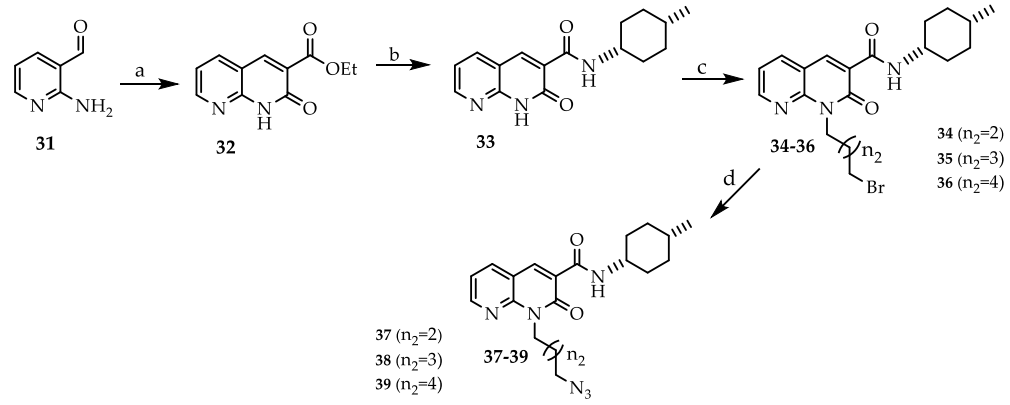

Scheme 4.2: Synthetic Route. ***a)*** *diethyl malonate, piperidine, 130 °C, overnight;* ***b)*** *4-methylcyclohexan-1-amine, 120 °C, 24 h;* ***c)*** *suitable alkyldibromide, CsF, DMF, 30 °C, 24 h;* ***d)*** *NaN_3, DMF, 60 °C, overnight.*

The synthetic procedure that led to the final compounds **18**-**23** is illustrated in *Scheme 4.3*. The reaction between intermediates **29**-**30** and **37**-**39** in presence of ascorbic acid and copper (II) sulfate pentahydrate ($CuSO_4 \cdot 5H_2O$) lead to the formation of triazole ring, providing final derivatives **18**-**23**. This cyclization represents an example of "Click"

Chemistry, a term which was firstly proposed by Sharpless et al. in 2001. [135] "Click" Chemistry includes simple and fast reactions, featuring high yields, high stereo specificity and less cytotoxic by-products. [136] It has recently emerged as a field of great interest, especially in pharmaceutical sciences, resulting as one of the most frequently used reaction to promote the connection of two different molecular portions through linkers of different structure and length. [137]

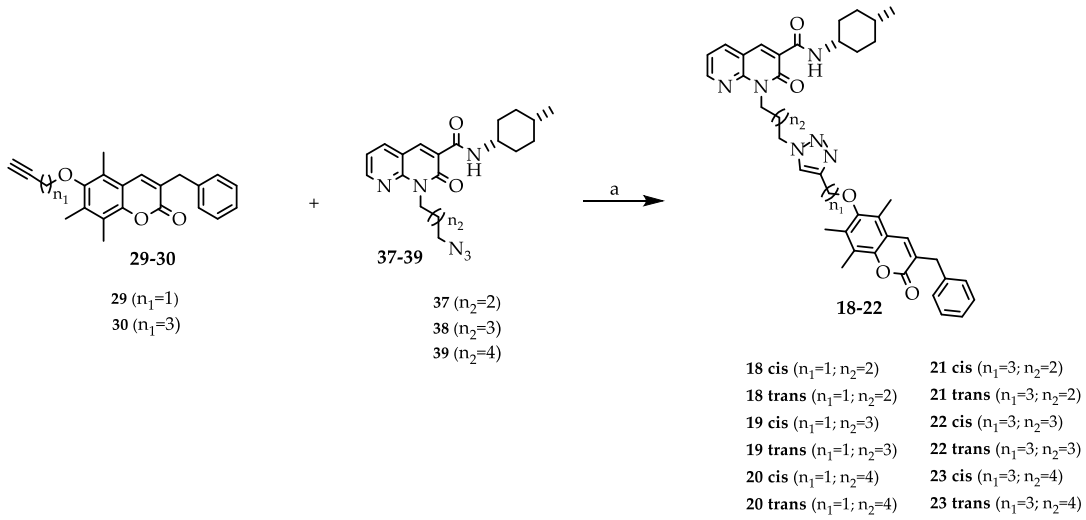

Scheme 4.3: Synthetic Route. ***a)*** *$CuSO_4 \cdot 5H_2O$, ascorbic acid, DMF, H_2O, 80 °C, 4h.*

4.2 Biological evaluation

During my study abroad experience, I also evaluated the affinity of these compounds toward GPR55 and CB_2R. Preliminary studies were performed on the mixture of isomers via radioligand binding using [^{3}H]CP55,940 (*see experimental section 6.2*). Results are reported in *Table 4.1*. Among all the developed compounds, derivatives **18** and **22** proved to be able to simultaneously bind both GPR55 and CB_2R, with K_i values included in the low nanomolar range. In addition, compounds **20** and **23**, bearing a *n*-hexyl chain between the naphthyridine-3-carboxamide scaffold **G** and the triazole ring, were unable to bind CB_2R (K_i > 10000). Moreover, this latter one, featuring the longest alkyl triazole linker of the series, did not bind GPR55 too (K_i > 10000).

Concerning the interesting data reported for compounds **18** and **22**, these derivatives will be further investigated, in order to assess the affinity and the fuctional activity of separate isomers toward GPR55 and CB_2R.

Table 4.1 Radioligand binding assays on *h*GPR55 and *h*CB_2R.[a]

Compound	n_1	n_2	K_i *h*GPR55 (nM)	K_i *h*CB_2R (nM)
CP55,940			30 (5.6 – 110)	49 (10 – 59)
18	1	2	2.2 (0.23 – 39)	16 (2.5 – 120)
19	1	3	0.21 (0.10 – 2.5)	n.c.
20	1	4	0.21 (0.09 – 2.3)	>10000
21	3	2	59 (18 – 790)	130 (56 – 640)
22	3	3	5.8 (0.63 – 42)	9.3 (2.6 – 190)
23	3	4	>10000	>10000

[a]*Affinity (K_i) was estimated for each compound using cell membranes (25 µg/sample) derived from CHO cells expressing either human GPR55 or CB_2R. Membranes were incubated with 1 nM [^{3}H]CP55,940 and 0.1 nM – 10 µM of each compound for 2 h and radioactivity was measured as previously described* [129]. *Data were fit to a 3-parameter non-linear regression in GraphPad (v. 9.0). Data are means with 95% confidence interval (CI). n = 3-4 independent experiments. Statistical analyses were by non-overlapping CI. *p < 0.05 relative to GPR55 within compound. Concentration-response curves are shown in Figure 5.3.*

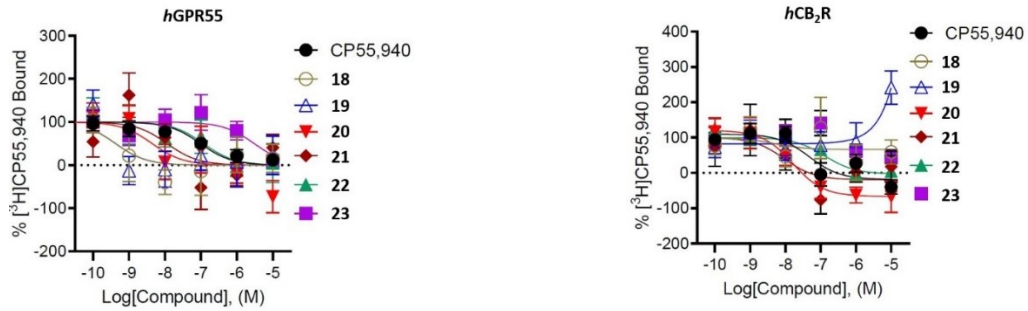

Figure 4.3. *In vitro characterization of [^{3}H]CP55,940 binding in the presence of compounds **18**-**23** at hGPR55 (a) and hCB_2R (c). Data are expressed as % change from 1 nM [^{3}H]CP55,940 binding and are means ± SEM (n = 3-4). All data were fit to a 3-parameter non-linear regression in GraphPad (v. 9.0). Analyses are presented in Table 5.1.*

5. Other targets

5.1 CB_1R ligands [138]

To study novel therapeutic targets useful for the treatment of neurodegenerative diseases, I took part in a study focused on the identification of novel ligands of CB_1 receptor, which is implicated in pathological processes ranging from memory deficits to neurodegenerative disorders. These compounds, which feature a variously substituted biphenilic structure **C** (*figure 5.1*), [138] were designed and synthesized by combining the pharmacophoric portions of derivatives **A** and **B**. In particular, derivatives **A** (*figure 5.1*) characterized by a 5-aryl substituted nicotinamide core, were reported in literature as selective CB_1R antagonists. [139] They presented structural similarities with compounds **B** (*figure 5.1*) which displayed selective CB_2R antagonist activity. [140] Interestingly, two of the newly synthesized compounds enhanced the binding of the radioligand [^{3}H]CP55940 on CB_1R, suggesting an allosteric behaviour, which was then investigated through computational studies. The analysis of their binding poses in two different binding cavities of the CB_1R surface revealed a probable negative allosteric modulation. [138]

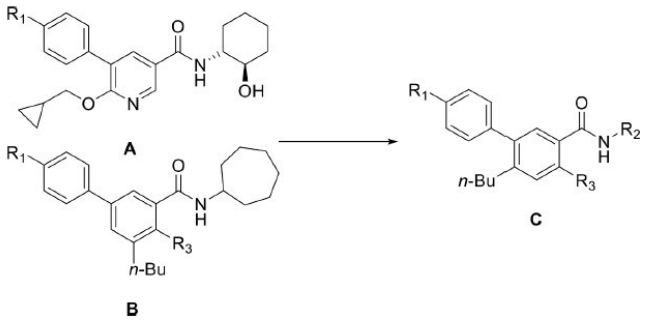

Figure 5.1 *Design and synthesis of novel variously substituted biphenilic compounds **C**.* [138]

5.2 CdK5 inhibitors [141]

I also took part in a project concerning a virtual screening of novel inhibitors of cyclin dependent kinase 5 (Cdk5), as innovative therapeutic target implicated in neurodegenerative processes, including PD and AD. Cdk5 is mainly located in the CNS, playing a key role in synaptic plasticity, neuronal survival and brain development. Its excessive activation lead to phosphorylation of an antioxidant enzyme Prx2 and to the to the formation of neurofibrillary tangles, which are associated with cell death in PD and AD, respectively. [142] Up to date, seliciclib and dinaciclib represent the prototype Cdk5 inhibitors in clinical trials. However, both of them are not selective, since they target other multiple kinases. [143] [144] In this contest, the identification of small molecules able to inhibit this enzyme is of great interest in the medicinal chemistry field. Employing a machine learning-based virtual screening protocol, this work provided the identification of two compounds, N-(2-(pyridin-3-yl)ethyl)-4-(1H-pyrrolo[2,3-b]pyridin-3-yl)piperidine-1-carboxamide **CPD1** and N^2-(3,4-dimethoxyphenyl)-N_6-(2-methoxyethyl)-7H-purine-2,6-diamine **CPD4** (*figure 5.2*), as potential lead compounds for the design and synthesis of novel potent and selective Cdk5 inhibitors. [141]

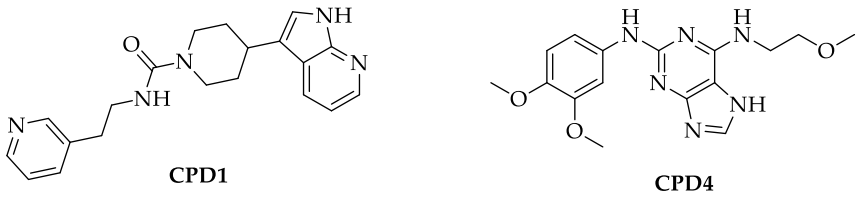

Figure 5.2. *Structures of derivatives **CPD1** and **CPD4** as potential lead compounds for the development of potent Cdk5 inhibitors.* [141]

5.3 Anedonia project [145]

During my abroad experience at University of Saskatchewan, I also took part on a project regarding the evaluation of the effect of some cannabinoid derivatives reported in literature in an *in vivo* mouse model of anhedonia. Anhedonia is referred to as the inability to feel pleasure from natural, non-drug sources, representing a core symptom of mood disorders such as depressive disorder [146] and anxiety disorders. [147] The endocannabinoid and the orexin systems play an important role in the multi-modal stress response, wakefulness, and mood. In particular, chronicstress seems to be correlated with a down-regulation of both systems, leading to the development of anhedonia. [148] [149] CB_1R activation following stress is correlated with antidepressant effects [150] On the other hand, orexin receptor antagonists are anxiolytic, inhibiting stress cue-associated hyperarousal in rodent models of post-traumatic stress disorder (PTSD). [151] [152] In order to provide additional information about the role of these systems in the onset and the development of the disease, some compounds able to target cannabinoid receptors and orexin receptors type 1 and 2 (, OX_1R, OX_2R) were selected and studied in 24-h restraint stress test (RST), which produced anhedonic behaviour in mice. [153] In particular, CP55940, Rimonabant, TCS 1102 (a dual orexin receptor antagonist [DORA]) (*figure 5.3*) and YNT 185 (an OX_2R agonist) (*figure 5.3*). The work demonstrated that combined stimulation of endocannabinoid and orexin systems provided an increase in consumption of sucrose because of an attenuation of chronic stress, confirming their involvement in anhedonia regulation. [145]

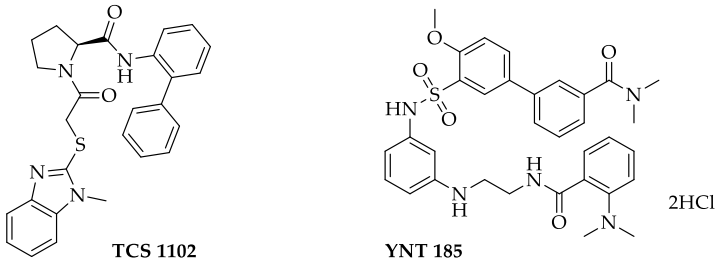

Figure 5.3 *Structures of derivatives* ***TCS 1102*** *and* ***YNT 185****.* [145]

6. Conclusion

In conclusion, during my phD, I designed and synthesized novel 3-benzylquinolin-2(1H)-ones, which resulted to be among the most potent and selective GPR55 ligands developed to date, representing potential tool compounds to understand the role of this receptor in neurodegenerative processes. In particular, derivative **1B** resulted as the most promising GPR55 agonist of the first set, showing not only high affinity (K_i = 14 nM) and potency (EC_{50} = 6.4 nM) toward GPR55, but also complete selectivity over both CBRs (K_i > 10,000 nM). In order to deepen the preliminary SAR for this class of molecules and provide further information about the features of the GPR55 binding site, we developed a second series of 3-benzyl-7-n-butyl-quinolin-2(1H)-ones. Among them, derivative **1C**, which differs from the reference compound **1B** only for the length of the alkyl side chain, displayed the greatest potency towards GPR55 within this new series (EC_{50} = 28 nM). Interestingly, this structural change shifted the functional activity from a pure agonism to an inverse agonist profile. Additionally, derivatives **3C** and **4D** shown K_i values of of 0.51 nM and 0.29 nM, respectively, resulting as ones of the compounds with the greatest observed affinity to date.

Moreover, I also designed and synthesized novel multitarget compounds, acting on both GPR55 and CB_2R, representing an innovative potential therapeutic option to counteract neurodegenerative diseases. Indeed, mutitarget approach has gained more and more relevance in the treatment of disorders which involve complex pathways, linked to the dysfunction of several biological targets. Among all the developed compounds, derivatives **18** and **22** proved to be able to simultaneously bind both GPR55 and CB_2R, with K_i values included in the low nanomolar range. Thus, these derivatives will be further investigated, in order to assess the affinity and the functional activity of separate isomers toward both targets.

7. Experimental section

7.1 Chemistry

7.1.1 Materials and methods

Unless otherwise stated, all reactions were performed under atmospheric air. All reagents, unless otherwise specified, were purchased from commercial sources (Sigma-Aldrich®, Alfa Aesar, Fluorochem) and used without further purification. All chemical reactions were monitored by thin-layer chromatography (TLC) on aluminium-backed silica gel 60 plates coated with the fluorescent indicator F_{254} (MERK) that were visualized under UV light (254-365 nm). The silica gel 60 Å (0.040-0.063 mm) used for flash chromatography was purchased from MERK and the evaporation was carried out in vacuo using a rotating evaporator. Compounds were characterized by ^{1}H-NMR and ^{13}C-NMR analysis: ^{1}H-NMR (400 MHz) and ^{13}C-NMR (100 MHz) spectra were recorded on a Bruker AVANCE III 400™ spectrometer. Chemical shifts (δ) were reported in parts per million related to the residual solvent signal, while coupling constants (*J*) were expressed in Hertz (Hz). Melting points were determined on a Büchi® B-540 melting point apparatus (TG: 1.0 °C). HRMS experiments were performed using a high resolution mass spectrometer Or-bitrap Q exactive plus (Thermo, San Jose, CA, USA) with HESI source. The mobile phase was constituted by a mixture of H_2O/AcOH (0.1% v/v) (eluent **A**) and ACN (eluent **B**). The flow rate was 0.8 mL/min. Retention times are given in minutes. Methods:

1. Isocratic elution with 70% of **B** and 30% of **A**.
2. Isocratic elution with 90% of **B** and 10% of **A**.
3. Gradient elution: 70% of **B** and 30% of **A** for 1 minute, then 90% of **B** and 10% of **A** in 6 minutes and it is maintained for 4 minutes. In 1 minutes the gradient return to 70% of **B** and 30% of **A** for 9 minute.

4. Gradient elution: 70% of **B** and 30% of **A** for 1 minute, then 90% of **B** and 10% of **A** in 9 minutes and it is maintained for 10 minutes. In 1 minutes the gradient return to 70% of **B** and 30% of **A** for 9 minute.

5. Gradient elution: 50% of **B** and 50% of **A** for 1 minute, then 70% of **B** and 30% of **A** in 10 minutes and it is maintained for 9 minutes. In 1 minutes the gradient return to 50% of **B** and 50% of **A** for 9 minute.

7.1.2 Synthetic procedures for novel GPR55 ligands

7.1.2.1 General procedure for the synthesis of variously substituted 1-alkyl-3-methoxy-5-nitrobenzene (6B, 6C, 6D, 6E)

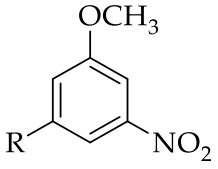

6B, 6C, 6D, 6E

Series B: R = -*n*butyl
Series C: R = -methyl
Series D: R = -*n*octyl
Series E: R = -isobutyl

General procedure: In a vial under nitrogen flux, commercial **3-bromo-5-nitro anisole 5** (1 eq) was dissolved in toluene (2 mL/mmol). Suitable alkylboronic acid (1.2 eq), NaOtBu (3 eq), distilled H_2O (0.2 mL/mmol), $Pd_2(dba)_3$ (0.02 eq) and Ruphos (0.04 eq) were added at room temperature. The vial was sealed and left under magnetic stirring at 80 °C overnight. After cooling to room temperature, the reaction mixture was filtered over silica pad and washed with AcOEt. The filtrate was evaporated under reduced pressure and the residue was purified by flash column chromatography on silica gel.

1-*n*-Butyl-3-methoxy-5-nitrobenzene

Starting from 300.0 mg of 3-bromo-5nitro anisole. Purification by flash column chromatography on silica gel (hexane/AcOEt 95:5). **6B** (210.0 mg, 1.00 mmol), white oil. Yield 78%.

^{1}H-NMR: (CDCl3) δ (ppm): 7.66-7.65 (m, 1H, ar); 7.55 (m, 1H, ar), 7.04-7.03 (m, 1H, ar), 3.87 (s, 3H, OCH_3), 2.66 (t, 2H, J = 7.7 Hz, $CH_2CH_2CH_2CH_3$), 1.66-1.58 (m, 2H, $CH_2CH_2CH_2CH_3$), 1.41-1.32 (m, 2H, $CH_2CH_2CH_2CH_3$), 0.93 (t, 3H, J = 7.3 Hz, $CH_2CH_2CH_2CH_3$).

1-Methyl-3-methoxy-5-nitrobenzene

Starting from 500.0 mg of 3-bromo-5nitro anisole. Purification by flash column chromatography on silica gel (hexane/AcOEt 94:6). **6C** (290.0 mg, 1.44 mmol), white oil. Yield 40%.

^{1}H-NMR: (CDCl3) δ (ppm): 7.65-7.64 (m, 1H, ar); 7.54-7.53 (m, 1H, ar); 7.04-7.03 (m, 1H); 3.86 (s, 3H, O-C*H*$_3$); 2.42 (s, 3H, CH$_3$).

1-*n*-Octyl-3-methoxy-5-nitrobenzene

Starting from 500.0 mg of 3-bromo-5nitro anisole. Purification by flash column chromatography on silica gel (hexane/AcOEt 96:4). **6D** (480.0 mg, 1.81 mmol), white oil. Yield 84%.

^{1}H-NMR: (CDCl3) δ (ppm): 7.66-7.65 (m, 1H, ar); 7.55-7.54 (m, 1H, ar), 7.04-7.03 (m, 1H, ar), 3.87 (s, 3H, O-C*H*$_3$), 2.65 (t, 2H, J = 7.6 Hz, C*H*$_2$-CH$_2$-CH$_2$-CH$_2$-CH$_2$-CH$_2$-CH$_2$-CH$_3$), 1.67-1.59 (m, 2H, CH$_2$-C*H*$_2$-CH$_2$-CH$_2$-CH$_2$-CH$_2$-CH$_2$-CH$_3$), 1.34-1.27 (m, 10H, CH$_2$-CH$_2$-C*H*$_2$-C*H*$_2$-C*H*$_2$-C*H*$_2$-C*H*$_2$-CH$_3$), 0.88 (t, 3H, J = 7.2 Hz, CH$_2$-CH$_2$-CH$_2$-CH$_2$-CH$_2$-CH$_2$-CH$_2$-C*H*$_3$).

1-Isobutyl -3-methoxy-5-nitrobenzene

Starting from 500.0 mg of 3-bromo-5nitro anisole. Purification by flash column chromatography on silica gel (hexane/AcOEt 96:4). **6E** (200.0 mg, 0.96 mmol), white oil. Yield 45%.

^{1}H-NMR: (CDCl3) δ (ppm): 7.64-7.63 (m, 1H, ar); 7.57-7.55 (m, 1H, ar), 7.02-7.01 (m, 1H, ar), 3.87 (s, 3H, O-C*H*$_3$), 2.53 (d, 2H, J = 7.2 Hz, C*H*$_2$CH(CH$_3$)$_2$), 1.96-1.86 (m, 1H, CH$_2$C*H*(CH$_3$)$_2$), 0.92 (d, 6H, J = 6.4 Hz, CH$_2$CH(C*H*$_3$)$_2$

7.1.2.2 General procedure for the synthesis of variously substituted 1-alkyl-3-methoxy-aniline (7B, 7C, 7D, 7E)

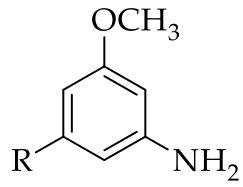

7B, 7C, 7D, 7E

Series B: R = -*n*butyl
Series C: R = -methyl
Series D: R = -*n*octyl
Series E: R = -isobutyl

General procedure: In a vial under nitrogen flux, intermediate **6B, 6C, 6D or 6E** (1 eq) was dissolved in a mixture of EtOH (12 mL/mmol) and H_2O (6 mL/mmol). After the addition of iron powder (0.62 g/mmol) and NH_4Cl (6 eq), the reaction mixture was stirred at reflux for 3h. After cooling to room temperature, the reaction mixture was filtered over celite pad and washed with EtOH. The filtrate was evaporated under *vacuo* and the residue was dissolved in AcOEt and washed with distilled H_2O. The organic phase was dried over Na_2SO_4, filtered and evaporated, affording desired compound, which was used for the next step without further purification.

1-*n*-Butyl-3-methoxy-aniline

Starting from 710.0 mg of intermediate 6B. **7B** (540.0 mg, 3.01 mmol). Brawn solid. Yield 95%.

^{1}H-NMR: (CDCl3) δ (ppm): 6.19-6.16 (m, 2H, ar), 6.10 (m, 1H, ar), 3.75 (s, 3H, OCH_3), 2.48 (t, 2H, J = 7.6 Hz, $CH_2CH_2CH_2CH_3$), 1.60-1.53 (m, 2H, $CH_2CH_2CH_2CH_3$), 1.37-1.32 (m, 2H, $CH_2CH_2CH_2CH_3$), 0.92 (t, 3H, J = 7.3 Hz, $CH_2CH_2CH_2CH_3$).

1-Methyl-3-methoxy-aniline

Starting from 460.0 mg of intermediate 6B. **7C** (350.0 mg, 2.55 mmol). Orange oil. Yield 93%.

^{1}H-NMR: (CDCl3) δ (ppm): 6.16-6.15 (m, 1H, ar); 6.14-6.13 (m, 1H, ar); 6.07-6.06 (m, 1H, ar); 3.76 (s, 3H, O-CH_3); 2.25 (s, 3H, CH_3).

1-*n*-Octyl-3-methoxy-aniline

Starting from 890.0 mg of intermediate 6B. **7D** (740.0 mg, 3.14 mmol). Brawn solid. Yield 94%.

^{1}H-NMR: (CDCl3) δ (ppm): 6.25-6.17 (m, 3H, ar), 3.76 (s, 3H, O-C*H*$_3$), 2.48 (t, 2H, J = 7.6 Hz, C*H*$_2$-CH$_2$-CH$_2$-CH$_2$-CH$_2$-CH$_2$-CH$_2$-CH$_3$), 1.59-1.54 (m, 2H, CH$_2$-C*H*$_2$-CH$_2$-CH$_2$-CH$_2$-CH$_2$-CH$_2$-CH$_3$), 1.33-1.24 (m, 10H, CH$_2$-CH$_2$-C*H*$_2$-C*H*$_2$-C*H*$_2$-C*H*$_2$-C*H*$_2$-CH$_3$), 0.87 (t, 3H, J = 7.2 Hz, CH$_2$-CH$_2$-CH$_2$-CH$_2$-CH$_2$-CH$_2$-CH$_2$-C*H*$_3$).

1-Isobutyl-3-methoxy-aniline

Starting from 740.0 mg of intermediate 6B. **7E** (550.0 mg, 3.07 mmol). Brawn solid. Yield 87%.

^{1}H-NMR: (CDCl3) δ (ppm): 6.15-6.09 (m, 3H, ar), 3.75 (s, 3H, O-C*H*$_3$), 2.34 (d, 2H, J = 7.2 Hz, C*H*$_2$CH(CH$_3$)$_2$), 1.89-1.79 (m, 1H, CH$_2$C*H*(CH$_3$)$_2$), 0.90 (d, 6H, J = 6.8 Hz, CH$_2$CH(C*H*$_3$)$_2$).

7.1.2.3 Synthesis of methyl 3-(2-hydroxyphenyl)propanoate (9)

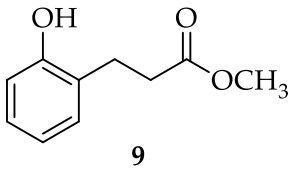

9

Procedure: Concentrated H_2SO_4 (0.28 mL) was added, under nitrogen atmosphere, to a solution of commercial **3,4-dihydrocumarine 8** (2.00 g, 13.5 mmol) in anhydrous MeOH and the resulting solution was heated overnight at reflux. Ambersep 900 OH resin was added until approximately pH 7.0 and then the solution was filtered and washed with AcOEt. The filtrate was evaporated under *vacuo* and the residue was dissolved in AcOEt and washed with distilled H_2O and brine. The organic phase was dried over Na_2SO_4, filtered and evaporated, affording intermediate **9** (2.14 g, 11.9 mmol) as yellow oil, which was used without further purification. Yield 88%.

^{1}H-NMR: (CDCl3) δ (ppm): 7.14-7.08 (m, 2H, ar), 7.07 (bs, 1H, OH), 6.89-6.85 (m, 2H, ar), 3.69 (s, 3H, O-C*H*$_3$), 2.91 (t, 2H, J = 6.8 Hz, CH_2CH_2(CO)), 2.72 (t, 2H, J = 7.2 Hz, CH_2CH_2(CO)).

7.1.2.4 Synthesis of methyl 3-(2-methoxyphenyl)propanoate (10)

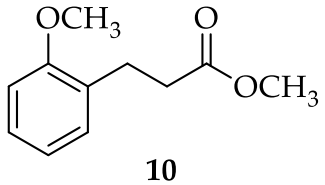

10

Procedure: Intermediate **9** (3.14 g, 17.4 mmol) was added to a suspension of NaH (60% dispersion in mineral oil) (1.44 g) in DMF (10 mL) at 0 °C and the reaction mixture was stirred at room temperature. After 30 minutes, CH_3I (2.17 mL, 34.8 mmol) was added dropwise at 0 °C and then the suspension was stirred at room temperature overnight. After the addition of about 10 mL of distilled H_2O, the aqueous phase was extracted with AcOEt. After washing with distilled H_2O, the organic phase was dried over anhydrous Na_2SO_4, filtered and evaporated, affording compound **10** (0.80 g, 4.07 mmol) as a transparent oil, which was used for the next step without further purification. Yield 92%.

^{1}H-NMR: (CDCl3) δ (ppm): 1H-NMR (CDCl3) δ (ppm): 7.22-7.13 (m, 2H, ar), 6.89-6.83 (m, 2H, ar), 3.96 (s, 3H, O-C*H*$_3$), 3.66 (s, 3H, O-C*H*$_3$), 2.94 (t, 2H, J = 7.6 Hz, CH_2CH_2(CO)), 2.61 (t, 2H, J = 7.6 Hz, C*H*$_2$$CH_2$(CO)).

7.1.2.5 Synthesis of 3-(2-Methoxyphenyl)propanoic acid (11)

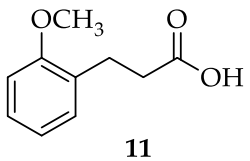

11

Procedure: LiOH (0.52 g, 21.76 mmol) was added to a solution of compound **10** (0.79 g, 4.07 mmol) in MeOH (16 mL)/H_2O (5 mL) and the reaction mixture was stirred at room temperature for 3h. MeOH was evaporated under reduced pressure and the residue was diluted with distilled H_2O and washed with AcOEt. The aqueous phase was acidified with HCl 1M until approximately pH 4 and the solution was extracted with AcOEt. The organic phase was dried over Na_2SO_4, filtered and evaporated, to afford derivative **11** (0.52 g, 2.88 mmol) as a white solid, which was used without further purification. Yield 71%.

^{1}H-NMR: (CDCl3) δ (ppm): 7.23-7.15 (m, 2H, ar), 6.90-6.84 (m, 2H, ar), 3.82 (s, 3H, O-C*H*$_3$), 2.95 (t, 2H, J = 7.6 Hz, CH_2CH_2COOH), 2.61 (t, 2H, J = 7.6 Hz, CH_2CH_2COOH).

7.1.2.6 Synthesis of 3-(2-Methoxyphenyl)propanoic acid (12)

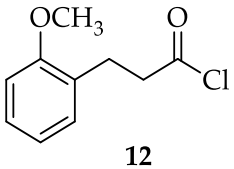

12

Procedure: In a vial, intermediate **11** (300.0 mg, 1.65 mmol) was dissolved in toluene (4.0 mL) under nitrogen flux. $SOCl_2$ (0.1 mL, 1.10 mmol) was added at room temperature and the vial was sealed and left under magnetic stirring at reflux for 3 h. The solvent and the excess of unreacted $SOCl_2$ were then removed under nitrogen flux, affording the desired compound **12** without any further purification as a brownish oil. No data are available for the yield due to the chemical instability of the compound.

^{1}H-NMR: δ (ppm): No data are available due to the chemical instability of the compound.

7.1.2.7 Synthesis of 3-(2-Methoxyphenyl)propanoic acid (17)

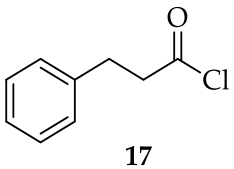

17

Procedure: In a reaction vial, compound **16** (395 mg, 2.63 mmol) was dissolved in toluene (5.6 mL). Under nitrogen flux, $SOCl_2$ (0.38 mL, 5.26 mmol) was added, and the reaction mixture was allowed to react in the sealed vial, stirring at reflux (~110 °C) for 3 h. After cooling the solution, the solvent was evaporated and the unreacted $SOCl_2$ was removed under inert atmosphere. The desired compound **17** was obtained without any further purification as a brownish oil. No data are available for the yield due to the chemical instability of the compound.

^{1}H-NMR: δ (ppm): No data are available due to the chemical instability of the compound.

7.1.2.8 General procedure for the synthesis of variously substituted 5-methoxyphenyl)-3-(2-methoxyphenyl)propanamide (13B, 13C, 13D, 13E, 13F)

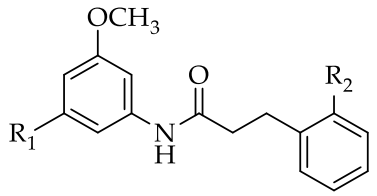

13B, 13C, 13D, 13E, 13F

Series B: R_1 = -*n*butyl; R_2 = -OCH_3
Series C: R_1 = -methyl; R_2 = -OCH_3
Series D: R_1 = -*n*octyl; R_2 = -OCH_3
Series E: R_1 = -isobutyl; R_2 = -OCH_3
Series F: R_1 = -*n*butyl; R_2 = -H

Procedure: In a round bottom flask, under nitrogen atmosphere, Et_3N (0.2 mL/mmol) was added to a solution of intermediate **7B**, **7C**, **7D** or **7E** (1 eq) in CH_2Cl_2 (7 mL/mmol). The acyl chloride **12** or **17** (1.2 eq) was added dropwise and the reaction was stirring at room temperature overnight. The resulting solution was diluted with CH_2Cl_2 and washed with an aqueous solution of NaOH (10% m/v), HCl 1M and distilled H_2O. The organic phase was dried over Na_2SO_4, filtered and evaporated, affording the desire derivative **13B**-**13F**, which was used without further purification.

N-(3-*n*-Butyl-5-methoxyphenyl)-3-(2-methoxyphenyl)propanamide

Starting from 450 mg of intermediate 7B. **13B** (370 mg, 1.26 mmol). Brown solid. Yield >99%.

^{1}H-NMR: (CDCl3) δ (ppm): 7.24-7.18 (m, 2H, ar), 7.06-7.03 (m, 2H, ar), 6.91-6.86 (m, 2H, ar), 6.74 (s, 1H, ar), 6.48 (bs, 1H, exchangeable, N*H*), 3.84 (s, 3H, O-C*H*$_3$), 3.78 (s, 3H, O-C*H*$_3$), 3.04 (t, 2H, J = 7.3 Hz, (C=O)C*H*$_2$CH$_2$), 2.63 (t, 2H, J = 7.8 Hz, (C=O)CH$_2$C*H*$_2$), 2.53 (t, 2H, J = 7.8 Hz, C*H*$_2$CH$_2$CH$_2$CH$_3$), 1.57-1.53 (m, 2H, CH$_2$C*H*$_2$CH$_2$CH$_3$), 1.36-1.31 (m, 2H, CH$_2$CH$_2$C*H*$_2$CH$_3$), 0.91 (t, 3H, J = 7.3 Hz, CH$_2$CH$_2$CH$_2$C*H*$_3$).

N-(3-Methyl-5-methoxyphenyl)-3-(2-methoxyphenyl)propanamide

Starting from 500.0 mg of intermediate 7B. **13C** (1.08 g, 3.61 mmol). Brown solid. Yield >99%.

^{1}H-NMR: (CDCl3) δ (ppm): 7.23-7.17 (m, 2H, ar), 7.04-7.01 (m, 2H, ar), 6.91-6.85 (m, 2H, ar), 6.76 (s, 1H, ar), 6.46 (bs, 1H, exchangeable, N*H*), 3.84 (s, 3H, O-C*H*$_3$), 3.77 (s, 3H, O-C*H*$_3$), 3.02 (t, 2H, J = 7.4 Hz, (C=O)C*H*$_2$CH$_2$), 2.62 (t, 2H, J = 7.4 Hz, (C=O)CH$_2$C*H*$_2$), 2.28 (s, 3H, CH$_3$).

N-(3- *n*-Octyl-5-methoxyphenyl)-3-(2-methoxyphenyl)propanamide

Starting from 740.0 mg of intermediate 7B. **13D** (1.24 g, 3.12 mmol). Brown solid. Yield >99%.

^{1}H-NMR: (CDCl3) δ (ppm): 7.23-7.16 (m, 2H, ar), 7.11-7.04 (m, 2H, ar), 6.91-6.85 (m, 2H, ar), 6.74 (s, 1H, ar); 6.47 (bs, 1H, exchangeable, N*H*), 3.83 (s, 3H, O-C*H*$_3$); 3.78 (s, 3H, O-C*H*$_3$), 3.03 (t, 2H, CH$_2$, J = 7.6 Hz, (C=O)C*H*$_2$CH$_2$), 2.63 (t, 2H, J = 7.2 Hz, (C=O)C*H*$_2$CH$_2$), 2.52 (t, 2H, J = 7.6 Hz, C*H*$_2$-CH$_2$-CH$_2$-CH$_2$-CH$_2$-CH$_2$-CH$_2$-CH$_3$), 1.59-1.55 (m, 2H, CH$_2$-C*H*$_2$-CH$_2$-CH$_2$-CH$_2$-CH$_2$-CH$_2$-CH$_3$), 1.29-1.26 (m, 10H, CH$_2$-CH$_2$-C*H*$_2$-C*H*$_2$-C*H*$_2$-C*H*$_2$-C*H*$_2$-CH$_3$), 0.88 (t, 2H, J = 6.8 Hz, CH$_2$-CH$_2$-CH$_2$-CH$_2$-CH$_2$-CH$_2$-CH$_2$-C*H*$_3$).

N-(3-Isobutyl-5-methoxyphenyl)-3-(2-methoxyphenyl)propanamide

Starting from 540.0 mg of intermediate 7B. **13E** (1.02 g, 2.99 mmol). Brown solid. Yield >99%.

^{1}H-NMR: (CDCl3) δ (ppm): 7.24-7.18 (m, 3H, ar), 7.11 (m, 3H, ar), 6.91-6.88 (m, 2H, ar), 6.71 (s, 1H, ar), 6.45 (bs, 1H, exchangeable, N*H*), 3.83 (s, 3H, O-C*H*$_3$), 3.77 (s, 3H, O-C*H*$_3$), 3.04 (t, 2H, J = 7.6 Hz, (C=O)C*H*$_2$CH$_2$), 2.64 (t, 2H, J = 7.6 Hz, (C=O)CH$_2$C*H*$_2$), 2.62 (d, 2H, J = 7.2 Hz, C*H*$_2$CH(CH$_3$)$_2$), 1.89-1.79 (m, 1H, CH$_2$C*H*(CH$_3$)$_2$), 0.89 (t, 6H, J = 6.8 Hz, CH$_2$CH(C*H*$_3$)$_2$).

N-(3-*n*-butyl-5-methoxyphenyl)-3-phenylpropanamide

Starting from 350.0 mg of intermediate 7B. **13F** (570.0 mg, 1.83 mmol). Brown solid. Yield 94%.

^{1}H-NMR: (CDCl3) δ (ppm): 7.33-7.26 (m, 2H, ar), 7.25-7.18 (m, 4H, ar), 7.04 (s, 1H, ar), 6.74 (bs, 1H, exchangeable, N*H*), 6.48 (s, 1H, ar), 3.78 (s, 3H, O-C*H*$_3$), 3.05 (t, 2H, J = 7.4 Hz, (C=O)C*H*$_2$CH$_2$), 2.64 (t, 2H, J = 7.4 Hz, (C=O)CH$_2$C*H*$_2$), 2.53 (t, 2H, J = 7.6 Hz, C*H*$_2$CH$_2$CH$_2$CH$_3$), 1.59-1.51 (m, 2H, CH$_2$C*H*$_2$CH$_2$CH$_3$), 1.36-1.30 (m, 2H, CH$_2$CH$_2$C*H*$_2$CH$_3$), 0.91 (t, 3H, J = 7.3 Hz, CH$_2$CH$_2$CH$_2$C*H*$_3$).

7.1.2.9 General procedure for the synthesis of variously substituted 2-chloro-5-methoxy-3-(2-methoxybenzyl)quinoline (14B, 14C, 14D, 14E, 14F)

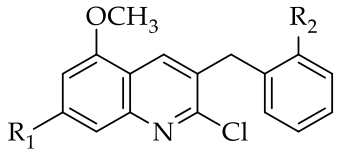

14B, 14C, 14D, 14E, 14F

Series B: R_1 = -*n*butyl; R_2 = -OCH_3
Series C: R_1 = -methyl; R_2 = -OCH_3
Series D: R_1 = -*n*octyl; R_2 = -OCH_3
Series E: R_1 = -isobutyl; R_2 = -OCH_3
Series F: R_1 = -*n*butyl; R_2 = -H

Procedure: In a vial, compound **14B**, **14C**, **14D**, **14E** or **14F** (1 eq) was dissolved in DMF (1 eq). $POCl_3$ (7 eq) was added at 10 °C under nitrogen flux and the vial was sealed and left under magnetic stirring at 80 °C overnight. The reaction mixture was poured out on ice, diluted with distilled H_2O and extracted with CH_2Cl_2. The organic phase was dried over Na_2SO_4, filtered, evaporated and the residue was purified by flash column chromatography on silica gel.

7-n-Butyl-2-chloro-5-methoxy-3-(2-methoxybenzyl)quinoline

Starting from 200.0 mg of intermediate 13B. Purification by flash column chromatography on silica gel (hexane/AcOEt 95:5). **14B** (70.0 mg, 0.19 mmol). White solid. Yield 32%.

m.p.: 82-84 °C.

^{1}H-NMR: ($CDCl_3$) δ (ppm): 8.19 (s, 1H, H4); 7.38 (s, 1H, H6'); 7.26-7.25 (m, 1H, H5'), 7.06-7.05 (m, 1H, H3'), 6.91-6.89 (m, 2H, H8, H4'), 6.65 (s, 1H, H6), 4.19 (s, 2H, H11), 3.92 (s, 3H, C2'-OC*H*$_3$), 3.82 (s, 3H, C5-OC*H*$_3$), 2.76 (t, 2H, J = 7.6 Hz, C*H*$_2$$CH_2CH_2CH_3$), 1.70-1.66 (m, 2H, CH_2C*H*$_2$$CH_2CH_3$), 1.41-1.36 (m, 2H, CH_2CH_2C*H*$_2$$CH_3$), 0.92 (t, 3H, J = 7.2 Hz, $CH_2CH_2CH_2$C*H*$_3$).

^{13}C-NMR: ($CDCl_3$) δ (ppm): 157.49 (C2'), 154.62 (C5), 152.24 (C2), 147.58 (C10), 145.30 (C7), 133.30 (C6'), 130.59 (C11), 130.30 (C3), 127.91 (C4'), 127.14 (C1'), 120.53 (C8), 118.83

(C5'), 118.38 (C9), 110.44 (C3'), 106.19 (C6), 55.55 (C5-OCH_3), 55.32 (C2'-OCH_3), 36.38 (C1''), 33.52 (C2''), 33.01 (C11), 22.28 (C3''), 13.95 (C4'').

HRMS (HESI): *m/z* calculated for $C_{22}H_{24}ClNO_2$ + H+ $[M + H]^+$: 370.15695. Found: 370.15683.

HPLC analysis: method 1, retention time = 16.65 min; peak area, 97.1% (280 nm).

7-Methyl-2-chloro-5-methoxy-3-(2-methoxybenzyl)quinoline

Starting from 320.0 mg of intermediate 13C. Purification by flash column chromatography on silica gel (CH_2Cl_2/ hexane 74:26). **14C** (140.0 mg, 0.468 mmol). White solid. Yield 22%.

m.p.: 158-160 °C.

^{1}H-NMR: ($CDCl_3$) δ (ppm): 8.18 (s, 1H, H4); 7.36 (s, 1H, H6'); 7.27-7.23 (m, 1H, H5'); 7.05 (d, 1H, H3', J = 6.8 Hz); 6.91-6.88 (m, 2H, H8, H4'); 6.63 (s, 1H, H6); 4.19 (s, 2H, H11); 3.91 (s, 3H, C2'-OCH_3); 3.82 (s, 3H, C5-OCH_3); 2.50 (s, 3H, CH_3)

^{13}C-NMR: ($CDCl_3$) δ (ppm): 157.49 (C2'); 154.55 (C5); 152.26 (C2); 147.58 (C10); 140.40 (C7); 133.27 (C6'); 130.56 (C11); 130.32 (C3); 127.93 (C4'); 127.11 (C1'); 120.54 (C8); 119.43 (C5'); 118.18 (C9); 110.45 (C3'); 106.82 (C6); 55.66 (C5-OCH_3); 55.33 (C2'-OCH_3); 33.52 (C1''); 22.53 (C11).

HRMS (HESI): *m/z* calculated for $C_{19}H_{18}ClNO_2$ + H+ $[M + H]^+$: 327.10265 Found: 327,1095.

HPLC analysis: method 1, retention time = 9.20 min; peak area, 99% (280 nm).

7-n-Octyl-2-chloro-5-methoxy-3-(2-methoxybenzyl)quinoline

Starting from 400.0 mg of intermediate 13D. Purification by flash column chromatography on silica gel (hexane/AcOEt 96:4). **14D** (205.0 mg, 0.48 mmol). White solid. Yield 47.5%.

m.p.: 56-58 °C.

^{1}H-NMR: (CDCl3) δ (ppm): 8.20 (s, 1H, H4), 7.40 (s, 1H, H6'), 7.26-7.22 (m, 1H, H5'), 7.06 (d, 1H, H3', J = 7.2 Hz), 6.91-6.88 (m, 2H, H8, H4'), 6.65 (s, 1H, H6), 4.20 (s, 2H, H11), 3.91 (s, 3H, C2'-OC*H*$_3$), 3.80 (s, 3H, C5-OC*H*$_3$), 2.75 (t, 2H, J = 7.6 Hz, C*H*$_2$-CH$_2$-CH$_2$-CH$_2$-CH$_2$-CH$_2$-CH$_2$-CH$_3$), 1.74-1.67 (m, 2H, CH$_2$-C*H*$_2$-CH$_2$-CH$_2$-CH$_2$-CH$_2$-CH$_2$-CH$_3$), 1.34-1.28 (m, 10H, CH$_2$-CH$_2$-C*H*$_2$-C*H*$_2$-C*H*$_2$-C*H*$_2$-C*H*$_2$-C*H*$_3$), 0.89 (t, 3H, J = 7.2 Hz, CH$_2$-CH$_2$-CH$_2$-CH$_2$-CH$_2$-CH$_2$-CH$_2$-C*H*$_3$).

^{13}C-NMR: (CDCl3) δ (ppm): 157.50 (C2'), 154.62 (C5), 152.22 (C2), 147.57 (C10), 145.37 (C7), 133.31 (C6'), 130.59 (C4), 130.30 (C3), 127.91 (C4'), 127.16 (C1'), 120.54 (C8), 118.81 (C5'), 118.39 (C9), 110.46 (C3'), 106.21 (C6), 55.66 (C5-OCH$_3$), 55.32 (C2'-OCH$_3$), 36.70 (C1''), 33.52 (C11, C2''), 31.88 (C3''), 30.87 (C4''), 29.48 (C5''), 29.25 (C6''), 22.67 (C7''), 14.10 (C8'').

HRMS (HESI): *m/z* calculated for $C_{26}H_{32}ClNO_2$ + H+ $[M + H]^+$: 425,2122. Found: 425,2190.

HPLC analysis: method 2, retention time = 12.07 min; peak area, 97.2% (280 nm).

7-Isobutyl-2-chloro-5-methoxy-3-(2-methoxybenzyl)quinoline

Starting from 575.0 mg of intermediate 13E. Purification by flash column chromatography on silica gel (hexane/AcOEt 94:6). **14E** (215.0 mg, 0.58 mmol). White solid. Yield 35%.

m.p.: 95-97 °C.

^{1}H-NMR: (CDCl3) δ (ppm): 8.20 (s, 1H, H4), 7.36 (s, 1H, H6'), 7.27-7.23 (m, 1H, H5'), 7.07-7.06 (m, 1H, H3'), 6.91-6.88 (m, 2H, H8, H4'), 6.65 (s, 1H, H6), 4.20 (s, 2H, H11), 3.92 (s, 3H, C2'-OC*H*$_3$), 3.82 (s, 3H, C5-OC*H*$_3$), 2.62 (d, 2H, J = 6.8 Hz, C*H*$_2$CH(CH$_3$)$_2$), 2.02-1.95 (m, 1H, CH$_2$C*H*(CH$_3$)$_2$), 0.93 (d, 6H, J = 6.8 Hz, CH$_2$CH(C*H*$_3$)$_2$).

^{13}C-NMR: (CDCl3) δ (ppm): 157.49 (C2'), 154.54 (C5), 152.24 (C2), 147.46 (C10), 144.16 (C7), 133.29 (C6'), 130.63 (C11), 130.30 (C3), 127.93 (C4'), 127.11 (C1'), 120.55 (C8), 119.73

(C5'), 118.42 (C9), 110.45 (C3'), 106.61 (C6), 55.66 (C5-O*C*H$_3$), 55.32 (C2'-O*C*H$_3$), 46.22 (C1''), 33.53 (C11), 29.94 (C2''), 22.45 (C3'').

HRMS (HESI): *m*/*z* calculated for $C_{22}H_{24}ClNO_2$ + H+ $[M + H]^+$: 369,1496. Found: 369,1567.

HPLC analysis: method 1, retention time = 22.49 min; peak area, 95.3% (280 nm).

3-benzyl-5-*n*-butyl-2-chloro-7-methoxyquinoline

Starting from 460.0 mg of intermediate 13F. Purification by flash column chromatography on silica gel (hexane/AcOEt 92:8). **14F** (130.0 mg, 0.38 mmol). White solid. Yield 26%.

m.p.: 50-52 °C.

^{1}H-NMR: ($CDCl_3$) δ (ppm): 7.87 (s, 1H, H4), 7.37-7.21 (m, 5H, H3', H4', H5'), 7.19 (d, 1H, J = 2.4 Hz, H2'), 6.99 (d, 1H, J = 2.4 Hz, H6'), 4.22 (s, 2H, H11), 3.90 (s, 3H, C2'-OC*H*$_3$), 2.82 (t, 2H, J = 7.6 Hz, C*H*$_2$CH$_2$CH$_2$CH$_3$), 1.59-1.51 (m, 2H, CH$_2$C*H*$_2$CH$_2$CH$_3$), 1.37-1.28 (m, 2H, CH$_2$CH$_2$C*H*$_2$CH$_3$), 0.88 (t, 3H, J = 7.2 Hz, CH$_2$CH$_2$CH$_2$C*H*$_3$)

^{13}C-NMR: ($CDCl_3$) δ (ppm): 154.60 (C2', C5), 152.00 (C2), 147.68 (C10), 145.68 (C7), 138.73 (C6'), 133.73 (C11), 130.84 (C3), 128.96 (C4'), 128.59 (C1'), 126.51 (C8), 118.82 (C5'), 118.29 (C9), 106.37 (C6, C3'), 55.69 (C5-O*C*H$_3$), 39.26 (C1''), 36.40 (C2''), 33.01 (C11), 22.29 (C3''), 13.95 (C4'').

HRMS (HESI): *m*/*z* calculated for $C_{21}H_{22}ClNO$ + H+ $[M + H]^+$: 339.13904. Found: 339.14630.

HPLC analysis: method 1, retention time = 22.01 min; peak area, 93.6% (280 nm).

7.1.2.10 General procedure for the synthesis of variously substituted 5-methoxy-3-(2-methoxybenzyl)quinolin-2(1H)-one (1B, 1C, 1D, 1E, 1F)

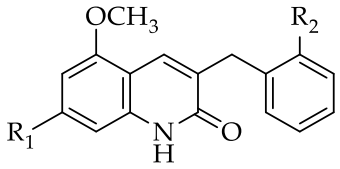

1B, 1C, 1D, 1E, 1F

Series B: R_1 = -*n*butyl; R_2 = -OCH_3
Series C: R_1 = -methyl; R_2 = -OCH_3
Series D: R_1 = -*n*octyl; R_2 = -OCH_3
Series E: R_1 = -isobutyl; R_2 = -OCH_3
Series F: R_1 = -*n*butyl; R_2 = -H

Procedure: In a reaction vial, HCl 6N (16 mL/mmol) was added to suitable intermediate **1B**, **1C**, **1D**, **1E** or **1F** (1 eq) and the resulting mixture was heated at reflux for 24 h. After cooling to room temperature, the reaction mixture was diluted with distilled H_2O and extracted with CH_2Cl_2. The organic phase was dried over anhydrous Na_2SO_4, filtered, evaporated and the residue was purified by flash column chromatography on silica gel.

7-*n*-Butyl-5-methoxy-3-(2-methoxybenzyl)quinolin-2(1H)-one

Starting from 100.0 mg of intermediate 14B. Purification by flash column chromatography on silica gel (hexane/AcOEt 70:30). **1B** (100.0 mg, 0.28 mmol). White solid. Yield 53%.

m.p.: 208-210 °C.

^{1}H-NMR: ($CDCl_3$) δ (ppm): 11.29 (bs, 1H, exchangeable, N*H*), 7.82 (s, 1H, H4), 7.30-7.28 (m, 1H, H6'), 7.24-7.19 (m, 1H, H5'), 6.92-6.88 (m, 2H, H3', H4'), 6.65 (s, 1H, H8), 6.40 (s, 1H, H6), 4.00 (s, 2H, H11), 3.86 (s, 3H, C2'-OC*H*$_3$), 3.82 (s, 3H, C5-OC*H*$_3$), 2.65 (t, 2H, J = 7.6 Hz, C*H*$_2$CH$_2$CH$_2$CH$_3$), 1.66-1.59 (m, 2H, CH$_2$C*H*$_2$CH$_2$CH$_3$), 1.42-1.35 (m, 2H, CH$_2$CH$_2$C*H*$_2$CH$_3$), 0.92 (t, 3H, J = 7.2 Hz, CH$_2$CH$_2$CH$_2$C*H*$_3$).

^{13}C-NMR: ($CDCl_3$) δ (ppm): 157.72 (C2), 155.46 (C5, C2'), 145.99 (C7), 138.57 (C10), 132.21 (C6'), 130.89 (C4), 127.95 (C3), 127.51 (C1', C4'), 120.49 (C8), 110.52 (C5'), 109.33 (C9),

107.43 (C3′), 103.45 (C6), 55.55 (C5-OCH_3), 55.40 (C2′-OCH_3), 36.40 (C1″), 33.42 (C11), 30.37 (C2″), 22.46 (C3″), 13.96 (C4″).

HRMS (HESI): *m*/*z* calculated for $C_{22}H_{25}NO_3$ + H+ [M + H]+: 352.19084. Found: 352.19072.

HPLC analysis: method 1, retention time = 11.01 min; peak area, 95.2% (280 nm).

7-Methyl-5-methoxy-3-(2-methoxybenzyl)quinolin-2(1H)-one

Starting from 80.0 mg of intermediate 14C. Purification by flash column chromatography on silica gel (hexane/AcOEt/ MeOH 70:28:2). **1C** (27.4 mg, 0.089 mmol). White solid. Yield 37%.

m.p.: 250-252 °C.

^{1}H-NMR: ($CDCl_3$) δ (ppm): 10.75 (bs, 1H, exchangeable, N*H*); 7.81 (s, 1H, H4); 7.28-7.19 (m, 2H, H5′, H6′); 6.90 (t, 2H, J = 7.6 Hz, H3′, H4′); 6.66 (s, 1H, H8); 6.39 (s, 1H, H6); 3.98 (s, 2H, H11); 3.84 (s, 3H, C2′-OC*H*$_3$); 3.81 (s, 3H, C5-OC*H*$_3$); 2.40 (s, 3H, CH_3).

^{13}C-NMR: ($CDCl_3$) δ (ppm): 164.06 (C2); 157.71 (C5); 155.43 (C2′); 140.91 (C7); 138.55 (C10); 132.15 (C6′); 130.85 (C4); 129.80 (C3); 127.91 (C1′); 127.52 (C4′); 120.51 (C8); 110.54 (C5′); 109.08 (C9); 107.95 (C3′); 104.18 (C6); 55.55 (C5-OCH_3); 55.40 (C2′-OCH_3); 30.34 (C1′′); 22.28 (C11).

HRMS (HESI): *m*/*z* calculated for $C_{19}H_{19}NO_3$ + H+ [M + H]$^+$: 309,1365. Found: 309,1439.

HPLC analysis: method 1, retention time = 3.37 min; peak area, 99.7% (280 nm).

7-*n*-Octyl-5-methoxy-3-(2-methoxybenzyl)quinolin-2(1H)-one

Starting from 200.0 mg of intermediate 14D. Purification by flash column chromatography on silica gel (hexane/AcOEt 70:30). **1D** (140.0 mg, 0.34 mmol). White solid. Yield 73%.

m.p.: 145-147 °C.

^{1}H-NMR: (CDCl3) δ (ppm): 11.43 (bs, 1H, exchangeable, N*H*), 7.84 (s, 1H, H4), 7.30-7.20 (m, 1H, H5', H6'), 6.92-6.88 (m, 2H, H3', H4'), 6.72 (s, 1H, H8), 6.40 (s, 1H, H6), 4.00 (s, 2H, H11), 3.85 (s, 3H, C2'-OC*H*$_3$), 3.82 (s, 3H, C5-OC*H*$_3$), 2.64 (t, 2H, J = 7.6 Hz, C*H*$_2$-CH$_2$-CH$_2$-CH$_2$-CH$_2$-CH$_2$-CH$_2$-CH$_3$), 1.67-1.60 (m, 2H, CH$_2$-C*H*$_2$-CH$_2$-CH$_2$-CH$_2$-CH$_2$-CH$_2$-CH$_3$), 1.31-1.25 (m, 10H, CH$_2$-CH$_2$-C*H*$_2$-C*H*$_2$-C*H*$_2$-C*H*$_2$-C*H*$_2$-CH$_3$), 0.86 (t, 3H, J = 7.2 Hz, CH$_2$-CH$_2$-CH$_2$-CH$_2$-CH$_2$-CH$_2$-CH$_2$-C*H*$_3$).

^{13}C-NMR: (CDCl3) δ (ppm): 164.82 (C2), 157.82 (C2'), 155.44 (C5), 146.02 (C10), 138.92 (C7), 132.30 (C6'), 131.00 (C4), 129.76 (C3), 128.16 (C4'), 127.56 (C1'), 120.56 (C8), 110.60 (C5'), 109.45 (C9), 107.88 (C3'), 103.40 (C6), 55.59 (C5-OCH$_3$), 55.47 (C2'-OCH$_3$), 36.83 (C1''), 31.98 (C11), 31.45 (C2''), 30.51 (C3''), 29.61 (C4''), 29.55 (C5''), 29.38 (C6''), 22.76 (C7''), 14.20 (C8'').

HRMS (HESI): *m*/*z* calculated for C$_{26}$H$_{33}$NO$_3$ + H+ [M + H]$^+$: 407,2460. Found: 407,2535.
HPLC analysis: method 1, retention time = 19.74 min; peak area, 98% (280 nm).

7-Isobutyl-5-methoxy-3-(2-methoxybenzyl)quinolin-2(1H)-one

Starting from 120.0 mg of intermediate 14E. Purification by flash column chromatography on silica gel (hexane/AcOEt 70:30). **1E** (60.0 mg, 0.17 mmol). White solid. Yield 53%.

m.p.: 231-233 °C.

^{1}H-NMR: (CDCl3) δ (ppm): 10.78 (bs, 1H, exchangeable, N*H*), 7.84 (s, 1H, H4), 7.29-7.20 (m, 2H, H5', H6'), 6.92-6.89 (m, 2H, H3', H4'), 6.64 (s, 1H, H8), 6.38 (s, 1H, H6), 3.99 (s, 2H, H11), 3.86 (s, 3H, C2'-OC*H*$_3$), 3.83 (s, 3H, C5-OC*H*$_3$), 2.51 (d, 2H, J = 7.2 Hz, C*H*$_2$CH(CH$_3$)$_2$), 1.96-1.89 (m, 1H, CH$_2$C*H*(CH$_3$)$_2$), 0.92 (t, 3H, J = 6.4 Hz, CH$_2$CH(C*H*$_3$)$_2$).

^{13}C-NMR: (CDCl3) δ (ppm): 158.02 (C2), 155.41 (C5, C2'), 144.95 (C7), 138.21 (C10), 132.21 (C6'), 130.87 (C4), 127.80 (C3), 127.57 (C1', C4'), 120.52 (C8), 110.52 (C5', C9), 107.86

(C3′), 104.12 (6), 55.58 (C5-OCH_3), 55.41 (C2′-OCH_3), 46.05 (C1′′), 30.33 (C11), 30.14 (C2′′), 22.44 (C3′′).

HRMS (HESI): *m*/*z* calculated for $C_{22}H_{25}NO_3$ + H+ $[M + H]^+$: 351,1834. Found: 351,1902.
HPLC analysis: method 1, retention time = 5.58 min; peak area, 99.1% (280 nm).

3-benzyl-7-*n*-butyl-5-methoxyquinolin-2(1*H*)-one

Starting from 120.0 mg of intermediate 14F. Purification by flash column chromatography on silica gel (hexane/AcOEt 70:30). **1F** (30.0 mg, 0.09 mmol). White solid. Yield 27%.

m.p.: 194-196 °C.

^{1}H-NMR: ($CDCl_3$) δ (ppm): 11.05-10.92 (bs, 1H, exchangeable, N*H*), 7.91 (s, 1H, H4), 7.38-7.27 (m, 4H, H2′, H3′, H5′, H6′), 7.20 (1H, t, J =7.2 Hz, H4′), 6.68 (s, 1H, H8), 6.43 (s, 1H, H6), 3.99 (s, 2H, H11), 3.88 (s, 3H, C2′-OCH_3), 2.65 (t, 2H, J = 7.6 Hz, C$H_2$$CH_2CH_2CH_3$), 1.67-1.59 (m, 2H, CH_2C$H_2$$CH_2CH_3$), 1.40-1.36 (m, 2H, CH_2CH_2C$H_2$$CH_3$), 0.94 (t, 3H, J = 7.3 Hz, $CH_2CH_2CH_2$CH_3).

^{13}C-NMR: ($CDCl_3$) δ (ppm): 164.21 (C2), 155.51 (C5, C2′), 146.86 (C7), 139.76 (C10), 138.50 (C6′), 133.43 (C4), 129.87 (C3), 129.29 (C1′), 128.54 (C4′), 126.32 (C8), 109.77 (C9, C5′), 107.96 (C3′), 103.97 (C6), 55.71 (C5-OCH_3), 36.57 (C1′′), 36.37 (C11), 33.47 (C2′′), 22.57 (C3′′), 14.09 (C4′′).

HRMS (HESI): *m*/*z* calculated for $C_{22}H_{25}NO_3$ + H+ $[M + H]^+$: 321.17288. Found: 321.18031.
HPLC analysis: method 1, retention time = 5.48 min; peak area, 95.7% (280 nm).

7.1.2.11 General procedure for the synthesis of variously substituted 5-methoxy-3-(2-methoxybenzyl)-1-methylquinolin-2(1H)-ones (2B, 2C, 2D, 2E, 2F)

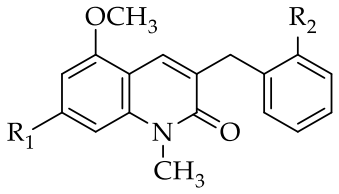

2B, 2C, 2D, 2E, 2F

Series B: R_1 = -*n*butyl; R_2 = -OCH_3
Series C: R_1 = -methyl; R_2 = -OCH_3
Series D: R_1 = -*n*octyl; R_2 = -OCH_3
Series E: R_1 = -isobutyl; R_2 = -OCH_3
Series F: R_1 = -*n*butyl; R_2 = -H

General procedure: NaH (48 mg/mmol) was added to a solution of compound **1B**, **1C**, **1D**, **1E** or **1F** (1 eq) in a mixture of anhydrous DMF (5 mL/mmol) and DME (14 mL/mmol), under nitrogen atmosphere. Upon the completion of gas evolution, CH_3I (1.2 eq) was added and the solution was stirred at room temperature overnight. The reaction mixture was diluted with distilled H_2O, to remove the excess of NaH, and extracted with CH_2Cl_2. The organic phase was dried over Na_2SO_4, filtered and evaporated. The residue was purified by flash column chromatography on silica gel.

7-n-Butyl-5-methoxy-3-(2-methoxybenzyl)-1-methylquinolin-2(1H)-one

Starting from 110.0 mg of compound 1B. Purification by flash column chromatography on silica gel (hexane/AcOEt 70:30). **2B** (60.0 mg, 0.16 mmol). Yellow solid. Yield 53%.

m.p.: 78-80 °C.

^{1}H-NMR: ($CDCl_3$) δ (ppm): 7.80 (s, 1H, H4), 7.26-7.19 (m, 2H, H5', H6'), 6.92-6.87 (m, 2H, H3', H4'), 6.73 (s, 1H, H8), 6.47 (s, 1H, H6), 3.97 (s, 2H, H11), 3.87 (s, 3H, C2'-OC*H*$_3$), 3.81 (s, 3H, C5-OC*H*$_3$), 3.72 (s, 3H, N-C*H*$_3$), 2.65 (t, 2H, J = 7.6 Hz, C*H*$_2$CH$_2$CH$_2$CH$_3$), 1.68-1.61 (m, 2H, CH$_2$C*H*$_2$CH$_2$CH$_3$), 1.44-1.34 (m, 2H, CH$_2$CH$_2$C*H*$_2$CH$_3$), 0.95 (t, 3H, J = 7.2 Hz, CH$_2$CH$_2$CH$_2$C*H*$_3$).

^{13}C-NMR: ($CDCl_3$) δ (ppm): 162.75 (C2), 157.73 (C2'), 155.87 (C5), 145.75 (C7), 140.22 (C10), 130.84 (C6'), 130.03 (C4), 129.58 (C3), 127.97 (C4'), 127.46 (C1'), 120.51 (C8), 110.53

(C5′), 109.38 (C9), 106.29 (C3′), 103.41 (C6), 55.69 (C5-O*C*H$_3$), 55.40 (C2′-O*C*H$_3$), 36.93 (C1″), 33.69 (C11), 31.34 (C2″), 30.08 (N-*C*H$_3$), 22.47 (C3″), 13.97 (C4″).

HRMS (HESI): *m*/*z* calculated for $C_{23}H_{27}NO_3$ + H+ $[M + H]^+$: 366.20649. Found: 366.20637.

HPLC analysis: method 1, retention time = 18.94 min; peak area, 97.7% (280 nm).

7-Methyl-5-methoxy-3-(2-methoxybenzyl)-1-methylquinolin-2(1H)-one

Starting from 120.0 mg of compound 1C. Purification by flash column chromatography on silica gel (hexane/AcOEt 70:30). **2C** (94.3 mg, 0.292 mmol). Yellow solid. Yield 75%.

m.p.: 132-134 °C.

^{1}H-NMR: ($CDCl_3$) δ (ppm): 7.79 (s, 1H, H4); 7.26-7.19 (m, 2H, H5′, H6′); 6.92-6.87 (m, 2H, H3′, H4′); 6.71 (s, 1H, H8); 6.45 (s, 1H, H6); 3.97 (s, 2H, H11); 3.84 (s, 3H, C2′-OC*H*$_3$); 3.81 (s, 3H, C5-OC*H*$_3$); 3.71 (s, 3H, N-C*H*$_3$); 2.44 (s, 3H, C*H*$_3$).

^{13}C-NMR: ($CDCl_3$) δ (ppm): 162.73 (C2); 157.75 (C2′); 155.82 (C5); 140.61 (C7); 140.24 (C10); 130.86 (C6′); 130.00 (C4); 129.54 (C3); 127.96 (C4′); 127.47 (C1′); 120.53 (C8); 110.57 (C5′); 109.17 (C9); 106.88 (C3′); 104.11 (C6); 55.67 (C5-O*C*H$_3$); 55.40 (C2′-O*C*H$_3$); 31.32 (C1″); 30.05 (N-*C*H$_3$); 22.76 (C11).

HRMS (HESI): *m*/*z* calculated for $C_{20}H_{21}NO_3$ + H+ $[M + H]^+$: 323,1521. Found: 323,1593.

HPLC analysis: method 1, retention time = 4.74 min; peak area, 99.8% (280 nm).

7-*n*-Octyl-5-methoxy-3-(2-methoxybenzyl)-1-methylquinolin-2(1H)-one

Starting from 150.0 mg of compound 1D. Purification by flash column chromatography on silica gel (hexane/AcOEt 80:20). **2D** (120.0 mg, 0.28 mmol). White solid. Yield 77%.

m.p.: 63-65 °C.

^{1}H-NMR: (CDCl3) δ (ppm): 7.81 (s, 1H, H4), 7.27-7.19 (m, 2H, H5', H6'), 6.92-6.87 (m, 2H, H3', H4'), 6.73 (s, 1H, H8), 6.47 (s, 1H, H6), 3.97 (s, 2H, H11), 3.86 (s, 3H, C2'-OCH_3), 3.81 (s, 3H, C5-OCH_3), 3.72 (s, 3H, N-CH_3), 2.68 (t, 2H, J = 7.6 Hz, CH_2-CH_2-CH_2-CH_2-CH_2-CH_2-CH_2-CH_3), 1.69-1.62 (m, 2H, CH_2-CH_2-CH_2-CH_2-CH_2-CH_2-CH_2-CH_3), 1.34-1.28 (m, 10H, CH_2-CH_2-CH_2-CH_2-CH_2-CH_2-CH_2-CH_3), 0.89 (t, 3H, J = 7.2 Hz, CH_2-CH_2-CH_2-CH_2-CH_2-CH_2-CH_2-CH_3).

^{13}C-NMR: (CDCl3) δ (ppm): 162.75 (C2), 157.73 (C2'), 155.86 (C5), 145.79 (C10), 140.22 (C7), 130.84 (C6'), 130.03 (C4), 129.57 (C3), 127.97 (C4'), 127.46 (C1'), 120.51 (C8), 110.52 (C5'), 109.38 (C9), 106.29 (C3'), 103.40 (C6), 55.69 (C5-OCH_3), 55.40 (C2'-OCH_3), 37.21 (C1''), 31.88 (C11), 31.56 (C2'', C3''), 30.08 (N-CH_3), 29.48 (C4''), 29.39 (C5''), 29.27 (C6''), 22.67 (C7''), 14.11 (C8'').

HRMS (HESI): *m/z* calculated for $C_{27}H_{35}NO_3$ + H+ $[M + H]^+$: 421,2617. Found: 421,2686.
HPLC analysis: method 1, retention time = 19.93 min; peak area, 99.3% (280 nm).

7-Isobutyl-5-methoxy-3-(2-methoxybenzyl)-1-methylquinolin-2(1H)-one

Starting from 80.0 mg of compound 1E. Purification by flash column chromatography on silica gel (hexane/AcOEt 80:20). **2E** (60.0 mg, 0.16 mmol). White solid. Yield 71%.

m.p.: 88-100 °C.

^{1}H-NMR: (CDCl3) δ (ppm): 7.81 (s, 1H, H4), 7.27-7.19 (m, 2H, H5', H6'), 6.92-6.87 (m, 2H, H3', H4'), 6.70 (s, 1H, H8), 6.45 (s, 1H, H6), 3.98 (s, 2H, H11), 3.86 (s, 3H, C2'-OCH_3), 3.82 (s, 3H, C5-OCH_3), 3.72 (s, 3H, N-CH_3), 2.56 (d, 2H, J = 7.2 Hz, CH_2CH(CH_3)$_2$), 1.99-1.89 (m, 1H, CH_2CH(CH_3)$_2$), 0.94 (d, 6H, J = 6.8 Hz, CH_2CH(CH_3)$_2$).

^{13}C-NMR: (CDCl3) δ (ppm): 162.74 (C2), 157.73 (C2'), 155.74 (C5), 144.56 (C7), 140.10 (C10), 130.86 (C6'), 129.60 (C4), 127.95 (C3), 127.50 (C4'), 127.49 (C1'), 120.53 (C8), 110.54 (C5'), 109.43 (C9), 107.02 (C3'), 103.99 (C6), 55.69 (C5-OCH_3), 55.40 (C2'-OCH_3), 46.59 (C1''), 31.34 (C2''), 30.33 (N-CH_3), 30.09 (C11), 22.46 (C4'').

HRMS (HESI): *m*/*z* calculated for $C_{23}H_{27}NO_3$ + H+ $[M + H]^+$: 365,1991. Found: 365,2061.

HPLC analysis: method 1, retention time = 9.55 min; peak area, 99.5% (280 nm).

3-benzyl-7-*n*-butyl-5-methoxy-1-methylquinolin-2(1H)-one

Starting from 75 mg of compound 1F. Purification by flash column chromatography on silica gel (hexane/AcOEt 70:30). **2F** (50.8 mg, 0.15 mmol). Yellow solid. Yield 66%.

m.p.: 65-67 °C.

^{1}H-NMR: ($CDCl_3$) δ (ppm): 7.89 (s, 1H, H4), 7.38-7.27 (m, 4H, H2', H3', H5', H6'), 7.23-7.17 (m, 1H, H4'), 6.73 (s, 1H, H8), 6.49 (s, 1H, H6), 3.97 (s, 2H, H11), 3.89 (s, 3H, C2'-OC*H*$_3$), 3.71 (s, 3H, N-C*H*$_3$), 2.69 (t, 2H, J = 7.6 Hz, C*H*$_2$CH$_2$CH$_2$CH$_3$), 1.69-1.61 (m, 2H, CH$_2$C*H*$_2$CH$_2$CH$_3$), 1.44-1.34 (m, 2H, CH$_2$CH$_2$C*H*$_2$CH$_3$), 0.96 (t, 3H, J = 7.3 Hz, CH$_2$CH$_2$CH$_2$C*H*$_3$).

^{13}C-NMR: ($CDCl_3$) δ (ppm): 162.70 (C2), 155.98 (C2'), 146.23 (C5), 140.42 (C7), 139.96 (C10), 130.87 (C6'), 130.30 (C4), 129.27 (C3), 128.49 (C4'), 126.21 (C1', C8), 109.32 (C5', C9), 106.44 (C3'), 103.59 (C6), 55.79 (C5-OCH$_3$), 37.51 (C1''), 37.05 (C11), 33.77 (C2''), 30.22 (N-CH$_3$), 22.58 (C3''), 14.08 (C4'').

HRMS (HESI): *m*/*z* calculated for $C_{23}H_{27}NO_3$ + H+ $[M + H]^+$: 335.18853. Found: 335.19632.

HPLC analysis: method 1, retention time = 9.91 min; peak area, 88.8% (280 nm).

7.1.2.12 General procedure for the synthesis of compounds 3B-3F and 4B-4F

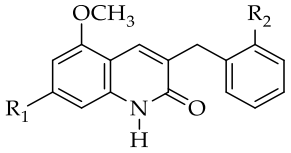

3B, 3C, 3D, 3E,3F

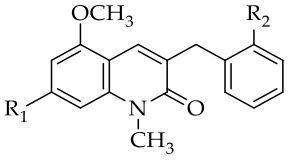

4B, 4C, 4D, 4E, 4F

Series B: R_1 = -*n*butyl; R_2 = -OCH_3
Series C: R_1 = -methyl; R_2 = -OCH_3
Series D: R_1 = -*n*octyl; R_2 = -OCH_3
Series E: R_1 = -isobutyl; R_2 = -OCH_3
Series F: R_1 = -*n*butyl; R_2 = -H

General procedure: A solution of BBr_3 in CH_2Cl_2 1M (4 eq) was added dropwise under nitrogen to a solution of compound **1B**-**1F** or **4B**-**4F** (1 eq) in CH_2Cl_2 (25 mL/mmol), previously cooled at -78 °C. The cold bath was then removed and the reaction mixture was stirred at room temperature overnight. The solution was quenched with distilled H_2O and organic and aqueous phase were separated. Water was then extracted with AcOEt and the combined organic layers were collected, dried with Na_2SO_4, filtered and evaporated. The residue was purified by flash column chromatography on silica gel.

Derivatives 3B-3F

7-*n*-Butyl-5-hydroxy-3-(2-hydroxybenzyl)quinolin-2(1*H*)-one

Starting from 100.0 mg of compound 1B. Purification by flash column chromatography on silica gel (hexane/AcOEt 70:30). **3B** (60.0 mg, 0.18 mmol). White solid. Yield 66%.

m.p.: 252-254 °C.

^{1}H-NMR: (DMSO-*d*$_6$) δ (ppm): 11.72 (bs, 1H, exchangeable, N*H*), 10.11 (bs, 1H, exchangeable, C5-O*H*), 9.63 (bs, 1H, exchangeable, C2'-O*H*), 7.71 (s, 1H, H4), 7.14 (dd, 1H, J = 7.6 Hz, J = 1.2 Hz, H6'), 7.07-7.03 (m, 1H, H5'), 6.80 (d, 1H, J = 7.2 Hz, H3'), 6.74 (t, 1H, J = 7.2 Hz, H4'), 6.41 (s, 1H, H8), 6.40 (s, 1H, H6), 3.72 (s, 2H, H11), 2.54-2-48 (m, 2H, C*H*$_2$CH$_2$CH$_2$CH$_3$), 1.54-1.47 (m, 2H, CH$_2$C*H*$_2$CH$_2$CH$_3$), 1.33-1.23 (m, 2H, CH$_2$CH$_2$C*H*$_2$CH$_3$), 0.88 (t, 3H, J = 7.6 Hz, CH$_2$CH$_2$CH$_2$C*H*$_3$).

^{13}C-NMR: (DMSO-*d*$_6$) δ (ppm): 163.37 (C2), 155.74 (C2'), 153.90 (C5), 145.69 (C7), 139.41 (C10), 131.61 (C6'), 131.17 (C4), 129.71 (C3), 127.94 (C4'), 126.44 (C1'), 119.63 (C8), 116.14 (C5'), 108.09 (C3'), 107.62 (C6), 105.63 (C9), 35.66 (C1''), 33.20 (C11), 30.70 (C2''), 22.17 (C3''), 14.25 (C4'').

HRMS (HESI): *m*/*z* calculated for $C_{20}H_{21}NO_3$ + H+ $[M + H]^+$: 324.15953. Found: 324.15942.

HPLC analysis: method 1, retention time = 5.49 min; peak area, 95.2% (280 nm).

7-Methyl-5-hydroxy-3-(2-hydroxybenzyl)quinolin-2(1H)-one

Starting from 100.0 mg of compound 1C. Purification by flash column chromatography on silica gel (hexane/AcOEt 70:30). **3C** (41.6 mg, 0.148 mmol). White solid. Yield 46%.

m.p.: 281-290 °C.

^{1}H-NMR: (MeOD) δ (ppm): 8.03 (s, 1H, H4); 7.20 (dd, 1H, J = 7.2 Hz, J = 1.0 Hz, H6'); 7.11-7.07 (m, 1H, H5'); 6.85-6.80 (m, 2H, H3', H4'); 6.64 (s, 1H, H8); 6.47 (s, 1H, H6); 3.88 (s, 2H, H11); 2.33 (s, 3H, CH_3).

^{13}C-NMR: (MeOD) δ (ppm): 164.38 (C2); 155.01 (C2'); 153.75 (C5); 141.57 (C7); 138.55 (C10); 132.92 (C6'); 130.42 (C4); 128.72 (C3); 127.46 (C4'); 126.10 (C1'); 119.68 (C8); 115.90 (C5'); 108.67 (C3'); 108.18 (C6); 106.01 (C9); 30.63 (C1''); 20.61 (C11).

HRMS (HESI): *m*/*z* calculated for $C_{17}H_{15}NO_3$ + H+ $[M + H]^+$: 281,1052. Found: 281,0950.
HPLC analysis: method 4, retention time = 3.20 min; peak area, 97.3% (280 nm).

7-*n*-Octyl-5-hydroxy-3-(2-hydroxybenzyl)quinolin-2(1*H*)-one

Starting from 80.0 mg of compound 1D. Purification by flash column chromatography on silica gel (hexane/AcOEt 70:30). **3D** (50.0 mg, 0.13 mmol). White solid. Yield 66%.

m.p.: 212-214 °C.

^{1}H-NMR: (CDCl3) δ (ppm): 8.02 (s, 1H, H4), 7.19 (dd, 1H, J = 7.6 Hz, J = 1.2 Hz, H6'), 7.11-7.07 (m, 1H, H5'), 6.84-6.80 (m, 2H, H3', H4'), 6.65 (s, 1H, H8), 6.48 (s, 1H, H6), 4.91 (s, 2H, H11), 2.59 (t, 2H, J = 7.6 Hz, C*H*$_2$-CH_2-CH_2-CH_2-CH_2-CH_2-CH_2-CH_3), 1.66-1.62 (m, 2H, CH_2-C*H*$_2$-CH_2-CH_2-CH_2-CH_2-CH_2-CH_3), 1.34-1.28 (m, 10H, CH_2-CH_2-C*H*$_2$-C*H*$_2$-C*H*$_2$-C*H*$_2$-C*H*$_2$-CH_3), 0.90 (t, 3H, J = 7.2 Hz, CH_2-CH_2-CH_2-CH_2-CH_2-CH_2-CH_2-C*H*$_3$).

^{13}C-NMR: (CDCl3) δ (ppm): 164.52 (C2), 155.80 (C2'), 153.69 (C5), 146.83 (C10), 138.95 (C7), 132.99 (C6'), 130.65 (C4), 129.74 (C3), 127.84 (C4'), 126.96 (C1'), 119.79 (C8), 117.53 (C5'), 108.75 (C9), 108.12 (C3'), 106.17 (C6), 35.91 (C1''), 31.74 (C11), 31.69 (C2'', C3''), 31.19 (C4''), 30.89 (C5''), 22.40 (C6'', C7''), 13.48 (C8'').

HRMS (HESI): *m*/*z* calculated for $C_{24}H_{29}NO_3$ + H+ $[M + H]^+$: 379,2147. Found: 379,2047.
HPLC analysis: method 1, retention time = 5.59 min; peak area, 91.2% (280 nm).

7-Isobutyl-5-hydroxy-3-(2-hydroxybenzyl)quinolin-2(1H)-one

Starting from 100.0 mg of compound 1E. Purification by flash column chromatography on silica gel (CH_2Cl_2/MeOH 98:2). **3E** (37.0 mg, 0.11 mmol). White solid. Yield 41%.

m.p.: 234-236 °C.

^{1}H-NMR: (CDCl3) δ (ppm): 8.03 (s, 1H, H4), 7.14 (d, 1H, J = 7.6 Hz, H6'), 7.11-7.07 (m, 1H, H5'), 6.84-6.80 (m, 2H, H3', H4'), 6.63 (s, 1H, H8), 6.46 (s, 1H, H6), 3.88 (s, 2H, H11), 2.46 (d, 2H, J = 7.2 Hz, C*H*$_2$CH(CH$_3$)$_2$), 1.93-1.87 (m, 1H, CH$_2$C*H*(CH$_3$)$_2$), 0.92 (d, 6H, J = 6.8 Hz, CH$_2$CH(C*H*$_3$)$_2$).

^{13}C-NMR: (CDCl3) δ (ppm): 164.40 (C2), 155.01 (C2'), 153.66 (C5), 145.37 (C7), 138.42 (C10), 133.03 (C6'), 130.43 (C4), 128.85 (C3), 127.47 (C4'), 126.08 (C1'), 119.69 (C8), 115.91 (C5'), 108.94 (C3'), 108.10 (C6), 106.21(C9), 45.41 (C1''), 30.68 (C11), 29.82 (C2''), 21.38 (C3'').

HRMS (HESI): *m*/*z* calculated for $C_{20}H_{21}NO_3$ + H+ $[M + H]^+$: 323,1521. Found: 323,1422.
HPLC analysis: method 3, retention time = 5.28 min; peak area, 98.5% (280 nm).

3-benzyl-7-*n*-butyl-5-hydroxyquinolin-2-(1*H*)-one

Starting from 90.0 mg of compound 1F. Purification by flash column chromatography on silica gel (hexane/AcOEt 50:50). **3F** (83.0 mg, 0.27 mmol). White solid. Yield 96%.

m.p.: 207-209 °C.

^{1}H-NMR: (Acetone-*d*$_6$) δ (ppm): 11.16 (bs, 1H, exchangeable, N*H*), 9.10 (bs, 1H, exchangeable, C5-O*H*), 7.89 (s, 1H, H4), 7.38-7.36 (m, 2H, H2', H6'), 7.28 (2H, t, J = 7.3 Hz, H3', H5'), 7.18 (1H, t, J = 7.3 Hz, H5), 6.74 (s, 1H, H8), 6.53 (s, 1H, H6), 3.92 (s, 2H, H11), 2.58 (t, 2H, J = 7.6 Hz, C*H*$_2$CH$_2$CH$_2$CH$_3$), 1.62-1.54 (m, 2H, CH$_2$C*H*$_2$CH$_2$CH$_3$), 1.38-1.30 (m, 2H, CH$_2$CH$_2$C*H*$_2$CH$_3$), 0.90 (t, 3H, J = 7.3 Hz, CH$_2$CH$_2$CH$_2$C*H*$_3$).

^{13}C-NMR: (Acetone-*d*$_6$) δ (ppm): 163.73 (C2), 154.46 (C2', C5), 146.90 (C7), 141.22 (C10), 140.48 (C6'), 132.49 (C4), 131.49 (C3), 129.99 (C4'), 129.14 (C1'), 126.86 (C8, C5'), 108.84

(C3′), 108.33 (C6), 106.69 (C9), 36.78 (C1″), 36.50 (C11), 34.04 (C2″), 22.93 (C3″), 14.18 (C4″).

HRMS (HESI): *m*/*z* calculated for $C_{20}H_{21}NO_3$ + H+ $[M + H]^+$: 307.15723. Found: 307.16441.

HPLC analysis: method 1, retention time = 2.72 min; peak area, 99.8% (280 nm).

Derivatives 4B-4F

7-*n*-Butyl-5-hydroxy-3-(2-hydroxybenzyl)-1-methylquinolin-2(1*H*)-one

Starting from 100.0 mg of compound 1B. Purification by flash column chromatography on silica gel (hexane/AcOEt/ MeOH 90:8:2). **4B** (20.0 mg, 0.06 mmol). White solid. Yield 42%.

m.p.: 223-225 °C.

^{1}H-NMR: (Acetone-d_6) δ (ppm): 9.97 (bs, 1H, exchangeable, C5-O*H*), 9.29 (bs, 1H, exchangeable, C2'-O*H*), 8.31 (s, 1H, H4), 7.34 (dd, 1H, J = 7.2 Hz, J = 1.6 Hz, H6'), 7.07 (dt, 1H, J = 7.2 Hz, J = 1.6 Hz, H5'), 6.93 (s, 1H, H8), 6.93-6.71 (m, 2H, H3', H4'), 6.70 (s, 1H, H6), 3.93 (s, 2H, H11), 3.75 (s, 3H, N-CH_3), 2.68 (t, 2H, J = 7.6 Hz, CH_2CH$_2$CH$_2$CH$_3$), 1.66-1.60 (m, 2H, CH$_2$CH_2CH$_2$CH$_3$), 1.40-1.35 (m, 2H, CH$_2$CH$_2$CH_2CH$_3$), 0.91 (t, 3H, J = 7.2 Hz, CH$_2$CH$_2$CH$_2$CH_3).

^{13}C-NMR: (Acetone-d_6) δ (ppm): 164.68 (C2), 156.62 (C5), 155.02 (C2'), 147.84 (C7), 141.08 (C10), 132.32 (C6'), 131.58 (C4), 129.75 (C3), 128.68 (C4'), 127.80 (C1'), 120.65 (C8), 118.20 (C5'), 109.83 (C9), 109.21 (C3'), 106.65 (C6), 36.97 (C1''), 34.22 (C11), 33.23 (C2''), 30.07 (N-*C*H$_3$), 22.99 (C3''), 14.15 (C4'').

HRMS (HESI): *m*/*z* calculated for $C_{21}H_{23}NO_3$ + H+ $[M + H]^+$: 338.17519. Found: 338.17507.

HPLC analysis: method 1, retention time = 8.24 min; peak area, 96.1% (280 nm).

7-Methyl-5-hydroxy-3-(2-hydroxybenzyl)-1-methylquinolin-2(1*H*)-one

Starting from 60.0 mg of compound 1C. Purification by flash column chromatography on silica gel (hexane/AcOEt 70:30). **4C** (23.1 mg, 0.078 mmol). White solid. Yield 41%.

m.p.: 236-238 °C.

^{1}H-NMR: (Acetone-d_6) δ (ppm): 8.32 (s, 1H, H4); 7.36 (dd, 1H, J = 7.2 Hz, J = 1.0 Hz, H6'); 7.11-7.06 (m, 1H, H5'); 6.92 (s, 1H, H8); 6.85-6.79 (m, 2H, H3', H4'); 6.69 (s, 1H, H6); 3.95 (s, 2H, H11); 3.75 (s, 3H, N-CH_3); 2.42 (s, 3H, CH_3).

^{13}C-NMR: (Acetone-d_6) δ (ppm): 163.80 (C2); 155.74 (C5); 153.92 (C2'); 141.96 (C7); 140.21 (C10); 130.70 (C6'); 128.88 (C4); 127.83 (C3); 127.82 (C4'); 126.90 (C1'); 119.79 (C8); 117.37 (C5'); 108.97 (C9); 108.68 (C3'); 106.45 (C6); 32.39 (C1''); 29.79 (N-CH_3); 21.44 (C11).

HRMS (HESI): *m*/*z* calculated for $C_{18}H_{17}NO_3$ + H+ $[M + H]^+$: 295,1208. Found: 295,1110.
HPLC analysis: method 1, retention time = 3.02 min; peak area, 99.5% (280 nm).

7-*n*-Octyl-5-hydroxy-3-(2-hydroxybenzyl)-1-methylquinolin-2(1*H*)-one

Starting from 200.0 mg of compound 1D. Purification by flash column chromatography on silica gel (hexane/AcOEt 84:16). **4D** (110.0 mg, 0.28 mmol). White solid. Yield 60%.

m.p.: 162-164 °C.

^{1}H-NMR: (Acetone-d_6) δ (ppm): 9.98 (bs, 1H, exchangeable, C5-O*H*), 9.32 (bs, 1H, exchangeable, C2'-O*H*), 8.34 (s, 1H, H4), 7.37 (dd, 1H, J = 7.6 Hz, J = 2 Hz, H6'), 7.09 (dt, 1H, J = 7.2 Hz, J = 1.6 Hz, H5'), 6.96 (s, 1H, H8), 6.85-6.80 (m, 2H, H3', H4'), 6.73 (s, 1H, H6), 3.96 (s, 2H, H11), 3.78 (s, 3H, N-CH_3), 2.71 (t, 2H, J = 7.2 Hz, CH_2-CH_2-CH_2-CH_2-CH_2-CH_2-CH_2-CH_3), 1.71-1.67 (m, 2H, CH_2-CH_2-CH_2-CH_2-CH_2-CH_2-CH_2-CH_3), 1.37-1.31 (m, 10H, CH_2-CH_2-CH_2-CH_2-CH_2-CH_2-CH_2-CH_3), 0.91 (t, 3H, J = 7.2 Hz, CH_2-CH_2-CH_2-CH_2-CH_2-CH_2-CH_2-CH_3).

^{13}C-NMR: (Acetone-d_6) δ (ppm): 162.81 (C2), 156.13 (C5), 154.63 (C2'), 146.52 (C7), 140.70 (C10), 131.60 (C6'), 130.65 (C4), 129.02 (C3), 128.28 (C4'), 126.59 (C1'), 119.93 (C8), 116.28 (C5'), 108.63 (C9), 108.45 (C3'), 105.88 (C6), 36.76 (C1''), 32.11 (C11), 31.78 (C2''), 31.61 (N-*C*H_3), 30.63 (C3''), 29.68 (C4''), 29.55 (C5''), 29.50 (C6''), 22.92 (C7''), 14.79 (C8'').

HRMS (HESI): *m*/*z* calculated for $C_{25}H_{31}NO_3$ + H+ $[M + H]^+$: 393,2304. Found: 393,2203.
HPLC analysis: method 1, retention time = 11.64 min; peak area, 99.7% (280 nm).

7-Isobutyl-5-hydroxy-3-(2-hydroxybenzyl)-1-methylquinolin-2(1*H*)-one

Starting from 150.0 mg of compound 1E. Purification by flash column chromatography on silica gel (hexane/AcOEt 70:30). **4E** (70.0 mg, 0.21 mmol). White solid. Yield 50%.

m.p.: 213-215 °C.

^{1}H-NMR: (Acetone-d_6) δ (ppm): 8.02 (s, 1H, H4), 7.18 (dd, 1H, J = 7.6 Hz, J = 1.2 Hz, H6'), 7.08 (dt, 1H, J = 7.6 Hz, J = 1.6 Hz, H5'), 6.83-6.79 (m, 2H, H3', H4'), 6.77 (s, 1H, H8), 6.53 (s, 1H, H6), 3.88 (s, 2H, H11), 3.73 (s, 3H, N-CH_3), 2.52 (d, 2H, J = 7.2 Hz, CH_2CH(CH$_3$)$_2$), 1.97-1.88 (m, 1H, CH$_2$CH(CH$_3$)$_2$), 0.93 (d, 6H, J = 6.8 Hz, CH$_2$CH(CH_3)$_2$).

^{13}C-NMR: (Acetone-d_6) δ (ppm): 163.66 (C2), 155.04 (C5), 154.08 (C2'), 145.53 (C7), 139.69 (C10), 130.48 (C6'), 128.14 (C4), 127.43 (C3), 126.01 (C4'), 119.64 (C1'), 115.78 (C8), 109.05 (C5'), 108.40 (C9, C3'), 105.76 (C6), 45.76 (C1''), 31.42 (C11), 29.97 (C2''), 29.39 (N-CH$_3$), 21.37 (C3'').

HRMS (HESI): *m*/*z* calculated for C$_{21}$H$_{23}$NO$_3$ + H+ [M + H]$^+$: 337,1678. Found: 337,1577.
HPLC analysis: method 1, retention time = 4.03 min; peak area, 98.3% (280 nm).

3-benzyl-7-*n*-butyl-5-methoxy-1-methylquinolin-2(1*H*)-one

Starting from 77.0 mg of compound 1F. Purification by flash column chromatography on silica gel (hexane/AcOEt 80:20). **4F** (50.8 mg, 0.16 mmol). White solid. Yield 69%.

m.p.: the solid decomposes beyond 217.3 °C.

^{1}H-NMR: (CDCl$_3$) δ (ppm): 7.91 (s, 1H, H4), 7.33-7.24 (m, 4H, H2', H3', H5', H6'), 7.23-7.15 (m, 1H, H4'), 6.69 (s, 1H, H8), 6.57 (s, 1H, H6), 3.99 (s, 2H, H11), 3.73 (s, 3H, N-CH_3), 2.62 (t, 2H, J = 7.6 Hz, CH_2CH$_2$CH$_2$CH$_3$), 1.63-1.56 (m, 2H, CH$_2$CH_2CH$_2$CH$_3$), 1.39-1.30 (m, 2H, CH$_2$CH$_2$CH_2CH$_3$), 0.91 (t, 3H, J = 7.3 Hz, CH$_2$CH$_2$CH$_2$CH_3).

^{13}C-NMR: (CDCl$_3$) δ (ppm): 162.99 (C2), 153.17 (C2', C5), 146.67 (C7), 140.34 (C10), 139.63 (C6'), 131,49 (C4), 129.68 (C3), 129.31 (C4'), 128.55 (C1'), 126.33 (C8, C5'), 108.94 (C3'),

108.67 (C6), 106.20 (C9), 37.41 (C1''), 36.60 (C11), 33.60 (C2''), 30.62 (N-CH_3), 22.52 (C3''), 14.06 (C4'').

HRMS (HESI): *m*/*z* calculated for $C_{21}H_{23}NO_3$ + H+ $[M + H]^+$: 321.17288. Found: 321.18061.

HPLC analysis: method 1, retention time = 3.92 min; peak area, 94.5% (280 nm).

7.1.3 Synthetic procedures for multitarget compounds

7.1.3.1 Synthesis of 1,4-dimethoxy-2,3,5-trimethylbenzene (25)

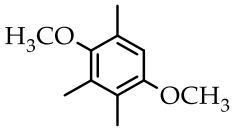

25

Procedure: The commercially available trimethylhydroquinone **24** (1.00 g, 6.57 mmol) was added to a suspension of NaH (60% dispersion in mineral oil) (0.85 g) in DMF (10 mL) at 0 °C and the reaction mixture was stirred at room temperature. After 30 minutes, CH_3I (1.64 mL, 26.3 mmol) was added dropwise at 0 °C and then the suspension was stirred at room temperature overnight. After the addition of about 10 mL of distilled H_2O, the aqueous phase was extracted with AcOEt. After washing with distilled H_2O, the organic phase was dried over anhydrous Na_2SO_4, filtered and evaporated, affording compound **25** (1.25 g, 6.93 mmol) as a transparent oil, which was used for the next step without further purification. Yields > 99%.

^{1}H-NMR: ($CDCl_3$) δ (ppm): 6.53 (s, 1H, ar), 3.78 (s, 3H, O-C*H*$_3$), 3.66 (s, 3H, O-C*H*$_3$), 2.28 (s, 3H, CH_3), 2.20 (s, 3H, CH_3), 2.12 (s, 3H, CH_3).

7.1.3.2 Synthesis of 2,5-dimethoxy-3,4,6-trimethylbenzaldehyde (26)

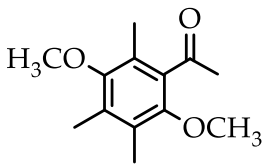

26

Procedure: Intermediate **25** (200 mg, 1.11 mmol) was added to a suspension of hexamethylenetetramine (202 mg, 1.44 mmol) in trifluoroacetic acid (TFA, 1.6 mL) and the reaction mixture was stirred at reflux overnight. After the addition of cold distilled H_2O (5 mL), the aqueous phase was neutralized with Na_2CO_3 2N and extracted with Et_2O (6 mL). After washing with distilled H_2O, the organic phase was dried over anhydrous Na_2SO_4, filtered, evaporated and purified by flash liquid chromatography on silica gel (hexane/AcOEt 90:10), providing compound **26** as an orange solid. Yield 78%.

^{1}H-NMR: ($CDCl_3$) δ (ppm): 10.48 (s, 1H, C*H*O), 3.77 (s, 3H, O-C*H*$_3$), 3.65 (s, 3H, O-C*H*$_3$), 2.49 (s, 3H, CH_3), 2.26 (s, 3H, CH_3), 2.20 (s, 3H, CH_3).

7.1.3.3 Synthesis of 2-hydroxy-5-methoxy-3,4,6-trimethylbenzaldehyde (27)

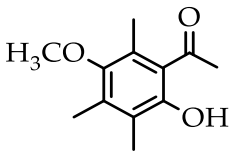

27

Procedure: In a flame-dried two-neck round-bottom flask equipped with a rubber septum, compound **27** (540 mg, 2.59 mmol) was dissolved in anhydrous DCM (25 mL) under nitrogen flux. Through the septum, a solution of BBr3 1M in DCM (2.59 mL, 2.59 mmol) was added dropwise into the reaction flask previously cooled in an ice-salt bath (-10 °C) and, after that, the mixture was stirred at r.t. for 2 h. After collecting the solution to ~10 °C, the reaction was quenched with H_2O until no more fumes were observed. The organic layer was separated from the aqueous one, which was then extracted with EtOAc. Once collected, the organic phase was dried over Na_2SO_4, filtered and evaporated under reduced pressure, affording derivative **27** (470 mg, 2.42) as a violet solid, which was used without further purification. Yield 93.4%.

^{1}H-NMR: ($CDCl_3$) δ (ppm): 12.20 (bs, 1H, exchangeable, OH), 10.23 (s, 1H, CO*H*), 3.64 (s, 3H, O-C*H*$_3$), 2.51 (s, 3H, CH_3), 2.26 (s, 3H, CH_3), 2.14 (s, 3H, CH_3).

7.1.3.4 Synthesis of 3-benzyl-6-methoxy-5,7,8-trimethyl-2H-chromen-2-one (28)

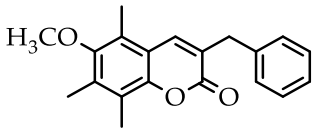

28

Procedure: Cinnamaldehyde (1.20 mL, 9.52 mmol), 1,3-dimethylimidazolium dimethyl phosphate (0.67 mL, 3.81 mmol) and K_2CO_3 (0.53 mg, 3.81 mmol) were added to a solution of intermediate **27** (740 mg, 3.81 mmol) in toluene (13 mL) under nitrogen flux and the suspension was stirred at 100 °C for 24 h. After cooling at room temperature, most of the solvent was evaporated under reduced pressure. The mixture was diluted with distilled H_2O (10 mL) and then extracted with CH_2Cl_2 (15 mL). The organic phase was dried over Na_2SO_4, filtered, evaporated and purified by flash liquid chromatography on silica gel (hexane/AcOEt 86:14), providing compound **28** (530 mg, 1.71) as a white solid. Yield 45%.

^{1}H-NMR: ($CDCl_3$) δ (ppm): 7.51 (s, 1H, ar), 7.34-7.28 (m, 4H, ar), 7.26-7.22 (m, 1H, ar), 3.89 (s, 2H, CH_2 benzylic), 3.65 (s, 3H, O-C*H*$_3$), 2.32 (s, 3H, CH_3), 2.30 (s, 3H, CH_3), 2.29 (s, 3H, CH_3).

7.1.3.5 Synthesis of 3-benzyl-6-hydroxy-5,7,8-trimethyl-2H-chromen-2-one (KIT17)

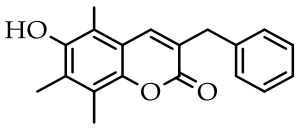

KIT17

Procedure: In a flame-dried two-neck round-bottom flask equipped with a rubber septum, compound **28** (530 mg, 1.72 mmol) was dissolved in anhydrous DCM (20 mL) under nitrogen flux. Through the septum, a solution of BBr3 1M in DCM (5.16 mL, 5.16 mmol) was added dropwise into the reaction flask previously cooled in an ice-salt bath (-10 °C) and, after that, the mixture was stirred at r.t. for 2 h. After collecting the solution to ~10 °C, the reaction was quenched with H_2O. The organic layer was separated from the aqueous one, which was then extracted with EtOAc. Once collected, the organic phase was dried over Na_2SO_4, filtered, evaporated under reduced pressure and purified by flash liquid chromatography on silica gel (hexane/AcOEt 80:20), affording derivative **KIT17** (390 mg, 1.32) as a violet solid, which was used without further purification. Yield 77%.

^{1}H-NMR: ($CDCl_3$) δ (ppm): 7.51 (s, 1H, ar), 7.36-7.24 (m, 5H, ar), 3.91 (s, 2H, CH_2 benzylic), 2.37 (s, 3H, CH_3), 2.28 (s, 3H, CH_3), 2.25 (s, 3H, CH_3).

7.1.3.6 Synthesis of 3-benzyl-6-(ethynyloxy)-5,7,8-trimethyl-2H-chromen-2-one (29) and 3-benzyl-6-(but-3-yn-1-yloxy)-5,7,8-trimethyl-2H-chromen-2-one (30)

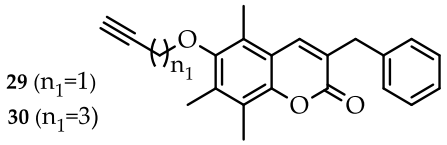

29-30

General procedure: Suitable 5-chloro-1-alkyne (1.5 eq) and K_2CO_3 (2 eq) were added to a solution of compound **KIT17** in DMF (6 mL/mmol) and the reaction mixture was stirred at 65 °C for 4 h. After evaporating most of the solved under reduced pressure, distilled H_2O (10 mL) was added and the aqueous phase was extracted with AcOEt. Once collected, the organic phase was washed with distilled H_2O, dried over Na_2SO_4, filtered and evaporated under reduced pressure, affording desire compounds, which were used without further purification.

3-benzyl-6-(ethynyloxy)-5,7,8-trimethyl-2H-chromen-2-one 29

Starting from 200 mg of intermediate KIT17. Derivative **29** (190 mg, 0.51 mmol) as a yellow solid. Yield 84%.

^{1}H-NMR: ($CDCl_3$) δ (ppm): 7.50 (s, 1H, ar), 7.35-7.29 (m, 4H, ar), 7.26-7.23 (m, 1H, ar), 4.43 (s, 2H, O-C*H*$_2$), 3.89 (s, 2H, CH_2 benzylic), 2.50 (t, 1H, CH alkyne), 2.34 (s, 3H, CH_3), 2.33 (s, 3H, CH_3), 2.32 (s, 3H, CH_3).

3-benzyl-6-(but-3-yn-1-yloxy)-5,7,8-trimethyl-2H-chromen-2-one 30

Starting from 200 mg of intermediate KIT17. Compound **30** (180 mg, 0.52 mmol) as a white solid. Yield 76%.

^{1}H-NMR: ($CDCl_3$) δ (ppm): 7.51 (s, 1H, ar), 7.35-7.24 (m, 5H, ar), 3.90 (s, 2H, CH_2 benzylic), 3.77 (t, 2H, J = 6.4 Hz, O-CH_2), 2.50 (dt, 2H, J = 6.8 Hz, J = 2.8 Hz, CH_2), 2.34 (s, 3H, CH_3), 2.29 (s, 6H, $2CH_3$), 2.05-1.98 (m, 3H, CH_2, CH alkyne).

7.1.3.7 Synthesis of ethyl 2-oxo-1,2-dihydro-1,8-naphthyridine-3-carboxylate (32)

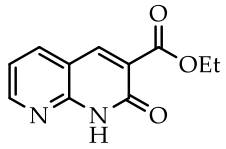

32

Procedure: Piperidine (0.20 ml) was added to a solution of commercial **2-aminonicotinaldehyde 31** (1.00 g, 8.19 mmol) and diethyl malonate (2.48 ml, 16.38 mmol) and the resulting mixture was heated overnight at 130 °C. After cooling to room temperature, the mixture was diluted with Et_2O (20 mL) and the obtained solid was collected by filtration, affording compound **32** (1.01 g, 4.63 mmol), which was used without further purification. Yellow oil. Yield 57%.

^{1}H-NMR: (MeOD) δ (ppm): 12.35 (bs, 1H, exchangeable, NH), 8.89-7.87 (m, 1H, ar), 8.47 (s, 1H, ar), 8.05-8.02 (dd, 1H, J = 7.8 Hz, J = 1.6 Hz, ar), 7.29-7.27 (m, 1H, ar), 4.44 (q, 2H, J = 7.1 Hz, CH_2-CH_3), 1.43 (t, 3H, J = 7.1 Hz, CH_2-CH_3).

7.1.3.8 Synthesis of N-4-methylcyclohexyl-2-oxo-1,2-dihydro-1,8-naphthyridine-3-carboxamide (33)

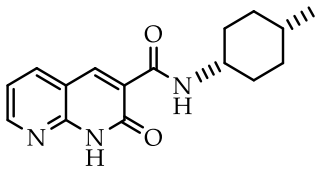

33

Procedure: In a vial, compound **32** (1.55 g, 7.11 mmol) was dissolved in 4-methylcyclohexan-1-amine (4.51 ml). The vial was sealed and left under magnetic stirring at 120 °C for 24h. After cooling to room temperature, the mixture was diluted with Et_2O (20 mL) and the obtained solid was collected by filtration, providing derivative **33** (1.66 g, 5.82 mmol), which was used without further purification. Yellow oil. Yield 82%.

^{1}H-NMR: ($CDCl_3$) δ (ppm): 11.98 (bs, 1H, exchangeable, NH), 9.93 (bs, 1H, exchangeable, NH, cis isomer), 9.51 (bs, 1H, exchangeable, NH, trans isomer), 8.94 (s,1H, ar cis), 8.93 (s,1H, ar trans), 8.85-8.83 (m, 1H, ar cis and trans), 8.14 (dd, 1H, J = 7.6 Hz, J = 1.2 Hz, ar cis and trans), 7.36-7.33 (m, 1H, ar cis and trans), 4.31-4.29 (m, 1H, CH cyclohexyl cis), 3.94-3.92 (m, 1H, CH cyclohexyl trans), 2.10-1.10 (m, 9H, cyclohexyl cis, cyclohexyl trans), 0.99 (d, 3H, J = 6.8 Hz, CH_3 cis), 0.92 (d, 3H, J = 6.4 Hz, CH_3 trans).

7.1.3.9 General procedure for the synthesis of 1-(3-bromoalkyl)-4-methylcyclohexyl-2-oxo-1,2-dihydro-1,8-naphthyridine-3-carboxamide (34-36)

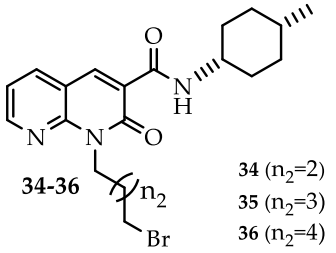

General procedure: CsF (3 eq) was added to a suspension of intermediate **33** (1 eq) in DMF (10 mL/mmol) and the resulting mixture was stirred at room temperature for 1h. After the addition of corresponding alkyldibromide (3 eq), the reaction mixture was heated at 30 °C for 24h. The solvent was evaporated and the residue was dissolved in H_2O and extracted with AcOEt. The organic phase was dried over Na_2SO_4, filtered and evaporated. Isomers cis and trans was separated by flash column chromatography on silica gel.

1-(4-bromobutyl)-N- (4-methylcyclohexyl)-2-oxo-1,2-dihydro-1,8-naphthyridine-3-carboxamide

Starting from 300 mg of intermediate 33. Purification by flash column chromatography on silica gel (hexane/AcOEt 50:50). **34** (440 mg, 0.93 mmol). White solid. Yield 89%.

^{1}H-NMR: (DMSO-d_6) δ (ppm) 1-(4-bromobutyl)-N-cis-(4-methylcyclohexyl)-2-oxo-1,2-dihydro-1,8-naphthyridine-3-carboxamide: 9.98 (bs, 1H, exchangeable, NH), 8.87 (s, 1H, ar), 8.71-8.69 (dd, 1H, J = 4.5 Hz, J = 1.9 Hz, ar), 8.08-8.06 (dd, 1H, J = 7.8 Hz, J = 1.8 Hz, ar), 7.29-7.27 (m, 1H, ar), 4.63 (t, 2H, J = 7.4 Hz, N-C*H*$_2$-CH$_2$-CH$_2$-CH$_2$-Br), 4.27-4.25 (m, 1H, CH cis cyclohexyl), 3.50 (t, 2H, J = 6.6 Hz, N-CH$_2$-CH$_2$-CH$_2$-C*H*$_2$-Br), 2.02-1.91 (m, 4H, cyclohexyl), 1.86-1.81 (m, 2H, N-CH$_2$-C*H*$_2$-CH$_2$-CH$_2$-Br), 1.70-1.60 (m, 5H, cyclohexyl), 1.35-1.25 (m, 2H, N-CH$_2$-CH$_2$-C*H*$_2$-CH$_2$-Br), 0.97 (d, 3H, J = 6.6 Hz, CH_3).

^{1}H-NMR: (DMSO-*d_6*) δ (ppm) 1-(4-bromobutyl)-N-trans-(4-methylcyclohexyl)-2-oxo-1,2-dihydro-1,8-naphthyridine-3-carboxamide: 9.60 (bs, 1H, exchangeable, NH), 8.87 (s, 1H, ar), 8.71-8.69 (dd, 1H, J = 4.5 Hz, J = 1.9 Hz, ar), 8.09-8.06 (dd, 1H, J = 7.8 Hz, J = 1.8 Hz, ar), 7.29-7.26 (m, 1H, ar), 4.61 (t, 2H, J = 7.4 Hz, N-C*H*$_2$-CH$_2$-CH$_2$-CH$_2$-Br), 3.93-3.89 (m, 1H, CH trans cyclohexyl), 3.49 (t, 2H, J = 6.5 Hz, N-CH$_2$-CH$_2$-CH$_2$-C*H*$_2$-Br), 2.10-2.04 (m, 2H, N-CH$_2$-C*H*$_2$-CH$_2$-CH$_2$-Br), 2.02-1.90 (m, 4H, cyclohexyl), 1.77-1.74 (m, 2H, N-CH$_2$-CH$_2$-C*H*$_2$-CH$_2$-Br), 1.40-1.05 (m, 5H, cyclohexyl), 0.91 (d, 3H, CH$_3$, J = 6.5 Hz).

1-(5-bromopentyl)-N-(4-methylcyclohexyl)-2-oxo-1,2-dihydro-1,8-naphthyridine-3-carboxamide

Starting from 500 mg of intermediate 33. Purification by flash column chromatography on silica gel (hexane/AcOEt 60:40). **35** (480 mg, 1.11 mmol). White solid. Yield 63%.

^{1}H-NMR: (DMSO-*d_6*) δ (ppm) 1-(5-bromopentyl)-N-cis-(4-methylcyclohexyl)-2-oxo-1,2-dihydro-1,8-naphthyridine-3-carboxamide: 9.99 (bs, 1H, exchangeable, NH), 8.85 (s, 1H, ar), 8.71-8.69 (dd, 1H, J = 4.7 Hz, J = 1.9 Hz, ar), 8.08-8.05 (dd, 1H, J = 7.8 Hz, J = 1.8 Hz, ar), 7.28-7.25 (m, 1H, ar), 4.60-4.57 (m, 2H, N-C*H*$_2$-CH$_2$-CH$_2$-CH$_2$-CH$_2$-Br), 3.27-3.23 (m, 1H, CH cis cyclohexyl), 3.44 (t, 2H, J = 6.8 Hz, N-CH$_2$-CH$_2$-CH$_2$-CH$_2$-C*H*$_2$-Br), 2.10-1.94 (m, 2H, N-CH$_2$-C*H*$_2$-CH$_2$-CH$_2$-CH$_2$-Br), 1.86-1.76 (m, 4H, cyclohexyl), 1.70-1.53 (m, 7H, cyclohexyl, N-CH$_2$-CH$_2$-CH$_2$-C*H*$_2$-CH$_2$-Br), 1.35-1.28 (m, 2H, N-CH$_2$-CH$_2$-C*H*$_2$-CH$_2$-CH$_2$-Br), 0.97 (d, 3H, CH$_3$).

^{1}H-NMR: (DMSO-*d_6*) δ (ppm) 1-(5-bromopentyl)-N-trans-(4-methylcyclohexyl)-2-oxo-1,2-dihydro-1,8-naphthyridine-3-carboxamide: 9.63 (bs, 1H, exchangeable, NH), 8.86 (s, 1H, ar), 8.71-8.69 (dd, 1H, J = 4.5 Hz, J = 1.8 Hz, ar), 8.09-8.06 (dd, 1H, J = 7.8 Hz, J = 1.8 Hz, ar), 7.29-7.27 (m, 1H, ar), 4.60-4.56 (m, 2H, N-C*H*$_2$-CH$_2$-CH$_2$-CH$_2$-CH$_2$-Br), 3.94-3.90 (m, 1H, CH trans cyclohexyl), 3.44 (t, 2H, J = 6.8 Hz, N-CH$_2$-CH$_2$-CH$_2$-CH$_2$-C*H*$_2$-Br), 2.10-2.07 (m, 2H, N-CH$_2$-C*H*$_2$-CH$_2$-CH$_2$-CH$_2$-Br), 2.00-1.93 (m, 2H, N-CH$_2$-CH$_2$-CH$_2$-C*H*$_2$-CH$_2$-Br), 1.83-1.73 (m, 4H, cyclohexyl), 1.64-1.29 (m, 5H, cyclohexyl), 1.15-1.06 (m, 2H, N-CH$_2$-CH$_2$-C*H*$_2$-CH$_2$-CH$_2$-Br), 0.91 (d, 3H, J = 6.4 Hz, CH$_3$).

1-(6-bromohexyl)-N-(4-methylcyclohexyl)-2-oxo-1,2-dihydro-1,8-naphthyridine-3-carboxamide

Starting from 300 mg of intermediate 33. Purification by flash column chromatography on silica gel (hexane/AcOEt 50:50). **36** (270 mg, 0.60 mmol). White solid. Yield 57%.

^{1}H-NMR: (DMSO-*d*$_6$) δ (ppm) 1-(6-bromohexyl)-N-cis-(4-methylcyclohexyl)-2-oxo-1,2-dihydro-1,8-naphthyridine-3-carboxamide: 9.98 (bs, 1H, exchangeable, NH), 8.83 (s, 1H, ar), 8.69-8.67 (dd, 1H, J = 4.7 Hz, J = 1.9 Hz, ar), 8.05-8.03 (dd, 1H, J = 7.8 Hz, J = 1.8 Hz, ar), 7.26-7.22 (m, 1H, ar), 4.56 (t, 2H, J = 7.8 Hz, N-C*H*$_2$-CH$_2$-CH$_2$-CH$_2$-CH$_2$-CH$_2$-Br), 4.24-3.22 (m, 1H, CH cis cyclohexyl), 3.39 (t, 2H, J = 8.8 Hz, N-CH$_2$-CH$_2$-CH$_2$-CH$_2$-CH$_2$-C*H*$_2$-Br), 1.89-1.71 (m, 6H, N-CH$_2$-C*H*$_2$-CH$_2$-CH$_2$-CH$_2$-CH$_2$-Br, N-CH$_2$-CH$_2$-CH$_2$-CH$_2$-C*H*$_2$-CH$_2$-Br, N-CH$_2$-CH$_2$-C*H*$_2$-CH$_2$-CH$_2$-CH$_2$-Br), 1.68-1.43 (m, 9H, cyclohexyl), 1.33-1.22 (m, 2H, N-CH$_2$-CH$_2$-CH$_2$-C*H*$_2$-CH$_2$-CH$_2$-Br), 0.95 (d, 3H, CH$_3$, J = 6.6 Hz).

^{1}H-NMR: (DMSO-*d*$_6$) δ (ppm) 1-(6-bromohexyl)-N-trans-(4-methylcyclohexyl)-2-oxo-1,2-dihydro-1,8-naphthyridine-3-carboxamide: 9.63 (bs, 1H, exchangeable, NH), 8.85 (s, 1H, ar), 8.70-8.68 (dd, 1H, J = 4.6 Hz, J = 1.7 Hz, ar), 8.07-8.05 (dd, 1H, J = 7.8 Hz, J = 1.8 Hz, ar), 7.27-7.24 (m, 1H, ar), 4.54 (t, 2H, J = 7.6 Hz, N-C*H*$_2$-CH$_2$-CH$_2$-CH$_2$-CH$_2$-CH$_2$-Br), 3.94-3.86 (m, 1H, CH trans cyclohexyl), 3.40 (t, 2H, J = 6.8 Hz, N-CH$_2$-CH$_2$-CH$_2$-CH$_2$-CH$_2$-C*H*$_2$-Br), 2.07-2.03 (m, 2H, N-CH$_2$-C*H*$_2$-CH$_2$-CH$_2$-CH$_2$-CH$_2$-Br), 1.91-1.84 (m, 2H, N-CH$_2$-CH$_2$-CH$_2$-CH$_2$-C*H*$_2$-CH$_2$-Br), 1.79-1.73 (m, 4H, cyclohexyl), 1.56-1.48 (m, 4H, cyclohexyl), 1.40-1.27 (m, 3H, cyclohexyl, N-CH$_2$-CH$_2$-C*H*$_2$-CH$_2$-CH$_2$-CH$_2$-Br), 1.14-1.06 (m, 2H, N-CH$_2$-CH$_2$-CH$_2$-C*H*$_2$-CH$_2$-CH$_2$-Br), 0.91 (d, 3H, CH$_3$, J = 6.5 Hz).

7.1.3.10 General procedure for the synthesis of 1-(3-azidoalkyl)-4-methylcyclohexyl-2-oxo-1,2-dihydro-1,8-naphthyridine-3-carboxamide (37-39)

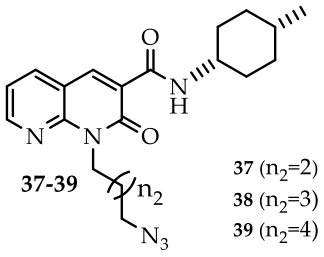

General procedure: In a reaction vial, suitable intermediate **34**-**36** (1 eq) was solubilized in DMF (5 mL/mmol) and sodium azide (3 eq) was added under nitrogen flux. The suspension is stirred at 60 °C overnight. After cooling to room temperature, the solvent was evaporated at 70 °C. The white residue was diluted with distilled H_2O (10 mL) and extracted with CH_2Cl_2 (15 mL). The organic phase was collected, dried over Na_2SO_4, filtered and evaporated, affording desire derivate as a white solid, which was used without further purification.

Cis derivatives

1-(4-azidobutyl)-N-cis-(4-methylcyclohexyl)-2-oxo-1,2-dihydro-1,8-naphthyridine-3-carboxamide

Starting from 410 mg of intermediate 34. Compound **37** (280 mg, 0.73 mmol). White solid. Yield 75%.

^{1}H-NMR: (DMSO-d_6) δ (ppm) cis isomer: 9.99 (bs, 1H, exchangeable, NH), 8.87 (s, 1H, ar), 8.73-8.71 (m, 1H, ar), 8.09 (dd, 1H, J = 7.6 Hz, J = 1.6 Hz, ar), 7.31-7.29 (m, 1H, ar), 4.66-4.62 (m, 2H, N-C*H*$_2$-CH$_2$-CH$_2$-CH$_2$-N$_3$), 4.29-4.25 (m, 1H, CH cis cyclohexyl), 3.28 (t, 2H, J = 6.8 Hz, N-CH$_2$-CH$_2$-CH$_2$-C*H*$_2$-N$_3$), 2.07-2.04 (m, 2H, N-CH$_2$-C*H*$_2$-CH$_2$-CH$_2$-N$_3$), 1.92-1.54 (m, 9H, cyclohexyl, CH$_2$), 1.34-1.26 (m, 2H, N-CH$_2$-CH$_2$-C*H*$_2$-CH$_2$-N$_3$), 0.99 (d, 3H, J = 6.8 Hz, CH$_3$).

1-(5-azidopentyl)-N-cis-(4-methylcyclohexyl)-2-oxo-1,2-dihydro-1,8-naphthyridine-3-carboxamide

Starting from 100 mg of intermediate 35. Compound **38** (70 mg, 0.18 mmol). White solid. Yield 77%.

^{1}H-NMR: (DMSO-d_6) δ (ppm): 10.02 (bs, 1H, exchangeable, NH), 8.87 (s, 1H, ar), 8.71-8.69 (m, 1H, ar), 8.07 (d, 1H, J = 7.8 Hz, ar), 7.28-7.25 (m, 1H, ar), 4.60 (t, 2H, J = 7.2 Hz, N-C*H*$_2$-CH$_2$-CH$_2$-CH$_2$-CH$_2$-N$_3$), 4.26-4.23 (m, 1H, CH cis cyclohexyl), 3.31 (t, 2H, J = 6.4 Hz, N-CH$_2$-CH$_2$-CH$_2$-CH$_2$-C*H*$_2$-N$_3$), 1.82-1.74 (m, 4H, N-CH$_2$-C*H*$_2$-CH$_2$-CH$_2$-CH$_2$-N$_3$, N-CH$_2$-CH$_2$-CH$_2$-C*H*$_2$-CH$_2$-N$_3$), 1.72-1.54 (m, 9H, cyclohexyl), 1.34-1.25 (m, 2H, N-CH$_2$-CH$_2$-C*H*$_2$-CH$_2$-CH$_2$-N$_3$), 0.97 (d, 3H, J = 6 Hz, CH$_3$).

1-(6-azidohexyl)-N-cis-(4-methylcyclohexyl)-2-oxo-1,2-dihydro-1,8-naphthyridine-3-carboxamide

Starting from 450 mg of intermediate 36. Compound **39** (326 mg, 0.79 mmol). White solid. Yield 79%.

^{1}H-NMR: (DMSO-d_6) δ (ppm): 10.02 (bs, 1H, exchangeable, NH), 8.88 (s, 1H, ar), 8.73-8.71 (m, 1H, ar), 8.08 (dd, 1H, J = 7.6 Hz, J = 1.6 Hz, ar), 7.29-7.26 (m, 1H, ar), 4.60 (t, 2H, J = 7.6 Hz, N-C*H*$_2$-CH$_2$-CH$_2$-CH$_2$-CH$_2$-CH$_2$-N$_3$), 4.29-4.25 (m, 1H, CH cis cyclohexyl), 3.29 (t, 2H, J = 6.8 Hz, N-CH$_2$-CH$_2$-CH$_2$-CH$_2$-CH$_2$-C*H*$_2$-N$_3$), 1.87-1.76 (m, 4H, N-CH$_2$-C*H*$_2$-CH$_2$-CH$_2$-CH$_2$-CH$_2$-N$_3$, N-CH$_2$-CH$_2$-CH$_2$-CH$_2$-C*H*$_2$-CH$_2$-N$_3$), 1.72-1.48 (m, 11H, cyclohexyl, N-CH$_2$-CH$_2$-C*H*$_2$-CH$_2$-CH$_2$-CH$_2$-N$_3$), 1.37-1.30 (m, 2H, N-CH$_2$-CH$_2$-CH$_2$-C*H*$_2$-CH$_2$-CH$_2$-N$_3$), 0.99 (d, 3H, J = 6.4 Hz, CH$_3$).

Trans derivatives

1-(4-azidobutyl)-N-trans-(4-methylcyclohexyl)-2-oxo-1,2-dihydro-1,8-naphthyridine-3-carboxamide

Starting from 200 mg of intermediate 34. Compound **37** (140 mg, 0.37 mmol). White solid. Yield 76%.

^{1}H-NMR: (DMSO-*d*$_6$) δ (ppm): 9.61 (bs, 1H, exchangeable, NH), 8.87 (s, 1H, ar), 8.71-8.70 (m, 1H, ar), 8.08 (dd, 1H, J = 7.6 Hz, J = 1.6 Hz, ar), 7.30-7.28 (m, 1H, ar), 4.61 (t, 2H, J = 7.2 Hz, N-C*H*$_2$-CH$_2$-CH$_2$-CH$_2$-N$_3$), 3.95-3.86 (m, 1H, CH trans cyclohexyl), 3.38 (t, 2H, J = 6.8 Hz, N-CH$_2$-CH$_2$-CH$_2$-C*H*$_2$-N$_3$), 2.09-2.05 (m, 2H, N-CH$_2$-C*H*$_2$-CH$_2$-CH$_2$-N$_3$), 1.90-1.82 (m, 2H, N-CH$_2$-CH$_2$-C*H*$_2$-CH$_2$-N$_3$), 1.77-1.70 (m, 4H, cyclohexyl), 1.40-1.05 (m, 5H, cyclohexyl), 0.91 (d, 3H, J = 6.8 Hz, CH$_3$).

1-(5-azidopentyl)-N-trans-(4-methylcyclohexyl)-2-oxo-1,2-dihydro-1,8-naphthyridine-3-carboxamide

Starting from 150 mg of intermediate 35. Compound **38** (140 mg, 0.35 mmol). White solid. Yield >99%.

^{1}H-NMR: (DMSO-*d*$_6$) δ (ppm): 9.62 (bs, 1H, exchangeable, NH), 8.84 (s, 1H, ar), 8.69-8.67 (m, 1H, ar), 8.07-8.04 (dd, 1H, J = 7.6 Hz, J = 1.6 Hz, ar), 7.27-7.24 (m, 1H, ar), 4.55 (t, 2H, J = 7.6 Hz, N-C*H*$_2$-CH$_2$-CH$_2$-CH$_2$-CH$_2$-N$_3$), 3.94-3.84 (m, CH trans cyclohexyl), 3.28 (t, 2H, J = 6.8 Hz, N-CH$_2$-CH$_2$-CH$_2$-CH$_2$-C*H*$_2$-N$_3$), 2.07-2.04 (m, 2H, N-CH$_2$-C*H*$_2$-CH$_2$-CH$_2$-CH$_2$-N$_3$), 1.81-1.65 (m, 6H, cyclohexyl, N-CH$_2$-CH$_2$-C*H*$_2$-CH$_2$-CH$_2$-N$_3$), 1.55-1.22 (m, 5H, cyclohexyl), 0.89 (d, 3H, J = 6.4 Hz, CH$_3$).

1-(6-azidohexyl)-N-trans-(4-methylcyclohexyl)-2-oxo-1,2-dihydro-1,8-naphthyridine-3-carboxamide 39

Starting from 200 mg of intermediate 36. Compound **39** (200 mg, 0.49 mmol). White solid. Yield 73%.

^{1}H-NMR: (DMSO-d_6) δ (ppm): 9.62 (bs, 1H, exchangeable, NH), 8.82 (s, 1H, ar), 8.68-8.66 (m, 1H, ar), 8.04 (dd, 1H, J = 7.6 Hz, J = 1.6 Hz, ar), 7.25-7.22 (m, 1H, ar), 4.53 (t, 2H, J = 7.6 Hz, N-C*H*$_2$-CH$_2$-CH$_2$-CH$_2$-CH$_2$-CH$_2$-N$_3$), 3.92-3.84 (m, 1H, CH trans cyclohexyl), 3.23 (t, 2H, J = 6.8 Hz, N-CH$_2$-CH$_2$-CH$_2$-CH$_2$-CH$_2$-C*H*$_2$-N$_3$), 2.05-2.03 (m, 2H, N-CH$_2$-C*H*$_2$-CH$_2$-CH$_2$-CH$_2$-CH$_2$-N$_3$), 1.73-1.71 (m, 4H, N-CH$_2$-CH$_2$-CH$_2$-CH$_2$-C*H*$_2$-CH$_2$-N$_3$, N-CH$_2$-CH$_2$-C*H*$_2$-CH$_2$-CH$_2$-CH$_2$-N$_3$), 1.63-1.56 (m, 2H, N-CH$_2$-CH$_2$-CH$_2$-C*H*$_2$-CH$_2$-CH$_2$-N$_3$), 1.48-1.43 (m, 4H, cyclohexyl), 1.40-1.21 (m, 5H, cyclohexyl), 0.87 (d, 3H, J = 6.8 Hz, CH$_3$).

7.1.3.11 General procedure for the synthesis of 1-(3-(4-(((3-benzyl-5,7,8-trimethyl-2-oxo-2H-chromen-6-yl)oxy)alkyl)-1H-1,2,3-triazol-1-yl)alkyl)-N-4-methylcyclohexyl)-2-oxo-1,2-dihydro-1,8-naphthyridine-3-carboxamide (18-23)

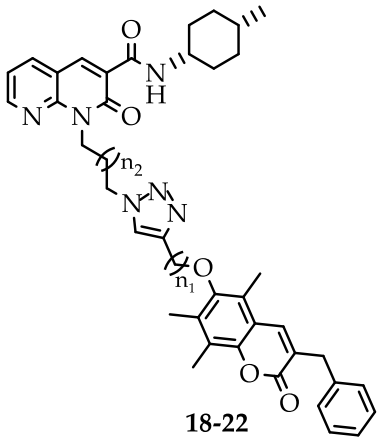

18-22

18 cis (n_1=1; n_2=4)
18 trans (n_1=1; n_2=4)
19 cis (n_1=1; n_2=5)
19 trans (n_1=1; n_2=5)
20 cis (n_1=1; n_2=6)
20 trans (n_1=1; n_2=6)
21 cis (n_1=3; n_2=4)
21 trans (n_1=3; n_2=4)
22 cis (n_1=3; n_2=5)
22 trans (n_1=3; n_2=5)
23 cis (n_1=3; n_2=6)
23 trans (n_1=3; n_2=6)

General procedure: Suitable intermediate **37**-**39** (1 eq), $CuSO_4 \cdot 5H_2O$ (1 eq) and ascorbic acid (3 eq) were added to a suspension of compound **29** or **30** (1 eq) in DMF (40 mL/mmol) and distilled H_2O (10 mL/mmol) and the reaction mixture was stirred at 80 °C for 5 h. After evaporating DMF ay 70 °C, the residue was dissolved in CH_2Cl_2 and the organic phase was washed with distilled H_2O. Once collected, the organic phase was dried over Na_2SO_4, filtered, evaporated under reduced pressure and purified by flash liquid chromatography on silica gel.

Cis derivatives 18-23

1-(4-(4-(((3-benzyl-5,7,8-trimethyl-2-oxo-2H-chromen-6-yl)oxy)methyl)-1H-1,2,3-triazol-1 yl)butyl)-N-cis-(4-methylcyclohexyl)-2-oxo-1,2-dihydro-1,8-naphthyridine-3-carboxamide

Starting from 55 mg of intermediate 29. Purification by flash column chromatography on silica gel (hexane/AcOEt/ MeOH 54:40:6). **18 cis** (60 mg, 0.09 mmol). White solid. Yield 56%.

m.p.: 95-97 °C.

^{1}H-NMR: ($CDCl_3$) δ (ppm): 9.95 (bs, 1H, exchangeable, N*H*), 8.89 (s, 1H, H4), 8.70-8.69 (m, 1H, H7), 8.09 (dd, 1H, J = 7.6 Hz, J = 1.6 Hz, H5), 7.71 (s, 1H, H5'' triazole), 7.51 (s, 1H, H4'), 7.36-7.27 (m, 6H, H6, H13', H14', H15', H16', H17'), 4.87 (s, 2H, O-C*H*$_2$), 4.66 (t, 2H, J = 7.2 Hz, (CO)N-CH$_2$-CH$_2$-CH$_2$-C*H*$_2$), 4.53 (t, 2H, J = 7.2 Hz, (CO)N-C*H*$_2$-CH$_2$-CH$_2$-CH$_2$), 4.28-4.25 (m, 1H, H13 cis), 3.91 (s, 2H, H11'), 2.34 (s, 3H, C5'-C*H*$_3$), 2.29 (s, 6H, C7'-C*H*$_3$, C8'-C*H*$_3$), 2.10-2.06 (m, 2H, (CO)N-CH$_2$-C*H*$_2$-CH$_2$-CH$_2$), 1.91-1.81 (m, 4H, m, 4H, H14 cyclohexyl, H18 cyclohexyl), 1.70-1.61 (m, 4H, H15 cyclohexyl, H17 cyclohexyl), 1.33-1.28 (m, 3H, H16 cyclohexyl, (CO)N-CH$_2$-CH$_2$-C*H*$_2$-CH$_2$, H16 cyclohexyl), 0.96 (d, 3H, J = 6.4 Hz, CH$_3$ cyclohexyl).

^{13}C-NMR: ($CDCl_3$) δ (ppm): 162.62 (C2), 161.79 (C2'), 161.74 (C11), 152.00 (C6'), 151.15 (C10), 149.59 (C7), 148.56 (C4''), 143.93 (C10'), 141.91 (C4'), 138.55 (C12'), 138.18 (C5), 136.96 (C4), 134.12 (C7'), 129.17 (C13', C17'), 128.67 (C5''), 127.42 (C14', C16'), 126.70 (C9'), 124.43 (C8'), 123.28 (C3'), 123.22 (C3), 122.78 (C15'), 119.19 (C5'), 116.62 (C9), 114.96 (C6), 66.51 (O-*C*H$_2$), 49.95 ((CO)N-CH$_2$-CH$_2$-CH$_2$-*C*H$_2$), 45.59 (C13), 40.77 (CO)N-*C*H$_2$-CH$_2$-CH$_2$-CH$_2$), 36.75 (C11'), 30.18 (C14, C18), 29.62 (C15, C17), 27.79 (C16), 24.84 ((CO)N-CH$_2$-CH$_2$-*C*H$_2$-CH$_2$), 21.58 ((CO)N-CH$_2$-*C*H$_2$-CH$_2$-CH$_2$, CH$_3$ cyclohexyl), 13.63 (C5'-*C*H$_3$), 11.86 (C7'-*C*H$_3$), 11.47 (C8'-*C*H$_3$).

HRMS (HESI): *m*/*z* calculated for $C_{19}H_{19}NO_3$ + H+ $[M + H]^+$: 714,3530. Found: 714,3599.

HPLC analysis: method 4, retention time = 9.51 min; peak area, 98% (280 nm).

1-(5-(4-(((3-benzyl-5,7,8-trimethyl-2-oxo-2H-chromen-6-yl)oxy)methyl)-1H-1,2,3-triazol-1-yl)pentyl)-N-cis-(4-methylcyclohexyl)-2-oxo-1,2-dihydro-1,8-naphthyridine-3-carboxamide

Starting from 70 mg of intermediate 29. Purification by flash column chromatography on silica gel ($CHCl_3$/ MeOH 98:2). **19 cis** (90 mg, 0.12 mmol). White solid. Yield 57%.

m.p.: 130-132 °C.

^{1}H-NMR: ($CDCl_3$) δ (ppm): 9.98 (bs, 1H, exchangeable, N*H*), 8.84 (s, 1H, H4), 8.68-8.67 (m, 1H, H7), 8.06-8.04 (m, 1H, H5), 7.66 (s, 1H, H5'' triazole), 7.50 (s, 1H, H4'), 7.32-7.23 (m, 6H, H6, H13', H14', H15', H16', H17'), 4.86 (s, 2H, O-C*H*$_2$), 4.56 (t, 2H, J = 7.6 Hz, (CO)N-CH$_2$-CH$_2$-CH$_2$-CH$_2$-C*H*$_2$), 4.42 (t, 2H, J = 7.2 Hz, (CO)N-C*H*$_2$-CH$_2$-CH$_2$-CH$_2$-CH$_2$), 4.27-4.23 (m, 1H, H13 cis), 3.88 (s, 2H, H11'), 2.32 (s, 3H, C5'-C*H*$_3$), 2.30 (s, 6H, C7'-C*H*$_3$, C8'-C*H*$_3$), 2.26-2.01 (m, 2H, (CO)N-CH$_2$-C*H*$_2$-CH$_2$-CH$_2$-CH$_2$), 1.83-1.80 (m, 4H, m, 4H, H14 cyclohexyl, H18 cyclohexyl), 1.67-1.51 (m, 7H, H16 cyclohexyl, H15 cyclohexyl, H17 cyclohexyl, (CO)N-CH$_2$-CH$_2$-CH$_2$-C*H*$_2$-CH$_2$), 1.32-1.26 (m, 2H, (CO)N-CH$_2$-CH$_2$-C*H*$_2$-CH$_2$-CH$_2$), 0.94 (d, 3H, J = 6.4 Hz, CH$_3$ cyclohexyl).

^{13}C-NMR: ($CDCl_3$) δ (ppm): 162.57 (C2), 161.85 (C2'), 161.80 (C11), 151.98 (C6'), 151.16 (C10), 149.65 (C7), 148.61 (C4''), 143.98 (C10'), 141.77 (C4'), 138.48 (C12'), 138.19 (C5), 136.97 (C4), 134.14 (C7'), 129.17 (C13', C17'), 128.67 (C5''), 127.45 (C14', C16'), 126.69 (C9'), 124.44 (C8'), 123.33 (C3'), 123.25 (C3), 122.58 (C15'), 119.06 (C5'), 116.65 (C9), 114.96 (C6), 66.52 (O-*C*H$_2$), 50.30 ((CO)N-CH$_2$-CH$_2$-CH$_2$-CH$_2$-*C*H$_2$), 45.66 (C13), 36.76 ((CO)N-*C*H$_2$-CH$_2$-CH$_2$-CH$_2$-CH$_2$), 30.94 (C11'), 30.21 (C14, C18), 29.97 (C15, C17), 29.59 (C16), 27.09 ((CO)N-CH$_2$-CH$_2$-CH$_2$-*C*H$_2$-CH$_2$), 23.93 ((CO)N-CH$_2$-*C*H$_2$-CH$_2$-CH$_2$-CH$_2$), 21.52 ((CO)N-CH$_2$-CH$_2$-*C*H$_2$-CH$_2$-CH$_2$, CH$_3$ cyclohexyl), 13.65 (C5'-*C*H$_3$), 11.88 (C7'-*C*H$_3$), 11.49 (C8'-*C*H$_3$).

HRMS (HESI): *m*/*z* calculated for $C_{19}H_{19}NO_3$ + H+ $[M + H]^+$: 728,3686. Found: 728,3771.

HPLC analysis: method 4, retention time = 10.84 min; peak area, 97.6% (280 nm).

1-(6-(4-(((3-benzyl-5,7,8-trimethyl-2-oxo-2H-chromen-6-yl)oxy)methyl)-1H-1,2,3-triazol-1-yl)hexyl)-N-cis-(4-methylcyclohexyl)-2-oxo-1,2-dihydro-1,8-naphthyridine-3-carboxamide

Starting from 70 mg of intermediate 29. Purification by flash column chromatography on silica gel (hexane/AcOEt/ MeOH 54:40:6). **20 cis** (90 mg, 0.12 mmol). White solid. Yield 58%.

m.p.: 113-115 °C.

^{1}H-NMR: ($CDCl_3$) δ (ppm): 9.99 (bs, 1H, exchangeable, N*H*), 8.87 (s, 1H, H4), 8.71-8.69 (m, 1H, H7), 8.07 (dd, 1H, J = 7.6 Hz, J = 1.6 Hz, H5), 7.65 (s, 1H, H5'' triazole), 7.51 (s, 1H, H4'), 7.36-7.25 (m, 6H, H6, H13', H14', H15', H16', H17'), 4.87 (s, 2H, O-C*H*$_2$), 4.58 (t, 2H, J = 7.6 Hz, (CO)N-CH$_2$-CH$_2$-CH$_2$-CH$_2$-CH$_2$-C*H*$_2$), 4.41 (t, 2H, J = 7.2 Hz, (CO)N-C*H*$_2$-CH$_2$-CH$_2$-CH$_2$-CH$_2$-CH$_2$), 4.26-4.24 (m, 1H, H13 cis), 3.91 (s, 2H, H11'), 2.34 (s, 3H, C5'-C*H*$_3$), 2.31 (s, 6H, C7'-C*H*$_3$, C8-C*H*$_3$), 2.02-1.94 (m, 2H, (CO)N-CH$_2$-C*H*$_2$-CH$_2$-CH$_2$-CH$_2$-CH$_2$), 1.85-1.45 (m, 17H, H16 cyclohexyl, H14 cyclohexyl, H18 cyclohexyl, H15 cyclohexyl, H17 cyclohexyl, (CO)N-CH$_2$-CH$_2$-CH$_2$-C*H*$_2$-CH$_2$-CH$_2$, (CO)N-CH$_2$-CH$_2$-CH$_2$-CH$_2$-C*H*$_2$-CH$_2$), 1.34-1.25 (m, 2H, (CO)N-CH$_2$-CH$_2$-C*H*$_2$-CH$_2$-CH$_2$-CH$_2$), 0.96 (d, 3H, J = 6.4 Hz, CH$_3$ cyclohexyl).

^{13}C-NMR: ($CDCl_3$) δ (ppm): 162.56 (C2,) 161.93 (C2'), 161.80 (C11), 151.16 (C6', C10), 149.68 (C7), 148.57 (C4''), 143.95 (C10'), 141.71 (C4'), 138.44 (C12'), 138.18 (C5), 136.99 (C4), 134.15 (C7'), 129.16 (C13', C17'), 128.67 (C5''), 126.70 (C14', C16'), 124.43 (C8', C9'), 123.28 (C3'), 123.18 (C3), 122.54 (C15'), 119.00 (C5'), 116.63 (C9), 114.92 (C6), 66.51 (O-*C*H$_2$), 50.42 ((CO)N-CH$_2$-CH$_2$-CH$_2$-CH$_2$-CH$_2$-*C*H$_2$), 45.68 (C13), 41.61 ((CO)N-*C*H$_2$-CH$_2$-CH$_2$-CH$_2$-CH$_2$-CH$_2$), 36.75 (C11'), 30.22 (C14, C18), 29.57 (C15, C17), 27.56 (C16), 26.39 ((CO)N-CH$_2$-CH$_2$-CH$_2$-CH$_2$-*C*H$_2$-CH$_2$), (CO)N-CH$_2$-*C*H$_2$-CH$_2$-CH$_2$-CH$_2$-CH$_2$), 26.18 ((CO)N-CH$_2$-CH$_2$-*C*H$_2$-CH$_2$-CH$_2$-CH$_2$), 21.49 ((CO)N-CH$_2$-CH$_2$-CH$_2$-*C*H$_2$-CH$_2$-CH$_2$, CH$_3$ cyclohexyl), 13.63 (C5'-*C*H$_3$), 11.86 (C7'-*C*H$_3$), 11.47 (C8'-*C*H$_3$).

HRMS (HESI): *m*/*z* calculated for $C_{19}H_{19}NO_3$ + H+ $[M + H]^+$: 742,3843. Found: 742,3915.

HPLC analysis: method 4, retention time = 12.08 min; peak area, 97.6% (280 nm).

1-(4-(4-(3-((3-benzyl-5,7,8-trimethyl-2-oxo-2H-chromen-6-yl)oxy)propyl)-1H-1,2,3-triazol-1-yl)butyl)-N-cis-(4-methylcyclohexyl)-2-oxo-1,2-dihydro-1,8-naphthyridine-3-carboxamide

Starting from 90 mg of intermediate 30. Purification by flash column chromatography on silica gel (hexane/AcOEt/ MeOH 60:36:4). **21 cis** (140 mg, 0.19 mmol). White solid. Yield 73%.

m.p.: 77-79 °C.

^{1}H-NMR: ($CDCl_3$) δ (ppm): 9.98 (bs, 1H, exchangeable, N*H*), 8.89 (s, 1H, H4), 8.71-8.69 (m, 1H, H7), 8.08 (dd, 1H, ar, J = 7.6 Hz, J = 1.6 Hz, H5), 7.51 (s, 1H, H5'' triazole), 7.43 (s, 1H, H4'), 7.37-7.27 (m, 6H, H6, H13', H14', H15', H16', H17'), 4.66 (t, 2H, J = 7.2 Hz, (CO)N-CH_2-CH_2-CH_2-C*H*$_2$), 4.49 (t, 2H, J = 7.2 Hz, (CO)N-C*H*$_2$-CH_2-CH_2-CH_2), 4.30-4.28 (m, 1H, H13 cis), 3.92 (s, 2H, H11'), 3.74 (t, 2H, J = 6.4 Hz, O-C*H*$_2$-CH_2-CH_2), 3.01-2.97 (m, 2H, O-CH_2-CH_2-C*H*$_2$), 2.34 (s, 3H, C5'-C*H*$_3$), 2.29 (s, 3H, C7'-C*H*$_3$), 2.28 (s, 3H, s, 3H, C8'-C*H*$_3$), 2.08-2.05 (m, 2H, O-CH_2-C*H*$_2$-CH_2), 1.89-1.84 (m, 4H, H14 cyclohexyl, H18 cyclohexyl), 1.73-1.56 (m, 6H, H15 cyclohexyl, H17 cyclohexyl, (CO)N-CH_2-C*H*$_2$-CH_2-CH_2), 1.35-1.28 (m, 3H, H16, (CO)N-CH_2-CH_2-C*H*$_2$-CH_2), 0.99 (d, 3H, J = 6.4 Hz, CH_3 cyclohexyl).

^{13}C-NMR: ($CDCl_3$) δ (ppm): 162.56 (C2), 161.90 (C2'), 161.83 (C11), 152.04 (C6'), 151.64 (C10), 149.52 (C7), 148.22 (C4''), 147.21 (C10'), 141.93 (C4'), 138.56 (C12'), 138.21 (C5), 137.13 (C4), 134.09 (C7'), 129.14 (C13', C17'), 128.64 (C5''), 127.10 (C14', C16'), 126.66 (C8'), 124.14 (C9'), 123.02 (C3', C3), 120.99 (C15'), 119.21 (C5'), 116.51 (C9), 114.89 (C6), 72.29 (O-*C*H_2-CH_2-CH_2), 49.71 ((CO)N-CH_2-CH_2-CH_2-*C*H_2), 45.54 (C13), 40.97 ((CO)N-*C*H_2-CH_2-CH_2-CH_2), 36.71 (C11'), 33.84 (O-CH_2-CH_2-*C*H_2), 31.08 (O-CH_2-*C*H_2-CH_2), 30.16 (C14, C18), 29.87 (C15, C17), 29.62 (C16), 27.75 ((CO)N-CH_2-*C*H_2-CH_2-CH_2), 24.84 ((CO)N-CH_2-CH_2-*C*H_2-CH_2), 21.63 (CH_3 cyclohexyl), 13.42 (C5'-*C*H_3), 11.78 (C7'-*C*H_3), 11.25 (C8'-*C*H_3).

HRMS (HESI): *m*/*z* calculated for $C_{19}H_{19}NO_3$ + H+ $[M + H]^+$: 742,3843. Found: 742,3912.

HPLC analysis: method 4, retention time = 10.53 min; peak area, 93.2% (280 nm).

1-(5-(4-(3-((3-benzyl-5,7,8-trimethyl-2-oxo-2H-chromen-6-yl)oxy)propyl)-1H-1,2,3-triazol-1-yl)pentyl)-N-(cis-4-methylcyclohexyl)-2-oxo-1,2-dihydro-1,8-naphthyridine-3-carboxamide

Starting from 100 mg of intermediate 30. Purification by flash column chromatography on silica gel (hexane/AcOEt/ MeOH 46:50:4). **22 cis** (90 mg, 0.12 mmol). White solid. Yield 41%.

m.p.: 105-107 °C.

^{1}H-NMR: ($CDCl_3$) δ (ppm): 9.98 (bs, 1H, exchangeable, N*H*), 8.87 (s, 1H, H4), 8.69-8.68 (m, 1H, H7), 8.07 (dd, 1H, ar, J = 8 Hz, J = 2 Hz, H5), 7.50 (s, 1H, H5'' triazole), 7.35-7.26 (m, 7H, H4', H6, H13', H14', H15', H16', H17'), 4.58 (t, 2H, J = 7.6 Hz, CO)N-CH_2-CH_2-CH_2-CH_2-C*H*$_2$), 4.38 (t, 2H, J = 7.2 Hz, (CO)N-C*H*$_2$-CH_2-CH_2-CH_2-CH_2), 4.28-4.24 (m, 1H, H13 cis), 3.89 (s, 2H, H11'), 3.74 (t, 2H, J = 6.4 Hz, O-C*H*$_2$-CH_2-CH_2), 2.98 (t, 2H, J = 7.2 Hz, O-CH_2-CH_2-C*H*$_2$), 2.32 (s, 3H, C5'-C*H*$_3$), 2.28 (s, 3H, C7'-C*H*$_3$), 2.27 (s, 3H, C8'-C*H*$_3$), 2.03-1.99 (m, 4H, O-CH_2-C*H*$_2$-CH_2, (CO)N-CH_2-CH_2-CH_2-C*H*$_2$-CH_2), 1.86-1.78 (m, 5H, H16 cyclohexyl, H14 cyclohexyl, H18 cyclohexyl), 1.71-1.53 (m, 6H, H15 cyclohexyl, H17 cyclohexyl, (CO)N-CH_2-C*H*$_2$-CH_2-CH_2-CH_2), 1.33-1.27 (m, 2H, (CO)N-CH_2-CH_2-C*H*$_2$-CH_2-CH_2), 0.97 (d, 3H, J = 6.8 Hz, CH_3 cyclohexyl).

^{13}C-NMR: ($CDCl_3$) δ (ppm): 162.55 (C2), 161.91 (C2'), 161.89 (C11), 152.02 (C6'), 151.66 (C10), 149.62 (C7), 148.27 (C4'', C10'), 147.28 (C4'), 141.78 (C12'), 138.21 (C5), 137.10 (C4), 134.11 (C7'), 129.16 (C13', C17'), 128.65 (C5'') 127.16 (C14', C16'), 126.67 (C8'), 124.15 (C9'), 123.14 (C3'), 123.08 (C3), 120.72 (C15'), 119.08 (C5'), 116.55 (C9), 114.91 (C6), 72.35 (O-*C*H_2-CH_2-CH_2), 50.04 ((CO)N-CH_2-CH_2-CH_2-CH_2-*C*H_2), 45.63 (C13), 41.39 ((CO)N-*C*H_2-CH_2-CH_2-CH_2-CH_2), 36.73 (C11'), 31.02 (O-CH_2-CH_2-*C*H_2), 30.19 (O-CH_2-*C*H_2-CH_2), 29.95 (C14, C18), 29.89 (C15, C17), 29.59 (C16), 27.09 ((CO)N-CH_2-*C*H_2-CH_2-CH_2-CH_2),

23.93 ((CO)N-CH_2-CH_2-CH_2-CH_2-CH_2), 22.40 ((CO)N-CH_2-CH_2-CH_2-CH_2-CH_2), 21.55 (CH_3 cyclohexyl), 13.45 (C5'-CH_3), 11.82 (C7'-CH_3), 11.29 (C8'-CH_3).

HRMS (HESI): *m/z* calculated for $C_{19}H_{19}NO_3$ + H+ $[M + H]^+$: 756,3999. Found: 756,4070.

HPLC analysis: method 4, retention time = 11.72 min; peak area, 96.4% (280 nm).

1-(6-(4-(3-((3-benzyl-5,7,8-trimethyl-2-oxo-2H-chromen-6-yl)oxy)propyl)-1H-1,2,3-triazol-1-yl)hexyl)-N-cis-(4-methylcyclohexyl)-2-oxo-1,2-dihydro-1,8-naphthyridine-3-carboxamide

Starting from 70 mg of intermediate 30. Purification by flash column chromatography on silica gel (hexane/AcOEt/ MeOH 54:40:6). **23 cis** (85 mg, 0.11 mmol). White solid. Yield 55%.

m.p.: 72-74 °C.

^{1}H-NMR: ($CDCl_3$) δ (ppm): 9.98 (bs, 1H, exchangeable, N*H*), 8.85 (s, 1H, H4), 8.68-8.67 (m, 1H, H7), 8.04 (dd, 1H, ar, J = 7.6 Hz, J = 1.6 Hz, H5), 7.49 (s, 1H, H5'' triazole), 7.33-7.22 (m, 7H, H4', H6, H13', H14', H15', H16', H17'), 4.55 (t, 2H, J = 7.6 Hz, (CO)N-CH_2-CH_2-CH_2-CH_2-CH_2-C*H*$_2$), 4.33 (t, 2H, J = 7.2 Hz, (CO)N-C*H*$_2$-CH_2-CH_2-CH_2-CH_2-CH_2), 4.26-4.24 (m, 1H, H13 cis), 3.88 (s, 2H, H11'), 3.72 (t, 2H, J = 6.4 Hz, O-C*H*$_2$-CH_2-CH_2), 2.96 (t, 2H, J = 7.6 Hz, O-CH_2-CH_2-C*H*$_2$), 2.30 (s, 3H, C5'-C*H*$_3$), 2.26 (s, 3H, C7'-C*H*$_3$), 2.25 (s, 3H, C8'-C*H*$_3$), 2.22-2.18 (m, 2H, O-CH_2-C*H*$_2$-CH_2), 1.95-1.92 (m, 2H, (CO)N-CH_2-CH_2-CH_2-CH_2-C*H*$_2$-CH_2), 1.85-1.60 (m, 8H, H14 cyclohexyl, H18 cyclohexyl, (CO)N-CH_2-C*H*$_2$-CH_2-CH_2-CH_2-CH_2, (CO)N-CH_2-CH_2-CH_2-C*H*$_2$-CH_2-CH_2), 1.54-1.40 (m, 5H, H16 cyclohexyl, H15 cyclohexyl, H17 cyclohexyl), 1.33-1.23 (m, 2H, (CO)N-CH_2-CH_2-C*H*$_2$-CH_2-CH_2-CH_2), 0.96 (d, 3H, J = 6.8 Hz, CH_3 cyclohexyl).

^{13}C-NMR: ($CDCl_3$) δ (ppm): 162.54 (C2), 161.94 (C2'), 161.88 (C11), 152.00 (C6'), 151.65 (C10), 149.66 (C7), 148.26 (C4''), 147.27 (C10'), 141.69 (C4'), 138.41 (C12'), 138.23 (C5), 137.06 (C4), 134.08 (C7'), 129.17 (C13', C17'), 128.65 (C5''), 127.18 (C14', C16'), 126.67 (C8'), 124.13 (C9'), 123.15 (C3'), 123.06 (C3), 120.61 (C15'), 119.00 (C5'), 116.54 (C9), 114.89

(C6), 72.33 (O-*C*H_2-CH_2-CH_2), 50.18 ((CO)N-CH_2-CH_2-CH_2-CH_2-CH_2-*C*H_2), 45.67 (C13), 41.60 ((CO)N-*C*H_2-CH_2-CH_2-CH_2-CH_2-CH_2), 36.73 (C11'), 30.22 (O-CH_2-CH_2-*C*H_2), 30.20 (O-CH_2-*C*H_2-CH_2), 29.88 (C14, C18), 29.56 (C15, C17), 27.55 (C16), 26.40 ((CO)N-CH_2-CH_2-CH_2-CH_2-*C*H_2-CH_2), 26.19 (CO)N-CH_2-*C*H_2-CH_2-CH_2-CH_2-CH_2), 22.39 ((CO)N-CH_2-CH_2-CH_2-CH_2-CH_2-CH_2), 21.49 ((CO)N-CH_2-CH_2-CH_2-*C*H_2-CH_2-CH_2, CH_3 cyclohexyl), 13.43 (C5'-*C*H_3), 11.80 (C7'-*C*H_3), 11.27 (C8'-*C*H_3).

HRMS (HESI): *m*/*z* calculated for $C_{19}H_{19}NO_3$ + H+ $[M + H]^+$: 770,4156. Found: 770,4227.

HPLC analysis: method 4, retention time = 12.69 min; peak area, 96.9% (280 nm).

Trans derivatives 18-23

1-(4-(4-(((3-benzyl-5,7,8-trimethyl-2-oxo-2H-chromen-6-yl)oxy)methyl)-1H-1,2,3-triazol-1 yl)butyl)-N-trans-(4-methylcyclohexyl)-2-oxo-1,2-dihydro-1,8-naphthyridine-3-carboxamide

Starting from 55 mg of intermediate 29. Purification by flash column chromatography on silica gel (hexane/AcOEt/ MeOH 60:36:4). **18 trans** (50 mg, 0.07 mmol). White solid. Yield 46%.

m.p.: 98-100 °C.

^{1}H-NMR: ($CDCl_3$) δ (ppm): 9.56 (bs, 1H, exchangeable, N*H*), 8.87 (s, 1H, H4), 8.69-8.67 (m, 1H, H7), 8.08 (dd, 1H, ar, J = 8 Hz, J = 2 Hz, H5), 7.70 (s, 1H, H5'' triazole), 7.50 (s, 1H, H4'), 7.35-7.22 (m, 6H, H6, H13', H14', H15', H16', H17'), 4.86 (s, 2H, O-C*H*$_2$), 4.63 (t, 2H, J = 7.6 Hz, (CO)N-CH$_2$-CH$_2$-CH$_2$-C*H*$_2$), 4.51 (t, 2H, J = 7.2 Hz, (CO)N-C*H*$_2$-CH$_2$-CH$_2$-CH$_2$), 3.92-3.83 (m, 1H, H13 trans, H11'), 2.32 (s, 3H, C5'-C*H*$_3$), 2.29 (s, 3H, C7'-C*H*$_3$), 2.28 (s, 3H, C8'-C*H*$_3$), 2.07-2.02 (m, 4H, H14 cyclohexyl, H18 cyclohexyl), 1.87-1.81 (m, 2H, (CO)N-CH$_2$-C*H*$_2$-CH$_2$-CH$_2$), 1.35-1.31 (m, 5H, H16 cyclohexyl, H15 cyclohexyl, H17 cyclohexyl), 1.29-1.23 (m, 2H, (CO)N-C*H*$_2$-CH$_2$-CH$_2$-CH$_2$), 0.90 (d, 3H, J = 6.4 Hz, CH$_3$ cyclohexyl).

^{13}C-NMR: ($CDCl_3$) δ (ppm): 162.57 (C2), 161.78 (C2'), 161.75 (C11), 152.04 (C6'), 151.16 (C10), 149.55 (C7), 148.57 (C4''), 143.97 (C10'), 142.07 (C4'), 138.57 (C12'), 138.18 (C5), 136.94 (C4), 134.12 (C7'), 129.17 (C13', C17'), 128.67 (C5''), 127.45 (C14', C16'), 126.70 (C9'), 124.43 (C8'), 123.29 (C3'), 123.14 (C3), 122.77 (C15'), 119.23 (C5'), 116.63 (C9), 114.98 (C6), 66.55 (O-*C*H$_2$), 49.92 ((CO)N-CH$_2$-CH$_2$-CH$_2$-*C*H$_2$), 48.79 (C13), 40.81 ((CO)N-*C*H$_2$-CH$_2$-CH$_2$-CH$_2$), 36.75 (C11'), 33.86 (C14, C18), 32.89 (C15, C17), 31.98 (C16), 27.79 ((CO)N-CH$_2$-CH$_2$-*C*H$_2$-CH$_2$), 24.83 ((CO)N-CH$_2$-*C*H$_2$-CH$_2$-CH$_2$), 22.22 (*C*H$_3$ cyclohexyl), 13.62 (C5'-*C*H$_3$), 11.85 (C7'-*C*H$_3$), 11.46 (C8'-*C*H$_3$).

HRMS (HESI): *m*/*z* calculated for $C_{19}H_{19}NO_3$ + H+ $[M + H]^+$: 714,3530. Found: 714,3605.

HPLC analysis: method 4, retention time = 9.87 min; peak area, 99.2% (280 nm).

1-(5-(4-(((3-benzyl-5,7,8-trimethyl-2-oxo-2H-chromen-6-yl)oxy)methyl)-1H-1,2,3-triazol-1-yl)pentyl)-N-trans-4-methylcyclohexyl)-2-oxo-1,2-dihydro-1,8-naphthyridine-3-carboxamide

Starting from 70 mg of intermediate 29. Purification by flash column chromatography on silica gel (hexane/AcOEt/ MeOH 54:40:6). **19 trans** (50 mg, 0.07 mmol). White solid. Yield 33%.

m.p.: 105-107 °C.

^{1}H-NMR: ($CDCl_3$) δ (ppm): 9.60 (bs, 1H, exchangeable, N*H*), 8.87 (s, 1H, H4), 8.70-8.68 (m, 1H, H7), 8.09- 8.07 (m, 1H, H5), 7.65 (s, 1H, H5'' triazole), 7.51 (s, 1H, H4'), 7.34-7.24 (m, 6H, H6, H13', H14', H15', H16', H17'), 4.88 (s, 2H, O-C*H*$_2$), 4.56 (t, 2H, J = 7.6 Hz, (CO)N-CH$_2$-CH$_2$-CH$_2$-CH$_2$-C*H*$_2$), 4.42 (t, 2H, J = 7.2 Hz, (CO)N-C*H*$_2$-CH$_2$-CH$_2$-CH$_2$-CH$_2$), 3.91-3.82 (m, 1H, H13 trans, H11'), 2.34 (s, 3H, C5'-C*H*$_3$), 2.31 (s, 6H, C7'-C*H*$_3$, C8'-C*H*$_3$), 2.08-2.03 (m, 4H, m, 4H, H14 cyclohexyl, H18 cyclohexyl), 1.84-1.72 (m, 4H, H15 cyclohexyl, H17 cyclohexyl), 1.54-1.48 (m, 2H, (CO)N-CH$_2$-C*H*$_2$-CH$_2$-CH$_2$-CH$_2$), 1.36-1.25 (m, 3H, H16 cyclohexyl, (CO)N-CH$_2$-CH$_2$-CH$_2$-C*H*$_2$-CH$_2$), 1.11-1.08 (m, 2H, (CO)N-CH$_2$-CH$_2$-C*H*$_2$-CH$_2$-CH$_2$), 0.90 (d, 3H, J = 6.4 Hz, CH$_3$ cyclohexyl).

^{13}C-NMR: ($CDCl_3$) δ (ppm): 162.52 (C2), 161.86 (C2'), 161.81 (C11), 152.04 (C6'), 151.16 (C10), 149.59 (C7), 148.61 (C4''), 143.99 (C10'), 141.95 (C4'), 138.53 (C12'), 138.18 (C5), 136.98 (C4), 134.14 (C7'), 129.17 (C13', C17'), 128.68 (C5''), 127.45 (C14', C16'), 126.70 (C9'), 124.44 (C8'), 123.33 (C3'), 123.14 (C3), 122.61 (C15'), 119.13 (C5'), 116.65 (C9), 114.98 (C6), 66.53 (O-*C*H$_2$), 50.33 ((CO)N-CH$_2$-CH$_2$-CH$_2$-CH$_2$-*C*H$_2$), 48.80 (C13), 41.45 ((CO)N-*C*H$_2$-CH$_2$-CH$_2$-CH$_2$-CH$_2$), 36.76 (C11'), 33.89 (C14, C18), 32.99 (C15, C17), 32.00 (C16), 29.98 ((CO)N-CH$_2$-CH$_2$-CH$_2$-*C*H$_2$-CH$_2$), 27.10 ((CO)N-CH$_2$-*C*H$_2$-CH$_2$-CH$_2$-CH$_2$), 23.96 (CO)N-CH$_2$-CH$_2$-*C*H$_2$-CH$_2$-CH$_2$), 22.23 (CH$_3$ cyclohexyl), 13.66 (C5'-*C*H$_3$), 11.88 (C7'-*C*H$_3$), 11.50 (C8'-*C*H$_3$).

HRMS (HESI): *m*/*z* calculated for $C_{19}H_{19}NO_3$ + H+ $[M + H]^+$: 728,3686. Found: 728,3762.

HPLC analysis: method 4, retention time = 11.25 min; peak area, 97.7% (280 nm).

1-(6-(4-(((3-benzyl-5,7,8-trimethyl-2-oxo-2H-chromen-6-yl)oxy)methyl)-1H-1,2,3-triazol-1-yl)hexyl)-N-trans-4-methylcyclohexyl)-2-oxo-1,2-dihydro-1,8-naphthyridine-3-carboxamide

Starting from 65 mg of intermediate 29. Purification by flash column chromatography on silica gel (hexane/AcOEt/ MeOH 54:40:6). **20 trans** (60 mg, 0.08 mmol). White solid. Yield 40%.

m.p.: 128-130 °C.

^{1}H-NMR: ($CDCl_3$) δ (ppm): 9.62 (bs, 1H, exchangeable, N*H*), 8.87 (s, 1H, H4), 8.71-8.69 (m, 1H, H7), 8.07 (dd, 1H, J = 7.6 Hz, J = 2 Hz, H5), 7.65 (s, 1H, H5'' triazole), 7.51 (s, 1H, H4'), 7.36-7.25 (m, 6H, H6, H13', H14', H15', H16', H17'), 4.87 (s, 2H, O-C*H*$_2$), 4.56 (t, 2H, J = 7.6 Hz, (CO)N-CH$_2$-CH$_2$-CH$_2$-CH$_2$-CH$_2$-C*H*$_2$), 4.40 (t, 2H, J = 7.2 Hz, (CO)N-C*H*$_2$-CH$_2$-CH$_2$-CH$_2$-CH$_2$-CH$_2$), 3.94-3.90 (m, 3H, H13 trans, H11'), 2.34 (s, 3H, C5'-C*H*$_3$), 2.31 (s, 6H, C7'-C*H*$_3$, C8'-C*H*$_3$), 2.10-2.05 (m, 2H, (CO)N-CH$_2$-CH$_2$-CH$_2$-CH$_2$-C*H*$_2$-CH$_2$), 1.99-1.96 (m, 2H, (CO)N-CH$_2$-C*H*$_2$-CH$_2$-CH$_2$-CH$_2$-CH$_2$), 1.80-1.47 (m, 5H, H16 cyclohexyl, H14 cyclohexyl, H18 cyclohexyl), 1.45-1.34 (m, 4H, H15 cyclohexyl, H17 cyclohexyl), 1.28-1.22 (m, 2H, (CO)N-CH$_2$-CH$_2$-CH$_2$-C*H*$_2$-CH$_2$-CH$_2$), 1.15-1.08 (m, 2H, (CO)N-CH$_2$-CH$_2$-C*H*$_2$-CH$_2$-CH$_2$-CH$_2$), 0.91 (d, 3H, J = 6.8 Hz, CH$_3$ cyclohexyl).

^{13}C-NMR: ($CDCl_3$) δ (ppm): 162.52 (C2), 161.91 (C2'), 161.80 (C11), 152.03 (C6'), 151.16 (C10), 149.63 (C7), 148.58 (C4''), 143.97 (C10'), 141.88 (C4'), 138.46 (C12'), 138.19 (C5), 136.98 (C4), 134.14 (C7'), 129.17 (C13', C17'), 128.67 (C5''), 127.42 (C14', C16'), 126.70 (C9'), 124.43 (C8'), 123.30 (C3'), 123.12 (C3), 122.50 (C15'), 119.05 (C5'), 116.63 (C9), 114.95 (C6), 66.55 (O-*C*H$_2$), 50.41 ((CO)N-*C*H$_2$-CH$_2$-CH$_2$-CH$_2$-CH$_2$-CH$_2$), 48.79 (C13), 41.70 ((CO)N-*C*H$_2$-CH$_2$-CH$_2$-CH$_2$-CH$_2$-CH$_2$), 36.76 (C11'), 33.90 (C14, C18), 32.99 (C15, C17), 32.00 (C16), 30.23 ((CO)N-CH$_2$-CH$_2$-CH$_2$-CH$_2$-*C*H$_2$-CH$_2$), 27.57 (CO)N-CH$_2$-*C*H$_2$-CH$_2$-CH$_2$-CH$_2$-CH$_2$), 26.44 ((CO)N-CH$_2$-CH$_2$-*C*H$_2$-CH$_2$-CH$_2$-CH$_2$), 26.19 ((CO)N-CH$_2$-CH$_2$-CH$_2$-*C*H$_2$-CH$_2$-CH$_2$), 22.24 (CH$_3$ cyclohexyl), 13.64 (C5'-*C*H$_3$), 11.87 (C7'-*C*H$_3$), 11.48 (C8'-*C*H$_3$).

HRMS (HESI): *m*/*z* calculated for $C_{19}H_{19}NO_3$ + H+ $[M + H]^+$: 742,3843. Found: 742,3914.

HPLC analysis: method 4, retention time = 12.42 min; peak area, 99.4% (280 nm).

1-(4-(4-(3-((3-benzyl-5,7,8-trimethyl-2-oxo-2H-chromen-6-yl)oxy)propyl)-1H-1,2,3-triazol-1-yl)butyl)-N-trans-(4-methylcyclohexyl)-2-oxo-1,2-dihydro-1,8-naphthyridine-3-carboxamide

Starting from 57 mg of intermediate 30. Purification by flash column chromatography on silica gel (hexane/AcOEt/ MeOH 60:36:4). **21 trans** (70 mg, 0.09 mmol). White solid. Yield 59%.

m.p.: 170-172 °C.

^{1}H-NMR: ($CDCl_3$) δ (ppm): 9.57 (bs, 1H, exchangeable, N*H*), 8.85 (s, 1H, H4), 8.67-8.66 (m, 1H, H7), 8.06 (dd, 1H, J = 7.6 Hz, J = 2 Hz, H5), 7.49 (s, 1H, H5'' triazole), 7.40 (s, 1H, H4'), 7.33-7.21 (m, 6H, H6, H13', H14', H15', H16', H17'), 4.60 (t, 2H, J = 7.6 Hz, (CO)N-CH_2-CH_2-CH_2-C*H*$_2$), 4.44 (t, 2H, J = 7.2 Hz, (CO)N-C*H*$_2$-CH_2-CH_2-CH_2), 3.90-3.86 (m, 3H, H13 trans, H11'), 3.71 (t, 2H, J = 6.4 Hz, O-C*H*$_2$-CH_2-CH_2), 2.96 (t, 2H, J = 7.6 Hz, O-CH_2-CH_2-C*H*$_2$), 2.30 (s, 3H, C5'-C*H*$_3$), 2.26 (s, 3H, C7'-C*H*$_3$), 2.25 (s, 3H, C8'-C*H*$_3$), 2.21-2.18 (m, 2H, O-CH_2-C*H*$_2$-CH_2), 2.07-2.04 (m, 5H, H16 cyclohexyl, H14 cyclohexyl, H18 cyclohexyl), 1.81-1.72 (m, 4H, H15 cyclohexyl, H17 cyclohexyl), 1.32-1.29 (m, 2H, (CO)N-CH_2-C*H*$_2$-CH_2-CH_2), 1.15-1.11 (m, 2H, (CO)N-CH_2-CH_2-C*H*$_2$-CH_2), 0.89 (d, 3H, J = 6.4 Hz, CH_3 cyclohexyl).

^{13}C-NMR: ($CDCl_3$) δ (ppm): 162.56 (C2), 161.92 (C2'), 161.80 (C11), 152.05 (C6'), 151.65 (C10), 149.54 (C7), 148.47 (C4''), 148.19 (C10'), 142.06 (C4'), 138.56 (C12'), 138.23 (C5), 137.07 (C4), 134.08 (C7'), 129.19 (C13', C17'), 128.67 (C5''), 127.22 (C14', C16'), 126.68 (C8'), 124.12 (C9'), 123.12 (C3'), 123.10 (C3), 120.87 (C15'), 119.23 (C5'), 116.71 (C9), 114.96 (C6), 72.30 (O-*C*H_2-CH_2-CH_2), 49.73 ((CO)N-CH_2-CH_2-CH_2-*C*H_2), 48.79 (C13), 40.88 ((CO)N-*C*H_2-CH_2-CH_2-CH_2), 36.74 (C11'), 33.87 (O-CH_2-CH_2-*C*H_2), 33.00 (O-CH_2-*C*H_2-CH_2), 32.00 (C14, C18), 29.88 (C15, C17), 27.81 (C16), 24.89 ((CO)N-CH_2-*C*H_2-CH_2-CH_2), 22.39 ((CO)N-CH_2-CH_2-*C*H_2-CH_2), 22.23 (CH_3 cyclohexyl), 13.44 (C5'-*C*H_3), 11.83 (C7'-*C*H_3), 11.27 (C8'-*C*H_3).

HRMS (HESI): *m*/*z* calculated for $C_{19}H_{19}NO_3$ + H+ $[M + H]^+$: 742,3843. Found: 742,3908.

HPLC analysis: method 4, retention time = 10.94 min; peak area, 99.8% (280 nm).

1-(5-(4-(3-((3-benzyl-5,7,8-trimethyl-2-oxo-2H-chromen-6-yl)oxy)propyl)-1H-1,2,3-triazol-1-yl)pentyl)-N-trans-(4-methylcyclohexyl)-2-oxo-1,2-dihydro-1,8-naphthyridine-3-carboxamide

Starting from 70 mg of intermediate 30. Purification by flash column chromatography on silica gel (hexane/AcOEt/ MeOH 70:28:2). **22 trans** (80 mg, 0.10 mmol). White solid. Yield 53%.

m.p.: 83-85 °C.

^{1}H-NMR: ($CDCl_3$) δ (ppm): 9.60 (bs, 1H, exchangeable, N*H*), 8.86 (s, 1H, H4), 8.69-8.67 (m, 1H, H7), 8.07 (dd, 1H, ar, J = 7.6 Hz, J = 1.6 Hz, H5), 7.49 (s, 1H, H5'' triazole), 7.33-7.24 (m, 7H, H4', H6, H13', H14', H15', H16', H17'), 4.54 (t, 2H, J = 7.6 Hz, (CO)N-CH_2-CH_2-CH_2-CH_2), 4.36 (t, 2H, J = 7.2 Hz, (CO)N-CH_2-CH_2-CH_2-CH_2-CH_2), 3.91-3.88 (m, 1H, H13 trans, H11'), 3.73 (t, 2H, J = 6.4 Hz, O-CH_2-CH_2-CH_2), 2.97 (t, 2H, J = 7.6 Hz, O-CH_2-CH_2-CH_2), 2.31 (s, 3H, C5'-CH_3), 2.28 (s, 3H, C7'-CH_3), 2.27 (s, 3H, C8'-CH_3), 2.09-1.99 (m, 4H, O-CH_2-CH_2-CH_2, (CO)N-CH_2-CH_2-CH_2-CH_2-CH_2), 1.81-1.73 (m, 5H, H16 cyclohexyl, H14 cyclohexyl, H18 cyclohexyl), 1.50-1.46 (m, 2H, (CO)N-CH_2-CH_2-CH_2-CH_2-CH_2), 1.37-1.28 (m, 4H, H15 cyclohexyl, H17 cyclohexyl), 1.14-1.08 (m, 2H, (CO)N-CH_2-CH_2-CH_2-CH_2-CH_2), 0.90 (d, 3H, J = 6.4 Hz, CH_3 cyclohexyl).

^{13}C-NMR: ($CDCl_3$) δ (ppm): 162.48 (C2), 161.90 (C2', C11), 152.07 (C6'), 151.66 (C10), 149.55 (C7), 148.26 (C10'), 147.28 (C4''), 141.95 (C4'), 138.51 (C12'), 138.21 (C5), 137.10 (C4), 134.10 (C7'), 129.15 (C13', C17'), 128.64 (C5''), 127.14 (C14', C16'), 126.66 (C8'), 124.15 (C9'), 123.06 (C3'), 123.03 (C3), 120.71 (C15'), 119.13 (C5'), 116.54 (C9), 114.92 (C6), 72.33 (O-*C*H_2-CH_2-CH_2), 50.02 ((CO)N-CH_2-CH_2-CH_2-CH_2-*C*H_2), 48.80 (C13), 41.46 ((CO)N-*C*H_2-CH_2-CH_2-CH_2-CH_2), 36.72 (C11'), 33.87 (O-CH_2-CH_2-*C*H_2), 32.97 (O-CH_2-*C*H_2-CH_2), 31.97 (C14, C18), 29.95 (C15, C17), 29.88 (C16), 27.12 ((CO)N-CH_2-*C*H_2-CH_2-

CH_2-CH_2), 23.97 ((CO)N-CH_2-CH_2-CH_2-CH_2-CH_2), 22.39 ((CO)N-CH_2-CH_2-CH_2-CH_2-CH_2), 22.24 (CH_3 cyclohexyl), 13.45 (C5'-CH_3), 11.81 (C7'-CH_3), 11.28 (C8'-CH_3).

HRMS (HESI): *m/z* calculated for $C_{19}H_{19}NO_3$ + H+ $[M + H]^+$: 756,3999. Found: 756,4065.

HPLC analysis: method 4, retention time = 12.13 min; peak area, 99.2% (280 nm).

1-(6-(4-(3-((3-benzyl-5,7,8-trimethyl-2-oxo-2H-chromen-6-yl)oxy)propyl)-1H-1,2,3-triazol-1-yl)hexyl)-N-trans-(4-methylcyclohexyl)-2-oxo-1,2-dihydro-1,8-naphthyridine-3-carboxamide

Starting from 55 mg of intermediate 30. Purification by flash column chromatography on silica gel (hexane/AcOEt/ MeOH 60:34:6). **23 trans** (80 mg, 0.10 mmol). White solid. Yield 65%.

m.p.: 112-114 °C.

^{1}H-NMR: ($CDCl_3$) δ (ppm): 9.62 (bs, 1H, exchangeable, N*H*), 8.84 (s, 1H, H4), 8.68-8.66 (m, 1H, H7), 8.04 (dd, 1H, J = 7.6 Hz, J = 1.6 Hz, H5), 7.48 (s, 1H, H5'' triazole), 7.33-7.21 (m, 7H, H4', H6, H13', H14', H15', H16', H17'), 4.52 (t, 2H, J = 7.6 Hz, (CO)N-CH_2-CH_2-CH_2-CH_2-CH_2-C*H*$_2$), 4.33 (t, 2H, J = 7.6 Hz, (CO)N-C*H*$_2$-CH_2-CH_2-CH_2-CH_2-CH_2), 3.91-3.88 (m, 1H, H13 trans, H11'), 3.72 (t, 2H, J = 6.4 Hz, O-C*H*$_2$-CH_2-CH_2), 2.96 (t, 2H, J = 7.6 Hz, O-CH_2-CH_2-C*H*$_2$), 2.29 (s, 3H, C5'-C*H*$_3$), 2.26 (s, 3H, C7'-C*H*$_3$), 2.25 (s, 3H, C8'-C*H*$_3$), 2.22-2.18 (m, 2H, O-CH_2-C*H*$_2$-CH_2), 2.08-2.04 (m, 2H, (CO)N-CH_2-CH_2-CH_2-CH_2-C*H*$_2$-CH_2), 1.94-1.90 (m, 2H, (CO)N-CH_2-C*H*$_2$-CH_2-CH_2-CH_2-CH_2), 1.75-1.72 (m, 4H, H14 cyclohexyl, H18 cyclohexyl), 1.51-1.27 (m, 7H, H16 cyclohexyl, H15 cyclohexyl, H17 cyclohexyl, (CO)N-CH_2-CH_2-CH_2-C*H*$_2$-CH_2-CH_2), 1.11-1.07 (m, 2H, (CO)N-CH_2-CH_2-C*H*$_2$-CH_2-CH_2-CH_2), 0.90 (d, 3H, J = 6.4 Hz, CH_3 cyclohexyl).

^{13}C-NMR: ($CDCl_3$) δ (ppm): 162.50 (C2), 161.93 (C2'), 161.88 (C11), 152.04 (C6'), 151.66 (C10), 149.61 (C7), 148.27 (C4''), 147.26 (C10'), 141.86 (C4'), 138.44 (C12'), 138.24 (C5), 137.05 (C4), 134.07 (C7'), 129.17 (C13', C17'), 128.65 (C5''), 127.20 (C14', C16'), 126.67 (C8'), 124.12 (C9'), 123.08 (C3'), 123.07 (C3), 120.60 (C15'), 119.04 (C5'), 116.54 (C9), 114.92

(C6), 72.32 (O-*C*H_2-CH_2-CH_2), 50.17 ((CO)N-CH_2-CH_2-CH_2-CH_2-CH_2-*C*H_2), 48.79 (C13), 41.68 ((CO)N-*C*H_2-CH_2-CH_2-CH_2-CH_2-CH_2), 36.74 (C11'), 33.89 (O-CH_2-CH_2-*C*H_2), 32.98 (O-CH_2-*C*H_2-CH_2), 32.00 (C14, C18), 30.21 (C15, C17), 29.88 (C16), 27.56 ((CO)N-CH_2-CH_2-CH_2-CH_2-*C*H_2-CH_2), 26.45 ((CO)N-CH_2-*C*H_2-CH_2-CH_2-CH_2-CH_2), 26.19 ((CO)N-CH_2-CH_2-*C*H_2-CH_2-CH_2-CH_2), 22.39 ((CO)N-CH_2-CH_2-CH_2-*C*H_2-CH_2-CH_2), 22.24 (CH_3 cyclohexyl), 13.43 (C5'-*C*H_3), 11.80 (C7'-*C*H_3), 11.27 (C8'-*C*H_3 20').

HRMS (HESI): *m*/*z* calculated for $C_{19}H_{19}NO_3$ + H+ $[M + H]^+$: 770,4156. Found: 770,4229.

HPLC analysis: method 4, retention time = 13.02 min; peak area, 99.8% (280 nm).

7.2 Biological evaluation

7.2.1 Cell culture

Chinese hamster ovary (CHO)-K1 cells, either untransfected or stably expressing *h*CB_1R or *h*CB_2R, have been already described in literature. [154] [155] According to the Lipofectamine 3000 standard operating procedure (ThermoFisher Scientific, Waltham, MA), CHO-K1 cells expressing *h*GPR55 were obtained by transfecting CHO-K1 cells with 2 μg pcDNA3.1+-*h*GPR55 plasmid (cDNA Resource Centre, Bloomsburg, PA; Cat No. GPR0550000). Cells were cultured at 37 °C, 5% CO_2 in F-12/DMEM containing 1 mM L-glutamine, 10% FBS, and 1% Pen/Strep. Hygromycin B (300 μg/mL) and G418 (600 μg/mL) were used for CHO *h*CB_1R cells, and G418 (400 μg/mL) was used for CHO *h*CB_2R cells. For the collection of membranes to be used in radioligand displacement assays, cells were grown in 15 cm^2 dishes to confluency, washed in 0.1 M phosphate-buffered saline (PBS), scraped from dishes, centrifuged, and frozen at − 80 °C until required.

7.2.2 [^{3}H]CP55,940 Radioligand Displacement Assay

Assays used 1 nM [^{3}H]CP55,940 and Tris binding buffer (50 mM Tris−HCl, 50 mM Tris−base, 0.1% BSA, pH 7.4), in a total assay volume of 500 μL. After homogenizing transfected *h*GPR55, *h*CB_1R, or *h*CB_2R CHO-K1 cells with Tris binding buffer, we proceeded with protein quantification according to the directions of the Pierce BCA protein assay kit (ThermoFisher, Waltham, MA). Binding was initiated by incubating six different concentrations of each compound (from 0.1 nM to 10 μM, obtained from 1.00 mM stock solutions in DMSO) at 37 °C with 25 μg of protein from *h*GPR55, *h*CB_1R, or *h*CB_2R CHO cell membranes and 1 nM [^{3}H]CP55,940 for 120 min. The assay was terminated quenching with ice-cold Tris binding buffer and filtrating under vacuum using a 24-well sampling manifold (Brandel Cell Harvester; Brandel, Inc., Gaithersburg, MD) and Brandel GF/B filters. The filtration was carried out washing each reaction well

with 1.2 mL of Tris binding buffer for six times. The filters were air-dried and then placed in 5 mL of scintillation fluid overnight (Ul-tima Gold XR, PerkinElmer). Liquid scintillation spectrometry was used for quantifying radioactivity. Specific binding was defined as the difference between the binding that occurred in the presence and absence of 1 μM unlabelled CP55,940. Data are presented as percentage of [^{3}H]CP55,940 bound displacement.

7.2.3 *In-cell* western quantification of ERK1/2 phosphorylation

Cells were seeded at approximately 2,000 cells/well in 96-well plates and treated with 0.1 nM – 10 μM compounds for 30 min. Cells were then fixed with 4% paraformaldehyde at room temperature for 10 min. Cells were washed 3 times with 100 μL 1X PBS for 5 min and incubated for 1 h at room temperature with blocking solution (PBS, 20% Odyssey blocking buffer, and 0.1% TritonX-100). Next, cells were exposed overnight at 4°C to primary antibodies for ERK1/2 (rabbit polyclonal IgG, Cat# sc-292838) (Santa Cruz Biotechnol-ogy, Santa Cruz, CA) or p-ERK1/2(T202/Y204) (mouse monoclonal IgG, Cat# sc-136521) diluted (1:200) in blocking solution and then washed 3 times with 100 μL PBS for 5 min. Cells were exposed to the secondary antibodies: goat polyclonal anti-mouse IgG IRDye680-conjugated antibody diluted 1:500 (Li-Cor Bio-sciences, IgG, Cat# P/N 925-68070, RRID AB-2651128, lot# C50113-17) and goat polyclonal anti-rabbit IgG IRDye800-conjugated antibody diluted 1:500 (Li-Cor Biosciences, IgG, Cat# P/S 926-32210, RRID AB-2687825, lot# C50113-18) at room temperature for 1 h. Cells were washed 3 times with 100 μL PBS for 5 min. Analyses were conducted using the Odyssey Imaging system and software (version 3.0; Li-Cor).

7.2.4 Data analysis

In [^{3}H]CP55,940 radioligand competition binding, data were calculated as % maximal ^{3}H bound (i.e. 100%). For p-ERK *in-cell* westerns functional assay, results are presented as

fold over vehicle response (i.e. 1). The values of K_i, EC_{50}, and E_{max} were determined using non-linear regression (3-parameters) (GraphPad, Prism, v. 9.0). P values < 0.05 were considered as significant. Values are showed as the mean ± the standard error of the mean (SEM) or 95% confidence interval (CI), as indicated in tables and figure legends.

7.3 Metabolic evaluation

7.3.1 Metabolic assay

Each compound (final concentration 10 μM) was incubated with 173 μL of phosphate buffer, pH 7.4, 4 μL of human liver microsomes (20 mg/mL) and 20 μL of NADPH solubilized in $MgCl_2$ 2.4 mM (final concentration 0.24 mM) to a final volume of 200 μL at 37 °C at different times up to 60 minutes. After blocking the reaction with 500 μL of ACN, each sample was centrifuged at 10000 rpm for 15 minutes. Supernatant was collected (680 μL), dried at 70 °C under nitrogen flux and suspended in 100 μL of ACN. The solution was analysed by using HPLC-HRMS. An isocratic elution with 90% of B and 10% of A was chosen.

MetaSite is a computational procedure which includes metabolic transformations related to CYP450 and reactions mediated by the flavin-containing monooxygenase (FMO). This program considers both the enzyme-substrate recognition, and chemical transformations induced by the enzyme, as thermodynamic and cynetic factors, respectively. The Molecular Interaction Fields (MIFs) in the CYP binding sites were obtained through GRID, [156] a computational procedure able to mimics the amino acid movements that occur in the CYP active site to accommodate different substrates according to their sizes, shapes, and interaction patterns. [157]

8. Bibliography

[1] H.-C. Lu, K. Mackie, An Introduction to the Endogenous Cannabinoid System, Biol. Psychiatry. 79 (2016) 516–525. https://doi.org/10.1016/j.biopsych.2015.07.028.

[2] E.L. Scotter, M.E. Abood, M. Glass, The endocannabinoid system as a target for the treatment of neurodegenerative disease: Endocannabinoids in neurodegenerative disease, Br. J. Pharmacol. 160 (2010) 480–498. https://doi.org/10.1111/j.1476-5381.2010.00735.x.

[3] W.A. Devane, L. Hanuš, A. Breuer, R.G. Pertwee, L.A. Stevenson, G. Griffin, D. Gibson, A. Mandelbaum, A. Etinger, R. Mechoulam, Isolation and Structure of a Brain Constituent That Binds to the Cannabinoid Receptor, Science. 258 (1992) 1946–1949. https://doi.org/10.1126/science.1470919.

[4] R. Mechoulam, S. Ben-Shabat, L. Hanus, M. Ligumsky, N.E. Kaminski, A.R. Schatz, A. Gopher, S. Almog, B.R. Martin, D.R. Compton, R.G. Pertwee, G. Griffin, M. Bayewitch, J. Barg, Z. Vogel, Identification of an endogenous 2-monoglyceride, present in canine gut, that binds to cannabinoid receptors, Biochem. Pharmacol. 50 (1995) 83–90. https://doi.org/10.1016/0006-2952(95)00109-D.

[5] C. Muller, P. Morales, P.H. Reggio, Cannabinoid Ligands Targeting TRP Channels, Front. Mol. Neurosci. 11 (2019) 487. https://doi.org/10.3389/fnmol.2018.00487.

[6] P. Morales, N. Jagerovic, Advances Towards The Discovery of GPR55 Ligands, Curr. Med. Chem. 23 (2016) 2087–2100. https://doi.org/10.2174/0929867323666160425113836.

[7] V. Di Marzo, L. De Petrocellis, Why do cannabinoid receptors have more than one endogenous ligand?, Philos. Trans. R. Soc. B Biol. Sci. 367 (2012) 3216–3228. https://doi.org/10.1098/rstb.2011.0382.

[8] R.G. Pertwee, Endocannabinoids and Their Pharmacological Actions, in: R.G. Pertwee (Ed.), Endocannabinoids, Springer International Publishing, Cham, 2015: pp. 1–37. https://doi.org/10.1007/978-3-319-20825-1_1.

[9] F. Fezza, M. Bari, R. Florio, E. Talamonti, M. Feole, M. Maccarrone, Endocannabinoids, Related Compounds and Their Metabolic Routes, Molecules. 19 (2014) 17078–17106. https://doi.org/10.3390/molecules191117078.

[10] D.A. Kendall, G.A. Yudowski, Cannabinoid Receptors in the Central Nervous System: Their Signaling and Roles in Disease, Front. Cell. Neurosci. 10 (2017). https://doi.org/10.3389/fncel.2016.00294.

[11] S. Zou, U. Kumar, Cannabinoid Receptors and the Endocannabinoid System: Signaling and Function in the Central Nervous System, Int. J. Mol. Sci. 19 (2018) 833. https://doi.org/10.3390/ijms19030833.

[12] T. Bisogno, M. Maccarrone, Endocannabinoid signaling and its regulation by nutrients: Endocannabinoid Signaling and Nutrients, BioFactors. 40 (2014) 373–380. https://doi.org/10.1002/biof.1167.

[13] K. Tsuboi, T. Uyama, Y. Okamoto, N. Ueda, Endocannabinoids and related N-acylethanolamines: biological activities and metabolism, Inflamm. Regen. 38 (2018) 28. https://doi.org/10.1186/s41232-018-0086-5.

[14] D.G. Deutsch, S.T. Glaser, J.M. Howell, J.S. Kunz, R.A. Puffenbarger, C.J. Hillard, N. Abumrad, The Cellular Uptake of Anandamide Is Coupled to Its Breakdown by Fatty-acid Amide Hydrolase, J. Biol. Chem. 276 (2001) 6967–6973. https://doi.org/10.1074/jbc.M003161200.

[15] M. Kaczocha, S.T. Glaser, D.G. Deutsch, Identification of intracellular carriers for the endocannabinoid anandamide, Proc. Natl. Acad. Sci. 106 (2009) 6375–6380. https://doi.org/10.1073/pnas.0901515106.

[16] S. Nicolussi, J. Gertsch, Endocannabinoid Transport Revisited, in: Vitam. Horm., Elsevier, 2015: pp. 441–485. https://doi.org/10.1016/bs.vh.2014.12.011.

[17] A.C. Howlett, M.E. Abood, CB 1 and CB 2 Receptor Pharmacology, in: Adv. Pharmacol., Elsevier, 2017: pp. 169–206. https://doi.org/10.1016/bs.apha.2017.03.007.

[18] S. Mallipeddi, D.R. Janero, N. Zvonok, A. Makriyannis, Functional selectivity at G-protein coupled receptors: Advancing cannabinoid receptors as drug targets, Biochem. Pharmacol. 128 (2017) 1–11. https://doi.org/10.1016/j.bcp.2016.11.014.

[19] J. Ramos, V.L. Cruz, J. Martínez-Salazar, N.E. Campillo, J.A. Páez, Dissimilar interaction of CB1/CB2 with lipid bilayers as revealed by molecular dynamics simulation, Phys Chem Chem Phys. 13 (2011) 3660–3668. https://doi.org/10.1039/C0CP01456G.

[20] C. Nogueras-Ortiz, G.A. Yudowski, The Multiple Waves of Cannabinoid 1 Receptor Signaling, Mol. Pharmacol. 90 (2016) 620–626. https://doi.org/10.1124/mol.116.104539.

[21] M.S. Ibsen, D.B. Finlay, M. Patel, J.A. Javitch, M. Glass, N.L. Grimsey, Cannabinoid CB1 and CB2 Receptor-Mediated Arrestin Translocation: Species, Subtype, and Agonist-Dependence, Front. Pharmacol. 10 (2019) 350. https://doi.org/10.3389/fphar.2019.00350.

[22] R.G. Pertwee, A.C. Howlett, M.E. Abood, S.P.H. Alexander, V. Di Marzo, M.R. Elphick, P.J. Greasley, H.S. Hansen, G. Kunos, K. Mackie, R. Mechoulam, R.A. Ross, International Union of Basic and Clinical Pharmacology. LXXIX. Cannabinoid Receptors and Their Ligands: Beyond CB $_1$ and CB $_2$, Pharmacol. Rev. 62 (2010) 588–631. https://doi.org/10.1124/pr.110.003004.

[23] A.R. Schatz, M. Lee, R.B. Condie, J.T. Pulaski, N.E. Kaminski, Cannabinoid Receptors CB1 and CB2: A Characterization of Expression and Adenylate Cyclase

Modulation within the Immune System, Toxicol. Appl. Pharmacol. 142 (1997) 278–287. https://doi.org/10.1006/taap.1996.8034.

[24] S.-J. Yu, D. Reiner, H. Shen, K.-J. Wu, Q.-R. Liu, Y. Wang, Time-Dependent Protection of CB2 Receptor Agonist in Stroke, PLOS ONE. 10 (2015) e0132487. https://doi.org/10.1371/journal.pone.0132487.

[25] R. Ferrisi, C. Ceni, S. Bertini, M. Macchia, C. Manera, F. Gado, Medicinal Chemistry approach, pharmacology and neuroprotective benefits of CB2R modulators in neurodegenerative diseases, Pharmacol. Res. 170 (2021) 105607. https://doi.org/10.1016/j.phrs.2021.105607.

[26] J. Wu, Cannabis, cannabinoid receptors, and endocannabinoid system: yesterday, today, and tomorrow, Acta Pharmacol. Sin. 40 (2019) 297–299. https://doi.org/10.1038/s41401-019-0210-3.

[27] A. Stumpf, D. Parthier, R.P. Sammons, A.V. Stempel, J. Breustedt, B.R. Rost, D. Schmitz, Cannabinoid type 2 receptors mediate a cell type-specific self-inhibition in cortical neurons, Neuropharmacology. 139 (2018) 217–225. https://doi.org/10.1016/j.neuropharm.2018.07.020.

[28] H.-Y. Zhang, M. Gao, Q.-R. Liu, G.-H. Bi, X. Li, H.-J. Yang, E.L. Gardner, J. Wu, Z.-X. Xi, Cannabinoid CB 2 receptors modulate midbrain dopamine neuronal activity and dopamine-related behavior in mice, Proc. Natl. Acad. Sci. 111 (2014). https://doi.org/10.1073/pnas.1413210111.

[29] A.V. Stempel, A. Stumpf, H.-Y. Zhang, T. Özdoğan, U. Pannasch, A.-K. Theis, D.-M. Otte, A. Wojtalla, I. Rácz, A. Ponomarenko, Z.-X. Xi, A. Zimmer, D. Schmitz, Cannabinoid Type 2 Receptors Mediate a Cell Type-Specific Plasticity in the Hippocampus, Neuron. 90 (2016) 795–809. https://doi.org/10.1016/j.neuron.2016.03.034.

[30] F.S. den Boon, P. Chameau, Q. Schaafsma-Zhao, W. van Aken, M. Bari, S. Oddi, C.G. Kruse, M. Maccarrone, W.J. Wadman, T.R. Werkman, Excitability of prefrontal cortical pyramidal neurons is modulated by activation of intracellular type-2 cannabinoid receptors, Proc. Natl. Acad. Sci. 109 (2012) 3534–3539. https://doi.org/10.1073/pnas.1118167109.

[31] H.S. Kwon, S.-H. Koh, Neuroinflammation in neurodegenerative disorders: the roles of microglia and astrocytes, Transl. Neurodegener. 9 (2020) 42. https://doi.org/10.1186/s40035-020-00221-2.

[32] Y. Tang, W. Le, Differential Roles of M1 and M2 Microglia in Neurodegenerative Diseases, Mol. Neurobiol. 53 (2016) 1181–1194. https://doi.org/10.1007/s12035-014-9070-5.

[33] S. Xu, J. Lu, A. Shao, J.H. Zhang, J. Zhang, Glial Cells: Role of the Immune Response in Ischemic Stroke, Front. Immunol. 11 (2020) 294. https://doi.org/10.3389/fimmu.2020.00294.

[34] V.H. Perry, J.A.R. Nicoll, C. Holmes, Microglia in neurodegenerative disease, Nat. Rev. Neurol. 6 (2010) 193–201. https://doi.org/10.1038/nrneurol.2010.17.

[35] A. Dhopeshwarkar, K. Mackie, CB 2 Cannabinoid Receptors as a Therapeutic Target—What Does the Future Hold?, Mol. Pharmacol. 86 (2014) 430–437. https://doi.org/10.1124/mol.114.094649.

[36] P. Morales, L. Hernandez-Folgado, P. Goya, N. Jagerovic, Cannabinoid receptor 2 (CB 2) agonists and antagonists: a patent update, Expert Opin. Ther. Pat. 26 (2016) 843–856. https://doi.org/10.1080/13543776.2016.1193157.

[37] T. Cassano, S. Calcagnini, L. Pace, F. De Marco, A. Romano, S. Gaetani, Cannabinoid Receptor 2 Signaling in Neurodegenerative Disorders: From Pathogenesis to a Promising Therapeutic Target, Front. Neurosci. 11 (2017). https://doi.org/10.3389/fnins.2017.00030.

[38] R.G. Pertwee, Pharmacology of cannabinoid receptor ligands, Curr. Med. Chem. 6 (1999) 635–664.

[39] J.W. Huffman, S. Yu, V. Showalter, M.E. Abood, J.L. Wiley, D.R. Compton, B.R. Martin, R.D. Bramblett, P.H. Reggio, Synthesis and Pharmacology of a Very Potent Cannabinoid Lacking a Phenolic Hydroxyl with High Affinity for the CB2 Receptor, J. Med. Chem. 39 (1996) 3875–3877. https://doi.org/10.1021/jm960394y.

[40] X.-Q. Xie, L.S. Melvin, A. Makriyannis, The Conformational Properties of the Highly Selective Cannabinoid Receptor Ligand CP-55,940, J. Biol. Chem. 271 (1996) 10640–10647. https://doi.org/10.1074/jbc.271.18.10640.

[41] L.S. Melvin, G.M. Milne, M.R. Johnson, B. Subramaniam, G.H. Wilken, A.C. Howlett, Structure-activity relationships for cannabinoid receptor-binding and analgesic activity: studies of bicyclic cannabinoid analogs, Mol. Pharmacol. 44 (1993) 1008–1015.

[42] L. Hanuš, A. Breuer, S. Tchilibon, S. Shiloah, D. Goldenberg, M. Horowitz, R.G. Pertwee, R.A. Ross, R. Mechoulam, E. Fride, HU-308: A specific agonist for CB 2 , a peripheral cannabinoid receptor, Proc. Natl. Acad. Sci. 96 (1999) 14228–14233. https://doi.org/10.1073/pnas.96.25.14228.

[43] C.C. Felder, K.E. Joyce, E.M. Briley, J. Mansouri, K. Mackie, O. Blond, Y. Lai, A.L. Ma, R.L. Mitchell, Comparison of the pharmacology and signal transduction of the human cannabinoid CB1 and CB2 receptors, Mol. Pharmacol. 48 (1995) 443–450.

[44] J. Huffman, The Search for Selective Ligands for the CB2 Receptor, Curr. Pharm. Des. 6 (2000) 1323–1337. https://doi.org/10.2174/1381612003399347.

[45] M.M. Ibrahim, H. Deng, A. Zvonok, D.A. Cockayne, J. Kwan, H.P. Mata, T.W. Vanderah, J. Lai, F. Porreca, A. Makriyannis, T.P. Malan, Activation of CB 2 cannabinoid receptors by AM1241 inhibits experimental neuropathic pain: Pain inhibition by receptors not present in the CNS, Proc. Natl. Acad. Sci. 100 (2003) 10529–10533. https://doi.org/10.1073/pnas.1834309100.

[46] M. Gallant, C. Dufresne, Y. Gareau, D. Guay, Y. Leblanc, P. Prasit, C. Rochette, N. Sawyer, D.M. Slipetz, N. Tremblay, K.M. Metters, M. Labelle, New class of potent ligands for the human peripheral cannabinoid receptor, Bioorg. Med. Chem. Lett. 6 (1996) 2263–2268. https://doi.org/10.1016/0960-894X(96)00426-X.

[47] R. Pertwee, G. Griffin, S. Fernando, X. Li, A. Hill, A. Makriyannis, AM630, a competitive cannabinoid receptor antagonist, Life Sci. 56 (1995) 1949–1955. https://doi.org/10.1016/0024-3205(95)00175-6.

[48] R.S. Landsman, A. Makriyannis, H. Deng, P. Consroe, W.R. Roeske, H.I. Yamamura, AM630 is an inverse agonist at the human cannabinoid CB1 receptor, Life Sci. 62 (1998) PL109–PL113. https://doi.org/10.1016/S0024-3205(97)01187-9.

[49] R.A. Ross, H.C. Brockie, L.A. Stevenson, V.L. Murphy, F. Templeton, A. Makriyannis, R.G. Pertwee, Agonist-inverse agonist characterization at CB $_1$ and CB $_2$ cannabinoid receptors of L759633, L759656 and AM630: L759633, L759656 and AM630, Br. J. Pharmacol. 126 (1999) 665–672. https://doi.org/10.1038/sj.bjp.0702351.

[50] D. Melck, L. De Petrocellis, P. Orlando, T. Bisogno, C. Laezza, M. Bifulco, V. Di Marzo, Suppression of Nerve Growth Factor Trk Receptors and Prolactin Receptors by Endocannabinoids Leads to Inhibition of Human Breast and Prostate Cancer Cell Proliferation1, Endocrinology. 141 (2000) 118–126. https://doi.org/10.1210/endo.141.1.7239.

[51] D.C. New, Y.H. Wong, BML-190 and AM251 act as inverse agonists at the human cannabinoid CB $_2$ receptor: signalling via cAMP and inositol phosphates, FEBS Lett. 536 (2003) 157–160. https://doi.org/10.1016/S0014-5793(03)00048-6.

[52] G. Griffin, E.J. Wray, Q. Tao, S.D. McAllister, W.K. Rorrer, M.M. Aung, B.R. Martin, M.E. Abood, Evaluation of the cannabinoid CB2 receptor-selective antagonist, SR144528: further evidence for cannabinoid CB2 receptor absence in the rat central nervous system, Eur. J. Pharmacol. 377 (1999) 117–125. https://doi.org/10.1016/s0014-2999(99)00402-1.

[53] M.-H. Rhee, S.-K. Kim, SR144528 as inverse agonist of CB2 cannabinoid receptor, J. Vet. Sci. 3 (2002) 179–184.

[54] M. Fujinaga, K. Kumata, K. Yanamoto, K. Kawamura, T. Yamasaki, J. Yui, A. Hatori, M. Ogawa, Y. Yoshida, N. Nengaki, J. Maeda, M.-R. Zhang, Radiosynthesis of novel carbon-11-labeled triaryl ligands for cannabinoid-type 2 receptor, Bioorg. Med. Chem. Lett. 20 (2010) 1565–1568. https://doi.org/10.1016/j.bmcl.2010.01.074.

[55] C. Presley, A. Abidi, S. Suryawanshi, S. Mustafa, B. Meibohm, B.M. Moore, Preclinical evaluation of SMM-189, a cannabinoid receptor 2-specific inverse agonist, Pharmacol. Res. Perspect. 3 (2015) e00159. https://doi.org/10.1002/prp2.159.

[56] P.L. Ferrarini, V. Calderone, T. Cavallini, C. Manera, G. Saccomanni, L. Pani, S. Ruiu, G.L. Gessa, Synthesis and biological evaluation of 1,8-naphthyridin-4(1H)-on-3-

carboxamide derivatives as new ligands of cannabinoid receptors, Bioorg. Med. Chem. 12 (2004) 1921–1933. https://doi.org/10.1016/j.bmc.2004.01.035.

[57] C. Manera, G. Saccomanni, B. Adinolfi, V. Benetti, A. Ligresti, M.G. Cascio, T. Tuccinardi, V. Lucchesi, A. Martinelli, P. Nieri, E. Masini, V. Di Marzo, P.L. Ferrarini, Rational design, synthesis, and pharmacological properties of new 1,8-naphthyridin-2(1H)-on-3-carboxamide derivatives as highly selective cannabinoid-2 receptor agonists, J. Med. Chem. 52 (2009) 3644–3651. https://doi.org/10.1021/jm801563d.

[58] A.M. Malfitano, C. Laezza, A. D'Alessandro, C. Procaccini, G. Saccomanni, T. Tuccinardi, C. Manera, M. Macchia, G. Matarese, P. Gazzerro, M. Bifulco, Effects on immune cells of a new 1,8-naphthyridin-2-one derivative and its analogues as selective CB2 agonists: implications in multiple sclerosis, PloS One. 8 (2013) e62511. https://doi.org/10.1371/journal.pone.0062511.

[59] V. Lucchesi, D.P. Hurst, D.M. Shore, S. Bertini, B.M. Ehrmann, M. Allarà, L. Lawrence, A. Ligresti, F. Minutolo, G. Saccomanni, H. Sharir, M. Macchia, V. Di Marzo, M.E. Abood, P.H. Reggio, C. Manera, CB2-selective cannabinoid receptor ligands: synthesis, pharmacological evaluation, and molecular modeling investigation of 1,8-Naphthyridin-2(1H)-one-3-carboxamides, J. Med. Chem. 57 (2014) 8777–8791. https://doi.org/10.1021/jm500807e.

[60] C. Manera, A.M. Malfitano, T. Parkkari, V. Lucchesi, S. Carpi, S. Fogli, S. Bertini, C. Laezza, A. Ligresti, G. Saccomanni, J.R. Savinainen, E. Ciaglia, S. Pisanti, P. Gazzerro, V. Di Marzo, P. Nieri, M. Macchia, M. Bifulco, New quinolone- and 1,8-naphthyridine-3-carboxamides as selective CB2 receptor agonists with anticancer and immuno-modulatory activity, Eur. J. Med. Chem. 97 (2015) 10–18. https://doi.org/10.1016/j.ejmech.2015.04.034.

[61] S. Pasquini, M. De Rosa, V. Pedani, C. Mugnaini, F. Guida, L. Luongo, M. De Chiaro, S. Maione, S. Dragoni, M. Frosini, A. Ligresti, V. Di Marzo, F. Corelli, Investigations on the 4-Quinolone-3-carboxylic Acid Motif. 4. Identification of New Potent and Selective Ligands for the Cannabinoid Type 2 Receptor with Diverse Substitution Patterns and Antihyperalgesic Effects in Mice, J. Med. Chem. 54 (2011) 5444–5453. https://doi.org/10.1021/jm200476p.

[62] S. Urwyler, Allosteric modulation of family C G-protein-coupled receptors: from molecular insights to therapeutic perspectives, Pharmacol. Rev. 63 (2011) 59–126. https://doi.org/10.1124/pr.109.002501.

[63] E.A. Wold, J. Chen, K.A. Cunningham, J. Zhou, Allosteric Modulation of Class A GPCRs: Targets, Agents, and Emerging Concepts, J. Med. Chem. 62 (2019) 88–127. https://doi.org/10.1021/acs.jmedchem.8b00875.

[64] L. Wang, B. Martin, R. Brenneman, L.M. Luttrell, S. Maudsley, Allosteric modulators of g protein-coupled receptors: future therapeutics for complex physiological disorders, J. Pharmacol. Exp. Ther. 331 (2009) 340–348. https://doi.org/10.1124/jpet.109.156380.

[65] F. Gado, S. Meini, S. Bertini, M. Digiacomo, M. Macchia, C. Manera, Allosteric modulators targeting cannabinoid cb1 and cb2 receptors: implications for drug discovery, Future Med. Chem. 11 (2019) 2019–2037. https://doi.org/10.4155/fmc-2019-0005.

[66] Z. Feng, M.H. Alqarni, P. Yang, Q. Tong, A. Chowdhury, L. Wang, X.-Q. Xie, Modeling, molecular dynamics simulation, and mutation validation for structure of cannabinoid receptor 2 based on known crystal structures of GPCRs, J. Chem. Inf. Model. 54 (2014) 2483–2499. https://doi.org/10.1021/ci5002718.

[67] P. Pandey, K.K. Roy, R.J. Doerksen, Negative allosteric modulators of cannabinoid receptor 2: protein modeling, binding site identification and molecular dynamics simulations in the presence of an orthosteric agonist, J. Biomol. Struct. Dyn. 38 (2020) 32–47. https://doi.org/10.1080/07391102.2019.1567384.

[68] V. Petrucci, A. Chicca, S. Glasmacher, J. Paloczi, Z. Cao, P. Pacher, J. Gertsch, Pepcan-12 (RVD-hemopressin) is a CB2 receptor positive allosteric modulator constitutively secreted by adrenals and in liver upon tissue damage, Sci. Rep. 7 (2017) 9560. https://doi.org/10.1038/s41598-017-09808-8.

[69] F. Gado, L. Di Cesare Mannelli, E. Lucarini, S. Bertini, E. Cappelli, M. Digiacomo, L.A. Stevenson, M. Macchia, T. Tuccinardi, C. Ghelardini, R.G. Pertwee, C. Manera, Identification of the First Synthetic Allosteric Modulator of the CB2 Receptors and Evidence of Its Efficacy for Neuropathic Pain Relief, J. Med. Chem. 62 (2019) 276–287. https://doi.org/10.1021/acs.jmedchem.8b00368.

[70] M. Sawzdargo, T. Nguyen, D.K. Lee, K.R. Lynch, R. Cheng, H.H.Q. Heng, S.R. George, B.F. O'Dowd, Identification and cloning of three novel human G protein-coupled receptor genes GPR52, ΨGPR53 and GPR55: GPR55 is extensively expressed in human brain, Mol. Brain Res. 64 (1999) 193–198. https://doi.org/10.1016/S0169-328X(98)00277-0.

[71] H. Yang, J. Zhou, C. Lehmann, GPR55 – a putative "type 3" cannabinoid receptor in inflammation, J. Basic Clin. Physiol. Pharmacol. 27 (2016). https://doi.org/10.1515/jbcpp-2015-0080.

[72] D.M. Shore, P.H. Reggio, The therapeutic potential of orphan GPCRs, GPR35 and GPR55, Front. Pharmacol. 6 (2015). https://doi.org/10.3389/fphar.2015.00069.

[73] S.W. Saliba, H. Jauch, B. Gargouri, A. Keil, T. Hurrle, N. Volz, F. Mohr, M. van der Stelt, S. Bräse, B.L. Fiebich, Anti-neuroinflammatory effects of GPR55 antagonists in LPS-activated primary microglial cells, J. Neuroinflammation. 15 (2018) 322. https://doi.org/10.1186/s12974-018-1362-7.

[74] J.D. Hill, V. Zuluaga-Ramirez, S. Gajghate, M. Winfield, U. Sriram, S. Rom, Y. Persidsky, Activation of GPR55 induces neuroprotection of hippocampal neurogenesis and immune responses of neural stem cells following chronic, systemic inflammation, Brain. Behav. Immun. 76 (2019) 165–181. https://doi.org/10.1016/j.bbi.2018.11.017.

[75] J.E. Lauckner, J.B. Jensen, H.-Y. Chen, H.-C. Lu, B. Hille, K. Mackie, GPR55 is a cannabinoid receptor that increases intracellular calcium and inhibits M current, Proc. Natl. Acad. Sci. 105 (2008) 2699–2704. https://doi.org/10.1073/pnas.0711278105.

[76] E. Ryberg, N. Larsson, S. Sjögren, S. Hjorth, N.-O. Hermansson, J. Leonova, T. Elebring, K. Nilsson, T. Drmota, P.J. Greasley, The orphan receptor GPR55 is a novel cannabinoid receptor: GPR55, a novel cannabinoid receptor, Br. J. Pharmacol. 152 (2007) 1092–1101. https://doi.org/10.1038/sj.bjp.0707460.

[77] S. Oka, S. Kimura, T. Toshida, R. Ota, A. Yamashita, T. Sugiura, Lysophosphatidylinositol induces rapid phosphorylation of p38 mitogen-activated protein kinase and activating transcription factor 2 in HEK293 cells expressing GPR55 and IM-9 lymphoblastoid cells, J. Biochem. (Tokyo). 147 (2010) 671–678. https://doi.org/10.1093/jb/mvp208.

[78] M. Alhouayek, J. Masquelier, G.G. Muccioli, Lysophosphatidylinositols, from Cell Membrane Constituents to GPR55 Ligands, Trends Pharmacol. Sci. 39 (2018) 586–604. https://doi.org/10.1016/j.tips.2018.02.011.

[79] C.M. Henstridge, N.A. Balenga, R. Schröder, J.K. Kargl, W. Platzer, L. Martini, S. Arthur, J. Penman, J.L. Whistler, E. Kostenis, M. Waldhoer, A.J. Irving, GPR55 ligands promote receptor coupling to multiple signalling pathways: GPR55 signalling, Br. J. Pharmacol. 160 (2010) 604–614. https://doi.org/10.1111/j.1476-5381.2009.00625.x.

[80] J. Kargl, N. Balenga, W. Platzer, L. Martini, J. Whistler, M. Waldhoer, The GPCR-associated sorting protein 1 regulates ligand-induced down-regulation of GPR55: GASP-1 regulates ligand-induced GPR55 sorting, Br. J. Pharmacol. 165 (2012) 2611–2619. https://doi.org/10.1111/j.1476-5381.2011.01562.x.

[81] S. Oka, K. Nakajima, A. Yamashita, S. Kishimoto, T. Sugiura, Identification of GPR55 as a lysophosphatidylinositol receptor, Biochem. Biophys. Res. Commun. 362 (2007) 928–934. https://doi.org/10.1016/j.bbrc.2007.08.078.

[82] A. Kapur, P. Zhao, H. Sharir, Y. Bai, M.G. Caron, L.S. Barak, M.E. Abood, Atypical Responsiveness of the Orphan Receptor GPR55 to Cannabinoid Ligands, J. Biol. Chem. 284 (2009) 29817–29827. https://doi.org/10.1074/jbc.M109.050187.

[83] C. Lipina, S.K. Walsh, S.E. Mitchell, J.R. Speakman, C.L. Wainwright, H.S. Hundal, GPR55 deficiency is associated with increased adiposity and impaired insulin signaling in peripheral metabolic tissues, FASEB J. 33 (2019) 1299–1312. https://doi.org/10.1096/fj.201800171R.

[84] T. Nevalainen, A. J. Irving, GPR55, a Lysophosphatidylinositol Receptor with Cannabinoid Sensitivity?, Curr. Top. Med. Chem. 10 (2010) 799–813. https://doi.org/10.2174/156802610791164229.

[85] S. Oka, T. Toshida, K. Maruyama, K. Nakajima, A. Yamashita, T. Sugiura, 2-Arachidonoyl-sn-glycero-3-phosphoinositol: A Possible Natural Ligand for GPR55, J. Biochem. (Tokyo). 145 (2008) 13–20. https://doi.org/10.1093/jb/mvn136.

[86] T. Okuno, T. Yokomizo, What is the natural ligand of GPR55?, J. Biochem. (Tokyo). 149 (2011) 495–497. https://doi.org/10.1093/jb/mvr022.

[87] L. Console-Bram, S.M. Ciuciu, P. Zhao, R.E. Zipkin, E. Brailoiu, M.E. Abood, N-arachidonoyl glycine, another endogenous agonist of GPR55, Biochem. Biophys. Res. Commun. 490 (2017) 1389–1393. https://doi.org/10.1016/j.bbrc.2017.07.038.

[88] B. A. Marichal-Cancino, A. Fajardo-Valdez, A. E. Ruiz-Contreras, M. Mendez-Díaz, O. Prospero-García, Advances in the Physiology of GPR55 in the Central Nervous System, Curr. Neuropharmacol. 15 (2017). https://doi.org/10.2174/1570159X14666160729155441.

[89] R. Rozenfeld, L.A. Devi, Receptor heteromerization and drug discovery, Trends Pharmacol. Sci. 31 (2010) 124–130. https://doi.org/10.1016/j.tips.2009.11.008.

[90] J. Kargl, N. Balenga, G.P. Parzmair, A.J. Brown, A. Heinemann, M. Waldhoer, The Cannabinoid Receptor CB1 Modulates the Signaling Properties of the Lysophosphatidylinositol Receptor GPR55, J. Biol. Chem. 287 (2012) 44234–44248. https://doi.org/10.1074/jbc.M112.364109.

[91] N.A. Balenga, E. Martínez-Pinilla, J. Kargl, R. Schröder, M. Peinhaupt, W. Platzer, Z. Bálint, M. Zamarbide, I.G. Dopeso-Reyes, A. Ricobaraza, J.M. Pérez-Ortiz, E. Kostenis, M. Waldhoer, A. Heinemann, R. Franco, Heteromerization of GPR55 and cannabinoid CB $_2$ receptors modulates signalling: Heteromerization of GPR55 and CB $_2$ receptors, Br. J. Pharmacol. 171 (2014) 5387–5406. https://doi.org/10.1111/bph.12850.

[92] E. Moreno, C. Andradas, M. Medrano, M.M. Caffarel, E. Pérez-Gómez, S. Blasco-Benito, M. Gómez-Cañas, M.R. Pazos, A.J. Irving, C. Lluís, E.I. Canela, J. Fernández-Ruiz, M. Guzmán, P.J. McCormick, C. Sánchez, Targeting CB2-GPR55 Receptor Heteromers Modulates Cancer Cell Signaling, J. Biol. Chem. 289 (2014) 21960–21972. https://doi.org/10.1074/jbc.M114.561761.

[93] E. Tudurí, M. Imbernon, R.J. Hernández-Bautista, M. Tojo, J. Fernø, C. Diéguez, R. Nogueiras, GPR55: a new promising target for metabolism?, J. Mol. Endocrinol. 58 (2017) R191–R202. https://doi.org/10.1530/JME-16-0253.

[94] C.M. Henstridge, N.A.B. Balenga, J. Kargl, C. Andradas, A.J. Brown, A. Irving, C. Sanchez, M. Waldhoer, Minireview: recent developments in the physiology and pathology of the lysophosphatidylinositol-sensitive receptor GPR55, Mol. Endocrinol. Baltim. Md. 25 (2011) 1835–1848. https://doi.org/10.1210/me.2011-1197.

[95] X. Zhang, Y. Maor, J. Wang, G. Kunos, J. Groopman, Endocannabinoid-like N-arachidonoyl serine is a novel pro-angiogenic mediator, Br. J. Pharmacol. 160 (2010) 1583–1594. https://doi.org/10.1111/j.1476-5381.2010.00841.x.

[96] K. Gupta, S. Kshirsagar, L. Chang, R. Schwartz, P.-Y. Law, D. Yee, R.P. Hebbel, Morphine stimulates angiogenesis by activating proangiogenic and survival-promoting signaling and promotes breast tumor growth, Cancer Res. 62 (2002) 4491–4498.

[97] V. Chiurchiù, M. Lanuti, M. De Bardi, L. Battistini, M. Maccarrone, The differential characterization of GPR55 receptor in human peripheral blood reveals a distinctive expression in monocytes and NK cells and a proinflammatory role in these innate cells, Int. Immunol. 27 (2015) 153–160. https://doi.org/10.1093/intimm/dxu097.

[98] A. Stančić, K. Jandl, C. Hasenöhrl, F. Reichmann, G. Marsche, R. Schuligoi, A. Heinemann, M. Storr, R. Schicho, The GPR55 antagonist CID16020046 protects against intestinal inflammation, Neurogastroenterol. Motil. 27 (2015) 1432–1445. https://doi.org/10.1111/nmo.12639.

[99] M. Celorrio, E. Rojo-Bustamante, D. Fernández-Suárez, E. Sáez, A. Estella-Hermoso de Mendoza, C.E. Müller, M.J. Ramírez, J. Oyarzábal, R. Franco, M.S. Aymerich, GPR55: A therapeutic target for Parkinson's disease?, Neuropharmacology. 125 (2017) 319–332. https://doi.org/10.1016/j.neuropharm.2017.08.017.

[100] J. Stephenson, E. Nutma, P. van der Valk, S. Amor, Inflammation in CNS neurodegenerative diseases, Immunology. 154 (2018) 204–219. https://doi.org/10.1111/imm.12922.

[101] T. Cassano, G. Serviddio, S. Gaetani, A. Romano, P. Dipasquale, S. Cianci, F. Bellanti, L. Laconca, A.D. Romano, I. Padalino, F.M. LaFerla, F. Nicoletti, V. Cuomo, G. Vendemiale, Glutamatergic alterations and mitochondrial impairment in a murine model of Alzheimer disease, Neurobiol. Aging. 33 (2012) 1121.e1-1121.e12. https://doi.org/10.1016/j.neurobiolaging.2011.09.021.

[102] G.G. Kovacs, H. Adle-Biassette, I. Milenkovic, S. Cipriani, J. van Scheppingen, E. Aronica, Linking pathways in the developing and aging brain with neurodegeneration, Neuroscience. 269 (2014) 152–172. https://doi.org/10.1016/j.neuroscience.2014.03.045.

[103] S. Kallendrusch, S. Kremzow, M. Nowicki, U. Grabiec, R. Winkelmann, A. Benz, R. Kraft, I. Bechmann, F. Dehghani, M. Koch, The G Protein-Coupled Receptor 55 Ligand L -α-Lysophosphatidylinositol Exerts Microglia-Dependent Neuroprotection After Excitotoxic Lesion: Microglia-Dependent GPR55-Driven Neuroprotection, Glia. 61 (2013) 1822–1831. https://doi.org/10.1002/glia.22560.

[104] C.-S. Wu, H. Chen, H. Sun, J. Zhu, C.P. Jew, J. Wager-Miller, A. Straiker, C. Spencer, H. Bradshaw, K. Mackie, H.-C. Lu, GPR55, a G-Protein Coupled Receptor for Lysophosphatidylinositol, Plays a Role in Motor Coordination, PLoS ONE. 8 (2013) e60314. https://doi.org/10.1371/journal.pone.0060314.

[105] J. Abe, A.T. Guy, F. Ding, P. Greimel, Y. Hirabayashi, H. Kamiguchi, Y. Ito, Systematic synthesis of novel phosphoglycolipid analogues as potential agonists of GPR55, Org. Biomol. Chem. 18 (2020) 8467–8473. https://doi.org/10.1039/D0OB01756F.

[106] M. Waldeck-Weiermair, C. Zoratti, K. Osibow, N. Balenga, E. Goessnitzer, M. Waldhoer, R. Malli, W.F. Graier, Integrin clustering enables anandamide-induced Ca2+ signaling in endothelial cells via GPR55 by protection against CB1-receptor-triggered repression, J. Cell Sci. 121 (2008) 1704–1717. https://doi.org/10.1242/jcs.020958.

[107] H. Yin, A. Chu, W. Li, B. Wang, F. Shelton, F. Otero, D.G. Nguyen, J.S. Caldwell, Y.A. Chen, Lipid G Protein-coupled Receptor Ligand Identification Using β-Arrestin PathHunter™ Assay, J. Biol. Chem. 284 (2009) 12328–12338. https://doi.org/10.1074/jbc.M806516200.

[108] H. Sharir, L. Console-Bram, C. Mundy, S.N. Popoff, A. Kapur, M.E. Abood, The Endocannabinoids Anandamide and Virodhamine Modulate the Activity of the Candidate Cannabinoid Receptor GPR55, J. Neuroimmune Pharmacol. 7 (2012) 856–865. https://doi.org/10.1007/s11481-012-9351-6.

[109] S. Anavi-Goffer, G. Baillie, A.J. Irving, J. Gertsch, I.R. Greig, R.G. Pertwee, R.A. Ross, Modulation of l-α-Lysophosphatidylinositol/GPR55 Mitogen-activated Protein Kinase (MAPK) Signaling by Cannabinoids, J. Biol. Chem. 287 (2012) 91–104. https://doi.org/10.1074/jbc.M111.296020.

[110] E. Stockings, D. Zagic, G. Campbell, M. Weier, W.D. Hall, S. Nielsen, G.K. Herkes, M. Farrell, L. Degenhardt, Evidence for cannabis and cannabinoids for epilepsy: a systematic review of controlled and observational evidence, J. Neurol. Neurosurg. Psychiatry. 89 (2018) 741–753. https://doi.org/10.1136/jnnp-2017-317168.

[111] J. Elliott, D. DeJean, T. Clifford, D. Coyle, B.K. Potter, B. Skidmore, C. Alexander, A.E. Repetski, V. Shukla, B. McCoy, G.A. Wells, Cannabis-based products for pediatric epilepsy: An updated systematic review, Seizure. 75 (2020) 18–22. https://doi.org/10.1016/j.seizure.2019.12.006.

[112] A. Morano, M. Fanella, M. Albini, P. Cifelli, E. Palma, A.T. Giallonardo, C. Di Bonaventura, Cannabinoids in the Treatment of Epilepsy: Current Status and Future Prospects, Neuropsychiatr. Dis. Treat. Volume 16 (2020) 381–396. https://doi.org/10.2147/NDT.S203782.

[113] L.S. Whyte, E. Ryberg, N.A. Sims, S.A. Ridge, K. Mackie, P.J. Greasley, R.A. Ross, M.J. Rogers, The putative cannabinoid receptor GPR55 affects osteoclast function in vitro and bone mass in vivo, Proc. Natl. Acad. Sci. 106 (2009) 16511–16516. https://doi.org/10.1073/pnas.0902743106.

[114] D.G. Johns, D.J. Behm, D.J. Walker, Z. Ao, E.M. Shapland, D.A. Daniels, M. Riddick, S. Dowell, P.C. Staton, P. Green, U. Shabon, W. Bao, N. Aiyar, T.-L. Yue, A.J. Brown, A.D. Morrison, S.A. Douglas, The novel endocannabinoid receptor GPR55 is activated by atypical cannabinoids but does not mediate their vasodilator effects: GPR55 and atypical cannabinoids, Br. J. Pharmacol. 152 (2007) 825–831. https://doi.org/10.1038/sj.bjp.0707419.

[115] V. Rempel, N. Volz, S. Hinz, T. Karcz, I. Meliciani, M. Nieger, W. Wenzel, S. Bräse, C.E. Müller, 7-Alkyl-3-benzylcoumarins: A Versatile Scaffold for the Development of Potent and Selective Cannabinoid Receptor Agonists and Antagonists, J. Med. Chem. 55 (2012) 7967–7977. https://doi.org/10.1021/jm3008213.

[116] V. Rempel, N. Volz, F. Gläser, M. Nieger, S. Bräse, C.E. Müller, Antagonists for the Orphan G-Protein-Coupled Receptor GPR55 Based on a Coumarin Scaffold, J. Med. Chem. 56 (2013) 4798–4810. https://doi.org/10.1021/jm4005175.

[117] Y.-J. Lee, Y.M. Lee, C.-K. Lee, J.K. Jung, S.B. Han, J.T. Hong, Therapeutic applications of compounds in the Magnolia family, Pharmacol. Ther. 130 (2011) 157–176. https://doi.org/10.1016/j.pharmthera.2011.01.010.

[118] W. Schuehly, J.M.V. Paredes, J. Kleyer, A. Huefner, S. Anavi-Goffer, S. Raduner, K.-H. Altmann, J. Gertsch, Mechanisms of Osteoclastogenesis Inhibition by a Novel Class of Biphenyl-Type Cannabinoid CB2 Receptor Inverse Agonists, Chem. Biol. 18 (2011) 1053–1064. https://doi.org/10.1016/j.chembiol.2011.05.012.

[119] V. Rempel, A. Fuchs, S. Hinz, T. Karcz, M. Lehr, U. Koetter, C.E. Müller, Magnolia Extract, Magnolol, and Metabolites: Activation of Cannabinoid CB $_2$ Receptors and Blockade of the Related GPR55, ACS Med. Chem. Lett. 4 (2013) 41–45. https://doi.org/10.1021/ml300235q.

[120] A. Fuchs, V. Rempel, C.E. Müller, The Natural Product Magnolol as a Lead Structure for the Development of Potent Cannabinoid Receptor Agonists, PLoS ONE. 8 (2013) e77739. https://doi.org/10.1371/journal.pone.0077739.

[121] S. Heynen-Genel, R. Dahl, S. Shi, L. Milan, S. Hariharan, Y. Bravo, E. Sergienko, M. Hedrick, S. Dad, D. Stonich, Y. Su, M. Vicchiarelli, A. Mangravita-Novo, L.H. Smith, T.D. Chung, H. Sharir, L.S. Barak, M.E. Abood, Screening for Selective Ligands for GPR55 - Agonists, in: Probe Rep. NIH Mol. Libr. Program, National Center for Biotechnology Information (US), Bethesda (MD), 2010. http://www.ncbi.nlm.nih.gov/books/NBK66152/ (accessed November 8, 2022).

[122] S. Heynen-Genel, R. Dahl, S. Shi, L. Milan, S. Hariharan, E. Sergienko, M. Hedrick, S. Dad, D. Stonich, Y. Su, M. Vicchiarelli, A. Mangravita-Novo, L.H. Smith, T.D. Chung, H. Sharir, M.G. Caron, L.S. Barak, M.E. Abood, Screening for Selective Ligands for GPR55 - Antagonists, in: Probe Rep. NIH Mol. Libr. Program, National Center for Biotechnology Information (US), Bethesda (MD), 2010. http://www.ncbi.nlm.nih.gov/books/NBK66153/ (accessed November 8, 2022).

[123] A.J. Brown, D.A. Daniels, M. Kassim, S. Brown, C.P. Haslam, V.R. Terrell, J. Brown, P.L. Nichols, P.C. Staton, A. Wise, S.J. Dowell, Pharmacology of GPR55 in Yeast and Identification of GSK494581A as a Mixed-Activity Glycine Transporter Subtype 1 Inhibitor and GPR55 Agonist, J. Pharmacol. Exp. Ther. 337 (2011) 236–246. https://doi.org/10.1124/jpet.110.172650.

[124] J. Kargl, A.J. Brown, L. Andersen, G. Dorn, R. Schicho, M. Waldhoer, A. Heinemann, A selective antagonist reveals a potential role of G protein-coupled receptor 55 in platelet and endothelial cell function, J. Pharmacol. Exp. Ther. 346 (2013) 54–66. https://doi.org/10.1124/jpet.113.204180.

[125] R.K. Paul, A. Wnorowski, I. Gonzalez-Mariscal, S.K. Nayak, K. Pajak, R. Moaddel, F.E. Indig, M. Bernier, I.W. Wainer, (R,R′)-4′-methoxy-1-naphthylfenoterol

targets GPR55-mediated ligand internalization and impairs cancer cell motility, Biochem. Pharmacol. 87 (2014) 547–561. https://doi.org/10.1016/j.bcp.2013.11.020.

[126] W. Poewe, K. Seppi, C.M. Tanner, G.M. Halliday, P. Brundin, J. Volkmann, A.-E. Schrag, A.E. Lang, Parkinson disease, Nat. Rev. Dis. Primer. 3 (2017) 17013. https://doi.org/10.1038/nrdp.2017.13.

[127] J.M. Long, D.M. Holtzman, Alzheimer Disease: An Update on Pathobiology and Treatment Strategies, Cell. 179 (2019) 312–339. https://doi.org/10.1016/j.cell.2019.09.001.

[128] C. Ceni, M.J. Benko, K.A. Mohamed, G. Poli, M. Di Stefano, T. Tuccinardi, M. Digiacomo, M. Valoti, R.B. Laprairie, M. Macchia, S. Bertini, Novel Potent and Selective Agonists of the GPR55 Receptor Based on the 3-Benzylquinolin-2(1H)-One Scaffold, Pharmaceuticals. 15 (2022) 768. https://doi.org/10.3390/ph15070768.

[129] A. Zagzoog, K.A. Mohamed, H.J.J. Kim, E.D. Kim, C.S. Frank, T. Black, P.D. Jadhav, L.A. Holbrook, R.B. Laprairie, In vitro and in vivo pharmacological activity of minor cannabinoids isolated from Cannabis sativa, Sci. Rep. 10 (2020) 20405. https://doi.org/10.1038/s41598-020-77175-y.

[130] R. Taniguchi, A. Inoue, M. Sayama, A. Uwamizu, K. Yamashita, K. Hirata, M. Yoshida, Y. Tanaka, H.E. Kato, Y. Nakada-Nakura, Y. Otani, T. Nishizawa, T. Doi, T. Ohwada, R. Ishitani, J. Aoki, O. Nureki, Structural insights into ligand recognition by the lysophosphatidic acid receptor LPA6, Nature. 548 (2017) 356–360. https://doi.org/10.1038/nature23448.

[131] L.M. Espinoza-Fonseca, The benefits of the multi-target approach in drug design and discovery, Bioorg. Med. Chem. 14 (2006) 896–897. https://doi.org/10.1016/j.bmc.2005.09.011.

[132] L. Pisani, M. Catto, F. Leonetti, O. Nicolotti, A. Stefanachi, F. Campagna, A. Carotti, Targeting Monoamine Oxidases with Multipotent Ligands: An Emerging Strategy in the Search of New Drugs Against Neurodegenerative Diseases, Curr. Med. Chem. 18 (2011) 4568–4587. https://doi.org/10.2174/092986711797379302.

[133] C. Ceni, D. Catarzi, F. Varano, D.D. Ben, G. Marucci, M. Buccioni, R. Volpini, A. Angeli, A. Nocentini, P. Gratteri, C.T. Supuran, V. Colotta, Discovery of first-in-class multi-target adenosine A2A receptor antagonists-carbonic anhydrase IX and XII inhibitors. 8-Amino-6-aryl-2-phenyl-1,2,4-triazolo [4,3-a]pyrazin-3-one derivatives as new potential antitumor agents, Eur. J. Med. Chem. 201 (2020) 112478. https://doi.org/10.1016/j.ejmech.2020.112478.

[134] V. Lucchesi, D.P. Hurst, D.M. Shore, S. Bertini, B.M. Ehrmann, M. Allarà, L. Lawrence, A. Ligresti, F. Minutolo, G. Saccomanni, H. Sharir, M. Macchia, V. Di Marzo, M.E. Abood, P.H. Reggio, C. Manera, CB2-selective cannabinoid receptor ligands: synthesis, pharmacological evaluation, and molecular modeling investigation of 1,8-Naphthyridin-2(1H)-one-3-carboxamides, J. Med. Chem. 57 (2014) 8777–8791. https://doi.org/10.1021/jm500807e.

[135] J.K. Pokorski, L.E. Smith, "Click" Chemistry for Medicine and Biology, Mol. Pharm. 15 (2018) 2891–2891. https://doi.org/10.1021/acs.molpharmaceut.8b00743.

[136] Y. Takayama, K. Kusamori, M. Nishikawa, Click Chemistry as a Tool for Cell Engineering and Drug Delivery, Molecules. 24 (2019) 172. https://doi.org/10.3390/molecules24010172.

[137] C.D. Hein, X.-M. Liu, D. Wang, Click Chemistry, A Powerful Tool for Pharmaceutical Sciences, Pharm. Res. 25 (2008) 2216–2230. https://doi.org/10.1007/s11095-008-9616-1.

[138] F. Gado, C. Ceni, R. Ferrisi, G. Sbrana, L.A. Stevenson, M. Macchia, R.G. Pertwee, S. Bertini, C. Manera, G. Ortore, CB1 receptor binding sites for NAM and PAM: A first approach for studying, new n-butyl-diphenylcarboxamides as allosteric modulators, Eur. J. Pharm. Sci. 169 (2022) 106088. https://doi.org/10.1016/j.ejps.2021.106088.

[139] S. Röver, M. Andjelkovic, A. Bénardeau, E. Chaput, W. Guba, P. Hebeisen, S. Mohr, M. Nettekoven, U. Obst, W.F. Richter, C. Ullmer, P. Waldmeier, M.B. Wright, 6-Alkoxy-5-aryl-3-pyridinecarboxamides, a New Series of Bioavailable Cannabinoid Receptor Type 1 (CB1) Antagonists Including Peripherally Selective Compounds, J. Med. Chem. 56 (2013) 9874–9896. https://doi.org/10.1021/jm4010708.

[140] S. Bertini, T. Parkkari, J.R. Savinainen, C. Arena, G. Saccomanni, S. Saguto, A. Ligresti, M. Allarà, A. Bruno, L. Marinelli, V. Di Marzo, E. Novellino, C. Manera, M. Macchia, Synthesis, biological activity and molecular modeling of new biphenylic carboxamides as potent and selective CB2 receptor ligands, Eur. J. Med. Chem. 90 (2015) 526–536. https://doi.org/10.1016/j.ejmech.2014.11.066.

[141] M. Di Stefano, S. Galati, G. Ortore, I. Caligiuri, F. Rizzolio, C. Ceni, S. Bertini, G. Bononi, C. Granchi, M. Macchia, G. Poli, T. Tuccinardi, Machine Learning-Based Virtual Screening for the Identification of Cdk5 Inhibitors, Int. J. Mol. Sci. 23 (2022) 10653. https://doi.org/10.3390/ijms231810653.

[142] K.K. Gupta, S.K. Singh, Cdk5: A main culprit in neurodegeneration, Int. J. Neurosci. 129 (2019) 1192–1197. https://doi.org/10.1080/00207454.2019.1645142.

[143] L. Meijer, A. Borgne, O. Mulner, J.P.J. Chong, J.J. Blow, N. Inagaki, M. Inagaki, J.-G. Delcros, J.-P. Moulinoux, Biochemical and Cellular Effects of Roscovitine, a Potent and Selective Inhibitor of the Cyclin-Dependent Kinases cdc2, cdk2 and cdk5, Eur. J. Biochem. 243 (1997) 527–536. https://doi.org/10.1111/j.1432-1033.1997.t01-2-00527.x.

[144] D. Parry, T. Guzi, F. Shanahan, N. Davis, D. Prabhavalkar, D. Wiswell, W. Seghezzi, K. Paruch, M.P. Dwyer, R. Doll, A. Nomeir, W. Windsor, T. Fischmann, Y. Wang, M. Oft, T. Chen, P. Kirschmeier, E.M. Lees, Dinaciclib (SCH 727965), a Novel and Potent Cyclin-Dependent Kinase Inhibitor, Mol. Cancer Ther. 9 (2010) 2344–2353. https://doi.org/10.1158/1535-7163.MCT-10-0324.

[145] H. Ji J. Kim, A. Zagzoog, C. Ceni, R. Ferrisi, N. Janz, R. B. Laprairie, Dual cannabinoid and orexin regulation of anhedonic behaviour caused by prolonged restraint stress, Brain Science (2023). Approved

[146] D.A. Pizzagalli, Depression, Stress, and Anhedonia: Toward a Synthesis and Integrated Model, Annu. Rev. Clin. Psychol. 10 (2014) 393–423. https://doi.org/10.1146/annurev-clinpsy-050212-185606.

[147] C.T. Taylor, S.N. Hoffman, A.J. Khan, Anhedonia in Anxiety Disorders, in: D.A. Pizzagalli (Ed.), Anhedonia Preclin. Transl. Clin. Integr., Springer International Publishing, Cham, 2022: pp. 201–218. https://doi.org/10.1007/7854_2022_319.

[148] S. Goldstein Ferber, A. Weller, G. Yadid, A. Friedman, Discovering the Lost Reward: Critical Locations for Endocannabinoid Modulation of the Cortico–Striatal Loop That Are Implicated in Major Depression, Int. J. Mol. Sci. 22 (2021) 1867. https://doi.org/10.3390/ijms22041867.

[149] M.A. Katzman, M.P. Katzman, Neurobiology of the Orexin System and Its Potential Role in the Regulation of Hedonic Tone, Brain Sci. 12 (2022) 150. https://doi.org/10.3390/brainsci12020150.

[150] E. Poleszak, S. Wośko, K. Sławińska, A. Szopa, A. Wróbel, A. Serefko, Cannabinoids in depressive disorders, Life Sci. 213 (2018) 18–24. https://doi.org/10.1016/j.lfs.2018.09.058.

[151] S. Soya, T. Sakurai, Evolution of Orexin Neuropeptide System: Structure and Function, Front. Neurosci. 14 (2020) 691. https://doi.org/10.3389/fnins.2020.00691.

[152] S.K. Prajapati, S. Krishnamurthy, Non-selective orexin-receptor antagonist attenuates stress-re-stress-induced core PTSD-like symptoms in rats: Behavioural and neurochemical analyses, Behav. Brain Res. 399 (2021) 113015. https://doi.org/10.1016/j.bbr.2020.113015.

[153] X. Chu, Y. Zhou, Z. Hu, J. Lou, W. Song, J. Li, X. Liang, C. Chen, S. Wang, B. Yang, L. Chen, X. Zhang, J. Song, Y. Dong, S. Chen, L. He, Q. Xie, X. Chen, W. Li, 24-hour-restraint stress induces long-term depressive-like phenotypes in mice, Sci. Rep. 6 (2016) 32935. https://doi.org/10.1038/srep32935.

[154] A. Zagzoog, K.A. Mohamed, H.J.J. Kim, E.D. Kim, C.S. Frank, T. Black, P.D. Jadhav, L.A. Holbrook, R.B. Laprairie, In vitro and in vivo pharmacological activity of minor cannabinoids isolated from Cannabis sativa, Sci. Rep. 10 (2020) 20405. https://doi.org/10.1038/s41598-020-77175-y.

[155] A. Zagzoog, A.L. Brandt, T. Black, E.D. Kim, R. Burkart, M. Patel, Z. Jin, M. Nikolaeva, R.B. Laprairie, Assessment of select synthetic cannabinoid receptor agonist bias and selectivity between the type 1 and type 2 cannabinoid receptor, Sci. Rep. 11 (2021) 10611. https://doi.org/10.1038/s41598-021-90167-w.

[156] E. Carosati, S. Sciabola, G. Cruciani, Hydrogen Bonding Interactions of Covalently Bonded Fluorine Atoms: From Crystallographic Data to a New Angular

Function in the GRID Force Field, J. Med. Chem. 47 (2004) 5114–5125. https://doi.org/10.1021/jm0498349.

[157] G. Cruciani, E. Carosati, B. De Boeck, K. Ethirajulu, C. Mackie, T. Howe, R. Vianello, MetaSite: Understanding Metabolism in Human Cytochromes from the Perspective of the Chemist, J. Med. Chem. 48 (2005) 6970–6979. https://doi.org/10.1021/jm050529c.

20/03/2023 09:52:57
COSTANZA CENI

Costanza Ceni